Xenia A. L. Domes

Cement grouting during installation of ground anchors in non-cohesive soils

Thesis for the degree of Philosophiae Doctor

Trondheim, June 2015

Norwegian University of Science and Technology
Faculty of Engineering Science and Technology
Department of Civil and Transport Engineering

NTNU – Trondheim
Norwegian University of
Science and Technology

The evaluation committee of this thesis comprised the following members:

Professor Adam Bezuijen
University of Gent

Professor Jürgen Grabe
Technische Universität Hamburg-Harburg

Professor Gudmund Eiksund
Norwegian University of Science and Technology

Academic supervisors:

Professor Thomas Benz
Norwegian University of Science and Technology

Dr. Markus Herten
Federal Waterways Engineering and Research Institute Karlsruhe

NTNU
Norwegian University of Science and Technology

Thesis for the degree of Philosophiae Doctor

Faculty of Engineering Science and Technology
Department of Civil and Transport Engineering

ISBN 978-82-326-0764-8 (printed ver.)
ISBN 978-82-326-0765-5 (electronic ver.)
ISSN 1503-8181

Doctoral theses at NTNU, 2015:51

Printed by NTNU Grafisk senter

Preface

The presented PhD study was carried out in cooperation with the Norwegian University of Science and Technology in Trondheim, Norway and the Federal Waterways Engineering and Research Institute in Karlsruhe, Germany. This project was made possible by financial support of the Federal Waterways Engineering and Research Institute in Karlsruhe. The field tests were carried out at their sites. The laboratory test series were done and test equipment was designed at the Norwegian University of Science and Technology. Their support is gratefully acknowledged. The work is presented as monograph.

Abstract

Pressure grouting during installation of grouted ground anchors is known to increase anchor capacity in non-cohesive soils, but little information is available on correlations between applied grouting pressures, duration of grouting, ground conditions and increase of anchor pull-out capacity.

The presented PhD study is concerned with processes taking place during installation of grouted ground anchors in non-cohesive soils, where filtration of the cement grout is assumed. It was aimed to determine the influence of pressure grouting on the stresses on the anchor body and the properties of the adjacent soil. The knowledge of those is considered prerequisite in order to determine the anchors pull-out capacity.

In the first part of the PhD thesis, a series of laboratory experiments is presented, which was carried out to understand the filtration process of cement grouts and to determine the properties of the filter cake material. Using a filtration press the rate of filter cake build-up was investigated, taking into account the influence of grouting pressure and initial water/cement ratio of the grout. The test results were used to evaluate different analytical approaches to simulate the filtration process: a two-phase filtration model and classical consolidation theory. Both models were found appropriate, and calculation parameters were determined. In addition to the filtration tests, the mechanical properties of the fresh, uncured, filter-cake material were investigated. Applying soil mechanical investigation methods, strength and stiffness properties could be determined.

In the second part of the PhD thesis in-situ tests during anchor installation in sands are presented. On three test sites the grout pressure was measured inside the borehole during and after anchor installation. Measurements confirmed a grout filtration inside the borehole and indicated the increase of radial stresses on the anchor body. Additional flat-dilatometer soundings (DMT) and cone penetration tests (CPT) showed the influence of the grouting process on the radial stresses in the adjacent soil.

In the third part of the thesis a numerical model is proposed to simulate the filtration process of cement grout in a fully coupled flow-displacement finite element analysis. Based on the two-phase filtration model a filter criterion was implemented, which defines the phase change from liquid to solid grout based on the discharge of water. The phase change was realised by changing the material properties of the grout elements. With the presented model the grouting during anchor installation was simulated and the influence of different parameters could be determined. The transfer of grouting pressures from the liquid grout to the soil through seepage forces in the filtercake is simulated and the residual stresses after grouting determined.

The findings can now be used as starting point to simulate the load transfer mechanisms of grouted ground anchors in numerical analysis, taking into account installation effects.

Acknowledgements

During my PhD research I had the privilege to be part of the geotechnical groups at the Norwegian University of Science and Technology (NTNU) in Trondheim as well as at the Federal Waterways Engineering and Research Institute (BAW) in Karlsruhe. However, I started my academic career setting me off into the topic of grouted ground anchors at the structural engineering department at the University of Applied Sciences in Münster. Along the way I met many people who have been supportive to me and my study in one way or the other. I would like to express my deepest gratitude to all of them.

First and foremost, I would like to thank my supervisor at NTNU, Professor Thomas Benz, for his support and encouragement. Thank you for always having an open mind for ideas and discussion, being interested and curious about my research, providing scientific support and even helping me in the field, giving me confidence and keeping me motivated.

I also owe my gratitude to my supervisor at BAW, Dr. Markus Herten, without whom it would not have been possible to conduct this research project. Thank you for your support, for having fate in the research project and facilitating the possibilities I had.

Further, I would like to thank Professor Gerhard Schaper of the FH Münster for evoking my interest in research and encouraging me to do a PhD.

The experimental part of this work would have been impossible without the help and effort of the technical staff at NTNU. Thank you Frank Stæli, Tage Westrum and Per Østensen for building the sensors and laboratory equipment and managing to get them ready in time so that I could finish my experiments within the tight travel schedule. Also many thanks to Rikke Marie Vollan for helping me with the laboratory experiments.

I am grateful for the secretary of the Geotechnical Division Marit Skjåk-Bræk for patiently helping me with all organizational and administrative matters and always being there when help is needed.

Over the years I have enjoined many discussions and meetings with past and present PhD candidates of different organizations. All of you provided inspiration and help which is highly appreciated. Amongst all other things, special thanks to Priscilla for supporting me to prepare for the exams at NTNU, Annika for the support with administrative matters, Stian for keeping the agenda up to date and Hilde for introducing me to the Norwegian culture. I would also like to thank Harriet, Jakob and Katharina for their versatile support and companionship.

Many thanks to all my colleges at BAW, who provided an inspiring and welcoming working environment. Thank you for the many suggestions and coffee break discussions. Special thanks to Eva Dornecker for sharing your knowledge about grouted ground anchors. Thank

you to Regina Kauther, Ingo Feddersen, Björn Mettig and Hermann Brauer for the support during the in-situ tests. I would also like to thank Dr. Bernhard Odenwald for the inspiring discussions about analytical solutions. I must also thank Olivia Wenzel for proofreading/editing my thesis.

Finally, my deepest gratitude goes to my family and friends with their unconditional support, everyone in their own way. Thank you to my father for motivating me achieving a goal and teaching me to become an independent person. Thank you Mama for your love and moral support regardless the time or distance. Thanks to my sisters Laura and Sophia for understanding and being patient. And last but not least I would like to thank my dear husband Fabian who accompanied me during the journey towards completing my PhD study. Thank you for encouraging me, enduring me and being faithful. You have been solid as a rock for me.

Table of Contents

List of Tables

List of Figures

Nomenclature

δ	piston deformation $[m]$
δ_{fin}	final sample deformation $[m]$
δ_{50}	50% of final deformation $[m]$
γ	unit weight $[kN/m^3]$
Δh	pressure head $[m]$
γ_w	unit weight of water $[kN/m^3]$
γ_{fc}	saturated bulk density of filter cake $[kN/m^3]$
γ_{sus}	saturated bulk density of liquid grout $[kN/m^3]$
ν	Poisson's ratio $[-]$
$\overrightarrow{n}_0$	normal vector on surface
$\overrightarrow{v}$	pore fluid velocity vector
ψ	dilation angle $[^\circ]$
σ'	effective stress $[kPa]$
σ'_v	vertical effective stress $[kPa]$
ε	strain $[-]$
φ	friction angle $[^\circ]$
A	area $[m^2]$
c_v	consolidation coefficient $[m^2/s]$
CPT	cone penetration test
$CRS-test$	oedometer test with constant strain rate
c	cohesion $[kPa]$
$D_{15,s}$	diameter where 15% of soil is finer $[mm]$
d_{50}	average grain diameter $[mm]$

$D_{85,g}$	diameter where 85% of grout is finer $[mm]$
d_{fc}	radial filter cake thickness $[m]$
$DMTA$	stationary flat dilatometer test
DMT	flat dilatometer test
e_g	grout void ratio $[-]$
E_{50}	secant Youngs modulus at 50% of the max. deviatoric stress $[kPa]$
e_{fc}	filter cake void ratio $[-]$
E_{oed}	Oedometer stiffness $[kPa]$
e	void ratio $[-]$
f_{eff}	efficiency factor $[-]$
G_g	shear modulus of the grout $[kPa]$
G_{fc}	shear modulus of the filter cake $[kPa]$
h_0	initial sample height $[m]$
h_{fin}	final sample height $[m]$
h	sample height $[m]$
K_0	at rest earth pressure coefficient $[-]$
k_{fc}	filter cake permeability $[m/s]$
L_c	filter cake thickness $[m]$
L_{fixed}	fixed anchor length $[m]$
L_{free}	free anchor length $[m]$
m_c	mass of cement particles $[kg]$
m_v	compressibility coefficient $[m^2/kN]$
N	groutability ratio $[-]$
Q_{filt}	total discharge of water into filter cake $[m^3]$
Q	discharge rate $[l/min]$
q	specific discharge rate $[m/s]$
r_b	borehole radius $[m]$

S	seepage force [kN]
t_50	time where 50% of the final deformation is reached [s]
T_m	ultimate bond capacity over a short length [kN]
t_{filt}	filtration time for a sample [t]
T_{ult}	ultimate anchor load [kN]
t	time [s]
U_{filt}	degree of consolidation at filtraiton point [$-$]
U	degree of consolidation [$-$]
u	pore pressure [kPa]
V_w	volume of water [m^3]
V_{fc}	filter cake volume [m^3]
V_{sus}	volume of liquid grout [m^3]
V	volume [m^3]
w/c_{fc}	water content of the filter cake [$-$]
w/c_{ini}	initial water content of the grout[$-$]
w/c_{sus}	water content of the liquid grout [$-$]
w/c	water content by weight [$-$]

Chapter 1

Introduction

Grouted ground anchors are widely used construction elements in geotechnical engineering. They are used in many cases where tension forces are transferred to the ground, for example to stabilise retaining walls or building pits, for uplift control of ship-locks, to anchor high towers or masts, or as reactive support for pile testing.

Grouted ground anchors have been proven to be efficient and reliable, although their load bearing mechanisms are not yet fully understood. Especially the influence of the applied installation techniques such as drilling and grouting remains unclear. Different concepts of the effect of pressure grouting on anchor capacity are present in literature. It is assumed that during grouting in non-cohesive soils water filters from the grout and a filter cake builds up which transfers the grouting pressure to the soil. However, information about the thickness of this filter cake and the amount of pressures transferred to the grout is not given. Applying pressure to the grout during anchor installation was found to increase anchor capacity by increasing the radial stresses on the grout body. But there is disagreement about the correlations between applied grouting pressures and anchor capacity.

Presented design formulae mostly consider the radial effective stress on the grout body as the main influential factor on anchor pull-out capacity because they are based on the concept of skin friction of the grout body. Experience however showed, that in non-cohesive soils the anchor capacity is much higher than would be expected by assuming the overburden pressure on the grout body. For that reason usually a factor is applied taking into account for higher radial forces. These factors are based on experience but correlations to installation parameters are not available. Thus, the design formulae only provide a rough estimate on anchor capacity. After installing the anchors, suitability and acceptance tests are carried out to ensure sufficient safety against anchor failure and creep. These tests provide safety against failure, but the real anchor capacity is unknown.

To predict realistic anchor capacity analytically or numerically, the load bearing mechanisms and installation effects need to be taken into account. Since little is known about the load transfer to the soils and the influence of various installation parameters no analytical or numerical methods are yet available to simulate realistic anchor behaviour and predict anchor capacity.

1.1 Motivation

The pull-out capacity of grouted ground anchors is highly influenced by installation effects even if installed in similar ground conditions. Understanding the effects of anchor installation and in particular cement grouting and identifying the main influential factors is essential for quality control on site and to ensure that the anchors perform as intended. Further, it is prerequisite to develop a numerical or analytical model to determine realistic anchor behaviour and calculate pull-out capacities.

1.2 Objectives

Aim of the presented study is to understand the processes taking place during anchor installation and to identify the effects of installation factors on the radial stresses acting on the grout body, focussing on grouting in non-cohesive soils. The main research questions are:

- What happens in the borehole during grouting?
- How and to what extend are the grouting pressures transferred to the soil?
- What is the level of radial stresses remaining after grouting?
- How do various factors influence the installation process?

To address these questions the study combines laboratory experiments, filed measurements and numerical simulations. Starting point is a review of the different concepts of the processes taking place during anchor installation and their influence on anchor capacity. The experimental laboratory tests cover the filtration behaviour of cement grouts and the material properties of the filter cake material. The field study investigates the anchor installation process in-situ, with concentration on the pressures in the borehole and adjacent soil. The numerical work relates to the filtration process of cement grout during anchor installation and investigates the radial stresses developing on the grout body surface in correlation to different factors. The objectives of the presented research are to:

- Contribute to the knowledge of installation effects of grouted ground anchors in sand.
- Experimentally investigate the filtration behaviour of cement grout suspension.
- Determine the material properties of cement grout filter cake.
- Evaluate models to describe cement grout filtration by back-calculating filtration tests.
- Observe what happens during anchor installation in-situ.
- Describe and measure the stress distribution in the borehole and adjacent soil during anchor installation.

- Develop a numerical model and simulate the filtration process of cement grouts in non-cohesive soils.
- Calculate the radial stresses on the grout body surface, taking into account various installation factors.
- Identify the main factors influencing the performance of anchor installation.

1.3 Scope and limitations

The installation process and effectiveness of grouted anchors differ significantly for different soil types, due to the varying mechanical properties and permeability. While water is drained from the grout in non-cohesive, permeable soils, this happens only to a small extend in impermeable soils.

Anchors in impermeable soils are therefore not considered in this study, but the understanding of processes taking place in non-cohesive soils also clears up processes in cohesive soils.

The grouting process and its impact on the radial stresses on the grout body are investigated. These essentially influence the anchor capacity, amongst other factors, for instance dilatancy effects, debonding, interlocking and swelling. Those are subject to further research and not investigated in the presented work. For that reason conclusions are limited to the effect of grouting on the radial stresses rather than pull-out capacity.

1.4 Outline of the thesis

The outline of the thesis is as follows

- Chapter 2 presents background information and definitions of grouted ground anchors used in this thesis. It gives an overview of previous studies and discusses different concepts of the processes taking place during anchor installation.
- Chapter 3 addresses the process of cement grout filtration. It gives an overview of previously applied models and calculation methods for cement grout filtration and material properties that were used for fresh cement grout and filter cake. Additionally a filtration model is developed to simulate radial filtration in a borehole.
- In Chapter 4 laboratory tests are presented. Filtration tests with standard Portland cement suspensions were carried out to investigate the filtration behaviour taking into account influences of water content and applied grouting pressure. Subsequently the mechanical properties of the cement grout filter cake were then determined in standard geotechnical laboratory tests. The calculation methods presented in the previous chapter are then evaluated by back-calculation of the test results.

- Chapter 5 is concerned with a field study examining the grouting process during in-situ anchor installation. Grouting pressures at different positions in the borehole were measured as well as stress changes in the adjacent soil.
- Chapter 6 presents numerical simulations of cement grout filtration during anchor installation. A model is developed to simulate the filtration process with the Finite Element Method by implementing the phase change from liquid grout to filter cake. With this model the grouting process inside the borehole is simulated and the influence of different grouting and material parameters investigated.
- Chapter 7 contains a summary and main conclusions of the presented work.

Chapter 2

Grouted ground anchors

2.1 Introduction

In the following chapter the definition of ‘grouted ground anchor’ is given as it is used in the presented study. An overview of the literature on grouted ground anchors with focus on the installation effects is given. Different concepts of the processes taking place during installation of grouted ground anchors and the effects of installation factors are summarised.

2.2 Definitions

Grouted ground anchors are used to transfer tension forces into the ground. Different terms such as ‘ground anchor’ ‘grouted anchor’ and ‘anchor’ are applied for many variations of anchorages in soil. In the presented study only anchorages with a cement grout anchor body are considered. The expression ‘grouted ground anchor’ is used to clarify that. The presented work is based on the construction type commonly executed in Europe, which is defined in the following sections.

2.2.1 Grouted ground anchors

According to the definition of ‘ground anchors’ in the European Standard EN 1537, an anchor consists of an anchor head, a free anchor length and a fixed anchor length, which is connected to the ground with cement grout. During anchor installation a tendon is placed into a pre-drilled borehole which is filled with cement grout to connect the tendon to the ground. The different parts of a grouted ground anchor are presented in Figure 2.1. Usually the tendon consists of one steel bar or several strands. The anchor is divided into two parts, the free anchor length L_{free} and the fixed anchor length L_{fixed}. In the fixed anchor length the anchor tendon is attached to the ground by the grout body. The free anchor length connects the grout body with the anchor head. The anchor head construction transfers the anchors load into the structure. After installing the anchor, the tendon is usually prestressed to minimize deformations of the retained structure to ensure a tight fit of the anchor head and prevent loosening in case of changing anchor forces.

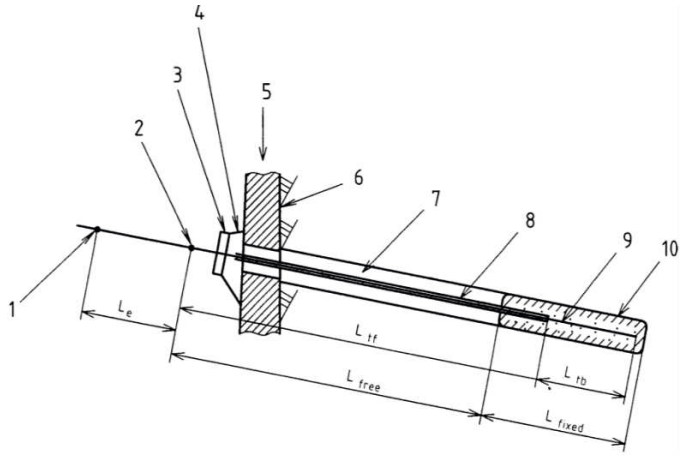

1. Anchorage point at jack during stressing
2. Anchorage point at anchor head in service
3. Bearing plate (or anchor plate)
4. Load transfer block
5. Structural element to be anchored
6. Soil-rock
7. Borehole
8. Debonding sleeve
9. Tendon
10. Grout body (if any)

Figure 2.1: Sketch of a grouted ground anchor (EN 1537:1999).

2.2.2 Micropiles

The structure of drilled micropiles is similar to grouted ground anchors (EN14199), though they do not provide a free anchor length and therefore cannot be prestressed after installation. Originally, they were designed as compressive piles in cases where site exhibits limited space for installation, but occasionally they are also used as tension piles. The installation process (drilling and grouting) of micropiles and grouted ground anchors is identical, except for flushing the free anchor length. Therefore, results of the presented work can also be applied for the installation of micropiles, as it focusses on the installation process, especially the grouting of the anchorages.

2.2.3 Installation methods of anchors

Detailed information about installation methods and execution recommendations for grouted ground anchors and micropiles in soils are given in Ostermayer and Barley (2002) and Wichter and Meiniger (2000). The most common drilling methods are presented in Figure 2.2, where the difference of these methods is mainly whether an outer drill casing is used to stabilise the borehole and how the cuttings are evacuated. For cased drilling the flushing liquid is pressed into the borehole through a hollow rod and flows back through the casing, flushing the cuttings to the top (internal flushing). For drilling without casing the flushing liquid flows between drilling rod and soil (external flushing), which may result in a larger, more irregular borehole shape. For external flushing non-cohesive soils, often cement and

bentonite is added to the flushing liquid to stabilise the borehole. After drilling is completed, the flushing liquid is replaced by cement grout and the anchor tendon is built in. Now, the grout is pressurised and the casing withdrawn until the end of the fixed anchor length is reached. To realise the free anchor length, excess cement grout in the free anchor length is usually flushed with water or bentonite slurry. In some cases the fixed anchor length is separated using packers so the fixed anchor length can be grouted at once and the pressure maintained until hardening. Sometimes post-grouting is applied approximately one day after the grout body is installed. Grout is injected under high pressure via one or more post-grouting pipes having valves in the fixed anchor length. The high pressure is supposed to fracture the grout body and increase the bonding to the ground. Post grouting is usually applied in cohesive soils.

Special installation methods with bells or under-reams which mechanically enlarge the borehole are not considered within the presented work.

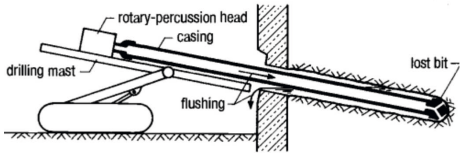

(a) Rotary or rotary-percussion drilling with lost bit crown (external flushing).

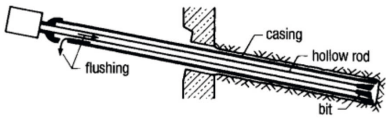

(b) Overburden drilling with casing and interior hollow rod for counterflush (internal flushing).

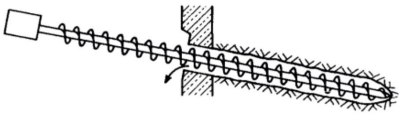

(c) Continuous flight augering without casing (no flushing).

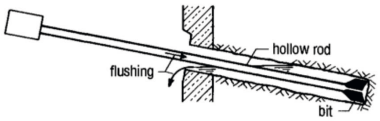

(d) Rotary drilling without casing.

Figure 2.2: Different drilling methods from Ostermayer and Barley (2002).

2.2.4 Anchor design

The anchor capacity is defined by the capacity of the individual structural parts such as anchor tendon and anchor head, and the pull-out capacity of the grout body. The design of the structural parts is straight forward, using the design load and capacity.

Determining the pull-out capacity analytically, however, is more complex. It is usually approximated by Coulomb's friction on the grout body surface and therefore depends on the radial stresses and the shear resistance. These values depend on various installation factors, whose influences are not yet fully investigated. Therefore, it is impossible to determine realistic values for the pull-out capacity on the basis of analytical formulae. For that reason,

according to EC 1997-1 the capacity of anchors needs to be determined in suitability tests on three anchors of each site to provide sufficient safety against creep and failure. In suitability tests the same installation technique and anchor type should be used as for the working anchors. Additionally, acceptance tests of each anchor ensure that the anchor can sustain the desired design load. Acceptance tests provide good safety and control if the anchors were installed properly. However, it only proves that the required factor of safety is met, but the real capacity of the anchor remains unknown. To determine the pull-out capacity of anchors, investigation tests where the anchor is loaded until failure have to be carried out.

2.3 Fundamentals and historic review

The application of grouted anchors in non-cohesive soils became popular in Germany and Europe when they were first used for strut-free excavations and other retaining structures after 1958 (Ostermayer and Barley, 2002). It was found that grouted anchors in cohesion-less soil provided pull-out capacities far beyond what would have been expected from classical soil mechanics, assuming Coulomb's friction on the anchor surface. This led to a number of research studies in the seventies and early eighties, in which a large number of in-situ and laboratory anchor tests were carried out to explain the observed high anchor pull-out capacity and to understand the load bearing mechanisms (e.g.: Littlejohn (1970), Ostermayer (1975), Jelinek and Ostermayer (1976), Littlejohn (1980), Mayer (1983), Scheele (1982), Shields (1978), Werner (1972) and Wernick (1978)).

Various researchers found similar factors influencing the pull-out capacity of grouted ground anchors in non-cohesive soils, but evaluated the significance of those differently:

- Soil properties (e.g. relative density, degree of uniformity, and dilatancy)
- Fixed anchor geometry and dimensions
- Drilling technique (boring with or without flushing)
- Grouting (grouting pressure, pumping rate of cement suspension)

The high capacity of grouted anchors in cohesion-less soils was ascribed primarily to the dilatancy effect in non-cohesive soils, creating a 'locking effect' of the grout body. This effect was verified by Werner (1972) and Wernick (1978). Both found that during anchor loading the soil adjacent to the anchor body dilates in reaction to the shear forces exerted to the ground. The dilation leads to a volume increase of the soil surrounding the anchor, which in turn increases the radial stress and thus facilitates higher shear forces on the shear plane.

Ostermayer and Barley (2002) give a comprehensive overview of the working principles of grouted ground anchors and recommendations for anchor installation. They propose to estimate the anchor capacity directly from design charts or from calculation formulae based on skin friction on the grout body. However, since it was found that the anchor's load bearing capacity is not linearly related to the anchor's fixed length and diameter, the formulae conflict with the assumption of Coulomb's friction on the anchor surface. This phenomenon

is explained by 'progressive failure' or 'de-bonding' of the tendon/cement/ground contact due to the 'incompatibility between the elastic modulus of the anchor tendon, of the anchor grout and of the ground' (Scheele (1982), Cornelius and Mehlhorn (1982) and Ostermayer and Barley (2002)). The shear force is said to gradually mobilise along the anchor body: First, shear forces are transferred in the proximal part of the fixed anchor length until the maximum (peak) force is exceeded and the force reduces to a residual value. Then the main part of shear forces are transferred further along the grout body until the load is concentrated at the distal end of the fixed anchor length just before failure (Barley and Windsor (2000), Ostermayer (2001), Ostermayer and Barley (2002) and Wichter and Meiniger (2000)). Ostermayer and Barley (2002) state that this non-linearity occurs for a fixed anchor length greater than 3 m and propose to use an efficiency factor f_{eff} to take into account the mobilisation of the shear strength when calculating the ultimate anchor load T_{ult}:

$$T_{ult} = T_m \times L_{fixed} \times f_{eff} \ , \tag{2.1}$$

where T_m is the ultimate bond capacity per metre over a short length, for which 'progressive failure' is negligible, and f_{eff} is a function of the fixed anchor length L_{fixed}.

In Germany however, the ultimate anchor capacity is directly estimated from a chart based on a large number of field tests rather than using design formulae (Figure 2.3).

The use of design diagrams or design formulae is however only accepted for pre-design, since anchor installation effects and soil conditions are not fully taken into account.

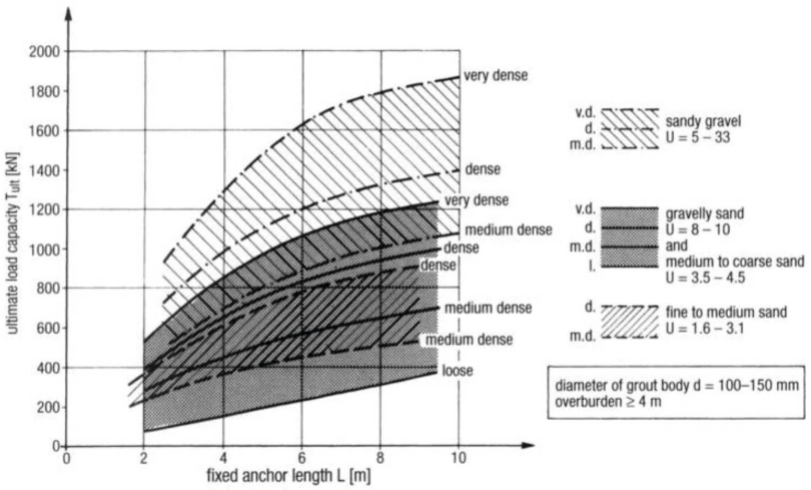

Figure 2.3: Ultimate load capacity of grouted anchors in non-cohesive soils based on empirical data from Ostermayer and Barley (2002).

2.3.1 Processes during grouting of ground anchors

Experience showed that applying pressure to the cement grout during anchor installation increases the anchor capacity in non-cohesive soils significantly. This effect is believed to be due to the increase of critical factors such as normal radial stress on the grout body and shear strength of the adjacent soil as a result of grouting. It remains unclear, how much the soil strength and stresses can be improved and how this improvement takes place. It is also uncertain how the radial stresses generated during grouting are retained permanently, since the grout pressure is released long before the cement grout starts to cure.

Reviewing literature and discussions with anchor professionals revealed, that there are different concepts present on what happens during grouting of ground anchors:

Some believe that the grout is injected into the soil's pores and the anchor diameter is increased. It is assumed that a transition zone of 'soil-concrete' develops around the anchor body and that the anchor capacity is increased either due to the enhanced shear strength of the material or the larger grout body diameter and thus larger shear surface. This idea came up when researchers first tried to explain the unexpected high capacity of grouted ground anchors in non-cohesive soils (see Mayer (1983)), but is still present today (Mecsi (2013) and Lee et al. (2012)).

The most frequent opinion present in literature is, however, that in non-cohesive soils water is pressed from the grout into the soil during grouting and a filter cake forms, which transfers grouting pressures to the soil.

Some assume a thin layer of impermeable filter cake building up at the borehole walls, similar to the bentonite filter cake during construction of a diaphragm wall. This filter cake would act as a membrane and transfer the full grouting pressure to the surrounding soil, causing densification of the soil and improved contact between grout and soil. However, the grout would still be liquid in the borehole centre and the borehole walls would be unloaded to the hydrostatic grout pressure after grouting.

Others assume the build-up of a thicker filter cake (Littlejohn (1970), Werner (1972), Shields (1978), McKinley (1993), Ostermayer and Barley (2002) and Bezuijen (2010)). It is believed that inside the borehole the grout thickens due to the expulsion of water and develops considerable strength and stiffness and some of the grouting pressure is 'locked in' when the grout filtrate restrains the rebound of the borehole walls after grouting pressure is released. Only vague information about the value of the grouting pressure locked in is given. Littlejohn (1970) reports that anchor pull-out tests in compact fine to medium sized sand indicate a residual radial stress in the range of 1.4 times the effective overburden pressure, but also reports that some contractors use grouting pressure dependent values.

Experiences in practice confirm the concept of cement grout filtration during grouting: Significant increases of anchor capacity due to pressure grouting were observed in non-cohesive, permeable soils, while little improvement could be achieved in cohesive soils, where excess water cannot filter into the surrounding soil. For cohesive soils, post-grouting has a stronger effect on anchor capacity. During post-grouting, grout is pressed into the

anchor body through post-grouting pipes attached to the anchor rod. The grout body is fractured and expanded, improving contact between grout and soil. Usually the grout is already too stiff to be fractured after primary grouting in non-cohesive soils. This indicates that a filtration of the grout takes place in non-cohesive soils and leads to the assumption that filtration plays a major role during anchor installation.

2.3.2 Influence of grouting pressure on anchor capacity

Even though there is common understanding that the installation process has a strong influence on the capacity of grouted anchors, installation effects were not emphasised within most of the reported anchor studies by the time they were carried out. For that reason, information about the installation methods and grouting procedures applied during anchor installation is seldom available because these factors were not recorded or published.

Just as different opinions exist on what happens during grouting of ground anchors, different concepts of the effect of pressure grouting on anchor capacity were found in literature: Mayer (1983) and Ostermayer (1993) for example state, that the application of grouting pressure sufficiently increases anchor capacity. Both found that the anchor capacity increases with an increasing value of grouting pressure up to a certain level, where it reaches an asymptotic limit and no further increase can be achieved. Mayer (1983) investigated the influence of grouting pressure on radial stresses and deformations in the soil. He found that the radial stresses increase underproportionally with applied grouting pressure and above 10 bar only marginal increases were observed. Pull-out tests showed that the capacity of the anchors corresponded directly to the radial stresses after unloading and could be increased with higher grouting pressures until 10 bar but for higher pressures minor increases were observed. He ascribes this effect to the fact that at a certain point the grout cannot be dewatered any further and the grout properties remain unchanged. Jelinek and Ostermayer (1976) and Ostermayer (1975) state that, in non-cohesive soils, a minimum grouting pressure of 10 bar improves the disturbed soil conditions due to grouting and filters water from the cement grout, leading to a higher quality of the grout body and better bond to the soil and thus increases anchor capacity. This concept was also stated by Werner (1972), who carried out model tests with cylindrical anchor bodies which were installed without grouting. The sand was filled into the test chamber after the anchor body was installed. He found similar pull-out capacities for the model anchors than for grouted in-situ anchors and concluded that the grouting pressure only ensures a good contact between grout body and soil. In a later study Werner (1975), however, assumes that if the soil density can be increased due to grouting, the anchor pull-out capacity also increases. Mayer (1983) states that pressure grouting increases the radial stresses on the grout body, but does not quantify the stress increase or the correlation to the applied grouting pressure. Xanthakos (1991) reports that usually grouting pressures between 3 and 7 bar are applied but that no evidence is given that pressures above 3 bar “will produce any real benefits”.

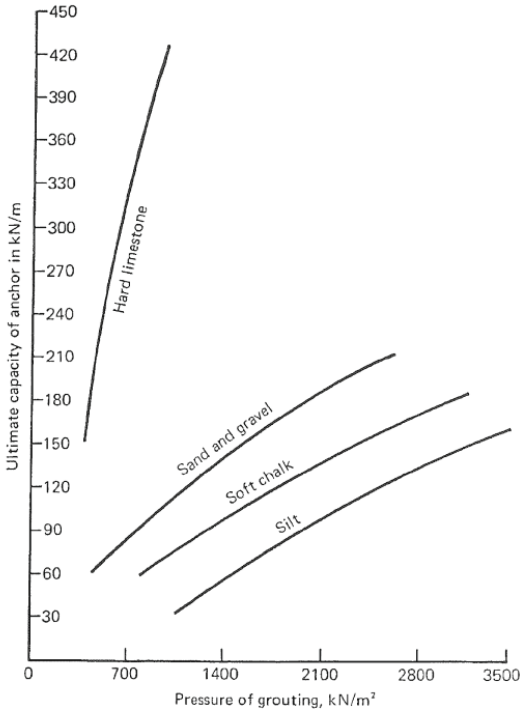

Figure 2.4: Influence of the grouting pressure on the pull-out capacity of anchors from Littlejohn (1980).

In contrast, Littlejohn (1980) reports that the pull-out capacity of grouted anchors is directly related to the value of the grouting pressure without an asymptotic limit (Figure 2.4). He assumes that in fine grained soils, the grouting pressure is transferred to the soil and a residual stress on the anchor surface is locked in due to the shear strength of the soil. He proposes that 1/3 to 2/3 of the grouting pressure should be assumed as residual stress on the grout body. However, in Littlejohns studies high-pressure grouted anchors with packers were used and he assumes that the grout body is enlarged due to hydro-fracturing. Littlejohn (1980) demands that more information is required at which grouting pressure the grout is permeated (densification) or hydro-fractured. This would result in completely different load bearing mechanisms for common grouted anchors with a straight shaft. Also Littlejohn points out that it is difficult to compare different studies, if some apply secondary grouting or grouting with packers.

More recent studies on grouted soil nails also show increasing pull-out capacities with increasing grouting pressure (Hong et al. (2013)). In this study packers were also applied which allowed to keep the grouting pressure constant for 4 hours. However, low grouting pressures (max. 2.5 bar) were applied, so the results do not necessarily contradict the assumption of Jelinek and Ostermayer (1976) and Ostermayer (1975) that pull-out capacity

cannot be increased for grouting pressures above 10 bar.

All reported studies found that applying pressure during grouting increases the anchor pull-out capacity. However, none of them described the precise installation process and no information on grouting stages and duration is given. Correlations between the magnitude of grouting pressure and anchor capacity are only given for anchors that were installed with packers, but those contradict the findings of studies where grouting without packers was applied.

2.3.3 Increase of radial stresses due to swelling of cement grout

Some researchers assume that the radial stress on the grout body of a grouted ground anchor is increased due to swelling of the cement grout during curing (Jessberger (1963), Mayer (1983) and Wichter and Meiniger (2000)). If during grouting excess water is filtered from the grout, the water content could fall below a critical limit for full hydration. It is assumed that in that case the grout pulls water from the surrounding soil and the grouts volume increases and induces additional radial stresses to the soil.

Mayer (1983) carried out sandbox tests where he measured radial deformations and stresses in the adjacent soil during grouting of anchors. He observed an increase of radial stresses and deformations due to swelling of the grout after grouting, which came to an end after 16 to 18 hours. An influence of grouting pressure on the swelling process could not be observed. Mayer (1983) reports 0.022 to 0.035 mm radial deformation corresponding to an increase or ca 100 kPa radial stress. The tests were carried out in dry sand and the water available for hydration was the water filtered from the grout before. If the sand is saturated, much more water is available for hydration and the swelling effect could be much higher.

Jessberger (1963) reports a volume increase of 2% to 4% of the grout due to the use of the additive Tricosal, which was originally added to increase flowability. He states that the volume increase causes additional interlocking of the grout body with the ground.

Paproth and Paproth (1966) compared the anchor installation with pure cement grout and cement mortar, where sand was added. They report that with pure cement grout better pull-out capacities were achieved and explain this with a stronger bonding of the grout body with the soil. Probably the capacity was increased because the pure grout provides a higher cement concentration and more subjected to swelling.

2.3.4 Characteristics of the grout body

The grout body shape primarily depends on the drilling technique and the soil properties. The different concepts of what happens during grouting (see Section 2.3.1) lead to different opinions on how the grout body is shaped.

Some believe, that in non-cohesive soils the grout is injected into the soil and the grout body diameter is enlarged (e.g. Mecsi (2013) and Lee et al. (2012)). However, no evidence of such grout bodies is given.

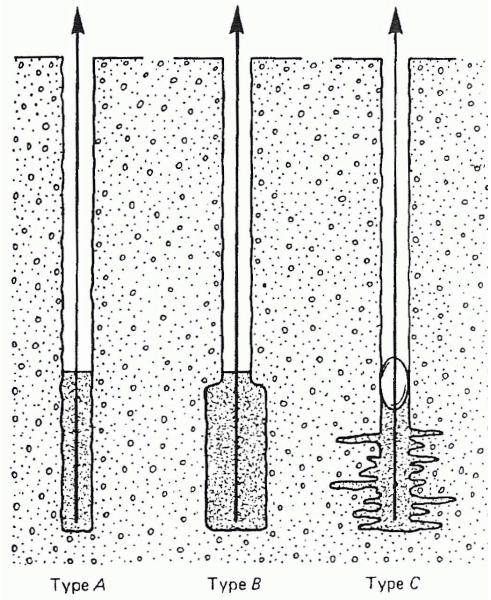

Figure 2.5: Types of grouted ground anchors from Littlejohn (1980):
Type A) Tremie-grouted
Type B) Low-pressure grouted
Type C) High-pressure grouted with hydro-fracturing of the soil

Littlejohn (1980) states that in non-cohesive soils the soil is compacted and the anchor diameter increases. He estimates effective diameters from grout consumption. For coarse sands or gravel the grout injects into the soil, and the initial borehole diameter is increased 3 to 4 fold. For finer soils, where compaction of the soil takes place, he reports that diameters of 1.2 to 2 times the initial diameter can be achieved with grouting pressures of 10 bar. It is not clear whether these values are intended as hypothetical values for calculation purposes or real anchor diameters, since they seem rather large. For higher grouting pressures Littlejohn (1980) presumes hydro-fracturing of the soil leading to a completely different anchor body shape (compare Figure 2.5). Excavations of anchor bodies as such are not reported. In contrary, Bezuijen (2010) found in his study on compensation grouting in sand, where fracturing of the soil is required, that it is difficult to achieve extensive fracturing in sand and that cement grouts with bentonite and high water contents are required.

In an extensive study on grouted ground anchors by the Belgian Building Research Institute (BBRI, 2008), grout bodies were excavated after testing (Figure 2.6). The excavations in sands showed that the grout does not inject into the soil. The encountered grout bodies where very straight and uniform and a distinct separation between grout body and soil was observed. The grout bodies almost looked like a ‘plaster cast’ of the borehole. No significant increase of anchor diameter due to grouting was seen and local diameter enlargements

seemed to result from borehole irregularities prior grouting. Only after postgrouting a small increase of diameter was observed and a bulge of cement built up along the cracks of the primary grout body.

Excavations of anchors in sand by 'Brückner Grundbau GmbH' are presented in Figure 2.7. It shows an excavated grout body which was cut at the soil edge. A clear border between cement and soil is visible. Next to the grout body is a circular area of compacted sand, which could be removed from the solid cement block easily.

Paproth and Paproth (1966) also excavated the grout bodies of grouted anchors installed in sand and report a thin layer (a few mm) sand crust on the grout body surface, but no grout was found elsewhere in the surrounding soil. They measured an increase of anchor diameter of 9 % due to pressure grouting compared to gravity grouting (without applied pressure). Ostermayer and Werner (1972) excavated grout bodies and found that the diameters were in the range of the borehole diameter plus twice the average grain diameter of the soil (d_{50}) and additional 5 mm.

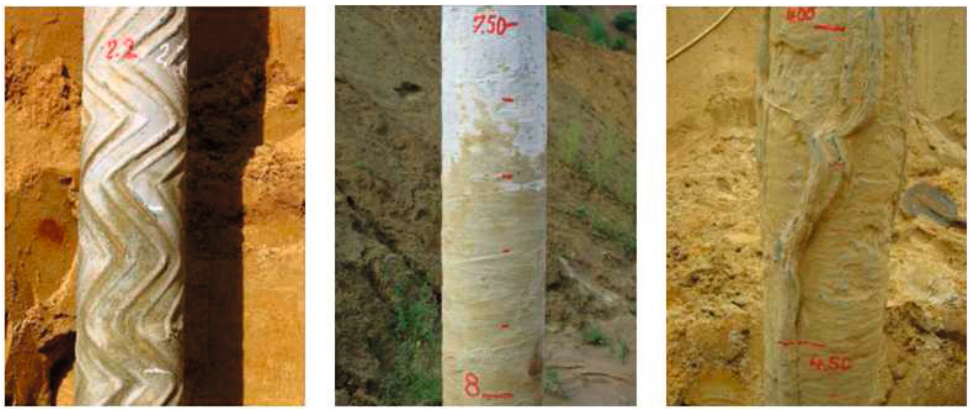

Figure 2.6: Excavated grout bodies from Tomboy and Huybrechts (2008): Cased drilling with internal flush (left), drilling with external flushing after primary grouting (centre) and after postgrouting (right).

Figure 2.7: Exposed grout body in sand (by Brückner Grundbau GmbH).

2.3.5 Influence of the drilling methods

Little systematic information is available on the effect of the drilling method on anchor performance. In his extensive test programme Ostermayer found no influence of the drilling method (ramming or boring with or without flush water) on the shape of the grout body and anchor pull-out capacity in non-cohesive soils, whereas in cohesive soil a significant influence of the drilling method and anchor capacity was found (Ostermayer and Werner (1972) and Ostermayer (1975)). Here, drilling without casing or with water flushing led to decreased pull-out capacities. It should be noted that drilling with external flushing was not applied in non-cohesive soils.

In BBRI (2008), however, an influence of the drilling method on anchor pull-out capacity in non-cohesive soils was reported. Especially for anchors drilled with internal or with external flushing. For anchors with external flushing only marginal grouting pressure could be applied because the grout leaked through the larger cavity between drill casing and borehole.

Those anchors were considered gravity grouted and lower pull-out forces were achieved than for anchors with internal flushing, where a larger grouting pressure could be applied. Additionally, external flushing produced an irregular grout body shape compared to internal flushing. It is therefore assumed that the drilling method only indirectly influences the anchor pull-out capacity.

2.3.6 Groutabiliy

Whether the grout is injected (permeation grouting) into the soil or the soil is compacted (compaction grouting) due to the expansion of the grout mass depends on the ability of the grout particles to permeate into the pores of the soil. This is influenced by many factors such as viscosity of the grout, porosity, hydraulic conductivity, and pore size of the soil, and grain size distribution of both materials. Both grouting methods, permeation grouting and compaction grouting require contrary grout and soil properties. Much research was conducted to investigate the injection of grouts into soil and various sophisticated models were developed. But a very simple approach where the grain size fractions of grout and soil particles are compared, was found very useful and is often applied. The grain sizes of soil and grout are related with the groutability ratio

$$N = \frac{D_{15,s}}{D_{85,g}}. \tag{2.2}$$

where $D_{15,s}$ is the diameter where 15% of soil is finer, and $D_{85,g}$ the fraction where 85% of the grout is finer. This relation is also known as Terzaghi filter criterion, where the filter stability of a soil matrix is estimated. If a soil is a stable filter for a grout material, grout particles do not permeate into soil pores and a filter cake builds at the border. For grouting, this means that not injection but compaction grouting takes place. Depending on whether injection or filtration is desired, the value of N should exceed or be lower than a certain limit. With respect to filter stability, Terzaghi et al. (1996) evaluated various studies and recommend values $N \leq 5$ as conservative values for satisfactory soil filters. To ensure successful injection, a minimum value of N in the order of 25 is mostly reported (e.g.: Akbulut and Saglamer (2002), De Paoli et al. (1992b), Semprich and Stadler (2002), or Zebovitz et al. (1989)). These values are based on experiments, but here not only the ability of grout to inject the pores but also the amount of grout was taken into consideration to judge if grouting was successful. In addition to a minimum value for N which ensures successful injection, sometimes also a lower limit is given which says that for $N < 11$ no injection is possible at all (Akbulut and Saglamer (2002) and De Paoli et al. (1992b)). But not only the grain size but also the water content of a grout was found to influence injection into soil (De Paoli et al. (1992a) and Akbulut and Saglamer (2002)). This is referred to the higher viscosity at low water contents, which hinders injection. However, Akbulut and Saglamer (2002) state that, regardless of other parameters, injection of standard cement is impossible for soils with

sufficient low grain sizes (below 0.6 mm). Terzaghi et al. (1996) also found that 'a clean cohesionless sand is [...] capable of effectively filtering even the finest silt and clay soils', which means that no injection takes place. Design tables based on grouting experiments also suggest that standard cement only injects into gravel (see Figure 2.8).

Even though using Terzaghi's filtration criterion is very crude, it gives a good idea whether injection or compaction should be expected during grouting. It indicates that for grouting standard cement in sands the grout does not inject into the soil.

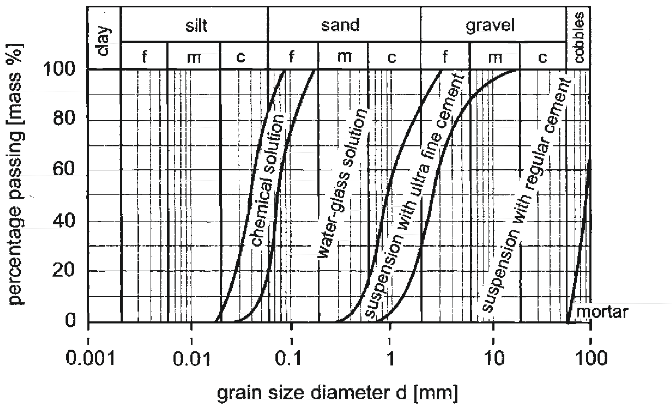

Figure 2.8: Limits for injection of different grouts in soil (Semprich and Stadler, 2002).

2.4 Chapter summary

Reviewing literature revealed that in previous studies on ground anchors the process of anchor installation was not emphasized. It is difficult to compare studies if different installation conditions were applied and the effects of these are unknown. This explains the varying concepts of the influence of grouting pressure on the anchor pull-out capacity and on the processes taking place, that developed with time.

However, the majority of sources indicate that during grouting in sand excess water drains into the soil and the liquid grout stiffens due to the water loss. Applying a simple filter criterion after Terzaghi indicated that sands are filter stable for grouting with standard cement and no injection of grout into the soil takes place. This complies well with observations in-situ, where a clear distinction between grout body and soil was detected. It is therefore assumed that during grouting filtration of excess water from the liquid grout takes place. It is yet unclear whether a thin filter cake builds up or the entire grout consolidates in the borehole.

In most studies it was found that applying pressure to the grout during grouting does increase the anchor pull-out capacity. Some state however that an increase of grouting pressure beyond 10 bar does not increase the capacity any further. This contradicts with findings

where pressure was applied using packers. It is hypothesised that using packers causes fracturing of the soil, but this effect is not validated.

It is assumed that applying grouting pressures during anchor installation in non-cohesive soils

- increases the radial stresses on the grout body
- reduces the water content of the grout
- compacts the surrounding soil
- enhances the contact between grout and soil
- creates an compact and flawless grout body and
- increases the grout body diameter

However, since the processes taking place during grouting are not resolved in detail, no direct correlations between value of grouting pressure and those factors could be drawn.

Chapter 3

Cement grout filtration - Background

3.1 Introduction

As discussed in Chapter 2, it is assumed that during grouting excess water is filtered from the liquid grout rather than the grout is injected into the soil. Prerequisite for further investigation of processes taking place during anchor installation is to access the properties of the fresh cement grout and the filtration process during grouting.

This chapter gives an overview of previous work on cement grout filtration and calculation methods. Material properties of fresh cement grout and filter cake are discussed and a filtration model is presented to simulate radial filtration in a borehole.

3.2 Fundamentals of cement grout filtration

Filtration describes the separation of solids and liquids from a suspension. Grouts with different water contents are used for anchor installation, but the water content is high enough to enable the grout to flow through the pumping equipment and the grout particles are suspended in the mixing water. If the grout is now pressed into a sufficient fine soil, water will be filtered from the suspension. The particle concentration in the suspension increases and a filter cake is formed. Following, the definition of 'filter cake' will be that the grout particles are in contact and are able to transfer effective stresses.

Filtration of suspensions is a complex multiphase problem which was addressed by various researchers and advanced analytical solutions were developed (see Bürger et al. (2001) and Lee and Wang (2000)). These advanced methods require a variety of calculation parameters which are unknown as well as advanced solution techniques.

Considering the filtration of cement grouts, in literature mostly two basic approaches were found appropriate to describe the filtration process in the scope of geotechnical engineering: The 'two-phase filtration model' which origins in fluid mechanics, and classical Terzaghi consolidation theory. These two theories may describe an upper and lower limit of the real material behaviour. One theory considers the initial cement grout suspension as liquid, the other as solid, granular material. The consistency of cement grout mixtures used for anchor installation lies just between viscous and plastic. They are neither a pure liquid nor a solid

material. Both theories are based on the assumptions that no injection of cement particles into the soil takes place.

3.2.1 Two-phase filtration model

McKinley (1993) as well as Bezuijen and Talmon (2003) propose a filtration model to describe the filtration process of cement grouts. This model considers the formation of filter cake as a distinct phase change from a liquid (suspension) to a solid phase (filter cake). It assumes that when water is filtered from the suspension, the cement particles pile up and a filter cake forms at the contact surface between suspension and filter medium. The drainage of excess water is assumed to be locally concentrated to this surface. The model assumes that the material properties of the filter cake do not change with time and also the suspension retains its initial particle concentration. Only the thickness of both layers changes with time. The principle of the two-phase filtration model is explained for a one dimensional filtration test presented in Figure 3.1, where constant pressure is applied to a grout sample, which is drained at the bottom: The amount of water expelled from the suspension controls the build up of the filter cake. The rate of filtration is influenced by the hydraulic resistance of the already existing filter cake and filter medium and the filtration pressure. Darcy's Law gives the discharge rate Q in relation to the filter cake's current thickness $L_c(t)$ and its permeability k_{fc}

$$Q = \frac{k_{fc}}{\gamma_w} \frac{\sigma}{L_c(t)} A \,, \tag{3.1}$$

where A is the drainage area and σ the total stress acting on top of the sample.

Assuming a constant concentration of cement particles within each phase, the calculation of filter cake formation with time is straight forward. The piston deformation during filtration $\delta(t)$, shown in Figure 3.1, can be calculated with the initial void ratio of the grout e_g and the final filter cake void ratio e_{fc}:

$$\delta(t) = L_c(t) \frac{e_g - e_{fc}}{1 + e_{fc}} \,. \tag{3.2}$$

If water and cement particles are regarded incompressible, the volume change of the sample is equal to discharge rate of water. Dividing Equation 3.1 by A gives

$$\frac{d\delta}{dt} = \frac{k_{fc}}{\gamma_w} \frac{\sigma}{L_c(t)} \,. \tag{3.3}$$

Replacing δ in Equation 3.3 with Equation 3.2 and rearranging gives

$$\frac{dL_c}{dt} \left(\frac{e_g - e_{fc}}{1 + e_{fc}} \right) = \frac{k_{fc}}{\gamma_w} \frac{\sigma}{L_c(t)} \tag{3.4}$$

Rearranging and integrating Equation 3.4 finally gives the filter cake thickness with time

$$\int L_c(t)\, dL_c = \int \frac{\sigma k_{fc}}{\gamma_w} \left(\frac{1 + e_{fc}}{e_g - e_{fc}} \right) dt$$
$$L_c(t)^2 = \frac{2\sigma k_{fc}}{\gamma_w} \left(\frac{1 + e_{fc}}{e_g - e_{fc}} \right) t \,. \tag{3.5}$$

The filtration process in a filtration press ends, when the piston reaches the filter cake at $t = t_{fin}$ and $L_{c,fin} = h_0 - \delta_{fin}$.

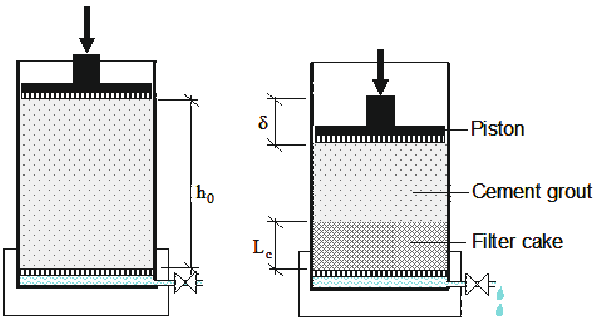

Figure 3.1: One-dimensional filtration test (adapted from McKinley and Bolton (1999)).

3.2.2 Consolidation theory

Other authors propose Terzaghi's classical consolidation theory to describe the filtration process of cement grouts (Kleyner and Krizek (1995), Lee et al. (2012), and Picandet et al. (2011)) because it is well known and readily available in geotechnical engineering. They found that the filtration process could be modelled reasonably well with this approach.

The classical consolidation theory is based on the assumption of homogeneous material properties within the sample remaining constant over time. In contrast to the filtration model, it assumes a gradual consolidation and thus change of particle concentration of the entire sample. The dissipation of excess pore pressures over sample height is

$$\frac{du}{dt} = c_v \frac{d^2u}{dz^2} \,, \tag{3.6}$$

where c_v is the consolidation coefficient, related to the permeability k and stiffness of the material

$$c_v = \frac{k}{\gamma_w m_v} \,. \tag{3.7}$$

The compressibility coefficient m_v is defined as

$$m_v = \frac{\varepsilon}{\sigma'} \tag{3.8}$$

where ε is the vertical strain caused by the effective stress σ'.

3.3 Analytical solution of radial filtration with constant pumping rate

The two-phase filtration model presented in Section 3.2.1 considers one-dimensional filtration due to a constant grouting pressure applied to the liquid grout. To estimate the filter cake build-up within a borehole, the two-phase filtration model is now adapted for radial flow and a constant pumping rate as observations of in-situ anchor installation showed that a more or less constant pumping rate is applied rather than constant grouting pressure. Consolidation theory is less suitable to determine the filter cake thickness and for that reason was not considered. In consolidation theory gradual consolidation of the whole grout is assumed and it does not distinguish between liquid grout and filter cake. The borehole walls are considered as a rigid boundary, which gives a constant cavity volume. With constant borehole volume, the volume of grout pumped into the cavity has to be equal to the volume of drained water. Assuming full saturation and incompressibility of water and cement particles, a certain volume of cement grout suspension results in a specific drainage water and filter cake volume $V_{sus} = V_w + V_{fc}$. The volume ratio f_{fc} between suspension and filter cake volume is defined by the change of water content:

$$f_{fc} = \frac{V_{fc}}{V_{sus}} = \frac{w/c_{fc} + 1}{w/c_{sus} + 1} \frac{\gamma_{sus}}{\gamma_{fc}} , \tag{3.9}$$

where γ_{sus} and γ_{fc} are the saturated bulk densities of suspension and filter cake respectively. Assuming a constant cavity volume, the volume of the expulsed water at a certain time is related to the pumping rate Q:

$$V_w(t) = V_{sus}(t) - V_{fc}(t) = (\frac{1}{f_{fc}} - 1) * V_{fc}(t) = Q * t . \tag{3.10}$$

The filter cake volume V_{fc} relates to the borehole radius r_b and the actual filter cake thickness d_{fc} with

$$V_{fc}(t) = \pi \left(r_b^2 - (r_b - d_{fc}(t))^2 \right) \, h, \tag{3.11}$$

where h is the grouting length. Combining Equations 3.10 and 3.11 gives the filter cake volume at a certain time t

$$V_{fc}(t) = Q \, t \left(\frac{f_{fc}}{1 - f_{fc}} \right) = \pi \left(r_b^2 - (r_b - d_{fc}(t))^2 \right) \, h . \tag{3.12}$$

Rearranging Equation 3.12 and normalising the inflow to a unit section length gives the filter cake thickness with time

$$d_{fc}(t) = r_b - \sqrt{r_b^2 - \frac{\frac{Q}{h}\, t \left(\frac{f_{fc}}{1 - f_{fc}}\right)}{\pi}} \,. \tag{3.13}$$

Equation 3.13 shows that for a constant pumping rate the filter cake build-up is independent of its permeability, contrary to the model with constant grouting pressure (see Equation 3.5). Figure 3.2 shows the filter cake build-up with time for different pumping rates. The higher the pumping rate, the faster the filter cake builds up.

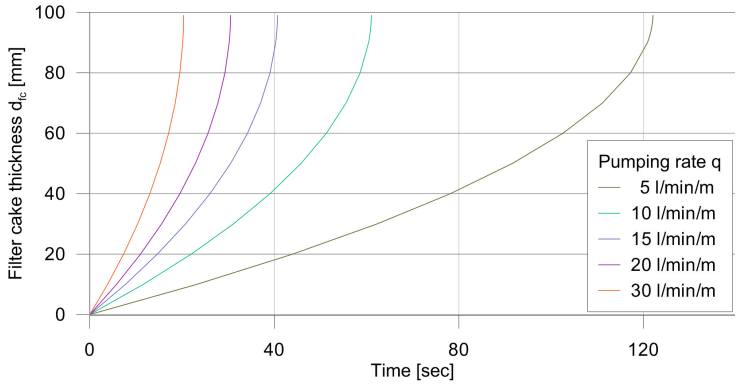

Figure 3.2: Analytical filter cake formation in a borehole with r = 100 mm, assuming $w/c_{sus} = 0.5$ and $w/c_{fc} = 0.3$.

3.4 Theoretical considerations about cement grout filter cake

During cement grout filtration, water is filtered from the suspension, while the cement particles cannot permeate through the filter medium. They pile up and build a 'filter cake' where the particles contact each other and build a solid, granular material.

Whether a cement/water mix or grout is liquid or should be regarded as solid depends on the concentration or packing density of the grains. For a high particle density, particles contact each other and the material acts as solid, while for a sufficient low particle concentration cement particles float in the mix water.

The notation 'filter cake' is in this work assigned to the point where the particles contact each other and effective stresses are transferred by inter-granular forces. It is now tried to theoretically define the water content at which the grout should be considered as filter cake by looking at the bulk density.

The concentration of particles where they start to contact each other could be compared

to the loosest packing of a material. The bulk density ρ without compaction of the used dry Ordinary Portland Cement ranges between $1.23\ g/cm^3$ and $1.38\ g/cm^3$. With a specific grain density ρ_s of $3.15\ g/cm^3$, the respective void ratio ranges from $e = 1.56$ to $e = 1.28$, using

$$e = \frac{V_p}{V_s} = \frac{\rho_s}{\rho_{tot}} - 1. \tag{3.14}$$

The particle concentration or water content of cement grouts is usually specified by the mass ratio $w/c = \frac{m_w}{m_c}$. Assuming all voids are fully saturated, the relation between e and w/c is

$$e = \frac{V_w}{V_c} = \frac{m_w}{m_c}\frac{\gamma_c}{\gamma_w}, \tag{3.15}$$

where m_w and m_c are the masses of water and cement respectively.

Therefore, the void ratio of the dry cement without compaction would correspond to a water content between $w/c = 0.5$ and $w/c = 0.4$. However, it should be considered that a water film develops around the particles when the cement is wetted. This film reduces the friction between the grains but also increases effective grain size. In suspension, the void ratio where a stable grain contact is achieved might therefore be below the loosest packing of the dry material.

The highest bulk density of the used cement, achieved by vibration, ranges from 1.6 - $1.9\ g/cm^3$, which corresponds to $w/c = 0.30$ - 0.21 for full saturation. For other dry Portland Cements bulk densities between 1.4 - $1.8\ g/cm^3$ were achieved by tamping (Reschke, 2001). These values correspond to $w/c = 0.34$ - 0.24, assuming full saturation.

3.5 Material properties of fresh cement grout

In literature, little information on material properties of fresh, uncured cement grouts is available, especially for grouts with low water contents.

Usually, only the strength of young concrete is of interest rather than properties of uncured grouts. Cement grout is a suspension of solid cement particles and mixing water and depending on the water content the behaviour can range from a viscous fluid to a friction material. Fresh cement grouts are usually considered non-Newtonian fluids or pastes. Properties, such as viscosity and internal friction are needed to assess workability and performance during grouting and depend on water content, grading, grain size and shape. Material properties of cement grout were found to change significantly with water content, grading and thus porosity. The material behaviour ranges from liquid to solid, and it is very difficult to define the border between those two consistencies. In general it can be stated that with lower porosity the internal friction increases as the space between the particles is reduced. However, the material behaviour is much more complex as size and shape of particles influence the internal friction, the grading and water content influence the void space between the grains which

in turn influences internal friction and adhesion forces.

Warner (2004) describes grout consistency viscous for water contents above $w/c = 0.6$ and as paste for water contents below $w/c = 0.4$. In between, it flows to some extent but is also capable to store some energy. Rounded particles also increase pumpability while angular particles increase internal friction. Bornemann (2005) investigated properties of fresh ('green') concrete and found that good grading increases the internal friction in the concrete while a high fines content combined with low water content increases the adhesion between the grains. For very low water contents it was found that fresh concrete behaves more like a granular material and can be described by soil-mechanical models (McKinley (1993) and Bolton and McKinley (1997)).

3.5.1 Previous laboratory tests on cement grout filtration

If water is filtered from the liquid grout, the particle concentration increases, the particles contact each other and a 'filter cake' builds up. Various researches simulated cement grout filtration in consolidation and laboratory chamber tests. The test type and grout properties determined in different studies are summed up in Table 3.1.

McKinley (1993) carried out consolidation tests with Ordinary Portland Cement (OPC) and Sulphate Resisting Cement (SRC) grouts, applying pressures between $5\,kPa$ and $60\,kPa$. He found filter cakes with water contents of approximately $w/c = 0.41$ for SRC and 0.35 for OPC but with a considerable scatter between 0.3 and 0.46. By back-calculation of the tests using the two-phase filtration model permeabilities of $k_{fc} = 7.2{\times}10^{-7}\ m/s$ and $k_{fc} = 4.3{\times}10^{-7}\ m/s$ were found, respectively. Assuming Terzaghi's consolidation theory for the whole sample height, an average consolidation coefficient for OPC was be estimated with $c_v = 0.197\ \frac{D^2}{t_{50}} = 2.8{\times}10^{-5}\ m^2/s$.

Consolidation tests followed by a pure filtration phase by applying a constant hydraulic gradient were presented by Picandet et al. (2011). From the consolidation phase with pressures of 30 kPa, consolidation coefficients of $c_v = 6.5{\times}10^{-7}\ m^2/s$ and $c_v = 3{\times}10^{-6}\ m^2/s$ were found for initial water contents of 0.3 and 0.4 respectively. From the pure filtration phase (constant pore pressure gradient) void ratio dependent permeabilities were determined with $k_{fc} = 4{\times}10^{-8}\ m/s$ and $k_{fc} = 1.5{\times}10^{-7}\ m/s$ for final water contents of 0.25 and 0.34 respectively.

Kleyner and Krizek (1995) carried out laboratory chamber tests where cement grouts were pressed into sand with 100 to 300 kPa. They back-calculated the filtration process using a combination of consolidation and cavity expansion theory and for n consolidation coefficient of $c_v = 5{\times}10^{-5}\ m^2/s$ (taken from Ahverdov (1981)) the results fitted well with the test results. This method was adopted by Lee et al. (2012) to back-calculate their laboratory chamber grouting tests of cement grout in clayey sand and decomposed residual soil and determined an average consolidation coefficient $c_v = 4.2{\times}10^{-5}\ m^2/s$ for initial water contents of $w/c = 0.5$ and grouting pressures between 200 and 400 kPa.

Table 3.1: Properties of fresh filter cake material determined for pure cement-water suspensions.

Reference	Method	w/c_{sus} [-]	w/c_{fc} [-]	c_v $[m^2/s]$	k_{fc} $[m/s]$	Pressure [kPa]
McKinley	Consolidation OPC	0.6-1.0	0.35	2.8×10^{-5}	4.3×10^{-7}	5-60
McKinley	Consolidation SRC	0.6-1.0	0.41		7.2×10^{-7}	5-60
Picandet et al.	Consolidation	0.3		6.5×10^{-7}		30
Picandet et al.	Consolidation	0.4		3.0×10^{-6}		30
Picandet et al.	Permeability test		0.25		4.0×10^{-8}	
Picandet et al.	Permeability test		0.34		1.5×10^{-7}	
Kleyner and Krizek	Grouting in sand	0.5	0.3	5.0×10^{-5}		100-300
Lee et al.	Grouting in silty sand and decomposed residual soil	0.5		4.2×10^{-5}		200 - 400

3.5.2 In-situ measurements

In some studies cement grout filtration was also observed during in-situ anchor installation and the water contents of the filter cake was determined: For example Jessberger (1963) reports that cement grouts with initial water contents between $w/c = 0.4$ and 0.5 reduce to values between 0.2 and 0.3 due to filtration. Also Paproth and Paproth (1966) report filter cake water contents of $w/c = 0.3$ from field and laboratory tests.

3.6 Chapter summary

Even though more advanced methods are available to simulate filtration of solids from a suspension, in literature mainly two approaches were found appropriate to describe the filtration of cement grouts: The two-phase filtration model and classical consolidation theory. The models represent an upper and lower limit of the real grout behaviour during filtration. This was also confirmed in laboratory tests which will be presented in Chapter 5. However, the two-phase filtration model uses more general parameters and was therefore chosen for further calculations.

The two-phase filtration model was adapted for radial filtration with constant pumping rate to simulate the filtration inside a borehole. To calculate the filter cake formation in the borehole, the water content of the filter cake needs to be known. From theoretical considerations based on the dry bulk density the grains would start to contact each other for water contents between $w/c = 0.4$ to 0.5 and could reduce as low as 0.2 after consolidation. However, these values seem too high to assume a stable grain contact, considering that cement grout suspension with $w/c = 0.5$ clearly acts as liquid.

Calculation parameters for the consolidation and two-phase filtration model were reviewed from previous studies. The presented filter cakes' water contents ranged from $w/c_{fc} = 0.25$

to 0.41, and also the permeabilities and consolidation coefficients show considerable scatter. However, the water contents comply with the theoretically expected values and confirm, that water contents in that range can be expected. In the studies different grouting pressures and initial water contents of the liquid grout were used, but the influence of those is unknown. Additionally, the grouting pressures applied were lower than pressures expected for grouting of ground anchors.

To further investigate the effects of cement grouting, the effective stresses acting on the soil should be determined. This requires the permeability of the filter cake in order to access the hydraulic resistance and calculate the seepage forces. Further, the mechanical behaviour of the soil and of the filter cake needs to be taken into account to simulate the unloading process and determine the effective stresses remaining after grouting.

Chapter 4

Cement grout filtration - Laboratory tests

4.1 Introduction

A series of laboratory tests is presented which were carried out to investigate the filtration behaviour of cement grouts and to determine their mechanical behaviour. Standard Portland cement was consolidated in a filtration press, applying varying grouting pressures and water contents of the initial grout. After filtration, the water contents and mechanical properties of the filter cake material were determined in soil-mechanical tests. These tests were then back-calculated using the two-phase filtration model as well as consolidation theory and the methods are evaluated.

4.2 Filtration tests - Experimental procedure

The filtration behaviour of fresh cement grouts was investigated in a series of laboratory tests, taking into account the effects of different grouting pressures and initial water contents. The filtration process was simulated with a filtration device similar to a confined compression test (oedometer-test) as presented in Figure 4.1. A constant pressure was applied on top of a grout sample and free drainage allowed at the bottom. Pore pressures and deformations were measured at the top of the sample. When the piston deformation declined and no further water was expelled from the sample the test was stopped. During the filtration test, water is drained out of the cement grout while cement particles are retained by the filter medium. The piston deformation δ and pore pressure u are recorded at the top of the sample during the test.

4.2.1 Materials

The filtration tests were designed to simulate cement grout filtration during anchor installation and therefore materials used in-situ were chosen.

For all filtration tests the grout was mixed with Norcem standard Portland cement and filtered, de-aired water. No aggregates such as gravel or sand was added. The cement had a specific grain density of $3.15\ g/cm^3$, the particle size distribution is given in Figure A.1 of

Appendix A. The retarding agent (Sika® Retarder) was added to the grout. An amount of 1.5% of the cement weight was successfully used to prevent setting during all tests.

4.2.2 Filtration press

The filtration press is constructed similar to an oedometer device drained at one end, only with a larger sample height. It consists of a steel cylinder, sitting on a bottom piece, and a moving piston on top. Drainage is allowed through the bottom piece and can be controlled through a valve. Constant pressure is applied with the moving piston on top. To record the actual pressure, a pore water pressure sensor is connected to the top piece with a thin flexible hose. Top and bottom pieces are equipped with drainage channels and porous filter blocks, preventing cement particles to be washed out or block the pore water pressure sensor. A sketch of the filtration device is presented in Figure 4.1. In first trial tests, an acrylic glass cylinder was used to observe the infiltration of cement into a sand layer and the formation of a filter cake. However, to be able to apply pressures up to 1500 kPa a steel tube was preferred for the test series presented in this study.

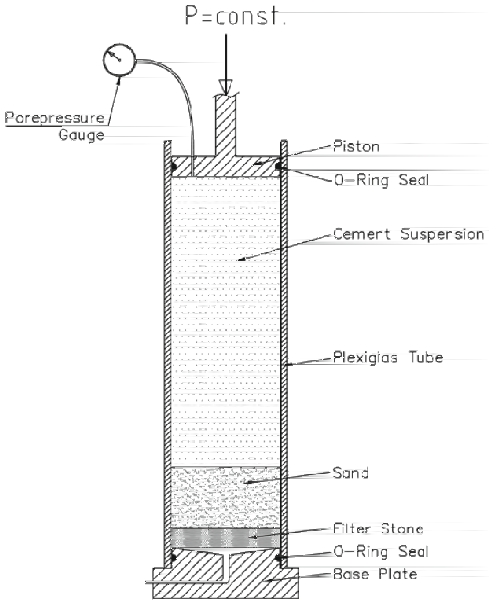

Figure 4.1: Filtration press used for filtration of cement grout suspension.

4.2.3 Experimental procedure

The cement grout was mixed in a conventional kitchen blender. Dry cement was placed in a mixing bowl and mixed at low speed while water and retarder were added, and at high

speed thereafter. One grout mixture was used for two to three filtration tests which were conducted one after another. Before each test, a filter paper was placed on top of the porous block at the bottom of the filtration press and the grout was filled into the cylinder to a height of 80 mm. Cylinder and piston were lubricated, to reduce friction. Filter paper was placed on the grout surface and some water was carefully poured on top of it. The filter paper prevented a mixing of water and cement. The piston was now placed on the sample. A valve in the tube connecting piston and pore pressure sensor allows air to escape during assembly of the piston. Before loading, the valve leading to the pressure sensor and the outlet valve at the bottom piece are closed. The now undrained sample was loaded with dead weights until the desired pore pressure was reached. A deformation transducer was adjusted on top of the piston and the recording of pressure and deformation started. To start the filtration process the drainage valve was opened quickly and allowed drainage at the bottom. The amount of expelled water from the sample was also recorded. The sample was loaded mechanically, using a customised oedometer press. In a first attempt the sample was loaded with a computer-operated pressure device but it turned out that the motor was not fast enough to ensure constant pressure for the fast deformations of the piston. This problem was avoided using a dead load applied mechanically.

4.2.4 Test series

In a first test series filtration tests with initial sample height h_{ini} of 80 mm were conducted with grouting pressures p_{ini} ranging from 100 to 1500 kPa and initial water contents w/c_{ini} from 0.4 to 0.6. Test parameters and results are presented in Appendix A, Table A.1. The first number in the name references the cement mix, next is the number of the test with this mix and in the third number the initial water content is indicated.

In the first test series, three additional tests were carried out with a layer of sand as filter (Table A.2). In these tests the infiltration of cement into sand during grouting and the effect of filter permeability was investigated.

A second test series was mainly carried out to create the filter cake material for triaxial testing. Here, the initial grout height was increased to achieve the required filter cake thickness for triaxial testing. These tests were all conducted with an initial water content of $w/c_{ini} = 0.4$ and grouting pressure of 500 kPa. Only during the last two tests a grouting pressure of 1000 kPa was applied (Table A.3).

4.2.5 Water content measurements

In geotechnical engineering water contents of soil samples are usually determined by oven drying the samples at $105\ °C$ for 24 hours. The drying time of 24 h was found sufficient and practical, but the exact time does not matter as long as the weight of the sample remains constant over time. However, for fresh cement grout mixtures the time is a relevant factor, because water binds to the cement particles during hydration and the amount of free water

changes with time. To reduce the drying time and thus reduce the hydration effects on the measured water content, the fresh cement mix was dried in a domestic microwave oven, which turned out to be reliable and practical.

For the second test series a combined drying method was applied, since drying samples in the microwave requires many runs until the weight remains constant. The samples were first dried in the microwave to evaporate the majority of pore water, followed by oven drying for 24 h.

4.2.6 Permeability measurements

Permeability tests were conducted in the filtration device directly after the filtration process was completed. The loading cap was removed and water poured on top of the sample. By replacing the loading cap on top of the sample and adding a dead weight, a constant hydraulic head between 8.08 and 9.60 m was applied for approximately 20 minutes. The piston deformation as well as outflow at the drained bottom was recorded to determine the filter cake permeability k_{fc}, based on Darcy's law:

$$q = k\frac{dh}{dz} \rightarrow k_{fc} = q\frac{h_{fin}}{\Delta h}, \tag{4.1}$$

where q is the specific discharge rate, Δh the applied pressure head and h_{fin} the sample height.

4.3 Filtration tests - Results

In the following section the results of the filtration tests are presented. A comprehensive overview of all results is given in Tables A.1 to A.3 of Appendix A.

4.3.1 Filtration behaviour

A typical filtration test is presented in Figure 4.2. All filtration tests showed a very similar filtration behaviour. The piston deformation is nearly linear with the square root of time $\sqrt{t}$ until it stagnates at a certain point, after which the deformation approaches a limit value δ_{fin}. The time t_{50} were 50% of the final deformation (δ_{50}) is reached is marked in the figure. The pore pressure at the top of the sample remains constant until it suddenly drops at a certain point in time (filtration time t_{filt}). This demonstrates that in a first phase of the tests some parts of the grout are still liquid and only hydrostatical stresses are transferred through the mix water. The drop of pore pressures at t_{filt} indicate the point where the piston touches the filter cake and all cement particles in the sample are in contact and transfer effective stresses.

The test results within one set of tests (tests from the same grout mix and with the same grouting pressure) were very consistent for most tests. Therefore, only the load deformation curve of the first test is plotted in comparison plots. Calculation parameters were derived

for each test. To plot results, mean values of all values derived from tests with the same test conditions were taken.

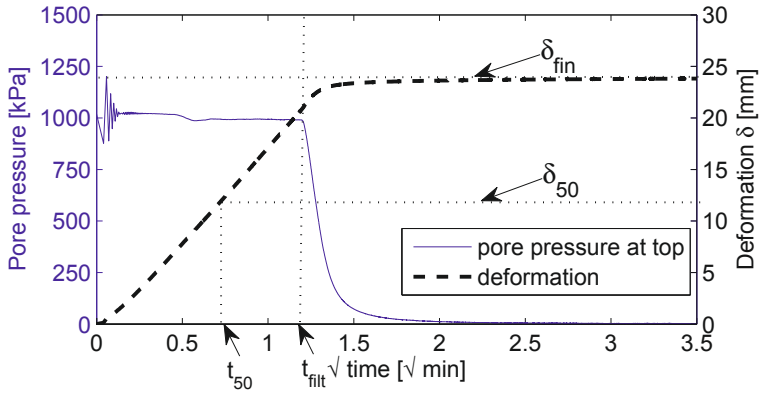

Figure 4.2: Typical deformation and pore pressures measured at the piston during filtration test with grouting pressure of 1000 kPa and $w/c = 0.5$.

Filtration test results for each parameter set are presented in Figure 4.3. The behaviour of all tests was very similar, regardless of grouting pressure or initial water content. All tests show a short filtration time t_{filt} below 4 minutes. When comparing tests with different grouting pressures, it appears in most cases that the higher the pressure, the faster filtration is completed.

Higher initial water contents w/c_{ini} of the grout result in larger deformations after filtration, which is reasonable as with equal initial sample height more water has to be expelled to reach the same filter cake water content. The deformation with time is larger for higher initial water contents, but at the same time a larger deformation is required in order to achieve full filtration of the sample. The initial sample height was constant for all tests, which means that, assuming a comparable void ratio of the filter cake, the final filter cake thickness is larger for lower initial water contents w/c_{ini}. At the same time filtration takes longer to for higher initial water contents than for lower ones because more water needs to be filtered out. These opposing effects of the initial water content could explain why the filtration time seems to be unaffected by it.

Even though the final deformations show considerable scatter, in general larger deformations are reached with higher grouting pressures, which indicates that the filter cake consolidates further, after the grains are in contact. The deformations after the filtration point are, however, very small compared to the difference for different grouting pressures, which leads to the assumption that a compression of the filter cake happens already during formation of the material.

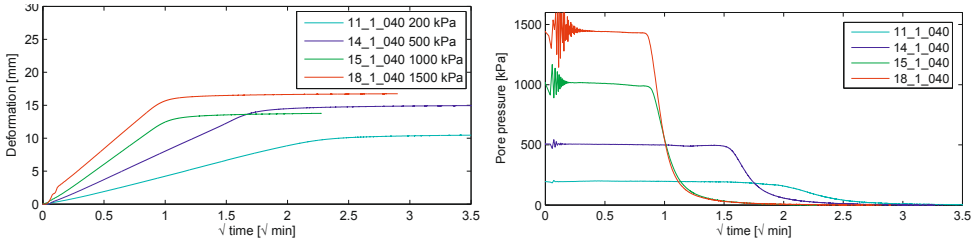

(a) $w/c_{ini} = 0.40$

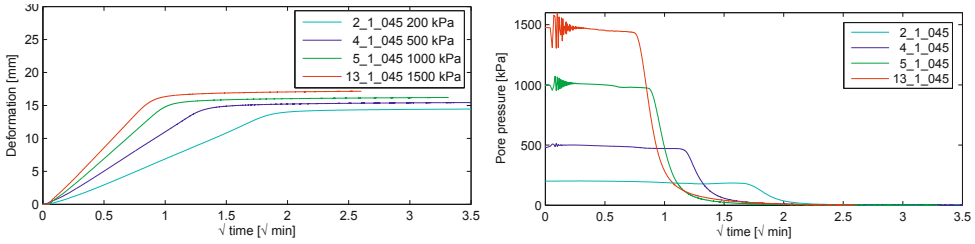

(b) $w/c_{ini} = 0.45$

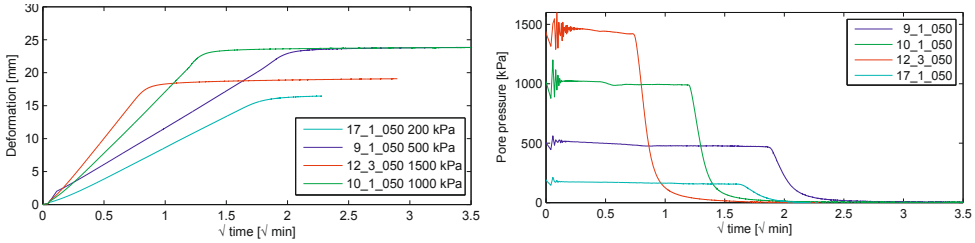

(c) $w/c_{ini} = 0.50$

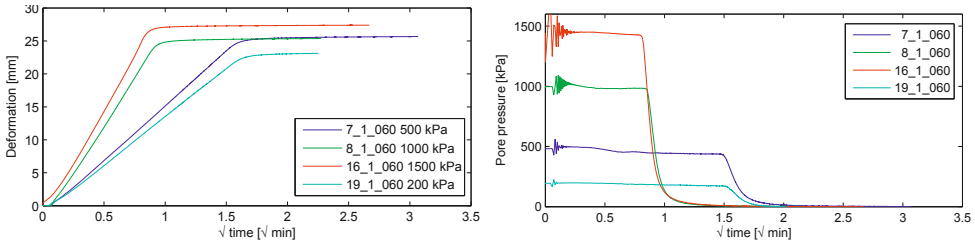

(d) $w/c_{ini} = 0.60$

Figure 4.3: Filtration test results for different initial water contents w/c_{ini}. Deformation and pore pressure measured on top of the sample.

4.3.2 Influence of sand as filter medium

The filtration tests were carried out with a filter consisting of a filter stone and a layer of filter paper, even though in-situ filtration takes place against sand. On the one hand, it was assumed that the influence of the sand as filter medium is negligible, on the other hand it was aimed to avoid additional inaccuracies accompanied with the compaction and saturating of the sand.

The influence of a sand layer on the filtration behaviour mainly depends on the hydraulic resistance of the material. The permeability of sand in the field ranges from $k = 1 \times 10^{-6}$ to $1 \times 10^{-3}\ m/s$. This is much higher than the expected filter cake permeability. As soon as a thin filter cake builds up, the filtration behaviour is governed by the filter cake itself and free drainage can be assumed through the sand layer and the porous block at the bottom of the filtration device. This was also stated by McKinley (1993), who investigated the effect of the porous block's permeability on the filtration process during similar tests on cement grout.

To investigate the influence of sand as filter medium, three tests of the first test series (3_1_045_S to 3_3_045_S) were conducted with a sand layer. Approximately 50 mm of sand were built in on top of the filter stone. The same amount of cement was used as for all tests of the first test series. Figure 4.4 shows the results of the filtration test compared to tests without sand filter but with identical test parameters. It shows that the sand layer has no significant influence on the filtration rate and the pore pressure development on the top of the sample. Variations between the tests with and without sand filter are in the same order than within one set of tests with the same conditions. These findings justified not to use a sand layer in the filtration tests.

4.3.3 Injection of grout into sand

Using a test set-up without a sand filter implies that injection of sand particles into the sand is insignificant for the filtration process.

The ability of a grout to permeating into a soil depends on the relation between the grouts grain size and the pore size of the soil. As presented in Section 2.3.6, the groutability or filter stability of grouts is usually accessed with the ratio N, where the grain sizes of grout and soil are related. With $D_{85,g}$ = 36 μm for the used standard Portland cement and $D_{15,s}$ = 250 μm of the sand, the groutability ratio becomes N = 6.9. This value is well below the recommended injection limit $N \geq 25$ and the value of $N \leq 11$ below which no injection is possible. The N value of the tests is still slightly above Terzaghi's filtration limit of $N \leq 5$, however, the filtration criterion is on the conservative side, providing a stable filter for water flowing through the filter for a period of time. It is also assumed that the relevant particle size increases after mixing the grout due to hydration and agglomeration. This is not taken into account in Terzaghi's filtration limits, but in the injection limits, which are based on injection with cement grouts. Therefore, N for injection might be more relevant in case of grouting.

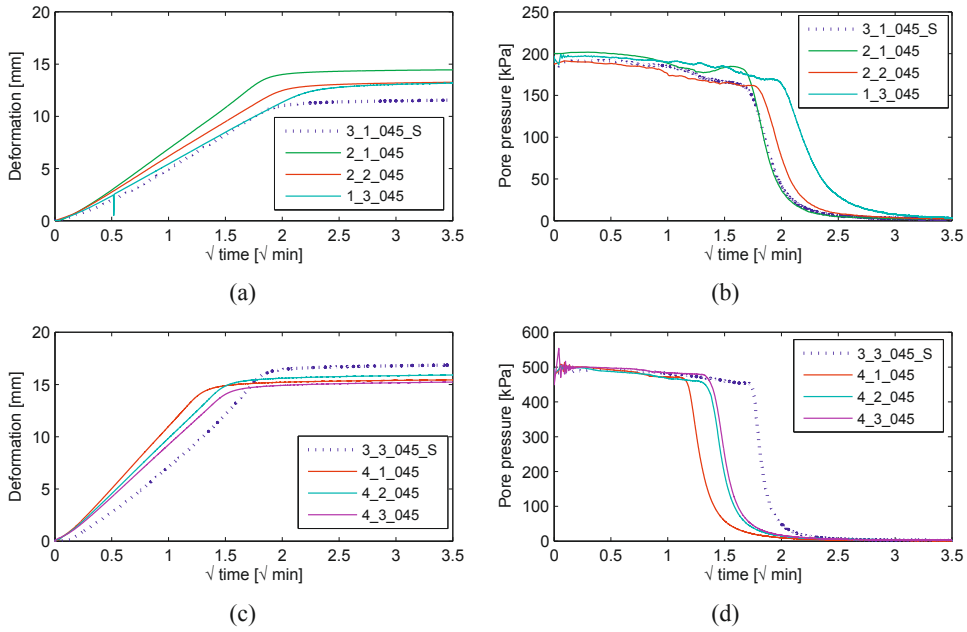

Figure 4.4: Filtration test results with sand filter compared to regular tests without sand filter. Initial water contents w/c = 0.45, filtration pressure 200 kPa (a and b) and 500 kPa (c and d).

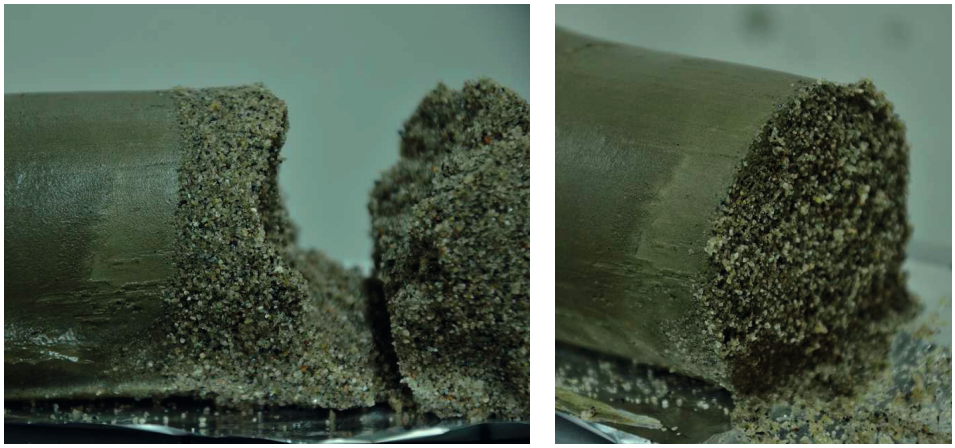

Figure 4.5: Uncured cement grout filter cake against sand filter.

Looking at the results of the filtration tests with a sand filter presented above (Figure 4.5), confirms that no infiltration of cement into the sand takes place. They exhibit a distinct border between grout filter cake and sand with no visible infiltration of cement particles into the sand. The sand was easily brushed off the filter cake. Only some particles sticked to the filter cake. The same effect was observed if the sand was removed only after curing of the cement. This shows that a transition zone where the sand is strengthened by infiltration of grout into sand does not occur and that the injection of grout particles into the soil is negligible.

4.3.4 Phase change

(a) Filter cake build-up after 30 s filtration time.

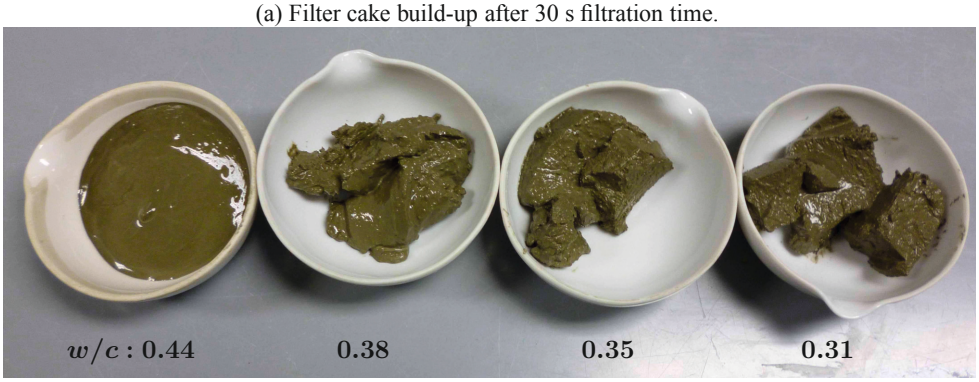

(b) Measured water contents along sample from top to bottom (left to right side).

Figure 4.6: Filter cake formation in cement grout suspension with initial $w/c = 0.5$ and grouting pressure of 5 bar.

One filtration test was stopped after 30 seconds to investigate if a distinct phase change is apparent during filtration. Figure 4.6a shows the extracted sample, the top end, where the pressure was applied on the left side, the drained end on the right side. The filter paper which was placed on top of the sample can be seen on the left. A distinct border between liquid and plastic material properties is clearly visible. Samples of the filter cake were taken and the stiffness appeared to increase gradually towards the drained end, from very soft to stiff. The water contents of the liquid grout and at three positions across the filter cake are presented in Figure 4.6b. The water contents decrease gradually within the filter cake but it seems that there is a certain w/c value or void ratio where the consistency changes instantaneously from liquid to solid.

4.3.5 Water contents

The water contents measured after microwave drying are compared to theoretical values in Figure 4.7. The measured water contents of the fresh grout were on average 8% lower than the intended w/c values. The lower water content can be explained by chemical bonding of water to the cement particles in the initial hydration phase or water evaporating during mixing and drying. Another possible explanation is that the samples were not dried completely during microwave drying and some moisture remained in the samples. In the second test series, the drying method was altered and the samples were additionally dried in the oven after initial microwave drying. With this method the difference between measured and theoretical water content was slightly smaller.

The water contents taken from one mix directly after mixing, before the second or the third filtration test did not decrease significantly. This indicates that curing processes were very little during the test period.

The measured filter cake water contents w/c_{fin} versus grouting pressure are presented in Figure 4.8. For grouting pressures up to 1000 kPa water contents decrease with increasing grouting pressure, which indicates stress dependent compaction of the material after a filter cake is built. Nevertheless, the water content is not reduced as much during grouting at higher grouting pressures. For higher initial water contents, the final water content was even higher for grouting pressures of 15 bar than for 10 bar. These findings could be either due to inaccuracy in determining the water content and values being very close to each other or due to the fact that for higher initial water contents a larger piston movement is required. If this is the case, the friction between piston and cylinder might increase due to cement particles sticking to it and leading to a reduction in grouting pressure. For lower initial water contents it seems like the final water content reaches an asymptotic limit for higher grouting pressures possibly because the material approaches its densest packing. Another explanation is that for higher grouting pressures full filtration is reached earlier, leaving less time for the filter cake to consolidate and thus resulting in higher filter cake water contents. This effect would be more distinct for higher than for lower initial water contents which can explain the results.

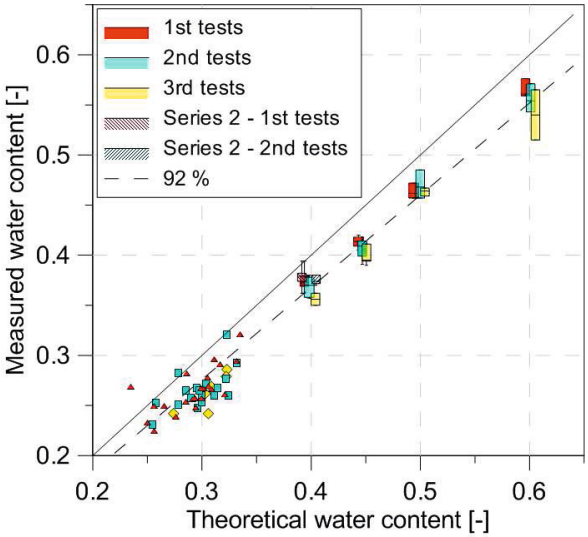

Figure 4.7: Measured versus theoretical water contents of cement grout. Values for fresh grout are presented in box-plots, filter cake values shown as symbols.

The difference between measured filter cake water contents and calculated values determined from the relation of initial volume, volume change and initial water content ranged from 2 to 20%. The difference between calculated and measured values were larger and more scattered than for the initial water contents of the grout because here the theoretical values are also subjected to uncertain parameters such as initial sample height or particle density. Taking the mean values for all tests based on the calculated values gives a final water content of around $w/c_{fin} = 0.29$ for pressures above $200\ kPa$ and $w/c_{fin} = 0.32$ for pressures at $200\ kPa$ (see Figure A.2 of Appendix A).

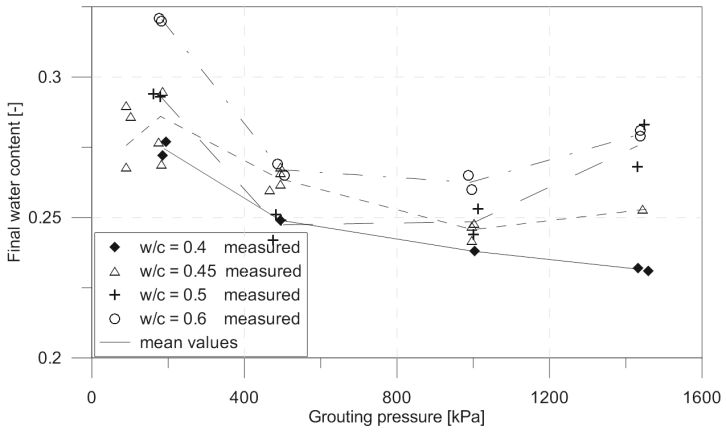

Figure 4.8: Measured filter cake water contents.

4.3.6 Permeabilities

The permeabilities of the filter cake material are presented in Table 4.1. They were determined in constant head permeability tests, where the discharge rate was measured. The discharge rate and therefore permeability reached a constant level in less than a minute (see Appendices A.3 and A.4) and permeabilities k_{fc} were taken as mean values of the constant part of the curves.

Table 4.1: Permeability test results.

File name	w/c_{ini}	p_{ini}	h_{fin} mm	Δh_{mean} m	e_{fc}	$k_{fc,mean}$ m/s
7_2_060	0.60	500	52.6	8.27	0.90	4.74E-08
8_2_060	0.60	1004	53.8	9.34	0.94	1.18E-07
9_2_050	0.50	497	58.3	9.42	0.88	4.55E-08
10_2_050	0.50	1024	56.3	9.57	0.81	5.01E-08
10_3_050	0.50	494	57.9	8.27	0.86	5.21E-08
12_3_050	0.50	1434	61.0	8.03	0.96	9.59E-08
13_2_045	0.45	1501	61.6	8.44	0.86	5.32E-08
14_2_040	0.40	491	67.8	8.09	0.92	3.88E-08
15_2_040	0.40	982	67.2	9.33	0.86	5.04E-08
16_2_060	0.60	1437	56.2	8.80	1.00	1.02E-07
17_3_050	0.50	203	64.0	8.25	1.05	1.22E-07
18_3_040	0.40	1472	65.3	8.74	0.83	4.44E-08
19_3_060	0.60	195	58.0	9.57	1.08	2.02E-07

In addition to the permeability tests, k_{fc} values were back-calculated from filtration tests, assuming the two-phase filtration theory presented in Section 3.2.1. A bilinear curve was fitted to the test results. The final filter cake height $L_{c,fin}$, deformation δ_{fin} and filtration

time t_{filt} were used to back-calculate the permeability by rearranging Equation (3.5) and inserting Equation (3.2) to

$$k_{fc} = \frac{\gamma_w \, L_{c,fin} \, \delta_{fin}}{2 \, \sigma \, t_{filt}} \, . \tag{4.2}$$

Measurements and back-calculated values of the filter cake permeability are presented in Figure 4.9. The measured values match with the calculated ones of the same test. As expected for granular materials, the permeabilities correlate to the void ratio of the filter cake material. Full saturation was assumed for the calculations and the water contents were directly related to the void ratios. Therefore, it is obvious that for a void ratio dependent permeability, similar correlations between permeability and grouting pressure were found as for water contents and grouting pressure. Plotting permeabilities k_{fc} against void ratio e_{fc} shows that the permeability decreases with void ratio (Figure 4.9). Picandet et al. (2011) proposed to use following function, initially published by Carman (1956), to correlate permeability of cement grouts to void ratio:

$$k = C_x \frac{e^3}{1+e} \tag{4.3}$$

but also used a logarithmic approach

$$\Delta(\log_{10} k) = \frac{\Delta e}{C_k} \tag{4.4}$$

suggested first by Taylor in 1948. The Carman equation fitted for permeability tests on cement grout filter cake carried out by Picandet et al. (2011) is plotted in Figure 4.9. For the permeability tests of this study, a better fit was found with Taylor's logarithmic relation given in Equation (4.4). Permeabilities from back-calculation using filtration theory fit well with the directly measured values.

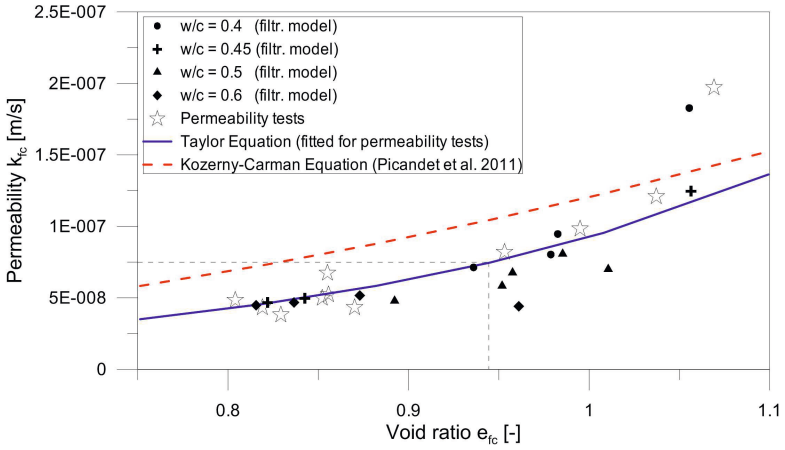

Figure 4.9: Permeability k_{fc} versus void ratio e_{fc}. Determined from permeability tests (☆) and mean values of all tests from back-calculation with filtration theory (◆ ▲ ✚ ●) compared to values from Picandet et al. (2011) (red dashed line).

4.3.7 Filtration rate

In Section 4.3.1 the inclination of the deformation-$\sqrt{t}$ curves was found to be influenced by grouting pressure and initial water content w/c_{ini}. The effects of these factors on filter cake formation are now investigated by comparing filtration rates of the different tests. The filtration rate was defined as the increase of filter cake thickness L_c with $\sqrt{t}$. The deformation curves of all tests were almost linear with $\sqrt{t}$ and the inclination of these linear parts were taken to calculate the filtration rates.

Applying the two-phase filtration model, the filter cake thickness L_c at a certain time was directly related to the deformation δ, using initial and final void ratios (Equation (3.2)). For a linear relation between deformation δ and $\sqrt{t}$, the inclination of the filtration curve was approximated with

$$\frac{d\delta}{d\sqrt{t}} \approx \frac{\delta_{50}}{\sqrt{t_{50}}} \,. \tag{4.5}$$

Combining Equation (4.5) and (3.2) yields the filtration rate

$$\frac{dL_c}{d\sqrt{t}} = \frac{\delta_{50}}{\sqrt{t_{50}}} \left(\frac{1 + e_{fc}}{e_g - e_{fc}} \right) . \tag{4.6}$$

Figure 4.10 shows filtration rates for different initial water contents and grouting pressures. Filtration rates clearly increase with grouting pressure, due to higher pressure gradients causing higher discharge rates (Equation (3.1)). Although the test results show some variance, a negative correlation can be seen between the filtration rate and initial water content.

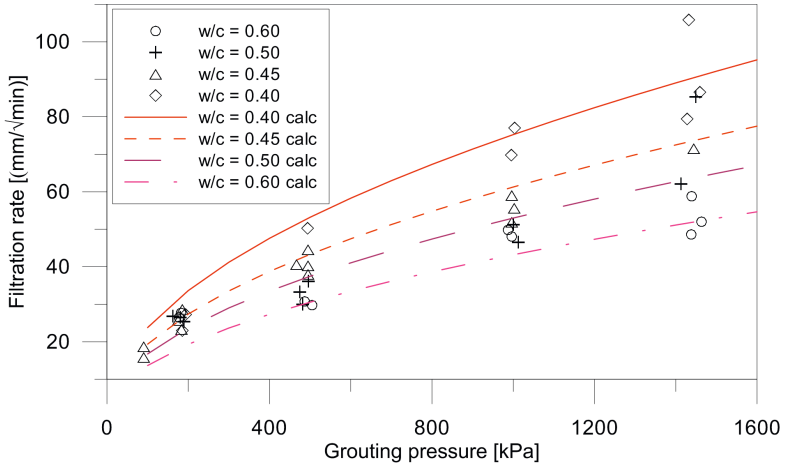

Figure 4.10: Filtration rate $\frac{dL_c}{d\sqrt{t}}$ versus grouting pressure. Test results (symbols) and calculated values from filtration approach - assuming $k_{fc} = 7.5 \times 10^{-8}\ m/s$ and $w/c_{fin} = 0.3$ (lines).

4.4 Simulation of filtration tests

4.4.1 Filtration model

The filtration tests were analytically back-calculated using the two-phase filtration model introduced in Section 3.2.1. The theoretical filtration rate was back-calculated for different initial water contents. Rearranging Equation (3.5) and differentiation with respect to $\sqrt{t}$ gives

$$\frac{dL_c}{d\sqrt{t}} = \sqrt{\left(\frac{2k_{fc}}{\gamma_w}\right)\left(\frac{1+e_{fc}}{e_g - e_{fc}}\right)\sigma}\ . \tag{4.7}$$

The filtration model requires the permeability of the filter cake and the initial and final void ratio of the cement grout. The initial void ratio was determined directly from the water content of the cement mix (Equation (3.15)). One representative filter cake water content $w/c_{fin} = 0.3$ was chosen as mean value of all tests. With the corresponding void ratio $e_{fc} = 0.945$ the permeability $k_{fc} = 7.5 \times 10^{-8} m/s$ was determined from Figure 4.9. The back-calculated filtration rates shown in Figure 4.10 fit well with the test data.

It was possible to back-calculate the filtration behaviour using the two-phase filtration model and only one set of parameters. However, the validity of this approach is restricted one-dimensional filtration.

4.4.2 Consolidation theory

The back-calculation with Terzaghi's consolidation theory requires two of the three parameters, the consolidation coefficient c_v, the compressibility coefficient m_v, or the mean permeability k_m. The coefficient of consolidation c_v was estimated from t_{50} at 50% consolidation, assuming the consolidation curve is linear with $\sqrt{t}$. The theoretical solution of Terzaghi's consolidation theory at this point gives the time parameter $T = c_v t_{50}/h^2 = 0.197$ and therefore the consolidation parameter is determined with

$$c_v = 0.197 \frac{h^2}{t_{50}} \,. \tag{4.8}$$

This method is a simplification of the '$\log(t)$-method' proposed by Casagrande and Fadum (1940), which additionally includes the determination of an initial and final deformation. For this study it was found adequate to assume $\delta_0 = 0$ and take the last measured deformation as δ_{fin}. The coefficients of consolidation c_v versus grouting pressure determined with this method are plotted in Figure 4.11. The coefficient of consolidation c_v increases with increasing grouting pressure, but c_v does not correlate to the initial water content of the grout. A linear function of c_v and grouting pressure was hence used for all back-calculations:

$$c_v = 6.07 \times 10^{-8} \cdot \sigma + 7.79 \times 10^{-6}. \tag{4.9}$$

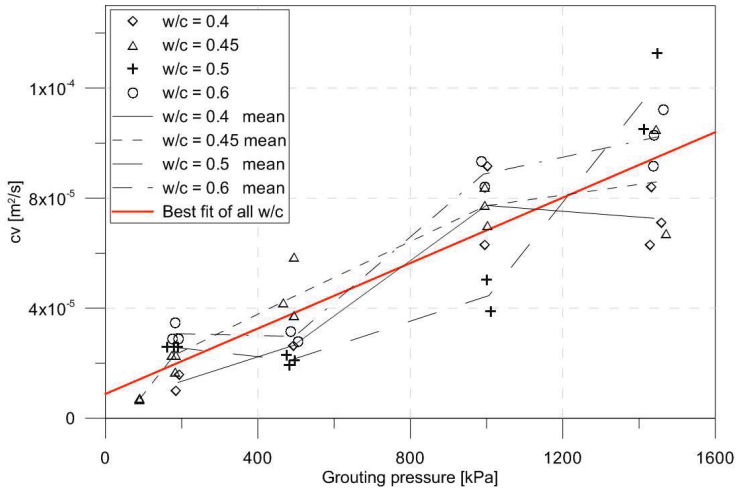

Figure 4.11: Consolidation parameter c_v versus grouting pressure. Best fit for all values $c_v = 6.07 \times 10^{-8}\sigma + 7.79 \times 10^{-6}$ with $R^2 = 0.976$.

The compressibility coefficient m_v was determined with Equation (3.8), assuming full

consolidation is achieved at the end of the test and therefore

$$\varepsilon = \frac{\delta_{fin}}{h_0} \,. \tag{4.10}$$

The determined compression parameter m_v should rather be considered as a parameter to adjust the calculated deformation as opposed to the physical stiffness of the grout material because the grout particles are initially not in contact with each other and volume changes are induced by water expelled from the suspension not by compression of the grain structure. For different initial water contents, different deformations are needed for complete filtration. Therefore, rather than using the deformation δ, the degree of consolidation U was applied to compare the test results. The degree of consolidation relates the actual and final deformation of the sample:

$$U = \frac{\delta}{\delta_{fin}} \,. \tag{4.11}$$

The calculated consolidation curves shown in Figure 4.12 fit reasonably well with the test results.

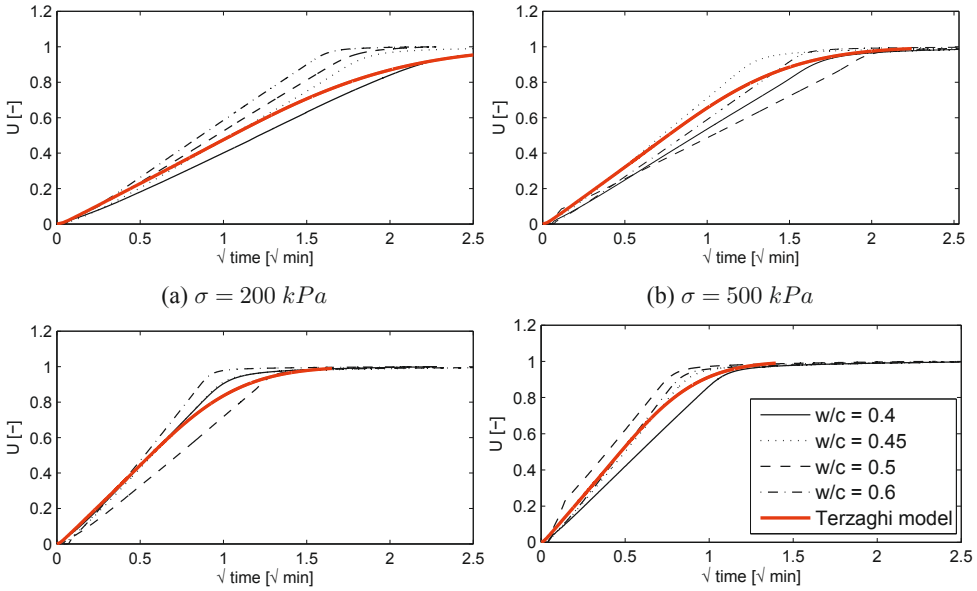

(a) $\sigma = 200\ kPa$ (b) $\sigma = 500\ kPa$

(c) $\sigma = 1000\ kPa$ (d) $\sigma = 1500\ kPa$

Figure 4.12: Degree of consolidation U versus $\sqrt{t}$ for $w/c = 0.4, 0.45, 0.5$ and 0.6 for different grouting pressures. Back-calculation of test results with Terzaghi consolidation theory (red line).

4.4.3 Modified consolidation theory

The assumption of a constant c_v value in classical consolidation theory might not be appropriate for cement grout because the material exhibits large changes in permeability and stiffness during the consolidation process. Both parameters, permeability k_m and compressibility m_v, decrease with the void ratio e or increasing effective stress σ'. Looking at Equation (3.7), c_v could either decrease, increase or stay constant with effective stress, dependent on which parameter changes more. It is usually assumed that the change of k_m and m_v cancels each other out and therefore c_v can be appropriately considered as a constant. This does not apply for all materials, and Abuel-Naga and Pender (2012) propose a modified consolidation approach with linear effective stress dependent c_v. Figure 4.13 shows the degree of consolidation $U = \delta/\delta_{fin}$ of a typical filtration test compared to consolidation curves for different values of c_v. The consolidation curve of the filtration test passes through different Terzaghian consolidation curves and shows that c_v changes gradually with degree of consolidation U and therefore with effective stress σ'.

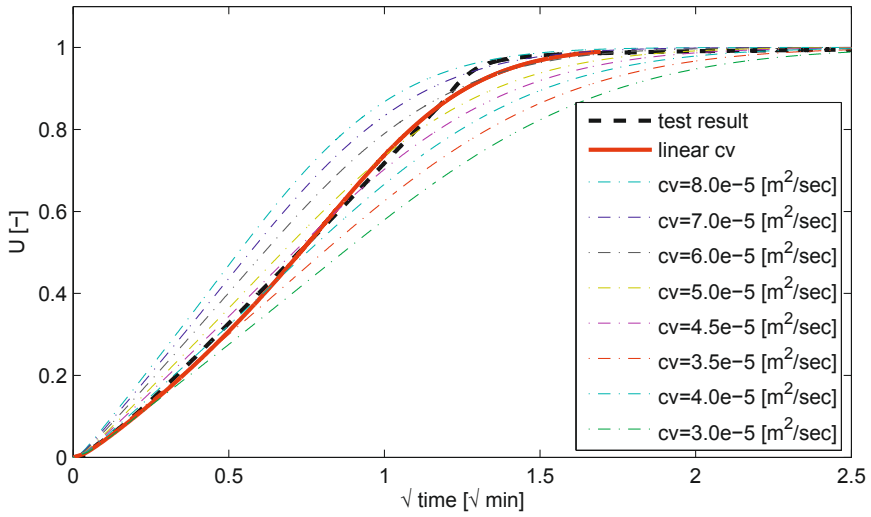

Figure 4.13: Consolidation curve of filtration test in comparison to back-calculation with constant c_v and effective stress dependent c_v ($c_{v,ini} = 2.5 \times 10^{-5}$; $c_{v,fin} = 8.0 \times 10^{-5}$).

A linear interpolation between the initial $c_{v,ini}$ and final $c_{v,fin}$ consolidation coefficient was used to back-calculate filtration tests:

$$c_v = c_{v,ini} + (c_{v,fin} - c_{v,ini})U. \tag{4.12}$$

The filtration tests were back-calculated using the finite difference method. The sample height was divided into 30 elements and for each time step the consolidation coefficient c_v

was updated in each element. The result of this back-calculation is shown in Figure 4.13 (solid line). Although the modified consolidation approach seems to characterise the single filtration test better than the classical Terzahgi consolidation theory, it was not possible to find a general correlation of c_v, grouting pressure and initial water content.

4.4.4 Estimation of filter cake thickness

To estimate the filer cake thickness during filtration, both theories, two-phase filtration and consolidation can be used. The two-phase filtration model assumes a distinct border between filter cake and grout. Therefore, for any time t before t_{filt} the cake thickness can be directly calculated with Equation (3.5).

In contrast, classical consolidation theory does not give the filter cake thickness directly. It assumes that the whole sample consolidates gradually with time and no distinction is made between fresh grout and filter cake. However, the border between filter cake material and grout can be assigned to a specific void ratio, at which stable contact between the grains is assumed. The filter cake thickness can then be related to the degree of consolidation U_{filt} at the time t_{filt} where the filter cake material reaches the top of the sample and pore pressures start to decrease. The degree of consolidation U_{filt}, shown in Figure 4.14, ranged from 0.75 to 0.95, which corresponds to void ratios between 0.88 and 1.13. Theoretically, the degree of consolidation at t_{filt} depends on the initial water content of the grout and the grouting pressure. w/c_{ini} defines the amount of expelled water, and therefore deformation needed to reach a certain mean water content in the sample. The level of grouting pressure defines how much the filter cake consolidates. Despite this, no significant correlation between initial water content, grouting pressure and U was found in Figure 4.14. This could be due to larger variations of the test results instead of parameter correlations. If all tests result in a final water content of 0.29 and a mean water content at the filtration time of $w/c_{filt} = 0.32$, U_{filt} values would be 0.75, 0.83, 0.87 and 0.91 for initial water contents of 0.4, 0.45, 0.5 and 0.6 respectively. Back-calculations with these values correspond to the range of the test results, even though the varying compression of filter cake at different grouting pressures is not taken into account.

4.4.5 Comparison of filtration and consolidation theory

Both models can be used to back-calculate the filtration tests. While the filtration model is designed to describe filtration of solid particles from a suspension, consolidation theory considers the expulsion of water from a solid. The used water contents of the cement grouts range between the liquid and plastic consistency limit and in this case the two models represent an upper and lower limit to describe the filtration process.

Required parameters for the filtration model are the initial and final water contents and the permeability of the filter cake. The filter cake material exhibits a void ratio dependent permeability k_{fc} between $3.81 \times 10^{-8} m/s$ and $1.97 \times 10^{-7} m/s$. The values calculated on the basis

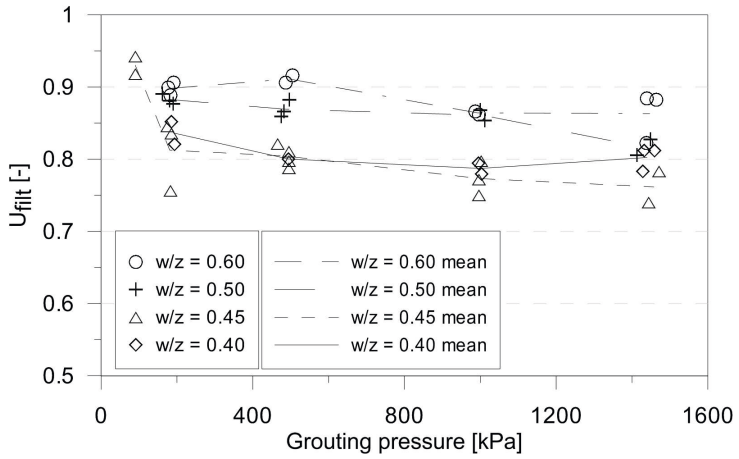

Figure 4.14: Degree of consolidation U at filtration time t_{filt}.

of filtration theory comply well with the directly measured values, which confirms that the filtration model is applicable. The filtration rate was back-calculated for all tested grouts and pressures, assuming a general final void ratio of $e_{fc} = 0.95$ and a corresponding permeability $k_{fc} = 7.5 \times 10^{-8}\ m/s$. The consolidation model requires the consolidation coefficient c_v and compressibility m_v of the material. The compressibility m_v can be determined from the strain required to achieve the final water content and the applied grouting pressure. Values for c_v ranged from $6.86 \times 10^{-6}\ m^2/s$ to $1.33 \times 10^{-4}\ m^2/s$, based on Terzaghi's consolidation theory. The mean values of all tests can be described with a linear function between c_v and grouting pressure. With this correlation, tests could be back-calculated. To determine the filtration point, it is proposed to use the degree of consolidation U. By assuming a final water content $w/c_{fin} = 0.29$, a mean water content at the filtration time $w/c_{filt} = 0.32$ was found as maximum value to set limits to the determined U values. The calculation parameters for both models depend on the final water content of the filter cake material which was found to vary between 0.25 and 0.35. No correlation between w/c_{fin} and grouting pressure could be identified. Therefore, it was not possible to determine the void ratio at which the grout actually acts like a solid and deformation is stress dependent. It seems that the scatter of test results exceed the influence of grouting pressure and initial water content for the range of water contents and grouting pressures of this study. Where no correlations could be identified, mean values of all tests were taken for back-calculation of test results, which gave reasonable results. These parameters might not be applicable for water contents and grouting pressures outside the test range. The filtration model allows a straight-forward determination of the filter cake thickness with time, but for an investigation of the filtration process in borehole geometry the use of consolidation theory could be favourable, as it is already implemented in common geotechnical FEM software. When using consolidation theory it is

not straight-forward to define the filtration time, especially as calculated deformations are inaccurate in the final part of the curve. However, a rough estimation of the minimum filtration time is possible.

4.5 Mechanical properties of fresh cement grout filtrate

4.5.1 Soil mechanical tests on filter cake material

The filter cake material was tested with various soil mechanical tests, to determine mechanical properties. The samples were taken directly after filtration and the tests were completed before setting was observed in reference probes of the unfiltered and filtered grout.

Unconfined compression test

Before triaxial tests and oedometer tests were conducted, some samples were loaded in unconfined compression to gain a first insight into failure mechanisms and shear strength of the material. During unconfined compression tests the sample was loaded with a constant rate of strain until failure occurred.

Split-ring oedometer

The oedometer stiffness E_{oed} and Poisson's ratio ν of the cement grout filtrate were determined with confined uniaxial compression tests carried out in a split-ring oedometer. This device is similar to a conventional oedometer, besides that additionally horizontal stresses are determined from deformation measurements at three points around the diameter at centre hight of the oedometer ring. Thus, the earth pressure coefficient K_0 and the Poisson's ratio ν can be investigated in addition to stiffness and consolidation properties. The oedometer ring is splitted into three sections which can be opened to build in a 20 mm heigh sample with a 54.5 mm diameter.

Samples of the cement grout filtrate were extracted from the filtration device directly after filtration was completed. The diameter of the filtration press complies with the oedometer ring and no cutting of the sample diameter was necessary. After extraction, one edge of the sample is cut straight and placed on the bottom plate of the oedometer. The three ring sections are clamped together to gain contact to the sample. The upper edge is then cut, a porous block and the top loading cap are placed on top and the sample is brought in contact with the load cell.

For each set of parameters at least one oedometer test was carried out (22 in total). The samples were loaded with constant strain rates between 3 and 4.5 % / h (CRS-test).

Drained triaxial tests

The shear strength of the filter cake material was determined with drained triaxial tests on 6 samples from the second test series. The first filtration test series found no significant influence of the initial water content of the cement grout and the grouting pressure on the properties of the filter cake. It was therefore considered appropriate to carry out triaxial tests with material with only an initial water content of 0.4 and grouting pressure of 500 kPa. The samples were built in directly after filtration was completed. After isotropic consolidation to 50, 75 or 100 kPa, a constant strain rate of $3\%/h$ was applied until a minimum strain of 10% was reached.

4.5.2 Soil mechanical properties of uncured cement grout filtrate

Material behaviour during failure

The samples loaded in unconfined compression showed brittle material behaviour during failure. The load/deformation curve was almost linear until sudden failure where diagonal failure patterns developed through the sample (Figure 4.15).

This shear plane failure pattern was also observed in most triaxial tests. However, a barrel shaped failure pattern and soft areas were also detected.

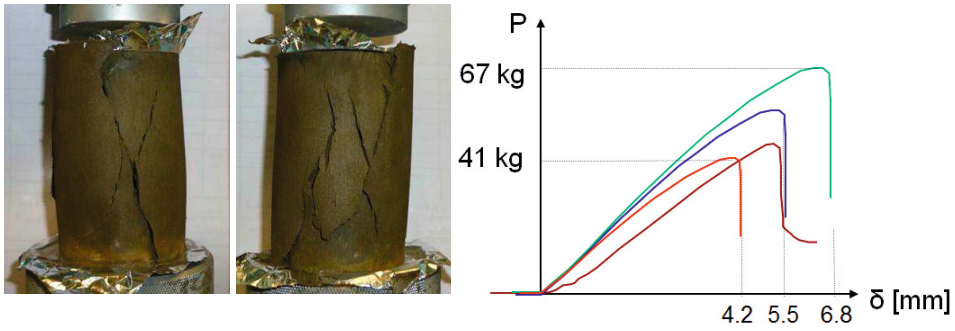

(a) 165 kPa (41 kg) (b) 265 kPa (67 kg) (c) Load/deformation curves.

Figure 4.15: Unconfined compression test results.

Oedometer Modulus E_{oed}

The constrained stiffness or oedometer modulus E_{oed} was determined from stress/strain increments during oedometer tests:

$$E_{oed} = \frac{\Delta\sigma'_v}{\Delta\varepsilon_v} \,. \tag{4.13}$$

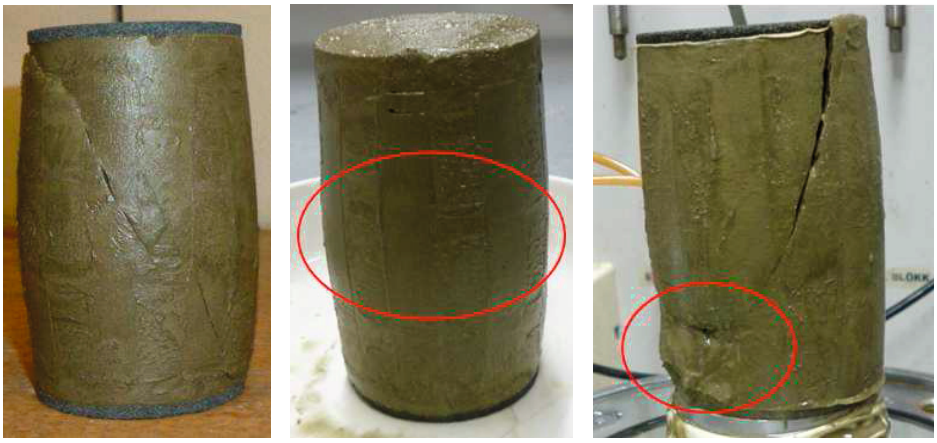

(a) Diagonal shear plane. (b) Barrel shape, soft centre region. (c) Shear plane with soft region at bottom.

Figure 4.16: Failure patterns observed during triaxial tests.

The test results showed a clear stress dependency of the stiffness. E_{oed} was expressed with the power function

$$E_{oed} = E_{oed,ref} \left(\frac{\sigma'_v}{\sigma_{ref}} \right)^m . \tag{4.14}$$

This formulation is usually used to describe soils and the exponent m varies with the soil type. Usually, m ranges from 0.3 to 0.7 for gravel, sand, or coarse silt, while a linear stress dependency is observed for normally consolidated clay (m = 1). A constant stiffness is often assumed for overconsolidated clay (m = 0). The oedometer moduli versus vertical effective stress are presented in Figure 4.17 for cement grout filtrates produced at different grouting pressures. E_{oed} increases with vertical stress level and using Equation (4.14) an exponent m = 0.75 fits well with the test data at primary loading. The reference stiffness $E_{oed,ref}$ at a reference stress $\sigma_{ref} = 100kPa$ ranges from 10 to 13.5 MPa (shaded area). Similar to overconsolidated clay, at vertical stresses below grouting pressure, oedometer moduli are higher than for primary loading, but return to the primary loading branch at stresses above grouting pressure levels. The oedometer stiffness on the primary loading branch seems independent on the level of grouting pressure and initial cement grout water content.

Young's Modulus E_{50}

The Young's Moduli E_{50} were determined from triaxial tests at different cell pressures σ'_h with

$$E_{50} = \frac{q_{50}}{\varepsilon_{v,50}}, \tag{4.15}$$

where q_{50} is 50% of the maximum deviatoric stress and $\varepsilon_{v,50}$ the corresponding strain.

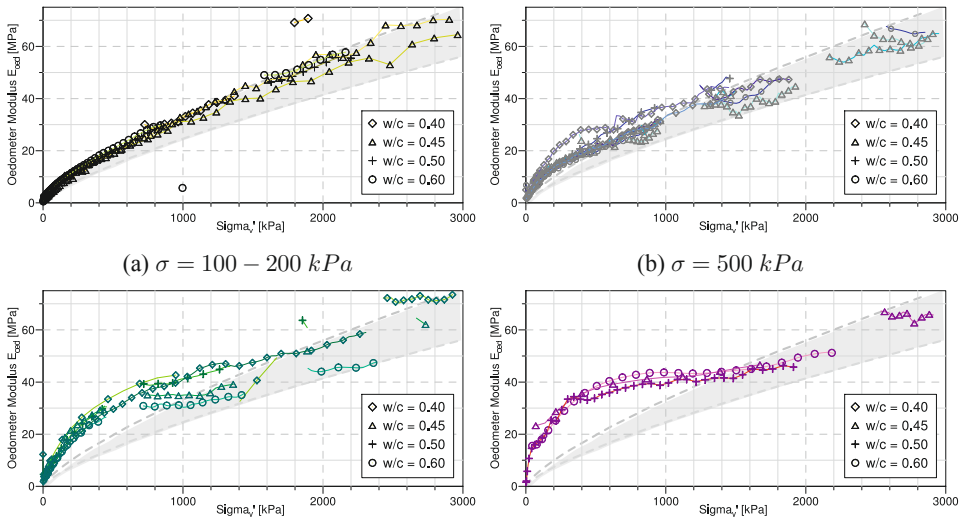

(a) $\sigma = 100 - 200\ kPa$ (b) $\sigma = 500\ kPa$

(c) $\sigma = 1000\ kPa$ (d) $\sigma = 1500\ kPa$

Figure 4.17: Oedometer modului E_{oed} at primary loading, for cement grout filtrates of different grouting pressures. Range of primary loading branches of all tests indicated by shaded area.

Equivalent oedometer moduli $E_{oed,eq}$ were calculated from E_{50} with

$$E_{oed,eq} = E_{50} \frac{1-\nu}{(1-2\nu)(1+\nu)}\ , \tag{4.16}$$

assuming a Poisson's ratio $\nu = 0.24$ as determined from split-ring oedometer tests (see following section). Results are presented in Table 4.2. The equivalent oedometer moduli determined from triaxial tests are similar to the oedometer test results for stresses below grouting pressure: they are slightly higher than the stiffness at primary loading and show some preconsolidation due to the grouting process.

Table 4.2: Stiffness moduli from triaxial tests.

Test Name	Filtration pressure kPa	Cell pressure σ_h kPa	E_{50} MPa	$E_{oed,eq}$ MPa
2-3-1	500	50	19.8	
2-4-1	500	100	17.9	21.1
2-4-2	500	50	15.2	17.9
2-5-1	500	75	21.8	25.7
2-5-2	500	75	21.8	25.7

Poisson's ratio

The Poisson's ratio was determined from split-ring oedometer tests, using stress increments:

$$\nu = \frac{\Delta\sigma_3'}{\Delta\sigma_3' + \Delta\sigma_1'} \,, \tag{4.17}$$

where σ_1' and σ_3' are the maximum and minimum principal stresses. Results presented in Figure 4.18 show a considerable variance during the tests, but a value of $\nu = 0.24$ as mean value throughout all tests could be estimated as reasonable value.

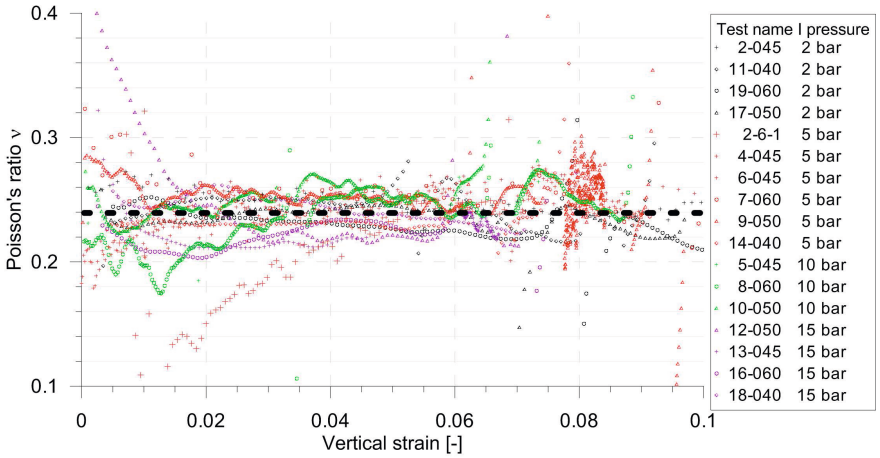

Figure 4.18: Poisson's ratio ν of cement grout filtrate.

Shear strength

The shear strength of the fresh cement grout filtrate was determined from drained triaxial tests with isotropic consolidation. As shown in Figure 4.19, a Mohr-Coulomb failure line with a friction angle φ = 38° and cohesion c = 30 kPa was determined from the maximum shear stress.

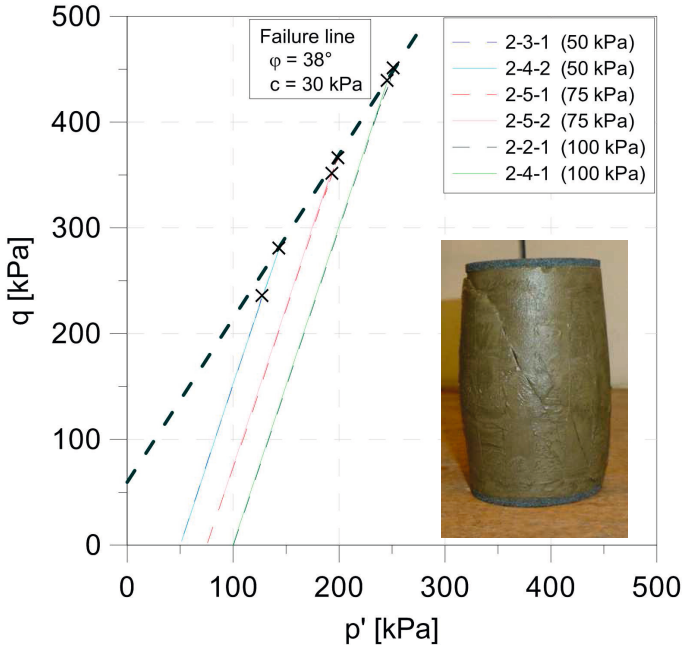

Figure 4.19: Drained triaxial test with isotropic consolidation. Test results and typical failure pattern.

4.6 Chapter summary

In a series of laboratory tests the filtration behaviour of cement grout was investigated. With increasing pressure the rate of filter cake build-up increased due to higher pressure gradients in the sample. However, the initial water content correlates negatively with the filtration time, as more water has to be expelled. The filter cakes void ratio decreased with increasing filtration pressure, as was to be expected for granular materials. For pressures above 500 kPa, the variation of test results was too large to confirm this trend. Interestingly, the initial water content of the cement grout influenced the void ratio and permeability of the filter cake. This effect was initially referred to the test set-up, but another explanation is a higher agglomeration of cement particles occurring during mixing for grouts with higher initial water contents. The agglomeration of grains leads to larger effective grain sizes and in turn to a higher porosity and therefore permeability.

It was found that in the test range the influence of calculation parameters, such as grouting pressure and initial water content, on the filtration and consolidation behaviour of the cement grout was small compared to the variation of test results. Therefore, no general correlations between all parameters could be determined. However, even though grouting pressure has little influence on filter cake properties, the value of grouting pressure could still affect the stress state and conditions of the surrounding soil.

During filtration tests with sand filter, it was observed that cement particles did not infiltrate the sand. Empirical methods to estimate groutability or filter stability by comparing grain size fractions confirm a negligible small amount of standard Portland cement infiltration. Furthermore, the sand filter does not influence the filtration behaviour of cement grout, due to its high permeability. As no infiltration of cement particles into the sand takes place, this high permeability is maintained and during grouting in sand free drainage can be assumed.

It was found that the cement filter cake behaves as granular material and can be described in terms of soil mechanical properties. An internal friction φ of $38°$ and a cohesion of $c = 30\ kPa$ was detected from triaxial tests. The stiffness for primary loading could be described by a stress dependent power function with an exponent m = 0.75 which lies between values common for clay (m = 1.0) and sand (m = 0.5). For stress states below grouting pressure a slightly higher stiffness was found due to the pre-consolidation of the material during to grouting.

The material properties were determined for fully consolidated material. In-situ filter cake material could exhibit lower strength and stiffness properties, if it was not pressurised long enough for full consolidation.

A distinct phase change of the grout from liquid to plastic was observed at a water content roughly around 38 %. The filtration process is a combination of filtration and consolidation. In a first phase water is expelled from the liquid grout until cement particles contact each other and a solid filter cake is created. This filter cake material transfers effective stresses and due to the applied pressure consolidates further.

Both models, the two-phase filtration model and consolidation theory could be used to back-calculate the filtration tests and roughly estimate filter cake thickness with time. The two-phase filtration model is based on a clear distinction between grout and filter cake, while in the consolidation approach the expulsion of water is associated with the dissipation of excess pore pressure which happens gradually. While in the filtration approach the pore pressures on top would theoretically stay constant until the piston reaches the filter cake, they decrease gradually from the beginning when using the consolidation approach. The processes taking place during filtration of cement grout turned out to be a combination of filtration and consolidation processes, and therefore the two basic models represent an upper and lower limit. The variation of test results was higher than the influence of grouting pressure and initial water content and therefore calculation parameters were determined from mean values of all tests. One set of parameters ($k_{fc} = 7.5 \times 10^{-8}\ m/s$ and $w/c_{fc} = 0.3$) gives reasonable results for the back-calculation with the filtration model. For the consolidation model the coefficient of consolidation c_v had to be adjusted to the grouting pressure. The results of all tests are very close to each other and the calculation parameters for both models are sufficient to roughly estimate the filtration time for the presented filtration tests. However, it seems that the filtration approach describes the test results slightly more accurate. And even though using consolidation theory would be convenient since it is readily

available in common finite element programs for geotechnical applications, it is less suitable for more general cases where the grouting pressure changes with time. Here, the calculation parameters for consolidation theory need to be adjusted to the grouting pressure, whereas one general set of parameters is sufficient filtration approach.

Chapter 5

Installation effects - Field measurements

5.1 Introduction

This chapter presents in-situ measurements of three test sites, which were conducted to gain a better understanding of the processes taking place during grouting of ground anchors in non-cohesive soils. Pressure levels were therefore measured within the grout and the surrounding soil during and after anchor installation. It was aimed to investigate the proportion of the grouting pressure acting as effective stresses on the soil during grouting and how stresses develop after grouting pressure is released. Pressure levels within the grout were measured with customised pressure sensors attached to the anchor tendon. To investigate the effect of grouting on the adjacent soil, flat dilatometer (DMT) and cone penetration (CPT) soundings were carried out close to the grouted length. Additionally, pore water pressures were measured during installation of nearby anchors. All three test sites are located in different parts of Germany and provided similar ground conditions where the grout bodies of the anchors were installed in sands.

5.2 Test sites and test programme

5.2.1 Test site Dörverden

In Dörverden, vertical micropiles were used as uplift control for a ship-lock excavation pit. During grouting of two piles, pressure measurements were taken inside the borehole. The vertical tension piles are approximately 18.15 m long, with 0.2 m grout body diameter. The planned grout body length was 14.65 m, ranging from 15.95 to 30.6 m below ground level. At the time of pile installation the excavation depth of the pit was 13.4 m below ground level and the water level in the pit approximately 0.65 m below ground level. Drilling and grouting was performed from a floating platform.

Site description

The soil investigation report (Schwab, 2008) identifies following soil layering in the ship lock area: First, an approximately 7 m thick fill of clayey silts with some thin sand interlayers. Below this layer, two sand layers were found, which are partly separated by an intermediate silty gravelly layer. In both sand layers coal inclusions were found with a thickness of several cm. The 'Upper Sands' layer, extending from approximately 7 to 15 m below surface, consists of medium sands, partly with fine or medium gravel fractions. In this layer two gravelly areas were detected. An 'Intermediate Layer' with varying fractions of silty clay and gravelly sands separates the two sand layers. In the region relevant for the test piles this layer is 1 - 2 m thick. Below extends a further sand layer ('Lower Sands') which is the relevant layer in which the micropile grout bodies are located. The 'Lower Sands' layer consists of narrow graded, fine sands, with a medium sand fraction (5.1). The sand grains have a round-edged, compact shape. CPT soundings showed high to very high tip resistance from 12 to 50 MPa. Soil parameters for the described soil layers are presented in Table 5.1.

Table 5.1: Soil properties at the test site in Dörverden.

Layer		Fill	Upper Sands	Interm. Layer	Lower Sands
Thickness	[m]	0-7	5-15	0-5	>25
Wet density	γ [kN/m^3]	19	18	18	18
Buoyant density	γ' [kN/m^3]	10.5	11	10.5	10.5
Permeability	k [m/s]	5×10^{-6}	1×10^{-4}	1×10^{-8}	5×10^{-4}
Undrained friction angle	$\varphi_{u,k}$ [°]	0	—	0	—
Undrained cohesion	$c_{u,k}$ [kPa]	40	—	100	—
Effective friction angle	φ' [°]	22.5	35	25	37.5-40
Effective cohesion	c' [kPa]	7.5	0	20	0

Micropile installation

The installation process of micropiles used in Dörverden is identical to installation of grouted ground anchors except that the fixed anchor length is not separated from the free anchor length by flushing. With a water level of 12.75 m above building pit bottom, the drill-rig was placed on a swimming platform to install the piles. The installation process is illustrated in Table 5.2 and Figure 5.10. The borehole was drilled using duplex drilling with internal flushing. After drilling, the inner drill rods were withdrawn while the outer casing was left to support the borehole walls. The borehole was then filled with cement grout and

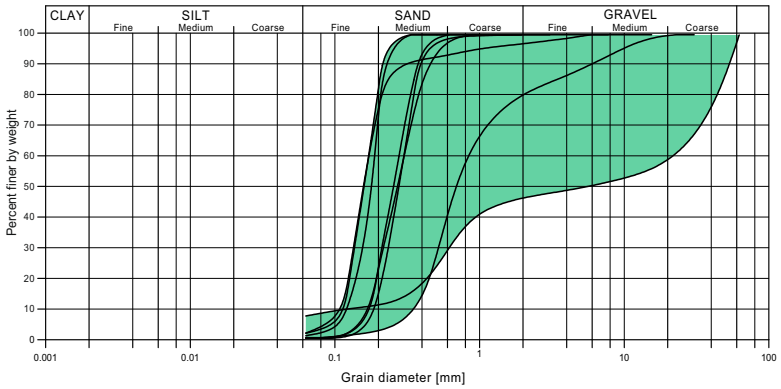

Figure 5.1: Grain size distribution of the ‘Lower Sands’ layer in Dörverden.

the GEWI steel rod was build in. For the grout, blast-furnace cement (Holcim-Duo 4 N Hochofenzement CEM III/A 42,5 N) was used with w/c = 0.5. The first casing section of 3 m was withdrawn and after applying the grouting cap, grout was pumped into the borehole with a pressure of up to 30 bar (measured at the cement pump). After a pressure of 30 bar was reached at the pump grouting was stopped and the next section of 3 m withdrawn and grouted. This procedure was repeated until 5 sections of 3 m were withdrawn and a length of 15 m was grouted. Measurements were taken during grouting, when the grouting cap was attached to the drill casing.

5.2.2 Test site Venhaus

In preparation of a reconstruction project of the ship lock Venhaus, a trial sheet-pile wall excavation pit with nine trial anchors was build on-site. Pressure measurements inside the borehole were conducted during grouting of three anchors. Additionally, stress changes in the soil next to the grout body were recorded during grouting of three anchors, using stationary flat dilatometer tests (DMTA). Also standard dilatometer tests were carried out next to two anchors, before and after anchor installation. The anchors in Venhaus are 19.5 m long, with nine strands. The drill casing diameter was 133 mm, the drill bit 141 mm, what is assumed as grout body diameter. The grouting length of the trial anchors varied in order to investigate the grout body length influence. Six anchors were planned with a grouted length of 5 m, three of these anchors were flushed to create a clear distinction between anchor body and free anchor length, while the other three were not flushed. The three remaining anchors were planned with a grouted length of 9 m and flushing. The dip angle of the anchors is 35°.

Site description

In the soil investigation report (Altenhöfer, 2013) following soil layering and parameters were identified in the area of the anchor tests: The first 2 to 3 m below ground level are

Table 5.2: Description of micropile installation process in Dörverden.

Step	Position from micropile end	Process description
①		Duplex drilling
②		Withdrawal of inner drill rods
③		Filling borehole with cement suspension
④		Install GEWI steel bar
⑤	0-3 m	Withdrawal of 1st drill casing section
⑥	0-3 m	Grouting
⑦	3-6 m	Withdrawal of 2nd drill casing section
⑧	0-6 m	Grouting
⑦	6-9 m	Withdrawal of 3rd drill casing section
⑧	0-9 m	Grouting
⑦	9-12 m	Withdrawal of 4th drill casing section
⑧	0-12 m	Grouting
⑦	12-15 m	Withdrawal of 5th drill casing section
⑧	0-15 m	Grouting
⑫		Removal of remaining sections

backfill materials consisting of sands, partly with organic and gravel fractions. Below this layer lies a narrow graded, medium to fine sand layer with medium to dense packing, in which the grout bodies of all anchors are located. The grain size distribution of the relevant sand layer is presented in Figure 5.2. In the sand layer, isolated, small gravelly or silty sand lenses were found. The layer reaches to a depth of around 15 m below ground. Below lies a transition zone of slightly plastic, sandy clay with irregular thickness between 0 to 1.4 m, followed by marly claystone with varying degrees of decomposition. The groundwater level was found approximately 3 m below ground level. Soil properties are given in Table 5.3. While for the fill only estimated values are given, the values for the other layers were determined from CPT correlations and geotechnical assessment of soil samples.

Table 5.3: Soil properties at the test site in Venhaus.

Layer		Fill	Medium Sands	Sandy Clay	Marly Claystone
Thickness	[m]	2-3	12-13	0-1.4	–
Wet density	γ [kN/m^3]	18	18	21	23
Buoyant density	γ' [kN/m^3]	10	10	11	13
Permeability	k [m/s]	–	1×10^{-4} – 1×10^{-3}	1×10^{-10} – 1×10^{-9}	1×10^{-9} – 5×10^{-6}
Effective friction angle	φ' [°]	30	35	25	25
Effective cohesion	c' [kPa]	0	0	5	20

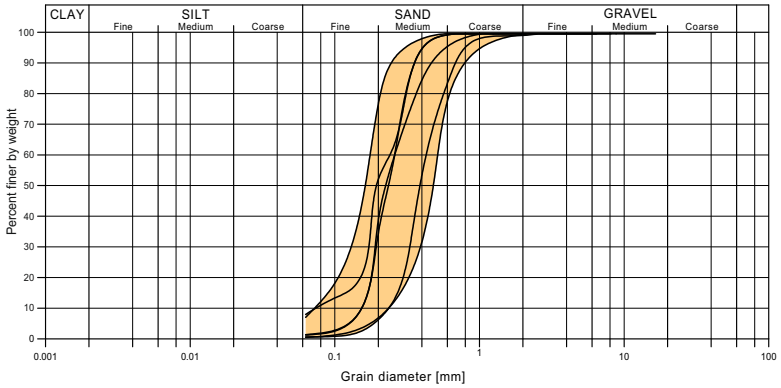

Figure 5.2: Grain size distribution of the sand layer in Venhaus.

Anchor installation

The anchor installation process in Venhaus is illustrated in Table 5.4. It was similar to micropile installation in Dörverden, except different anchor dimensions and inclination. For

the grout standard Portland cement (CEM I 42,5 R) was used with w/c = 0.45. The borehole was drilled using duplex drilling with auger. After drilling to the desired depth, the inner drill rods were withdrawn and the outer casing left to support the borehole walls. The tendon was installed in the borehole which was then filled to 50 % with cement grout. It was found that the cement grout filtered very fast in the given soil conditions, so that the first 2.5 m of casing were withdrawn without pressurising the grout. In one case, pressure was applied in the first meters which led to a blockage of the tendon inside the drill-casing. When the casing was withdrawn, the tendon was pulled out of the borehole. This was explained by the filtration of cement grout inside the drill-casing, building a blockage between tendon and drill-casing. After removing the first 2.5 m of drill-casing, the borehole was filled with grout completely and grouting pressure up to 10 bar was applied to the grout while the next casing section of 1.5 m was withdrawn. Just before the full length of a section was withdrawn and removed, the pressure was released. This procedure was repeated 5 times, until the full length of 9 m was grouted. Then, the borehole was flushed and benotnite was filled into the borehole to support the soil before the remaining casing sections were removed.

Table 5.4: Description of anchor installation process in Venhaus.

Step	Position from distal anchor end	Process description
①		Duplex drilling
②		Withdrawal of inner drill rods
③		Installing anchor into borehole
④		Filling borehole to 50 % with cement suspension
⑤	0 - 2.5 m	Withdrawal and removal of drill casing section 1 and 2
⑥		Filling borehole to 100 % with cement suspension
⑦	2.5 - 4.0 m	Grouting while 1.5 m of casing is withdrawn
⑧		Removal of 3rd casing section
⑨	4.0 - 5.5 m	Grouting while 1.5 m of casing is withdrawn
⑩		Removal of 4th casing section
⑪	5.5 - 7.0 m	Grouting while 1.5 m of casing is withdrawn
⑫		Removal of 5th casing section
⑬	7.0 - 8.5 m	Grouting while 1.5 m of casing is withdrawn
⑭		Removal of 6th casing section
⑮	8.5 - ca. 9.5 m	Grouting while 1 m of casing is withdrawn
⑯	10.0 m	Flushing of free anchor length and filling with bentonite
⑰		Removal of remaining sections

5.2.3 Test site Horstwalde

On the test site in Horstwalde, grouted anchors were used to tie down a test apparatus for loading piles. At this site, pressures were measured within the borehole during grouting of five anchors. Additionally, the effect of grouting on the surrounding soil was investigated with pore pressure measurements, stationary dilatometer tests (DMTA) and CPT soundings.

The anchors in Horstwalde are 19.5 m long with a 6 m long grout body. The boreholes were drilled with an inclination of 10°, using external flushing. The outer diameter of the drill casing was 133 mm, but the actual anchor diameter could be larger due to external flushing.

Site description

In Horstwalde, the soil investigation was conducted up to a depth of 25 m (Bergholz, 2011). Below a 0.5 to 1 m thick humus layer, medium sands were found which were divided into three main layers: 'Upper Sands', 'Intermediate Sands', and 'Lower Sands'. The Upper Sands reach until 8 to 9 m below ground level and consist of dense, fine to medium sand with a small coarse fraction. Within this layer a thin layer of sandy, clayey silt was found at a depth of 6 m below ground level. From 8 to 9 m below ground the Intermediate Sands consisting of medium sands with less fines content extends to a depth of 16 to 17 m. CPT soundings show a significantly lower resistance in this layer than in the Upper Sands. Below 16 to 17 m until the investigation depth of 25 m, the Lower Sands, medium sands with more coarse fractions were found. Varying CPT tip resistance in this layer shows the existence of gravel in some places, which was also detected during sampling. The grout bodies of the anchors are mainly located in the Intermediate Sand layer and lie partly in the Lower Sands. The general groundwater level was found between 1.5 to 3 m below ground level, during the test period the groundwater level was determined on two days with 1.6 and 1.9 m below ground level. Determined soil properties from the soil investigation programme are presented in Table 5.5.

Table 5.5: Soil properties at the test site in Horstwalde.

Layer		Upper Sands	Intermediate Sands	Lower Sands
From depth	[m from GL]	0.5 - 1	8 - 9	16 - 17
To depth	[m from GL]	8-9	16-17	–
Wet density	γ [kN/m^3]	18	16.5	17.5
Buoyant density	γ' [kN/m^3]	10.5	9	10
Permeability	k [m/s]	9×10^{-5} – 3×10^{-4}	2×10^{-4} – 6×10^{-4}	3×10^{-4} – 2×10^{-3}

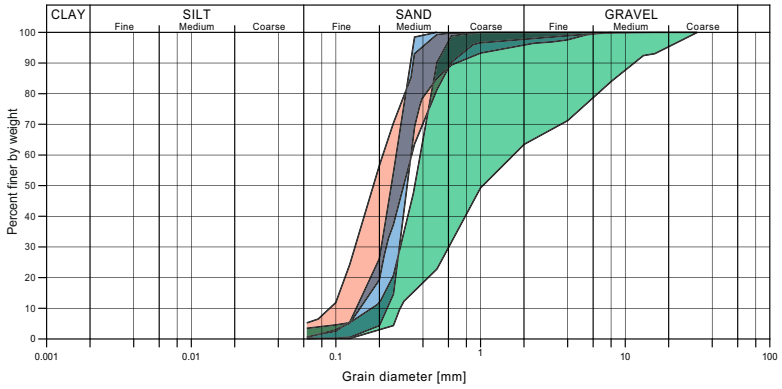

Figure 5.3: Grain size distribution in Horstwalde: Upper Sands (red), Intermediate Sands (blue), and Lower Sands (green).

Anchor installation

The boreholes were drilled with external flushing as illustrated in Figure 5.4. Flushing liquid was a cement/water suspension with w/c = 3.3. After drilling, the borehole was filled to 50% with cement grout with w/c = 0.45. Bentonite was added to the cement in small quantities. The borehole was filled with grout completely after the tendons were placed. Then, 1 m of drill casing was withdrawn and the grouting process started. While the drill casing sections were withdrawn from the borehole, the pressure was increased by pumping more grout into the borehole until a pressure 5 to 8 bar was reached or the rotation resistance of the drill casing increased significantly. Each section of 4 m was grouted continuously, then the pressure was released and the section built out. After grouting was completed at a length of 7 m, water was flushed into the drill-rods to create a defined fixed anchor length.

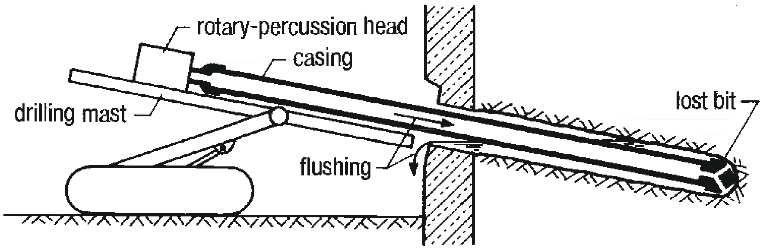

Figure 5.4: Rotary drilling with lost bit crown and external flushing from Ostermayer and Barley (2002).

Table 5.6: Description of anchor installation process in Horstwalde.

Step	Position from distal end	Process description
①		Rotary drilling with external flushing
②		Knocking off lost crown
③		Filling borehole to 50% with cement suspension
④		Install anchor
⑤		Fill borehole with cement suspension
⑥	1 m	Withdrawal of approx. 1 m casing
⑦	1 - 4 m	Grouting while 3 m of casing is withdrawn
⑧		Removal of first casing section
⑨	4 - 7 m	Grouting while 3 m of casing is withdrawn
⑩	7 - 8 m	1 m of casing is withdrawn
⑪		Removal of second casing section
⑫	8 - 19 m	Flushing and removal of sections

5.3 Test methods

5.3.1 Pressure measurements within the borehole

For measuring grouting pressures within the borehole during anchor installation, measurement equipment had to be customised and a certain test set-up was developed for each site. It was aimed to keep the installation process as close as possible to 'real life' conditions and to minimise delays and alternations due to testing. Therefore, pressure sensors, cables, and connections had to resist pressures up to 30 bar and rough treatment during anchor installation. The sensors also had to be very small due to limited space available between the anchors' tendon and the casing. Depending on the drill-rig used, a way had to be found to connect the sensors to a data logger, as the drill-rig and drill casing build a closed system during grouting.

At the first test site in Dörverden, an 'off-the-shelf' pore water pressure sensor was used. A gel pad was applied to the sensor tip to prevent cement particles blocking the water filter and to enable the measurement of total stresses within the grout (Figure 5.5). Due to their size, the sensors were attached parallel to the anchor tendon to fit them into the drill casing. Therefore, measurements were only taken in vertical direction.

To enable pressure measurements in radial direction of the anchor body, smaller, customised pressure sensors were developed for the tests in Venhaus (Figure 5.6). A very small piezoresistive pressure transducer was attached to a steel plate, which could be mounted

Figure 5.5: Pore pressure sensor used for measurements in Dörverden. The gel pad allows measurement of total stresses.

on the tendon. A layer of silicone compound applied in a mould on top of the transducer protected the very thin transducer membrane against damage from solid particles. The composition of the compound was chosen to be flexible enough to not influence the readings. Additional protection was achieved by placing a spacer just above the sensor (Figure 5.6c). At the tests site in Horstwalde, slightly more space was available within the borehole and it was possible to fit two transducers into one sensor, facing in radial and parallel direction. This made a comparison of radial and vertical stresses possible.

Depending on the drill-rig and grouting procedure deployed at the test sites, individual solutions were developed to connect the sensors to a data logger in order to record the measured data. At the first test site in Dörverden, a grouting cap was placed on top of the drill casing and grout was pumped into the borehole through a hose attached to the grouting cap (Figure 5.7). After grouting of each section, the cap was removed and the drill casing section withdrawn and built out. For testing, a special grouting cap was designed where the cables were led outside the drill casing to connect the sensors to an external data logger. After grouting, the cables were disconnected again and placed inside the casing, so that it could be attached to the drill-rig and be withdrawn. A swimmer was attached to the cables to keep them on the surface.

In contrast to the site in Dörverden, a continuous anchor installation process was employed at the sites in Venhaus and Horstwalde. Here, grout was pumped into the borehole through the drill-rig while the casing sections were withdrawn. The drill-rig and casing built a closed system and it was not possible to lead cables out of the casing to connect to a data logger. Therefore, miniature data loggers were used and placed inside a steel casing together with a 9 V block battery (as power supply for the sensors). The container was attached to the tendon and fitted into the drill casing completely (Figure 5.8). With this closed system solution, data

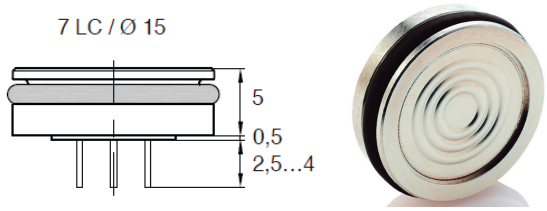

(a) Piezoresistive pressure transducer [mm].

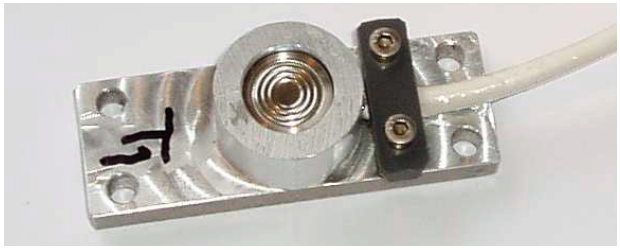

(b)

(c)

Figure 5.6: Customised pressure sensor measuring in radial direction (b), attached to the anchor (c).

Figure 5.7: Modified grouting cap used to pump grout into the borehole in Dörverden.

was recordable continuously during the whole installation process. The system, however, was much more vulnerable to failure because the containers had to be watertight to more than 20 bar. The employed data loggers had the size of a common USB stick and could record on four channels. Therefore, pressure was measured either in vertical and radial direction at two positions, or in radial direction in three positions. In the latter case, temperature transducers were included into one of the sensors, and the remaining channel was used to record temperatures during anchor installation.

Figure 5.8: Casing for data logger and power supply attached to the tendon.

5.3.2 Flat Dilatometer Tests (DMT and DMTA)

Flat dilatometer tests (DMT) were conducted close to the anchors grout body to investigate the stress changes in the surrounding soil due to grouting.

The flat dilatometer or 'Marchetti Dilatometer' was initially developed by S. Marchetti to investigate the stiffness modulus E of a soil for laterally loaded driven piles (Marchetti, 1975). But it was also found useful as pressure sensing element, when the dilatometer test is modified and the blade is kept at one constant position and several measurements are taken one after another over a period of time (Stationary DMTA test, see Marchetti et al. (2001))

The DMT test can also be used for compaction control by comparing results before and after soil treatment. Schmertmann (1988) found that the degree of compaction can be detected and Marchetti et al. (2001) states that the DMT is better suited for compaction control than CPT because the increase of the dilatometer modulus M_{DMT} is more distinctive than the increase of tip resistance q_c in a CPT test.

Figure 5.9a shows the flat dilatometer blade consisting of a steel blade with a flat circular membrane in one of its sides. The blade is pushed into the ground (similar to a CPT cone) and at testing depth the membrane is inflated and pressures are measured at different membrane positions (Figure 5.9b). During a standard dilatometer test (DMT) the blade is then pushed to the next test position (usually 30 cm) and the procedure is repeated. For stationary DMTA

measurements, the blade is kept at a constant position and a series of readings is taken one after another over a period of time. Due to its flat shape, the dilatometer blade causes less disruption than a CPT cone when pressed into the ground. However, some stress changes still occur and in the beginning of the stationary test, directly after DMT insertion, several readings are required until the values stabilise.

The parameters gained from DMT are used in several correlations to obtain soil properties, such as compressibility and soil behaviour classification. The dilatometer has been used and calibrated for various different soil types. A comprehensive description of the working principle, the application possibilities and correlations of the DMT is given in Marchetti et al. (2001).

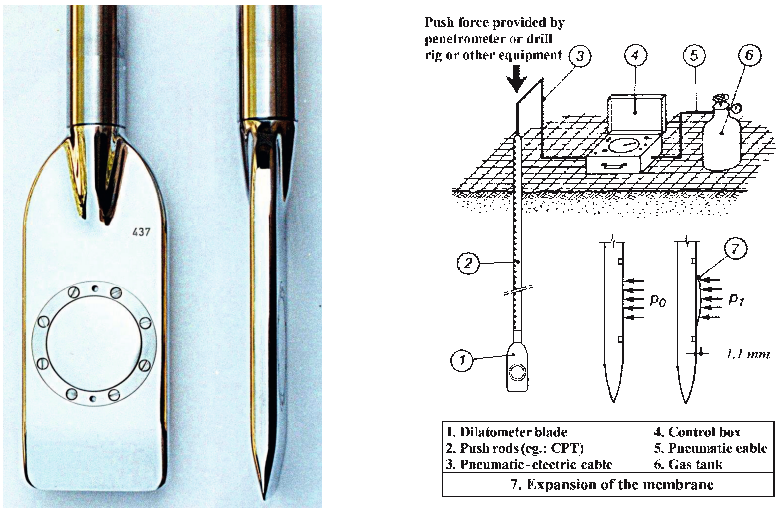

(a) Dilatometer blade, front and side view. (b) General layout of Dilatometer test.

Figure 5.9: Flat Dilatometer testing from Marchetti et al. (2001).

Interpretation of test results

The Flat Dilatometer measures three pressures, each corresponding to a certain membrane position. The first value ('A-reading') is the pressure needed to inflate the membrane to position A, where the membrane is in line with the dilatometer blade. The second value ('B-reading') is the pressure needed to inflate the membrane 1.1 mm outwards of the dilatometer blade to position B. The third value ('C-reading') is the pressure where the membrane returns back to position A. To avoid plastic soil deformations, inflating the membrane to position B is omitted during stationary dilatometer tests (DMTA). The pressures p_0 and p_1 acting on the membrane/soil interface at position A and B are determined by correcting the readings with

correction factors for the test equipment

$$p_0 = 1.05(A - Z_M + \Delta A) - 0.05(B - Z_M - \Delta B) \tag{5.1}$$

and

$$p_1 = B - Z_M - \Delta B, \tag{5.2}$$

where Δ A and Δ B are the correction factors determined from pressures necessary to reach position A and B when the blade is in air contact. Z_M is the pressure gage reading at atmospheric pressure. The correction factors were determined for each DMT blade prior each test.

During stationary DMTA tests, only A values are taken and therefore only pressure variations are determined as the B-readings are required in order to estimate absolute stresses. Provided that the A readings have stabilised sufficiently after insertion of the dilatometer blade, the change ΔA represents the change of total stresses $\Delta\sigma$ in the soil.

For interpretation of DMT tests, two dilatometer parameters were directly determined from p_0 and p_1: The material index

$$I_D = \frac{p_1 - p_0}{p_0 - u_0} \tag{5.3}$$

and the horizontal stress index

$$K_D = \frac{p_0 - u_0}{\sigma'_{v0}}, \tag{5.4}$$

where u_0 is the assumed pre-insertion pore pressure and σ'_{v0} the assumed pre-insertion overburden stress. With these direct DMT parameters, further soil parameters can be determined, using correlations for different soil types. In this study, the coefficient of earth pressure $K_{0,DMT}$ and the friction angle φ'_{DMT} were determined. φ'_{DMT} was estimated with

$$\varphi_{save,DMT} = 28^\circ + 14.6^\circ log K_D - 2.1^\circ log^2 K_D \tag{5.5}$$

as proposed by Marchetti et al. (2001). It is stated that the correlation is not as precise as correlations using additional CPT data, but gives a good lower bound value. This is reasonable, because it is looked for relative changes of values before and after grouting rather than for precise soil parameters.

Due to the stress change during insertion of the dilatometer blade, the horizontal stress index K_D differs from the in-situ coefficient of earth pressure $K_{0,DMT}$. Various correlations are available to determine $K_{0,DMT}$ from K_D in clays, but for sands K_0 also depends on the friction angle φ and relative density D_r, and therefore K_0-K_D correlations are not applicable (Marchetti et al., 2001). For the interpretation of the test results a $K_0 - K_D - \varphi$ correlation

was adapted from Schmertmann (1983), using $\varphi_{save,DMT}$ estimated with 5.5:

$$K_0 = \frac{40 + 23K_D - 86K_D(1 - sin\varphi) + 152(1 - sin\varphi) - 717(1 - sin\varphi)^2}{192 - 717(1 - sin\varphi)} . \quad (5.6)$$

For comparison also a $K_0 - K_D - q_c$ correlation was used as recommended by Marchetti et al. (2001):

$$K_0 = 0.376 + 0.095K_D - 0.002\frac{q_c}{\sigma'_v 0} , \quad (5.7)$$

where q_c is the tip resistance from a CPT test in the same soil. Although it is difficult to determine $K_{0,DMT}$ in sands, Marchetti et al. (2001) state that the $K_{0,DMT}$ profile can be estimated appropriately, even though the $K_{0,DMT}-$values might not be correct.

5.4 Field test results

5.4.1 Measurements in Dörverden

Test set-up

In Dörverden two micropiles were instrumented with three pressure sensors each. The pressure sensors described in Section 5.3.1 were attached to the GEWI steel bars at distances of 1, 7, and 13 m from the distal end of the anchor, with the measuring membrane facing downwards. The sensors were connected to a data logger through cables. These led to a data logger through a special grouting cap which had to be removed for withdrawal of the casing sections. Therefore, measurements were only taken during grouting but were interrupted during withdrawal and removing of the drill sections. Measurements were taken after the anchor was placed into the borehole, during each grouting stage and when installation was completed. The micropiles were grouted in 5 stages of 3 m, as illustrated in Figure 5.10.

Pressures measured inside the borehole

The measured total stresses during grouting of the two micropiles GEWI1 and GEWI2 are presented in Figure 5.11 and Figure 5.12 respectively. They are compared to the theoretical hydrostatic suspension pressure (green lines) and to pore pressures (blue lines), which were calculated from suspension weight and groundwater level. The reference time starts with the mixing of the cement grout, although during grouting of the anchors new grout was mixed consistently. Grouting of each section took less than 1.5 minutes. After grouting of one section the measurements had to be interrupted for approximately 20 minutes, when the section was built out.

The first measurement was taken directly after filling the borehole with grout and placing the pile into the borehole and the pressures were consistent with the theoretical suspension pressure at all positions. But 30 to 60 minutes after filling the grout into the borehole,

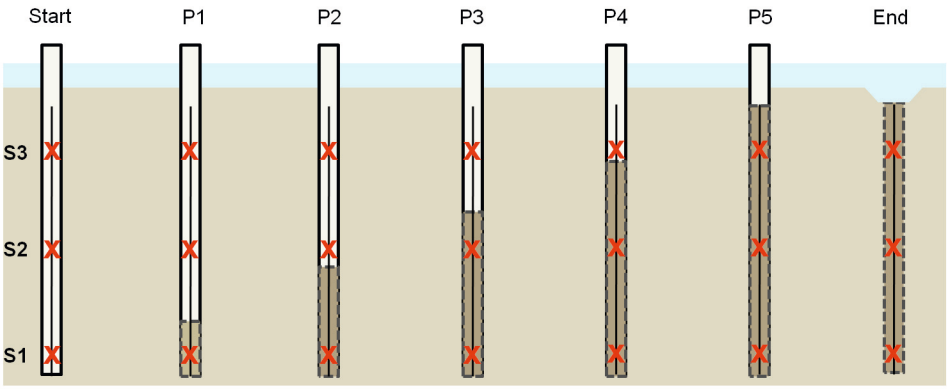

Figure 5.10: Installation of a grouted micropile in 5 grouting steps.

(a) Top sensor S3, 13 m from distal anchor end.

(b) Middle sensor S2, 7 m from distal anchor end.

(c) Bottom sensor S1, 1 m from distal anchor end.

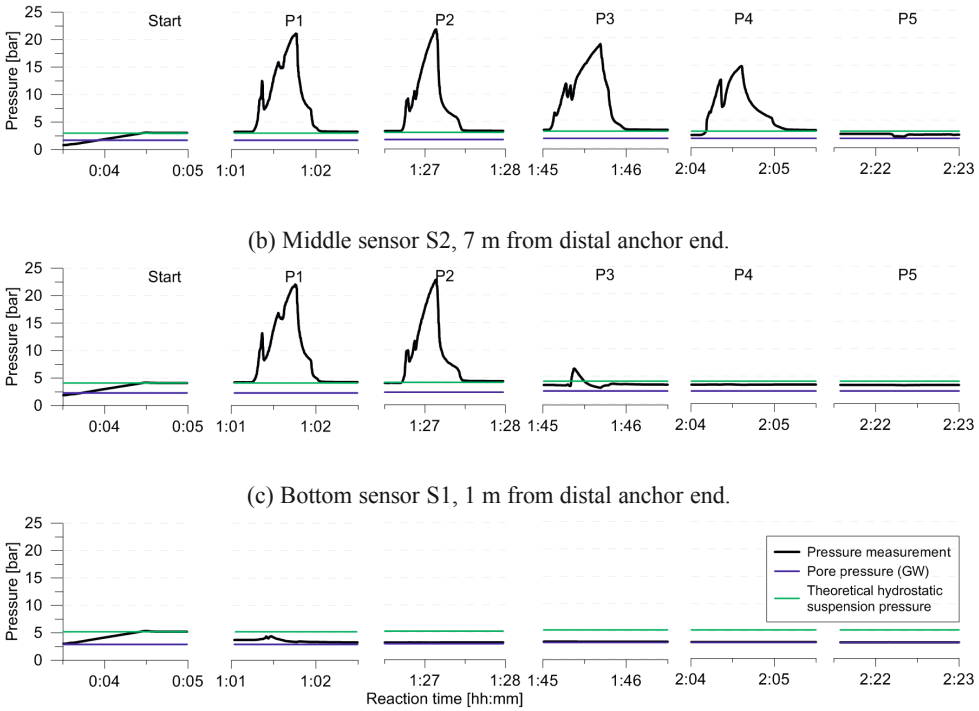

Figure 5.11: Pressure measured inside the borehole during installation of micropile GEWI1 in Dörverden.

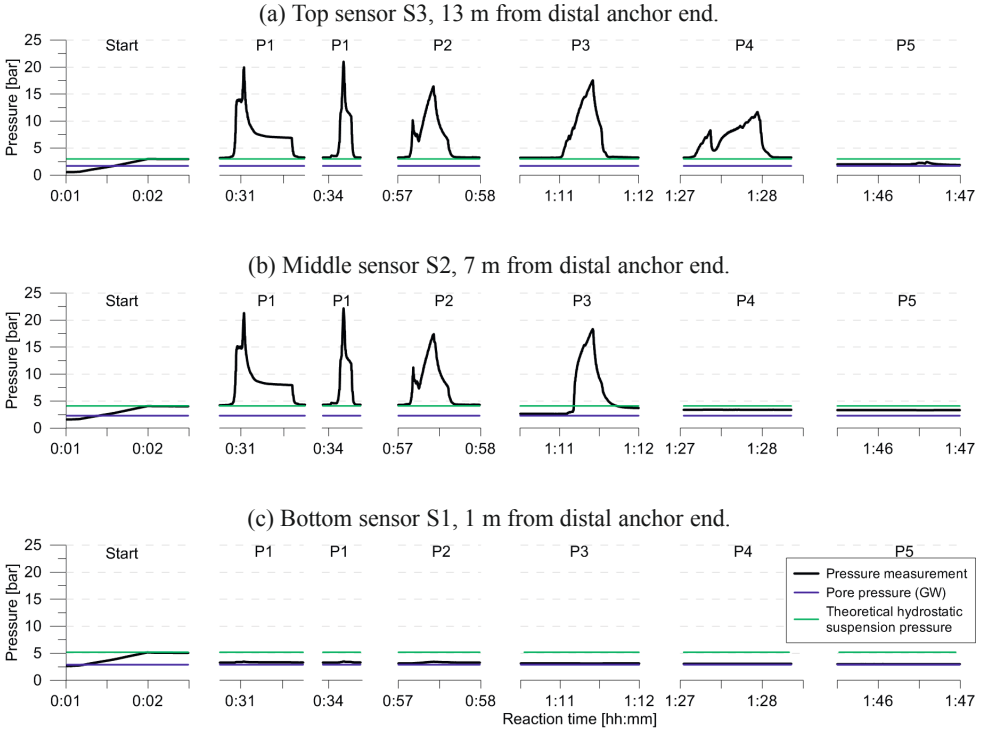

Figure 5.12: Pressure measured inside the borehole during installation of micropile GEWI2 in Dörverden.

the pressures at the borehole bottom (position S1) had reduced almost to groundwater pore pressure at both anchors, while the full suspension pressure was measured at in the centre and top positions (S2 and S3).

In the first grouting stage (P1), where the first 3 m of casing were withdrawn, the bottom sensor S1 was located in the grouting area (direct contact between grout and soil), whereas S2 and S3 were still located within the borehole casing. During grouting, S1 showed only marginal stress increase, but both sensors inside the casing measured full grouting pressure. After grouting, pressures reduced to suspension pressure in S2 and S3, while they fell to groundwater pore pressure level at S1. During the second grouting stage (P2), full grouting pressure was measured at S2 and S3, but S1 stayed unaffected from this point onward. In (P3), where the drill casing was pulled above the middle sensor, the stresses at middle and top position started to diverge. At grouting stage P3 slightly different observations were made for GEWI1 and GEWI2. At GEWI1 (Figure 5.11) the pressures measured at sensor S2 increased only 2.5 bar, then shortly dropped to groundwater level and increased again to a level just below suspension pressure. At GEWI2 (Figure 5.12) the pressures at S2 had reduced to groundwater level during removal of the third section. During grouting, pressures increased some seconds delayed but reached a value slightly higher than S3. After grouting they dropped to a value just below suspension pressure level. S3 measured full grouting pressure at both piles which reduced to suspension pressure after grouting. In stage (P4) only a fraction of the grouting pressure (10-15 bar) was measured at the top sensor and in the last stage (P5), where the free grouting area reached S3, the sensor barely showed a hint of stress increase. At GEWI1 pressures even drop down to groundwater level during grouting. Pressures measured directly after grouting were just below suspension pressure at top and middle position (S2 and S3) and at groundwater pore pressure level at the bottom (S1).

Long-term measurements of both anchors are presented in Figure 5.13. At GEWI1 the pressures decreased slightly in the first hours but started to increase significantly 8 to 12 hours after grout mixing. In contrast, at GEWI2 pressures stayed at a constant level during the measurement time of 16 hours.

Interpretation of test results in Dörverden

The hydrostatic pressure distribution of the measured total stresses inside the borehole directly after the grout was filled into the borehole shows that the grout initially acts as liquid. During grouting, sensors lying inside the casing showed hydrostatical stress distribution with the full grouting pressure, while pressures where almost unaffected by the grouting process outside the casing, where the grout was directly in contact with the soil. In this region, the measured stresses ranged between suspension and pore water pressures. This indicates that in regions where water can be drained from the grout, the grout behaviour changes as soon as it filtrates. The cement grains start to contact each other and the liquid grout transforms into a friction material and effective stresses are transferred through grain contact. The stress

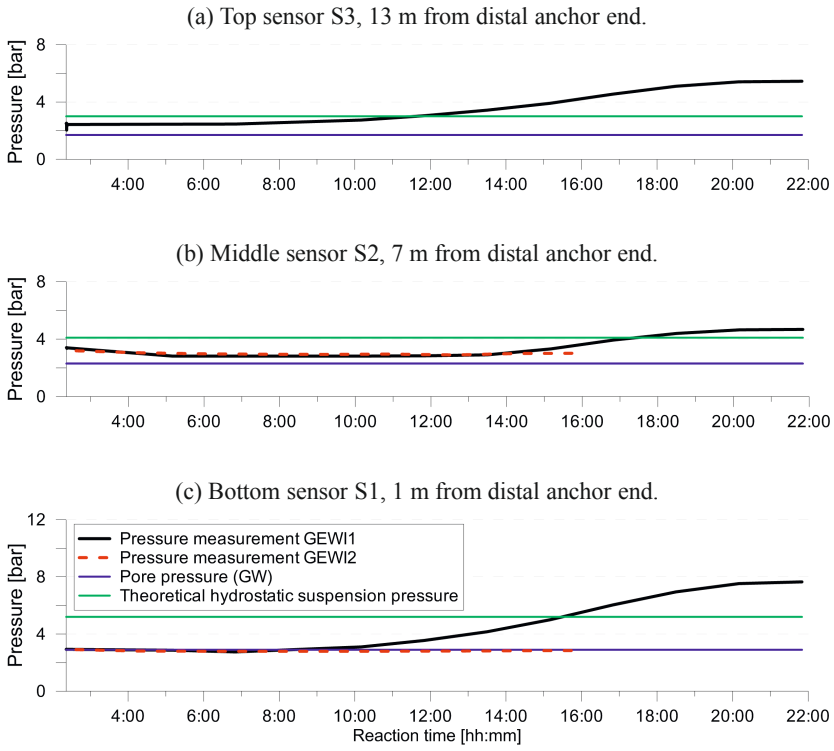

Figure 5.13: Long-term measurements of pressures inside the borehole after installation of micropiles GEWI1 and GEWI2 in Dörverden.

Figure 5.14: Drill casing after grouting in Dörverden.

distribution is not hydrostatically any more. After grouting, stiff, clay-like grout filter cake was found sticking inside the drill casing (see Figure 5.14). This confirms, that filtration takes place and transforms the grout into a plastic/solid material, as it was previously observed in laboratory tests. Measurements before grouting showed that the grout inside the casing already thickened in the bottom part of the borehole due to sedimentation or filtration through the borehole bottom. Pressures measured one meter from the borehole bottom had reduced significantly 30 minutes after filling the borehole with grout, and did not represent hydrostatic stress distribution any more. After grouting the full pile length, pressures inside the borehole were even below the theoretical suspension pressure.

These findings were surprising and question the benefit of grouting if the stresses after grouting are lower than before. Experience however showed that the anchor capacity is increased due to pressure grouting presumably due to an stress increase.

But possibly the stress increase due to grouting only occurs in radial direction and was not captured because only vertical stresses were measured. When the grout filters and transforms into a friction material, the stress distribution is heterogeneous and vertical stresses might diverge from radial stresses. An other explanation of the low vertical pressures could be that instead of total stresses only pore pressures were measured. Maybe once the grout filters a column of stiffened grout is pressed down the borehole during grouting and a cavity forms below the sensors which is then filled with water. In this case, no effective stresses are transferred to the sensor and only pore pressures are measured.

The long term measurements at anchor GEWI1 showed stress increases during setting of the grout, supporting the theory that stresses increase when the grout swells during curing because it draws water from the surrounding soil. However, at anchor GEWI2, stresses stayed constant during curing.

5.4.2 Measurements in Venhaus

Test set-up

On the test site in Venhaus grouting pressures were measured inside the borehole during installation of three anchors. Pressure sensors were installed on the anchor strands with a distance of 1.8, 4.8, and 8 m from the distal end of the anchor, facing in radial direction. At one anchor, the temperature was measured in the middle sensor. The voltage level of the power supply was measured at two anchors. The anchor installation process in Venhaus was similar to Dörverden, except that sections of 1.5 m were grouted continuously. The borehole was first filled to 50% with grout, then 2.5 m of casing were withdrawn before it was filled completely and grouting started. Experience of the contractor showed that the grout filters very quickly in the present soil conditions and in cases where the first 2.5 m were grouted, filtrate formed inside the drill casing, causing the anchor to get stuck to the drill casing. For that reason the anchor was pulled out of the borehole when the casing was withdrawn. When the first 2.5 m were withdrawn without grouting, filtration of the grout

took place in the uncased borehole rather than within the casing and the anchor remained in the borehole. Pressure changes in the adjacent soil were measured during anchor installation, using standard (DMT) and stationary (DMTA) dilatometer tests. Stationary tests were conducted during installation of three anchors. The dilatometer blades were placed at depth of the intended grouting section in a distance of 40 cm from the anchor axis (Figure 5.15). Additionally, two standard DMT measurements were taken close to the anchor body after anchor installation and compared to reference measurements in the undisturbed soil (DMT Ref).

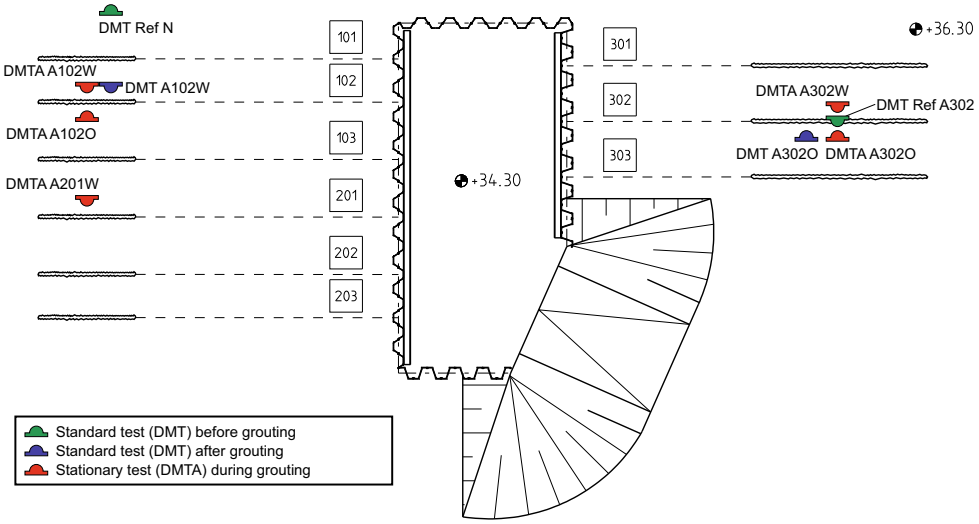

Figure 5.15: Sketch of DMT and DMTA sounding positions at test site in Venhaus.

Pressures measured inside the borehole

Figure 5.16 shows the pressure development of three test anchors while they are placed into the borehole, which was thereafter filled with cement grout. When the borehole was first filled with grout to 50 %, stresses increased hydrostatically to suspension pressure and declined as soon as the casing was withdrawn, because the suspension level dropped. When the borehole was then filled with grout to 100 % (⑥), pressures at the middle and top position (Sensor S2 and S3) increased proportional to each other, corresponding to hydrostatic pressure distribution, whereas pressures at the bottom sensor (S1) increased irregularly and stayed below grout self-weight. Directly after the borehole was filled, all pressures dropped below the theoretical suspension pressure level. The stress at the middle and top sensor developed proportionally to each other, while stresses at bottom position decreased with a delay and fell even below pressures measured at S2 and S3.

The pressure development during grouting is presented in Figure 5.17. The reference time started with filling the grout into the borehole. The duration of the grouting stages varied

(a) Anchor 301

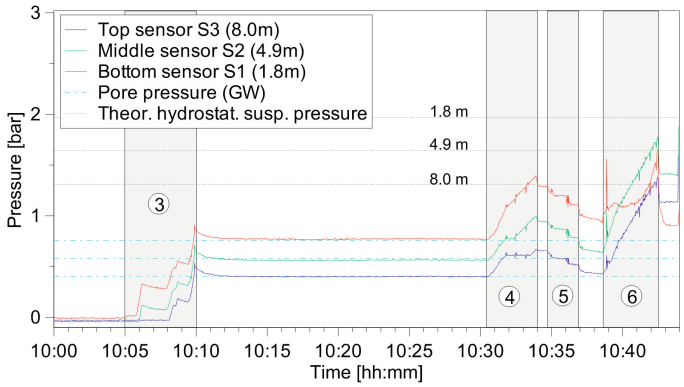

(b) Anchor 302

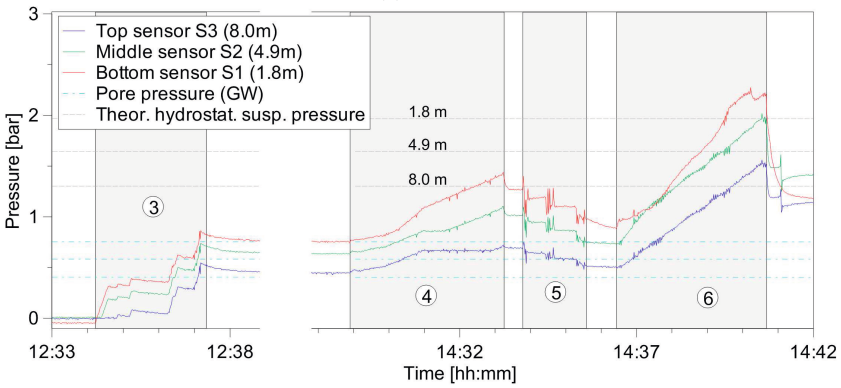

(c) Anchor 303

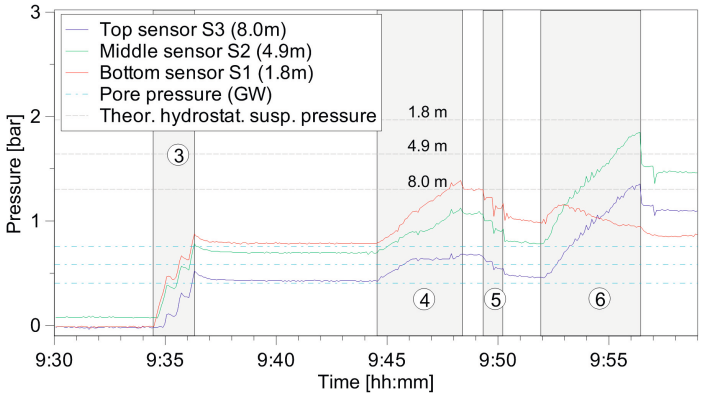

Figure 5.16: Anchor installation in Venhaus. Installing anchor into the borehole ③. Filling borehole to 50% with grout ④. Withdrawal of 2.5 m casing ⑤. Filling borehole to 100% with grout ⑥.

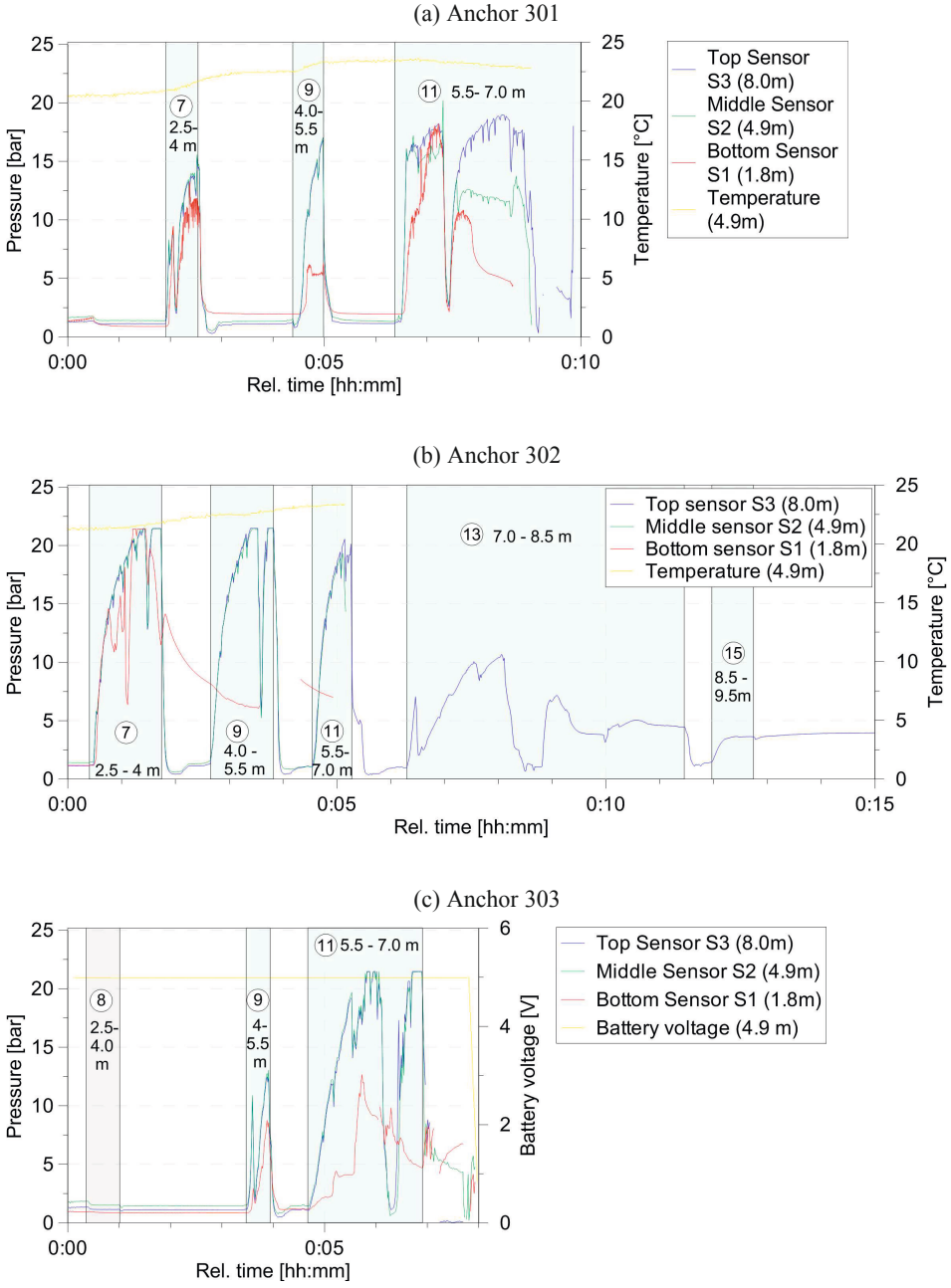

Figure 5.17: Pressure measurements in the borehole during grouting of test anchors in Venhaus. Grouting from 2.5 to 4.0 m ⑦. Withdrawal of 3rd section (no grouting pressure) ⑧. Grouting from 4.0 to 5.5 m ⑨ .Grouting from 5.5 to 7.0 m ⑪. Grouting from 7.0 to 8.5 m ⑬. Grouting from 8.5 to 9.5 m ⑮.

from 30 seconds to 5 minutes. Unfortunately, the test equipment failed during the tests and the installation process was only partly recorded.

At the first grouting stage from 2.5 to 4.0 m (⑦) the middle and top sensors S2 and S3, still lying within the drill casing, showed identical, full grouting pressures, while pressures at the bottom sensor S1 (1.8 m from the distal anchor end) deviated from hydrostatic stress distribution. At Anchor 301, pressures at S1 developed similar to S2 and S3 but with smaller values, while at Anchor 302 pressures first were lower but reached a peak above measuring limit of 23 bar. At both anchors the pressure at S1 stayed above suspension pressure after grouting while S2 and S3 fell down to suspension pressure. The first 4 m were not grouted at anchor 303.

In the next grouting stage from 4.0 to 5.5 m the grouting area reaches sensor S2, but at all anchors still full grouting pressure is measured at S2 and S3. The bottom Sensor S1 only shows a fraction of the grouting pressure. At Anchor 302 no pressure increase was observed at this stage but the sensor failed shortly after, so it is unclear until when results are reliable. After grouting, S2 and S3 fell down on suspension pressure level, while S1 fell to the level before this grouting stage. At Anchor 301, pressures of all sensors started to diverge in the next grouting stage from 5.5 to 7.0 m, the top sensor measured the highest pressure, while the bottom sensor showed the lowest. At Anchor 302 and 303, the sensors S2 and S3 still showed the same pressures in this stage. The following grouting stages were only measured by the top sensor S3 of Anchor 302. The pressures did not reach full grouting pressure but remain at a higher level that suspension pressure after grouting pressure is released.

Standard DMT tests before and after anchor installation

The influence of anchor installation and grouting on the surrounding soil was investigated by comparing standard DMT tests before and after grouting. The sounding positions are illustrated in Figure 5.15.

Two standard DMT tests were conducted as reference before grouting. For ‘DMT Ref N’ 30 cm steps were chosen and the sounding was carried out until 11 m below ground level. At ‘DMT Ref A302’ the blade could only be brought to a depth of 9.20 m, from where the resistance was too high for further insertion. After withdrawal, the dilatometer blade exhibited strong deformations, which indicated that it hit an obstacle. It is assumed that it might have been a stone or even the anchor drill rods of anchor A302 for which the borehole was already drilled, but the drill casing still remained in the borehole. Measurements were taken in 1 m steps until 8 m below ground and in 30 cm steps from 8 to 9.20 m.

Results of both reference measurements are presented in Figure 5.18. In the first 3 m below ground level the corrected DMT readings of Ref A302 show higher pressures than Ref N, while from 5 to 6 m pressures are lower. At 4 m, and from 7 to 9.2 m, measurements coincide very well, even though Ref A302 was taken after drilling the borehole. Figure 5.19 shows the DMT and soil parameters determined from reference DMT readings. The material index lies well in the range for sand and stays constant with depth.

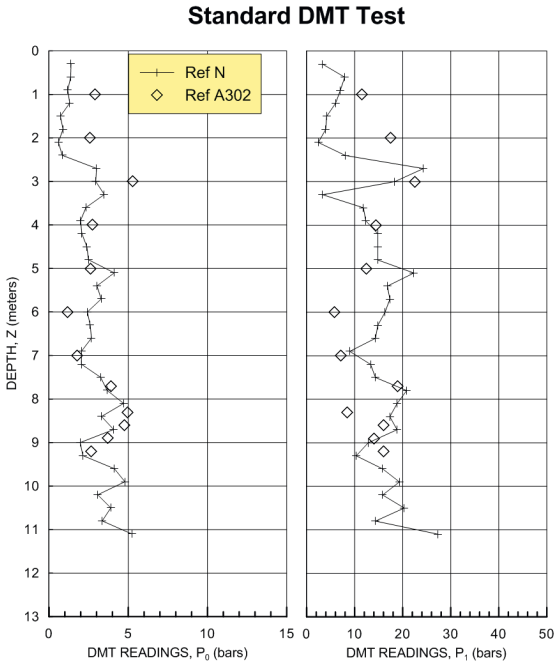

Figure 5.18: Corrected DMT readings before anchor installation in Venhaus.

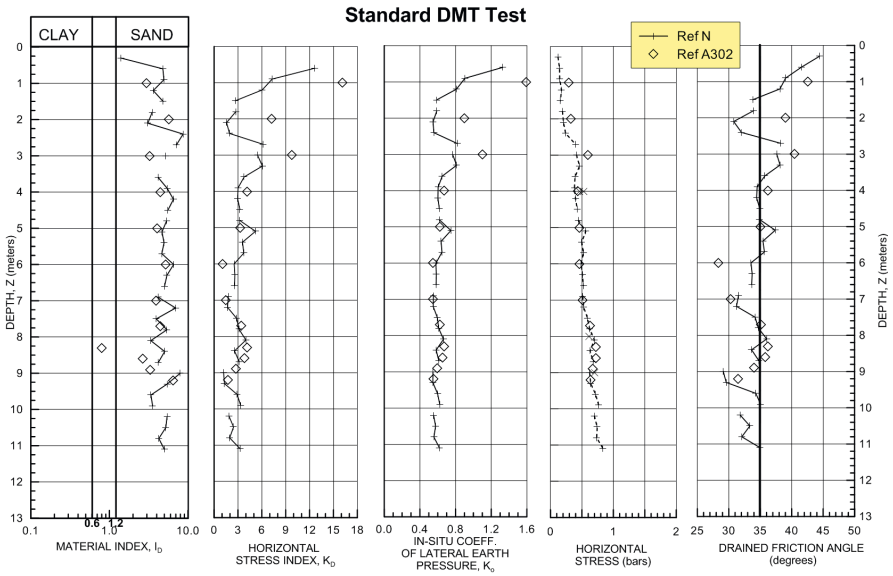

Figure 5.19: Soil parameters determined from DMT reference tests before anchor installation in Venhaus.

The horizontal stress index K_D and the derived value K_0 (calculated with Equation 5.6) are fairly high in the first 3 meters below ground level, especially at DMT Ref A302. This could be because this layer is above groundwater level and subjected to wetting and drying, which can cause overconsolidation effects. Below 3 m K_0 falls to a value around 0.6, which is still higher than would be expected, but both measurements show very similar K_0 profiles. This indicates that the development of the K_0 values with depth is reasonable, even though the values are potentially unrealistic.

The determined friction angle φ varies between 30°and 45°. In the soil investigation report for the site, φ = 30°was given for the fill layer (0 to 2-3m) and $\varphi = 35°$for the sand layer below.

To evaluate the DMT interpretation method, K_0 was additionally determined with the $K_0 - K_D - q_c$ correlation given in Equation 5.7. The CPT soundings used for correlation are presented in Figure B.1; 'CPT-V07' was used as reference for DMT Ref N and DMT A102, and 'CPT-S26' for DMT REF 302 and DMT A302 respectively. Figure B.2 in Appendix B compares the two correlations and Equation 5.7 gives K_0 values closer to the expected value of $K_0 = 1 - sin\varphi$ = 0.43. However, CPT results are not always available to calibrate DMT results and the additional parameter q_c gives additional uncertainty for test interpretation, especially if the CPT soundings are not very close to the DMT position. The $K_0 - K_D - \varphi$ correlation is only dependent on DMT results and even though the K_0 values might be inaccurate, a good K_0-profile is achieved to compare different tests and evaluate the effect of grouting.

After installing and grouting the anchors, two DMT tests were carried out close to the grout body. The dilatometer blade was inserted at 40 cm distance from the anchor axis with the membrane facing towards the grout body and measuring radial stresses. Results for 'DMT A102' are presented in Figure 5.20. The planned grout body of anchor A102 lies between 8.9 m and 11.8 m below ground level. The dilatometer blade was inserted at 12 m distance from the sheet pile wall, where the grout body is located at 9.6 m depth. Results for 'DMT A302' are presented in Figure 5.21. The blade was inserted 10 m from the sheet pile wall, where the grout body is located at approximately 8.2 m depth, ranging from in total 6.6 to 11.8 m.

The DMT measurements are in good agreement with the reference measurements in the first meters, while higher pressures occur in the area around the intended anchor body. In the first 4 m below ground level, where the reference measurements differed from each other, the DMT tests after grouting correspond well to the reference test close by. DMT A102 fits well with DMT Ref N, whereas DMT A302 fits better to DMT Ref A302. This indicates that the variations of the reference measurements are due to inhomogeneities of the fill layer. Below 4 m, the measured pressures are in the range of the reference measurements until approximately 9 m depth from where the A and B-readings are larger after grouting than before. This is more distinct for Anchor A102 than for Anchor A302. The pressure increases are observed just below the assumed grout body location.

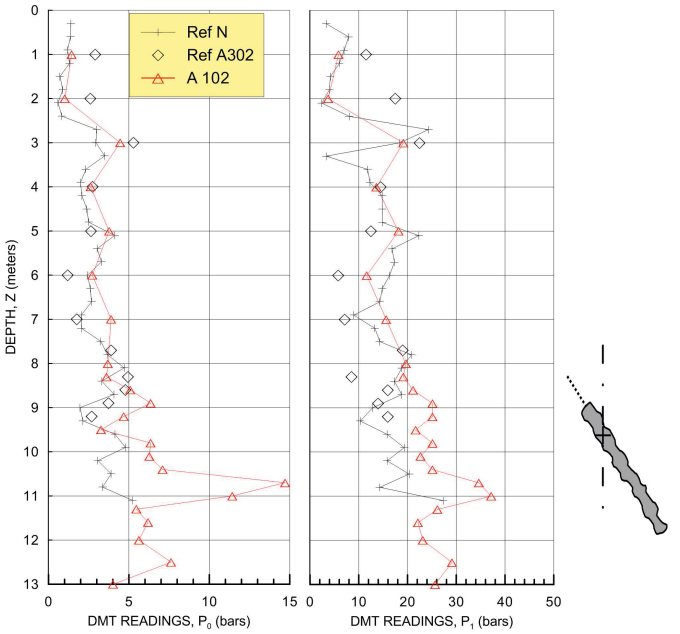

Figure 5.20: Standard DMT tests before and after installation of Anchor 102 in Venhaus.

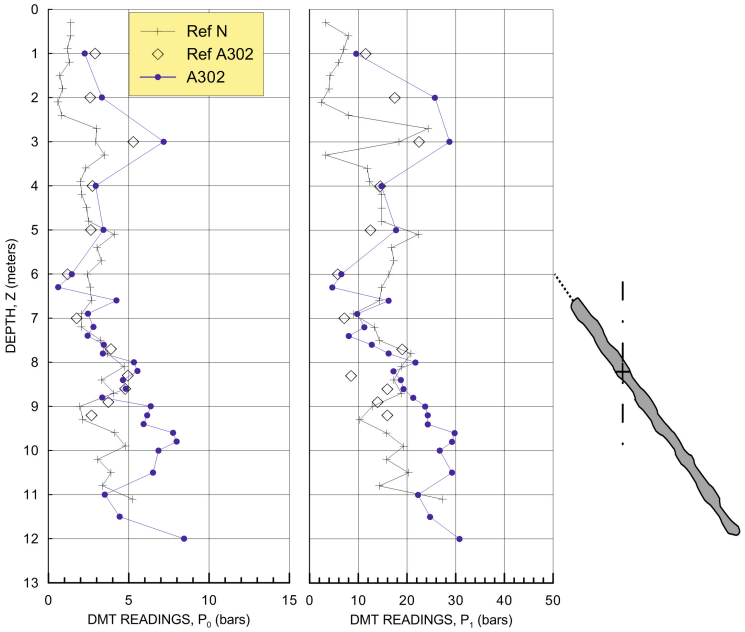

Figure 5.21: Standard DMT tests before and after installation of Anchor 302 in Venhaus.

Parameters determined from the standard DMT tests before and after anchor installation are presented in Figure 5.22. Both pressures, P_0 and P_1, increased after grouting and consequently, all derived parameters also increase in this region. Only the material index I_D stays at a value of 3, unaffected by grouting, which identifies the soil type as sand before and after grouting. I_D relates the difference of total stresses P_0 and P_1 to the effective stress P_0' and gives information on the 'rigidity' of the soil. For all other parameters a relatively large variation is observed in the first 4 meters below ground level which are referred to the inhomogeneous soil properties of this area. From 4 m to 8.5 m the parameters before and after grouting are very similar. Approximately 8.5 m below ground level, the values before and after grouting start to diverge and a clear increase of horizontal stresses is observed. The vertical effective stress σ'_{v0}, which was used to determine K_D and therefore K_0 and σ'_{H0}, was determined with

$$\sigma'_{v0} = \gamma' \times z, \tag{5.8}$$

where z is the depth below ground level in meters. The groundwater pore pressures were calculated assuming a groundwater level 3 m below ground level. An increase of vertical stresses during grouting was disregarded. The reference measurements were stopped at 11 m below ground level, but extrapolating the values linearly with depth, the values from DMT after grouting seem to return back to the initial values below 11 and 11.2 m. Measurements indicate an increase of horizontal (radial) stresses in the soil adjacent to the grout body.

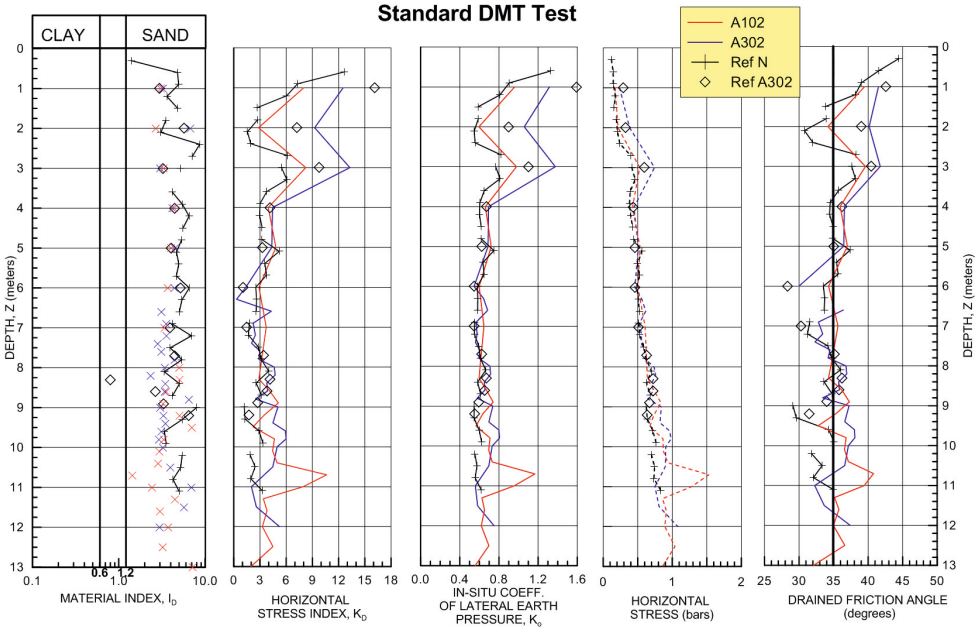

Figure 5.22: Soil parameters determined from DMT tests before and after installation of anchors A102 and A302 in Venhaus.

Stationary DMTA tests during anchor installation

In addition to before/after soundings, five stationary DMTA tests were conducted to investigate stress changes in the soil adjacent to the grouted length during grouting. The dilatometer blades were positioned 40 cm from the anchor axis, facing towards the grout body (see Figure 5.15). Tests 'DMTA A102O' and 'DMTA A102W' were placed on both sides of Anchor 102, test 'DMTA A202W' next to Anchor 202. The blades were positioned 13 m from the sheet-pile wall at a depth of 10.40 m. Tests 'DMTA A302O' and 'DMTA A302W', next to Anchor 302, were positioned 11.3 m from the sheet-pile wall, at 9.20 and 9.05 m depth respectively. 'DMTA A302W' could not be brought down below 9.05 m because the resistance was too high. Presumably a stone or even the drill rod was hit.

Figure 5.23 shows the A-readings measured during grouting. The pressures decreased during the first few measurements and remained at a constant level thereafter until anchor grouting was started. Only at Anchor 201 was a pressure decrease observed during the entire test period, possibly due to test equipment working insufficiently. At all tests a clear pressure increase was measured when grouting started. While at Anchors 102 and 201 stresses rose instantaneously when the first grouting stage started, at Anchor 302 they increased during the second grouting stage only. The measured peak pressures during grouting varied largely between the tests. However, only few measurements could be taken during the short grouting period, so it is unclear if the peak pressures were captured. After grouting was completed, the pressures declined and reached a value between 100 and 300 kPa above the initial level. The DMTA pressure measurements do not represent actual earth pressures but detect the relative stress changes, which were clearly visible during and after grouting. Only total stresses are measured and therefore, the peak pressures measured during grouting could be partly due to excess pore pressures induced by the pressure impulse during grouting. However, the surrounding sand is very permeable and it can be assumed that the excess pore pressures dissipate very quickly. The remaining stresses decline slightly after grouting, as a result of dissipation of excess pore pressures and relaxation of the soil. They approach a stress level well above the initial stress level.

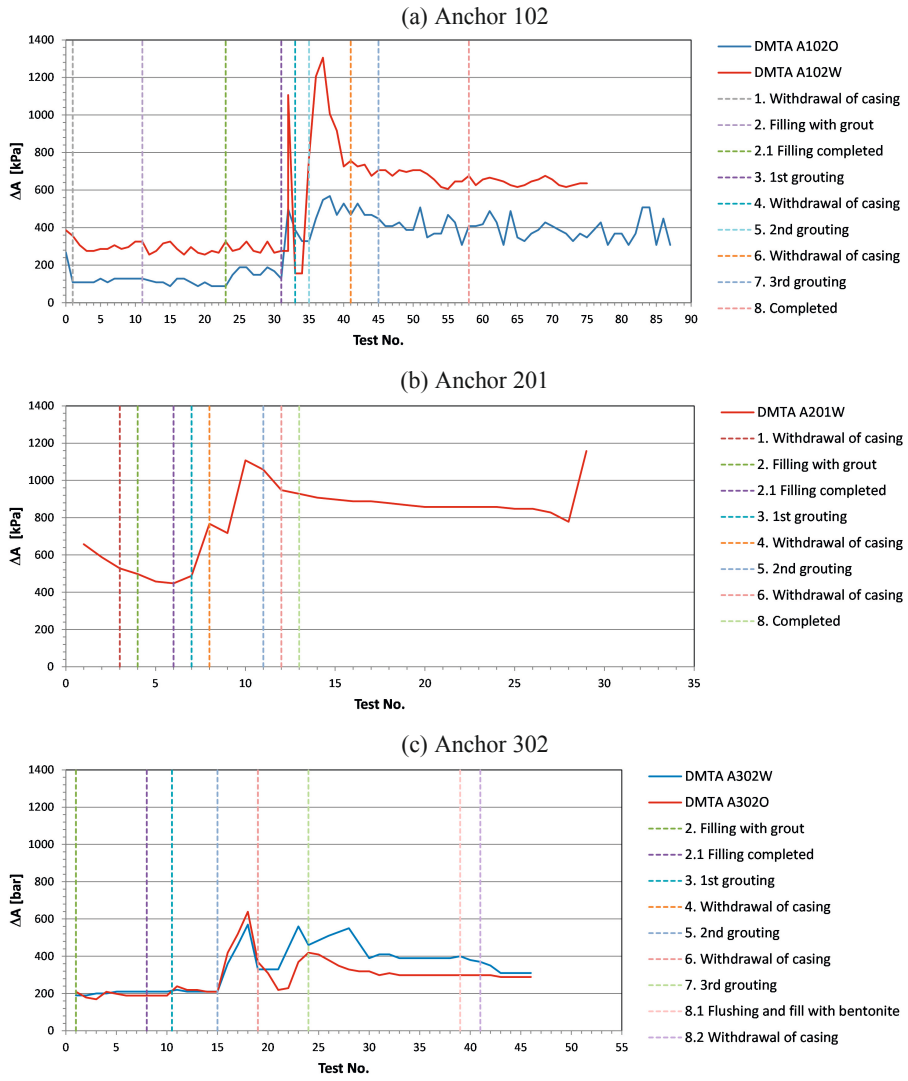

Figure 5.23: Stationary DMTA tests during anchor installation in Venhaus. Installation stages are indicated by vertical dashed lines.

Interpretation of measurements in Venhaus

The hydrostatic stress distribution during filling the borehole with grout shows that the grout initially behaves as liquid. But directly after the grout was filled into the borehole, stresses at the bottom sensor started to develop disproportional to the other positions and even fell below suspension pressure. This indicates that the grout at the bottom position, 1.8 meters from the distal anchor end, filtered only minutes after the borehole was filled. But during the first grouting stage, the bottom sensor, located in the free grouting length, showed only slightly less pressure than measured within the casing, where full grouting pressure was measured. Although the grout at the bottom position seemed to have filtered during filling of grout, almost full grouting pressures were measured at this position when grouting started. Possibly, within the filtrate only little friction was generated during filling of grout or the contact between the grains was so weak that the grout liquefied again during grouting. In the second grouting stage, stresses at bottom position were significantly lower than grouting pressures, indicating that the filtration was more distinct at this stage. After grouting, radial stresses at bottom position stayed well above suspension pressure, indicating that the grouting pressure was locked in to some extend. The centre position sensor showed full grouting pressure in the grouting stage where it was just located in the free grouting length, showing that filtration was not completed to the centre and did not progress into the casing. Further grouting stages were only recorded at the top sensor of one anchor. Here, it occurred that when the top sensor reached free anchor length only a fraction of grouting pressure was measured. After grouting, the remaining radial stresses were 250 kPa above suspension pressure. The dilatometer tests conducted at a distance of 40 cm from the anchor axis showed similar results. During standard DMT tests before and after grouting, local stress increases were detected between 9 and 11 m depth, just below the intended grout body. Maximum stress increases of 25 kPa and 75 kPa were measured at anchors A 102 and A 302 respectively. Stationary dilatometer tests (DMTA) showed pressure impulses of up to 1000 kPa during grouting. After grouting was completed, stress declined to a level between 100 and 300 kPa above initial pressure. These measurements show clearly that the stress state of the soil is influenced by the grouting process, although only a fraction of the grouting pressure remains as radial stress within grout and soil.

5.4.3 Pressure measurements in Horstwalde

Test set-up

At the test site in Horstwalde, grouting pressures were measured within the borehole during and after grouting of five anchors. Three anchors were equipped with three radial sensors each at positions of 1.5, 3.5, and 5.5 m from the distal end of the anchor. A temperature sensor was added to one of the sensors additionally. At two anchors, pressure sensors were installed at two positions at 3 and 5 m from the distal end and radial and vertical stresses were recorded at the same position. The lower vertical sensor at 3 m faced upwards, while

the other one at 5 m faced downwards. In addition to the pressure measurements inside the borehole, pressure changes were also measured within the soil. Measurement positions are presented in Figure 5.24. Stationary DMTA tests were taken next to anchors 10, 15, 16, 19, and 25. After the borehole was drilled, the dilatometer blades were brought down at 30 cm distance from the anchor axis. Due to the large anchor length and steep angle, the anchors grout bodies were much deeper than in Venhaus, resulting in higher inaccuracies of the dilatometer position. The influence of grouting was also determined with CPT soundings next to anchor 10 before and 16 hours after installation. Also pore pressures were recorded at two positions during installation of anchor 7 and anchor 10. Contrary to the other test sites, in Horstwalde boreholes were drilled with external flushing and small quantities of bentonite were added to the flushing suspension and the cement grout. Sections of 3 m were grouted while the drill casing was withdrawn continuously.

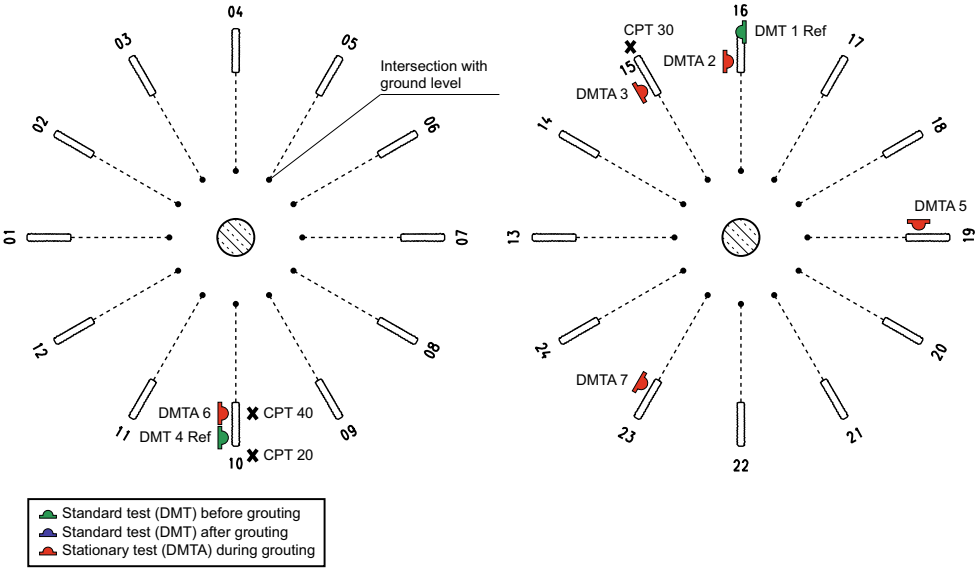

Figure 5.24: Position of CPT and DMT soundings in Horstwalde.

Pressures measured inside the borehole

Pressures measured during placing the anchors into the borehole correspond to the theoretical pressure of the flushing suspension (w/c = 3.3). The pressure distribution during placing the anchors into the borehole leads to the assumption that for the test anchors, the borehole was just filled with grout when grouting started. In contrast to observations at the sites in Venhaus and Dörverden, pressures remained constant until grouting started, even 40 minutes after installation. Only at Anchor 19 a slight decrease of pressures was observed.

Pressure measurements during grouting in radial direction at three positions are presented

(a) Anchor 7

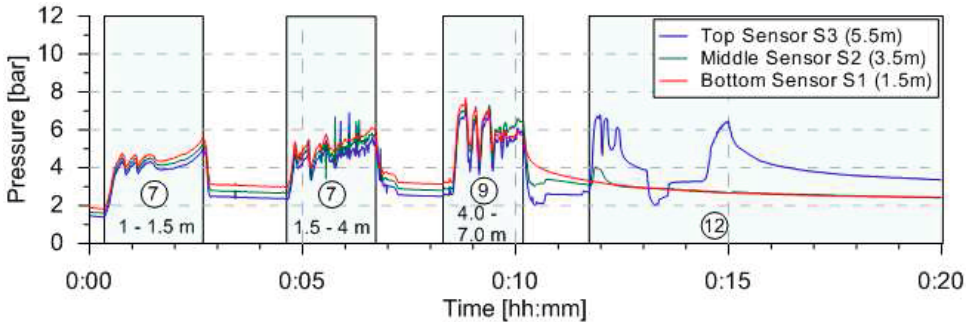

(b) Anchor 10

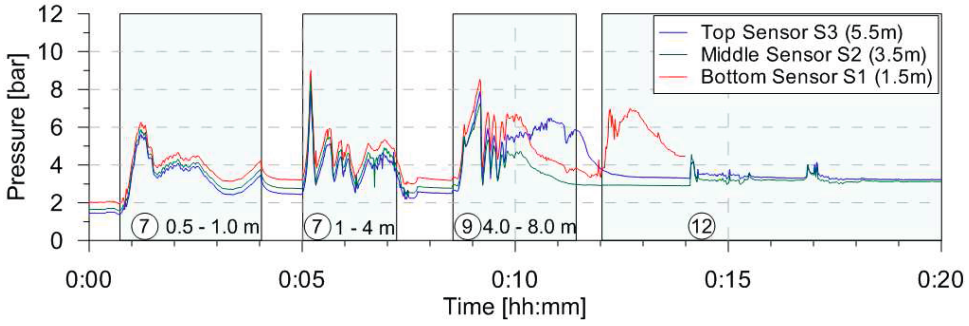

(c) Anchor 19

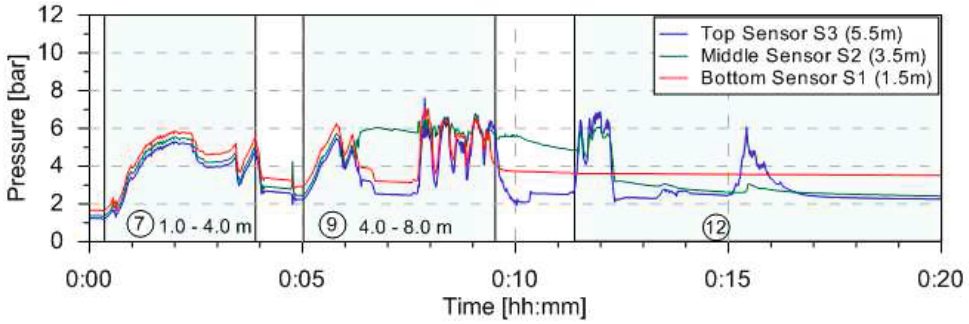

Figure 5.25: Horizontal pressure measurements in the borehole during anchor installation in Horstwalde. Grouting from 0.5/1.0 m to 4.0 m ⑦, grouting from 4.0 to 7 m ⑨, flushing and removal of sections 8.0 m - end ⑫.

in Figure 5.25. In the first grouting stage (1.0 to 4.0 m, ⑦), full grouting pressure was measured with a proportional distribution at all positions, even though both sensors S1 and S2 were located in the grouting area. After grouting, all pressures fell back to hydrostatic grout pressure and decreased slightly before the next grouting stage. In the second grouting stage (4.0 to 7.0 m, ⑨) the pressure distribution started to diverge and the pressures were no longer proportional at the three positions. After grouting, pressures fell down to suspension pressure at some sensors but remained at a higher level at others. Flushing of the free anchor length was measured as pressure increase of around 7 bar at the top sensors, while the middle sensor showed less increase and no pressure change was observed for the bottom sensor. Only measurements at Anchor 10 showed different results, but one sensor failed during flushing and it is unclear until when the results are trustworthy.

At Anchors 8 and 13, vertical and radial stresses were measured at two positions. Results are presented in Figure 5.26. In the first grouting stage ⑦, stresses increased proportionally at both positions with identical values in radial and vertical direction. Afterwards grouting pressures reduced to hydrostatic suspension pressure. In the next grouting stage, pressures started to diverge. Higher stresses developed at the top position compared to the middle position. Vertical and radial stresses were still identical at top, but they started to diverge at the middle position. After grouting, the vertical stresses fell to a level below suspension pressure, while radial stresses remained at a higher level. Pressures at top position fell down to suspension pressure. During flushing, no increase of stresses was observed at middle position. At top position pressures increase. Now, vertical and radial stresses also started to diverge at this position. During flushing vertical stresses were higher than radial stresses, but fell below suspension pressure after flushing. The radial stresses stayed at a higher level at Anchor 8 while they fell to a lower level at Anchor 13.

(a) Anchor 8

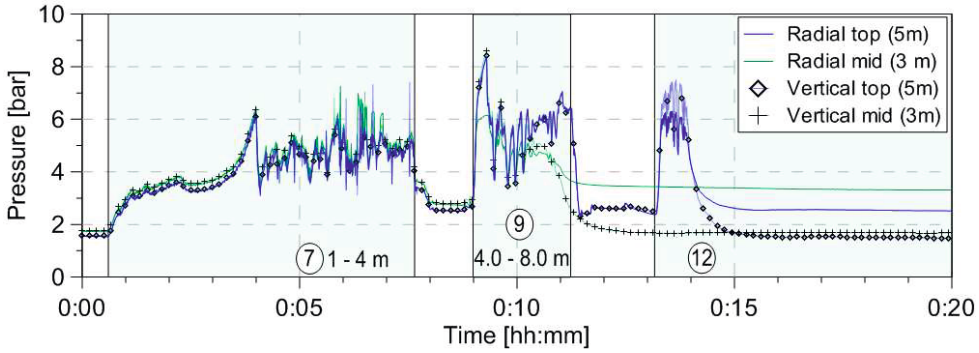

(b) Anchor 13

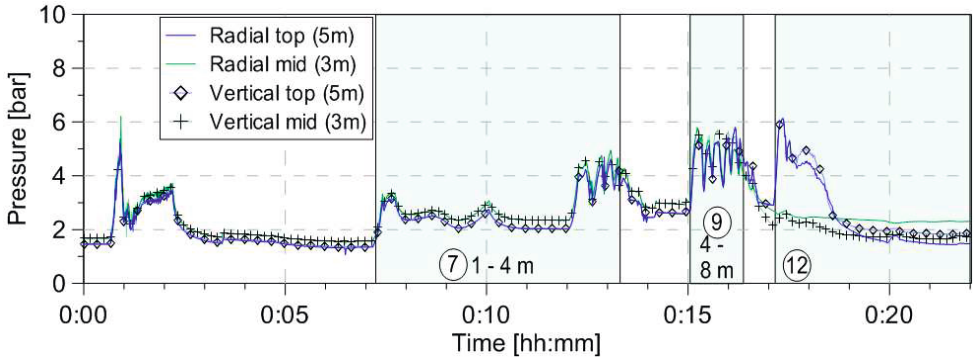

Figure 5.26: Pressure measurements in the borehole during anchor installation in Horstwalde. Radial stresses (solid lines) compared to vertical stresses at the same position (symbols). Grouting from 0.5/1.0 m to 4.0 m ⑦, grouting from 4.0 to 7 m ⑨, flushing and removal of sections 8.0 m - end ⑫.

Pore pressure measurements

Pore water pressures were measured at two positions at a depth of 14.42 and 11.00 m below ground level. As shown in Figure 5.27, a slight pressure increase is noticeable for a short period of time during installation of the adjacent anchors 7 and 10. Measurements were only taken during installation of these two anchors.

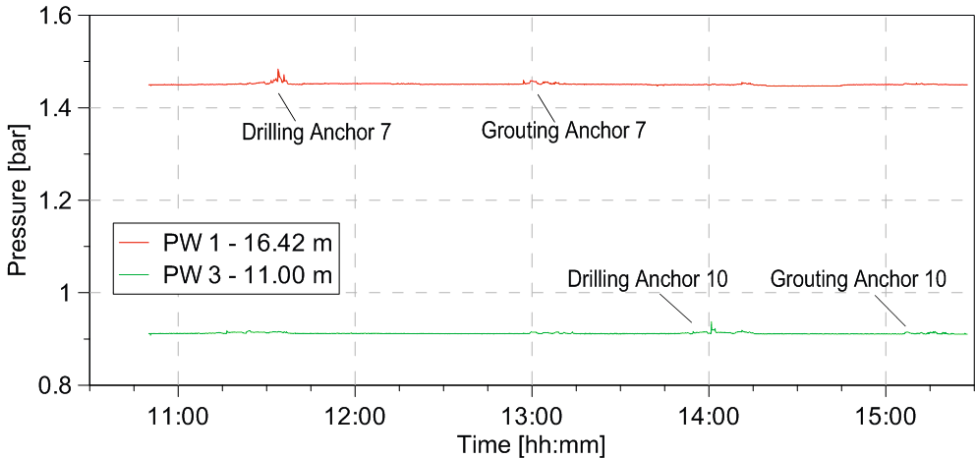

Figure 5.27: Pore pressure measurements

Stationary DMTA tests during anchor installation

Results of stationary DMTA tests in Horstwalde are presented in Figure 5.28 and Figure 5.29. The grouting stages are indicated with dashed vertical lines, although the times are only rough estimations as it was not possible to identify the transition between the different phases precisely. The test results in Horstwalde are not as consistent as in Venhaus. This might be due to varying ground conditions or inaccurate dilatometer positions. In all tests, the A-readings decrease in the first few measurements as expected for a stationary DMTA test. But grouting was started before the values had stabilised and therefore it is uncertain at what level the decrease would have stopped. Only at DMTA6, grouting was started after the readings reached a plateau of 210 kPa. The decrease of the A-reading value during the first few measurements of the tests in Venhaus is in the same range as in Horstwalde. During withdrawal and grouting of the first 3 meters, stresses decreased within the borehole at DMTA2, DMAT5, and DMTA6 (possibly due to relaxation of the soil when the casing was removed), while at DMTA3 and DMTA7 stresses increased clearly. However, during the second grouting stage a small increase of stresses was observed at all anchors. It seems that due to grouting the soil stresses were either recovered after drilling or even increased.

(a) Anchor 16 DMTA2

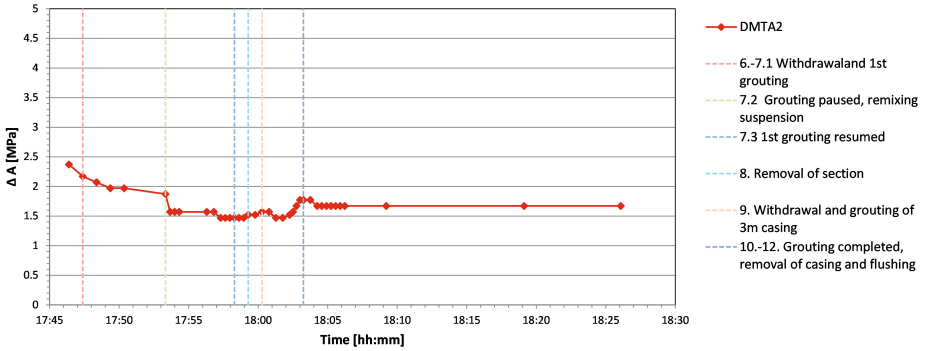

(b) Anchor 15 DMTA3

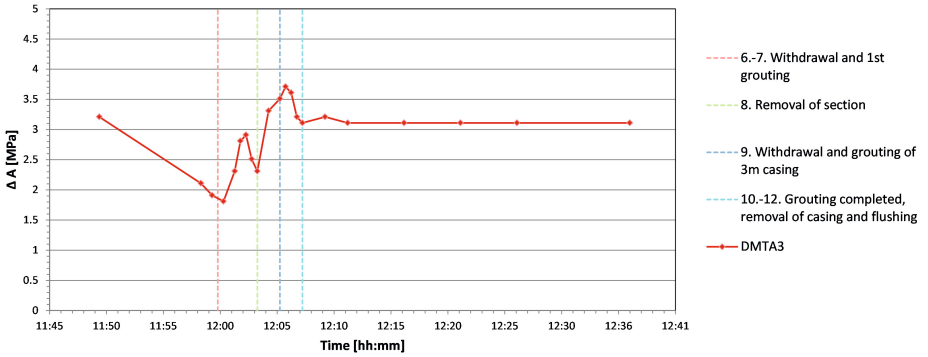

(c) Anchor 19 DMTA5

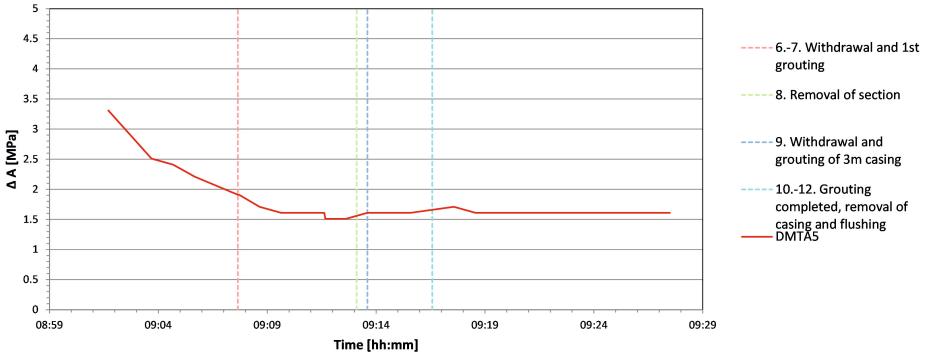

Figure 5.28: Stationary DMTA tests during anchor installation in Horstwalde. DMTA2, DMTA3 and DMTA5. Installation stages are indicated by vertical dashed lines.

(a) Anchor 10 DMTA6

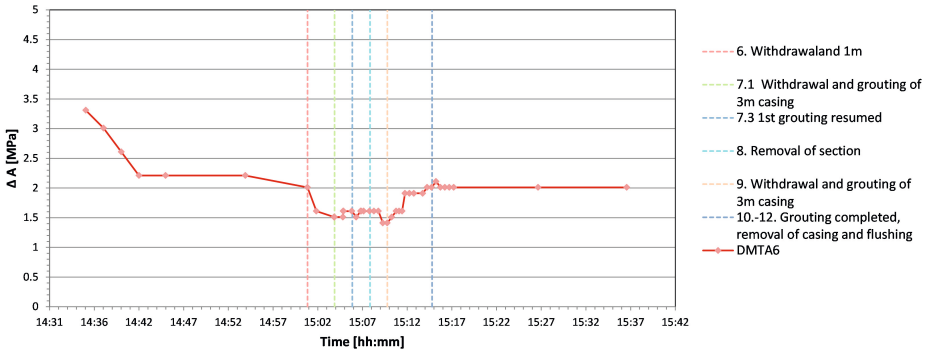

(b) Anchor 23 DMTA7

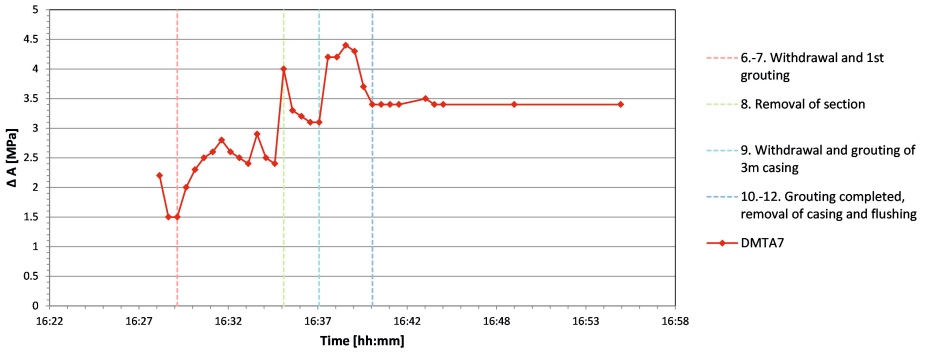

Figure 5.29: Stationary DMTA tests during anchor installation in Horstwalde. DMTA6 and DMTA7. Installation stages are indicated by vertical dashed lines.

CPT Soundings

The influence of grouting on the surrounding soil was also investigated by comparing CPT soundings before and after anchor installation. Two CPT soundings were conducted at a distance of 30 cm from Anchor 10.'CPT20', carried out after anchor installation, shows lower tip resistance and skin friction than the reference test 'CPT40' until a depth of 16 m. Below 16 m, skin friction and tip resistance seem to have increased due to grouting. The lower values could be induced by soil disturbances due to the drilling process with external flushing.

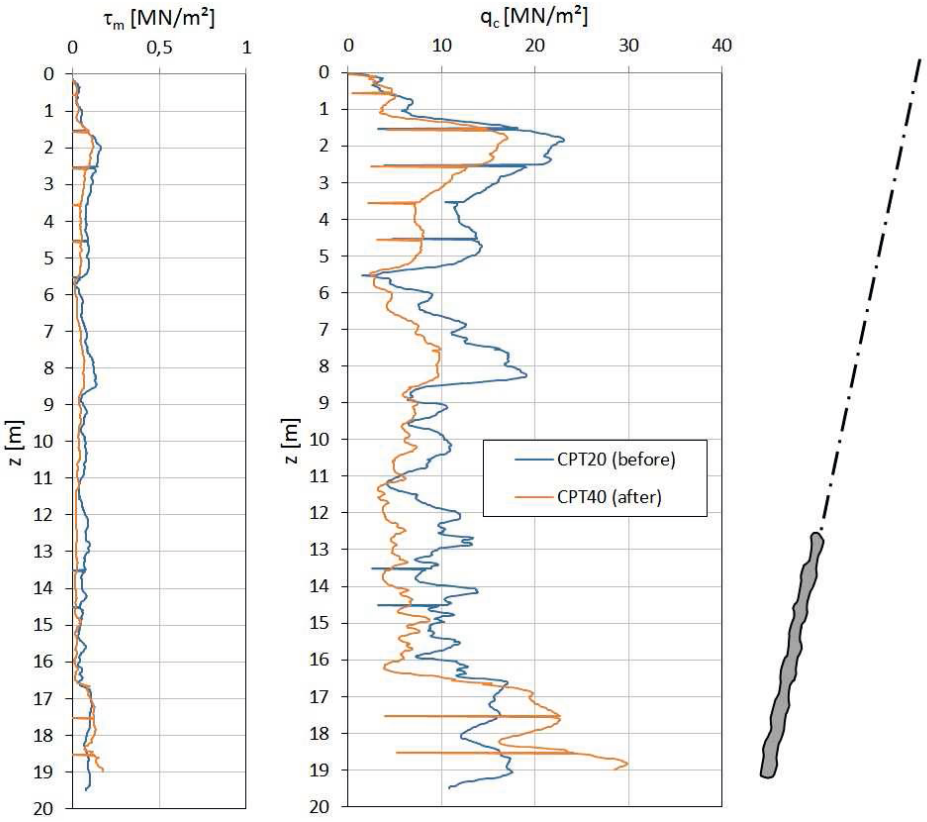

Figure 5.30: CPT measurements before and after Anchor installation in Horstwalde

Interpretation of measurements in Horstwalde

In Horstwalde some sensors measured vertical and radial stresses at the same position, making it possible to identify the point where stresses start to develop inhomogeneous and the grout changes from liquid to friction material. When the anchors were lowered into the borehole, it was filled with flushing liquid, a cement/water suspension with w/c = 3.3 and

some bentonite. The stress distribution was hydrostatic and stresses remained constant until grouting started. This shows that the suspension acts as liquid and no water was drained through the borehole bottom during this period. It is assumed that due to external flushing and the use of bentonite, a thin filter cake formed and sealed the borehole walls, so that no drainage occurred due to self-weight of the grout and the grout remained liquid within the borehole. Measurements during grouting confirm this assumption. In the first grouting stage, all sensors showed hydrostatic stress distribution and fell back to suspension pressure after grouting. This shows that the grout was still fully liquid. In the second grouting stage, stress developments started to diverge at the different positions, indicating that filtration started. From this point the residual stresses between the grouting stages started to alter from suspension pressure, but some were above, some below. Comparisons between vertical and radial stresses at the same position confirmed that the grout is liquid initially, but changes its behaviour to a heterogeneous material at a certain point. During the first grouting stage stresses developed hydrostatically and radial and vertical measurements were the same, proving that the grout is still liquid. In the second grouting stage stresses at the mid sensor started to diverge and fell below stresses measured at the top sensor. During grouting, vertical stresses were higher than radial stresses, but thereafter vertical stresses fell below suspension pressure, while radial stresses remained at a higher level. This indicates that the grout changes from liquid to a friction material. During vertical loading only a fraction of the stress was transferred in radial direction, but during unloading vertical stresses decreased, while radial stresses were locked in. After the grouting pressure was released, vertical stresses fell below suspension pressure which is believed to be due to arching of the filtrate inside the borehole where the grouts weight is partly transferred to the surrounding soil. Similar observations were made at the top position sensor, but only during flushing of the free anchor length. Pore pressure measurements close to the anchors show that during grouting only a short and tiny pressure impulse occurred in the groundwater and dissipated very quickly. Stationary dilatometer tests show varying results, but it can be concluded that due to grouting, radial stresses were increased or at least recovered after drilling. CPT measurements before and after grouting of one anchor showed loosening of the soil due to drilling, but increased strength below 16 m. These findings indicate that in Horstwalde the soil is disturbed and loosened by the external flushing drilling method, but due to grouting, this was recovered or the soil was even improved. However, this improvement was not achieved for the full grout body length but only in the bottom part. The pressure measurements indicate that during grouting the grout was still liquid in the top part of the grouting length and only filtered after grouting was already completed. Thus, possibly less pressure was transferred to the surrounding soil at the top of the grouting length. In Horstwalde, test results varied significantly from anchor to anchor, but also the grouting pressures and durations applied at the different anchors varied.

5.4.4 Summary

Comparison of test sites

Pressure measurements were taken at three different sites with similar ground conditions, but slightly varying drilling and grouting methods were applied. In Dörverden, casing sections of 3 m were withdrawn and the full length was grouted at once with 20 to 22 bar. At the other sites continuous grouting was applied. The casing was withdrawn continuously, while grout was pressed into the borehole. In Venhaus 1.5 m sections were grouted with 15 to 20 bar, while in Horstwalde only 6 to 8 bar were applied to 4 m sections. During continuous grouting, pumping was usually stopped before the full section was withdrawn, and not the full pressure was applied to the remaining length. At all sites, it was observed that the grouting pressure was not constant during the grouting process but build up successively.

The grouting suspension at all sites consisted of a mixture of standard Portland cement and water. In Dörverden, pure water/cement mix with w/c = 0.50 was used, in Venhaus the water content was w/c = 0.45, and in Horstwalde small quantities of bentonite were added to the grout with w/c = 0.45. Also the applied drilling method varied between the sites. External flushing was applied in Horstwalde, whereas duplex drilling was used at the other sites. Drilling with external flushing disturbs the soil more than when the drillings are flushed within the casing. During external flushing, cement and bentonite was added to the flushing liquid to stabilise the borehole. It is assumed that some filter cake already builds at the borehole walls when water is filtered from the flushing liquid during drilling. These small differences in anchor installation methods observed at the test sites reflect common practice, where each contractor uses different methods, depending on their individual experience. However, the installation methods influence the anchors performance and it was reported that even at the same building site anchors of one contractor would fail the required capacity, while anchors installed by another contractor perform sufficient. All test anchors were around 19 m long, but the geometry varied between the sites. In Dörverden, vertical micropiles with a grouted length of 15 m were used, while in Venhaus anchors were inclined 55°, with a grouting length of 6 and 9 m, and in Horstwalde inclination was 10° and the grouting length was 6 m.

Pressure measurements inside the borehole

At all sites the total stresses were measured, only the measuring direction varied. In Dörverden the sensors faced downwards, in Venhaus radial stresses were measured and in Horstwalde stresses were measured in radial and longitudinal direction.

Measurements before grouting showed that at all sites the grout initially acts as liquid with hydrostatic pressure distribution within the borehole. In Dörverden and Venhaus it was observed that the grout already filtered before grouting started and stresses started to decrease at the borehole bottom. In Dörverden, sensors 1 m above borehole bottom showed almost no reaction to the grouting process, indicating that the material was already fully filtered

due to self-weight. Although in Venhaus grouting was started shortly after the borehole was filled, and the grout remained in the borehole only for a short time, filtration due to self-weight was also observed here. However, the effect was not as distinct as in Dörverden. At this site, 2.5 m of casing were already withdrawn before the borehole was filled with grout completely. Also, the deepest measurement position 1.8 m above borehole was much higher than in Dörverden. In Horstwalde no filtration took place after lowering the anchor into the borehole. At this time the borehole was filled with flushing suspension with w/c = 3.3, which had a lower self-weight than the grout. It is also assumed that a thin bentonite filter cake laid down at the borehole walls during drilling already, sealing the borehole. This is confirmed by the observation that the flushing suspension showed hydrostatical pressure distribution even 40 minutes after filling the borehole and no water loss due to filtration took place. At all sites during grouting, full grouting pressures were measured with sensors placed within the drill casing. Outside the casing, only a fraction of pressures were measured after a certain point in time. This observation indicates that the grout filtrates and transforms from a liquid to a friction material. However, the filtration time where the entire grout in the grouting length is filtered enough to change its properties varied from site to site. In Dörverden, as soon as the sensors were outside the casing, hardly any grouting pressure was measured, indicating full filtration, while the sensors inside the casing showed full grouting pressure. In Venhaus, stresses outside the casing were only slightly smaller than inside, but the development differed from hydrostatic stress distribution, indicating a stiffening of the grout in the grouting length. In Horstwalde, filtration took even longer and the stresses outside the casing started to diverge from hydrostatic stress distribution just when grouting was completed. This difference in filtration time can be referred to the installation method. In Dörverden, it took approximately 20 minutes to build out one casing section after each grouting step and the whole grouting process per anchor took much longer than at the other sites. This allowed the grout to filtrate due to self-weight between grouting steps. In Venhaus the removal of the casing sections took less than two minutes, and the grouting pressure was lower, which explains why filtration of the grout throughout the full borehole section was achieved later. In Horstwalde even less grouting pressure was applied and the permeability of the filter cake was reduced due to the use of bentonite, leading to filtration starting even later in the grouting process.

Comparison of radial and vertical measurements in Horstwalde confirmed that after a certain point of filtration (when vertical and radial pressures started to diverge) the grout develops some internal friction and stress distribution is inhomogeneous. When pressure was applied in the next grouting stage the vertical stress in the filtered area increased more than the radial stress, but when pressure was released vertical stresses reduced to a low level, while radial stresses remained on a higher level. In Dörverden, filtration already started before grouting within the lowest part of the drill casing and each section was almost fully filtered after it was grouted. In Venhaus, sensors showed full grouting pressure even when they reached the free grouting area, which shows that filtration took a bit longer. Similar

observations were made in Horstwalde. Here the grout started to filtrate only during flushing of the grout after grouting was completed. However, the divergence of radial and vertical stresses indicates that filtration was achieved.

It was observed at all anchors that after each grouting stage, the pressures reduced to suspension pressure level in the unfiltered grout, but remained on a higher level in the filtered material. This pressure level seemed to be higher in radial than in vertical direction. However, the level varied between the different anchors and therefore gives no quantitative information on the stress levels after grouting. Possibly the measurements inside the filtered grout were imprecise because arching actions around the sensors influenced the measured total stresses. In Dörverden is was even assumed that due to the downwards orientation a cavity formed below the sensors and instead of total stresses only pore pressures were measured.

It was not possible to draw general conclusions on the long term development of the stresses in the borehole because too little data is available. Long term measurements in Dörverden gave contradicting results and no reliable long term measurements could be taken at the other sites.

Pressure measurements in the adjacent soil

Comparing CPT and DMT soundings before and after anchor installation showed the influence of grouting on the surrounding soil. DMT measurements in Venhaus showed horizontal stress increases between 25 and 75 kPa. In Horstwalde CPT tests showed a decrease of tip resistance above 16 m and an increase below. This indicates that the soil is loosened due to the external flushing but recovered due to grouting. At both sites the influenced area was detected just below the assumed grout body. This indicates that grouting was more effective in the bottom part of the grout body. Pressure measurements inside the borehole indicated that at least in Horstwalde full filtration during grouting was only achieved in the bottom part of the grout body. Even though full filtration was achieved in the top part during flushing, the filter cake was not subjected to the full grouting pressure at this stage.

Stationary DMTA tests in Venhaus showed stress increases between 100 and 200 kPa in the surrounding soil, whereas results in Horstwalde were subjected to much more variation. This is referred to the deeper position of the DMT blade which leads to higher deviations of the intended position and orientation. However, it was found that the stress state was increased or at least recovered, after it decreased when the drill-casing was withdrawn.

5.5 Conclusion of field measurements

Pressure measurements inside the borehole gave insight in processes taking place during anchor installation. Tests were conducted at sites with similar soil conditions, but with slightly varying installation techniques. It was observed that the variations in anchor installation technique made a significant difference in pressure development within the grout.

Measurements proved that initially the cement grout acts as liquid and grouting pressures are transferred isotropically. After sufficient grouting time, the grout in the grouting length (outside the casing) changes from a liquid to a friction material with anisotropic stress distribution whereas the grout inside the casing is still liquid. It is assumed that the grout thickens because water drains from the grout suspension and contact establishes between the cement particles. The time until the grout was filtered within the full borehole section varied at the different sites, but measurements indicate that at all sites full filtration of the grout along the entire grouting length was achieved. It was also found that the grout filters even without being pressurised, due to its own self-weight. This would lead to the conclusion that grouting pressure is not required for the grout to filtrate, as long as sufficient time is given for filtration. But, if the grout filtrate is considered as friction material which constrains the borehole walls to collapse back inwards after grouting, the value of grouting pressure would influence the radial stresses locked in. After grouting an increase of radial stresses was measured in the grout as well as in the adjacent soil, confirming this assumption.

The measured values of radial stresses after grouting varied significantly for the different test anchors and positions, possibly caused by long grouting sections, different sensor positions and varying grouting pressures within the tests. The increase of radial stresses measured in Venhaus seemed slightly larger than in Horstwalde. Here, smaller grouting pressures were applied, but possibly also the drilling process with external flushing disturbed the soil beforehand. Test results indicate that in Horstwalde filtration was only completed in the bottom part of the grouting length, whereas the grout in the top part only filtered after grouting. It is assumed that due to the external flushing only small grouting pressures could be achieved and that the use of bentonite hindered filtration. The CPT sounding showed that the soil was compacted only in the area of the bottom part of the grout body.

Too little data is available and variations of test results were too high to determine correlations between grouting pressure and radial stresses after grouting. But in general, the tests confirmed that the grout filtrates throughout the borehole and grouting increases or at least recovers radial stresses in the soil.

Chapter 6

Modelling cement grout filtration with FEM

6.1 Introduction

The following chapter covers the numerical analysis of cement grout filtration during anchor installation. A method is developed to simulate the filtration process by applying the finite element analysis (FEM). The two-phase filtration model, which was found sufficient to simulate cement grout filtration in Chapter 4, is implemented into the constitutive model of the grout and the material parameters are changed according to the discharge of mixing water during filtration. After validating the proposed numerical method for one-dimensional and radial flow, an axisymmetric FEM model is prepared based on the conditions of the Dörverden test site (presented in Chapter 5) and the grouting process inside the borehole is simulated. Finally, parametric studies were carried out where the influence of different grouting and material parameters was investigated. Details about the used software package ABAQUS, the functionality and implementation of the presented model as well as the source code are given in Appendix C.

6.2 Implementation of cement grout filtration into the finite element method (FEM)

The grouting process is simulated using Lagrangian finite element analysis (FEM), provided in the program package ABAQUS, version 6.11. To implement cement grout filtration in the FEM analysis, the analytical solution for two-phase filtration is included into the constitutive model.

The intention of the numerical simulations was to determine the effects of grouting on the stress state and properties on the surrounding soil. It was aimed as a calculation tool that could directly be used to simulate the anchor behaviour after grouting (e.g. to simulate anchor pull-out), applying the changed soil conditions. For that reason the FEM method was chosen rather than other methods, which probably would be more suitable to simulate the filtration process separately, but less appropriate to simulate the pull-out tests. For example Kabir and Gamwo (2011) use computational fluid dynamics (CFD) to numerically simulate

filter cake formation, which considers filtration of multiphase drilling fluids. This model allows to take into account flow of the suspension and material properties in relation to particle concentration. Others use numerical methods to solve the analytical filtration equations for specified boundary conditions: Bürger et al. (2001) propose an advanced upwind finite difference method to simulate one-dimensional filtration of suspensions, and Zinati et al. (2009) simulate the filter cake build-up in a wellbore.

Using Lagrangian FEM, the ability of the unfiltered, liquid grout to flow through the borehole is only indirectly modelled because the elements relative position remains unchanged during calculation. The simulation of flow of the liquid grout is approximated by using a very high permeability and low stiffness for the liquid grout material so that in a coupled flow/deformation FEM analysis the flow of the pore water in the liquid grout elements represents the grout flow.

To simulate the grout filtration, the material properties of the cement grout are switched from properties for the liquid grout to properties of the filter cake. The material parameters for the grout are defined dependent on a field variable, which gives information whether the grout is liquid or filter cake.

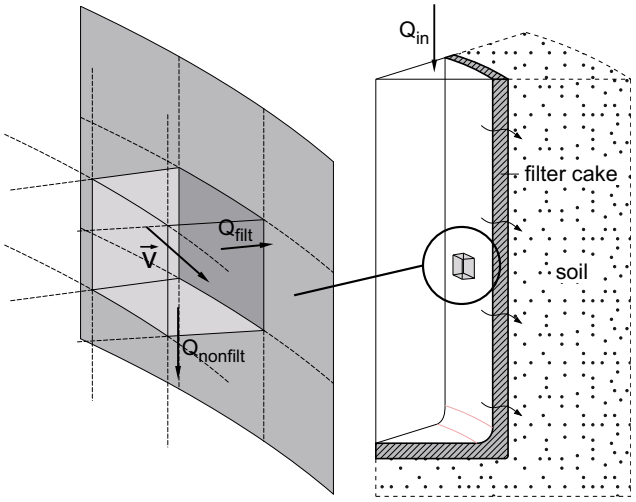

Figure 6.1: Principle sketch of modelling grouting in a borehole.

The material change of one element from liquid to filter cake is controlled by a filter criterion ('critical volume ratio') which relates the discharge of pore water from the grout to the element volume $CVR = \frac{Q_{filt}}{V_{el}}$. This filter criterion is based on the two-phase filtration model presented in Chapter 3. Before stresses and velocities are calculated for a Gauss integration point, this filter criterion is checked to define its material properties.

To calculate the total discharge of the element, only the flow of water into adjacent elements, which already act as filter medium, must be considered, as indicated in Figure 6.1.

This is to distinguish between flow of the liquid grout itself, which also includes flow of particles, and expulsion of water from the grout. Elements located inside the liquid grout should not be considered for filtration because in these elements the flow of pore water only represents flow of grout and does not cause the element to filtrate.

To identify the elements considered for filtration, information about the advancing front of filtration needs to be available during calculation and only elements located directly next to the filter cake material are allowed to change their material properties.

If the actual element is located next to a filter element, the total discharge into this filter element is calculated by transponing the velocity vector at the current integration point in direction of the common surfaces' normal and integrating with time and surface area. If more than one neighbour is filter cake material, the discharge into these elements is cumulated. If the current element was at the filtration front in previous calculation increments, the actual discharge is added to the discharge from previous increments, divided through the element volume and compared to the filter criterion. If elements with more than one integration point would be used, only a proportion of the element volume and common surface area should be taken into account, dependent on the number of integration points per element.

At the time the filter criterion is met, the field variable, which defines the material information, is changed and the filtration front progresses.

Following items need to be included into the FEM code to simulate filtration:

→ Filter criterion $\frac{Q_{filt}}{V_{el}}$

→ Volume of actual element

→ Identification of neighbouring elements

→ Accessing if neighbouring elements are filter cake

→ Discharge into the adjacent filter elements

→ Integrating discharge over time from point where adjacent element becomes filter medium

→ Change material properties if filter criterion is met

6.2.1 Filter criterion

Based on the two-phase filtration theory, the material change from liquid to filter cake is defined by the discharge Q of water from the grout. Assuming full saturation of the grout, the volume change due to filtration is equal to the volume of dissipated water, as the mass of cement particles remains constant (see Figure 6.2). The discharge of water required to filter liquid suspension with w/c_{ini} until a filer cake with w/c_{fc} forms is given by

$$Q_{filt} = \frac{m_c}{\gamma_w}(w/c_{ini} - w/c_{fc}) \,, \tag{6.1}$$

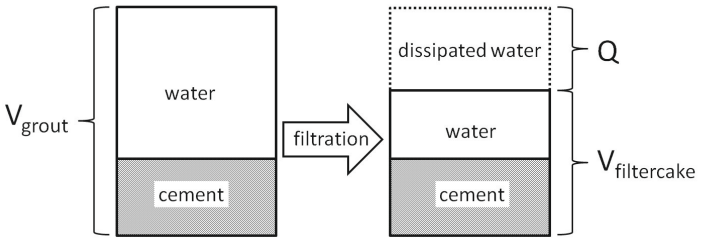

Figure 6.2: Schematic volume relations of liquid grout and filter cake.

where m_c is the mass of the cement particles and γ_w the water density. To control the filtration in the FEM simulation, the discharge of water of one element is compared to its volume, which will then be the filter cake volume $V_{el} = V_{fc}$. The filter criterion therefore is the ratio between the discharge Q_{filt} and the filter cake volume V_{fc}. The filter cake volume is given by

$$V_{fc} = \frac{(w/c_{fc} + 1)m_c}{\gamma_{fc}}, \tag{6.2}$$

where γ_{fc} is the filter cakes density. Combining Equations 6.1 and 6.2 gives the filter criterion

$$CVR = \frac{Q_{filt}}{V_{fc}} = \frac{w/c_{ini} - w/c_{fc}}{w/c_{fc}\frac{\gamma_c}{\gamma_w} + 1} \frac{\gamma_c}{\gamma_w} . \tag{6.3}$$

Assuming an initial water content of $w/c_{ini} = 0.5$ and a filter cakes water content of $w/c_{fc} = 0.3$ gives a critical volume ratio of $CVR = Q_{filt}/V_{fc} = 32.3\%$.

6.2.2 Identification of neighbouring elements

To evaluate whether one element is located next to a filter cake element, the element connectivity is determined. The neighbouring elements of each element can be identified by finding common nodes with other elements in the model: The algorithm **'ele_con'** presented in Section C.2.1 of Appendix C reads the list of elements and corresponding nodes from the input file and compares them. The element connectivity is then stored in an 'common block', which can be accessed by all subroutines in the FEM calculation.

6.2.3 Discharge into the adjacent filter elements

To determine the discharge of one element into a neighbouring element, the flow perpendicular to the common face of both elements is determined by transponing the pore-fluid flow velocity vector $\overrightarrow{v}$. The velocity vector is treated in an explicit way and is provided for each integration point as a result of the previous calculation step. The discharge is then obtained by integrating the velocity over time and the surface area (see also Appendix C.2.1).

6.2.4 Calculating the advancing filtration front

The information whether an element is liquid or filter cake is associated to a field variable ($FIELD(1)$), which is available for all elements during calculation. By accessing this field variable, the filtration front is identified (see Section C.2.2 of Appendix C). During the routine, which evaluates the filter criterion, the value of $FIELD(1)$ of the neighbouring element is checked. Only if the neighbouring element is filter cake, the discharge into this element is taken into account. As the accessible field variables are from the previous calculation increment, the filtration front can only progress one element layer in one increment and small enough time increments need to be chosen.

6.3 Materials

6.3.1 Constitutive laws

In the FEM simulations, different constitutive laws where applied of which a short description is given in C.1 of Appendix C. Detailed descriptions of the material models can be for example found in Brinkgreve et al. (2012), ABAQUS 6.11 (2011b) and Benz (2007).

The grout was modelled linear-elastic for the validation calculations, but the Mohr-Coulomb model with stress dependent stiffness was applied to calculate the grouting process in the borehole.

For calculations where it was focussed on the filtration process of the grout, the soil was modelled linear-elastic, but for the parametric studies, where the radial stresses and the influence of material properties was investigated the Hardening Soil model with small-strain stiffness (HSsmall) was applied for the soil to achieve more realistic results.

The drill casing was modelled linear-elastic.

6.3.2 Material properties

Filter cake

Material properties for the filter cake material were determined based on the geotechnical laboratory tests presented in Chapter 4. For the determination of the radial stresses retained after grouting, the Mohr-Coulomb model with an exponential stiffness formulation dependent on the pressure stress p' was used:

$$G = G^{ref}(\frac{p'}{p_{ref}})^m \,. \tag{6.4}$$

To determine realistic radial stresses after grouting, the unloading after grouting was considered most relevant and the reloading/unloading stiffness of the filter cake material was chosen for calculation. It was determined from the initial part of the oedometer tests, where

an overconsolidation due to grouting was observed. The stiffness below grouting pressure was larger than the assumed primary loading stiffness, and was therefore regarded as unloading/reloading stiffness. A reference stiffness of G^{ref} = 8.8 MPa and an exponent m = 0.6 was determined. The Poisson's ratio was found ν = 0.24. For the Mohr-Coulomb failure criterion the friction angle φ =38°and cohesion coefficient c = 30 kPa were found in triaxial tests. The determined permeability was 7.5×10^{-8} m/s.

Soil

The material parameters for the soil were based on the conditions of the Döverden site presented in Section5.2.1. The material parameters for the 3D calculations were determined based on CPT correlations.

For the parametric studies more general material sets were used to represent a 'loose' and a 'dense' packed sand. They were determined after empirical formulae for quartz sands to correlate relative density (RD) to soil parameters as proposed by Brinkgreve et al. (2010).

The mean permeability was determined from the grain size distributions of several samples of the material using correlations after Hazen (1893): $k = 5 \times 10^{-4}$ m/s.

6.4 Validation of one-dimensional cement grout filtration

The implementation of cement grout filtration into the FEM analysis is validated for a one-dimensional flow scenario similar to the filtration tests in Chapter 4. Various model parameters are varied to investigate their influence on the numerical filtration simulation.

6.4.1 Model definition

A sketch of the one-dimensional filtration model is presented in Figure 6.3. A 10 cm heigh grout sample was modelled using one row of 3D continuum elements (C3D8RP); the element size was 1 cm. The boundary conditions for this validation model were chosen in accordance to the laboratory filtration tests: At the bottom surface vertical deformations were restrained and horizontal deformations were restrained at the element sides. At the top surface free deformation was allowed. Per default, all model boundaries are initially set impermeable.

In a first calculation step, the grouting pressure was applied to the model: A surface load (total stress) of 1000 kPa was applied at the top of the model. Additionally, the pore pressure boundary is set to 1000 kPa to achieve zero effective stress. In a second, transient flow step the pore pressure at the bottom surface of the model was then set to zero to simulate free drainage of the pore water and dissipation of the excess pore pressures.

To define the material properties of the grout, the value of the field variable FIELD(1) is assigned initially. All elements represent cement grout and are assigned to a value of FIELD(1)=0 for liquid grout, except the bottom element which, to allow the filtration to

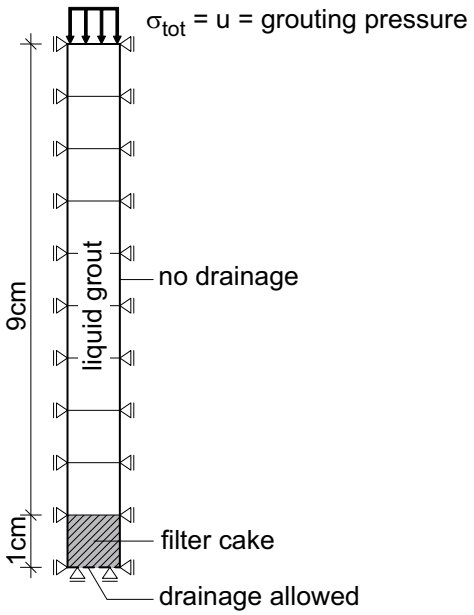

Figure 6.3: Sketch of the one-dimensional filtration model.

start, is considered as filter cake material already and has the value of FIELD(1)=1. Gravity loading is not taken into account for this validation model.

Linear-elastic material behaviour was used to simulate the grout material. Initially a low stiffness modulus and high Poisson's ratio of ν = 0.49 is assigned to the grout elements to approximate liquid material behaviour. At the time, the filter criterion is met in one element, the material's shear modulus and Poisson's ratio are changed to the filter cake properties. The remaining parameters stay unchanged.

6.4.2 Validation results

The numerical simulation of the cement grout was evaluated by comparing the filter cake growth with time to the analytical solution of the two-phase filtration model presented in Section 3.2.1. To allow for a starting point for the filtration, the FEM simulation was started with 1 cm filter cake already. To compare the analytical filtration time, it was therefore adjusted to start at 1 cm filter cake thickness ($t = t - t_{1cm}$). It should be noted that in the numerical simulation no deformation comparable to the piston deformation in the laboratory tests was determined. The element volume in the FEM model corresponds to the filter cake volume after filtration and it is assumed that liquid grout is replenished continuously at the top of the model. The filtration is completed by the time all elements in the model have switched to filter cake material properties. As shown in Figure 6.4, the filtration time determined in the FEM simulation is very similar to the analytical two-phase filtration solution.

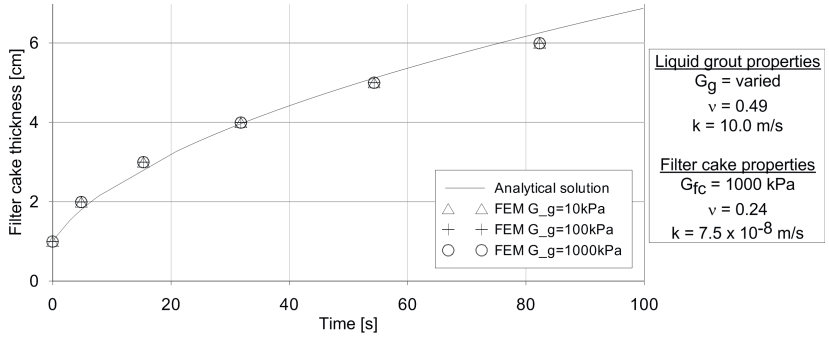

Figure 6.4: Filtration time for varying values of liquid grout stiffness G_g and a filter cake stiffness of $G_{fc} = 1000$ kPa.

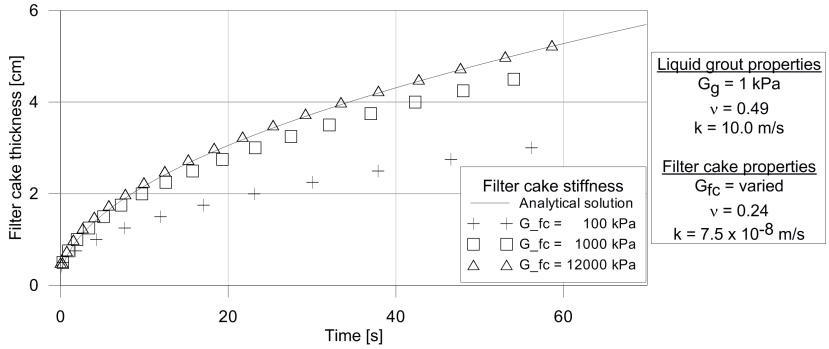

Figure 6.5: Influence of filter cake stiffness on filtration time.

For the numerical simulation, a shear stiffness needs to be defined for the liquid grout elements which is unknown and also physically incorrect. It was however assumed that excess pore pressures govern the filtration process and therefore the shear modulus chosen for the liquid cement grout is insignificant. A variation of the liquid grout's shear modulus G_g showed that its value does not affect the filtration time (Figure 6.4) and confirms that modelling the liquid grout as solid material is applicable in this case.

The filter cake's shear modulus G_{fc}, however, influences the filtration time. Figure 6.5 shows that for a lower value of G_{fc}, the filtration time increases. For higher values, the numerical simulation approaches the analytical solution.

The analytical two-phase filtration model assumes that the filter cake material is rigid, and therefore compression and thus consolidation of the filter cake is not taken into account. It also assumes steady-state flow resulting in a constant pore pressure gradient in the filter cake. Uniform pore pressure is assumed in the liquid phase. In contrast, in the FEM simulation the filter cake compresses and thus consolidates during filtration. The coupled FEM analysis allows for transient flow and the stress gradient in the filter cake changes with time since pore pressures consolidate after the material has changed. The dissipation time depends on

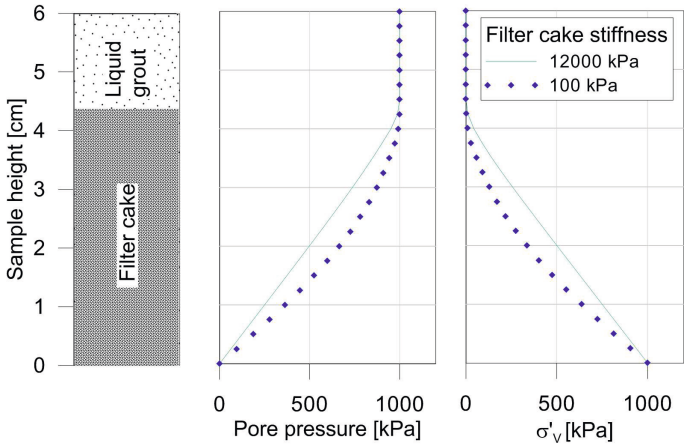

Figure 6.6: Stress distribution in the filter cake - influence of filter cake stiffness on FEM result.

the permeability and stiffness assigned to the filter cake material. Therefore, the filter cake stiffness influences the stress gradient in the filter cake and the flow velocity at the filtration front. For a very stiff filter cake the numerical simulation approaches the analytical results, assuming a rigid filter cake: excess pore pressures dissipate quickly and the pore pressure gradient is linear. For the stiffness determined in laboratory tests the results are very close to the analytical (rigid) solution. The pore water flow induced by the pressure gradient creates seepage forces, resulting in effective stresses in the filter cake. Figure 6.6 shows the stress distribution in the filter cake.

The influence of the element size was investigated by refining the mesh to 0.5 and 0.25 cm. Figure 6.7 shows that the applied mesh size has no influence on the filtration time. Of course, due to the finer discretisation, the filter cake expansion is modelled more precisely with higher resolution, whereas larger elements are less accurate, as the filter cake grows one element at a time. In general, it needs to be ensured that the calculation increments are sufficient small for the chosen element size. Only one element layer next to the filter cake can filtrate within one increment, even if the filter cake growth would be larger analytical. The next element layer is not taken into account for filtration until the next time increment. Therefore, too large time increments would delay the filter cake growth. The smaller the elements, the smaller the maximum allowed time increments should be.

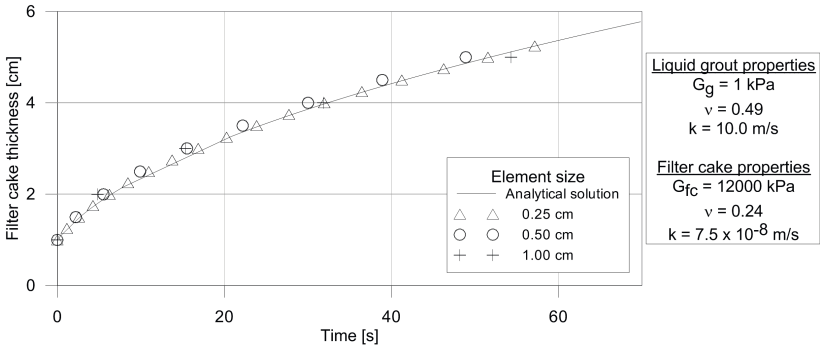

Figure 6.7: Filtration time for different mesh sizes.

6.5 Validation of radial cement grout filtration

After validating the FEM filtration model for one-dimensional flow, it was now applied to radial flow: The radial cement grout filtration due to a constant pumping rate was simulated inside a borehole, using a quasi-axisymmetric model presented in Figure 6.8. Using 3D continuum elements, a 22.5°section of the axisymmetric geometry was modelled.

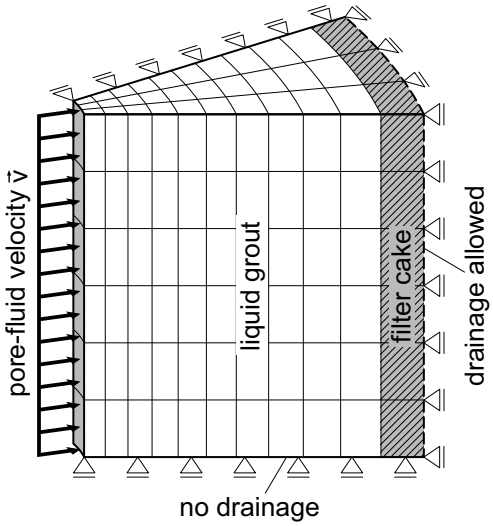

Figure 6.8: Sketch of the quasi-axisymmetric FEM model with radial flow.

6.5.1 Model definition

In this quasi-axisymmetric model a cylindrical coordinate system was introduced to apply the boundary conditions. The side surfaces, representing the symmetry plane of the model

were restrained in tangential direction. The curved outer surface or the model was restrained in radial direction. Bottom and top surfaces were restrained in vertical direction. To create a surface where radial flow could be applied to the model, a small cavity (r = 0.2 cm) was left out in the model centre.

Similar to the 1D model, the field variable FIELD(1) was used to define the material properties of the grout. Initially, the liquid grout was assigned to a value of 0. One element layer at the outer diameter was assigned to a value of 1, to allow the filtration to start. The pore pressure was initially set to zero in the whole model. Per default all model boundaries were set impermeable. Gravity loading was not taken into account.

Only one calculation phase was used for the simulation. A constant inflow velocity of -1 cm/s was applied to the created cavity surface at the model centre. The pore pressure boundary at the outer model radius was set to zero to allow for free drainage. As in the 1D model, linear-elastic material behaviour was assumed for the grout.

6.5.2 Validation results

To validate the FEM simulation, the filter cake formation was compared to the analytical two-phase filtration solution for radial flow, presented in Section 3.3. Figure 6.9 shows that also for the radial model with constant pumping rate the FEM simulation complies well with the analytical solution. The slightly faster filtration in the FEM simulation towards the end of the test can be explained by the element shape in quasi-radial geometry: The discharge is calculated from the fluid velocity at the integration point rather than the velocity at the element surface, resulting in a slightly larger discharge than in the analytical solution. The pore pressure development at the model centre (representing the grouting pressure of the liquid grout) is presented in Figure 6.10. Compared to the analytical steady state solution the porepressures increase stepwise in the FEM simulation just when the filter cake progresses one element row.

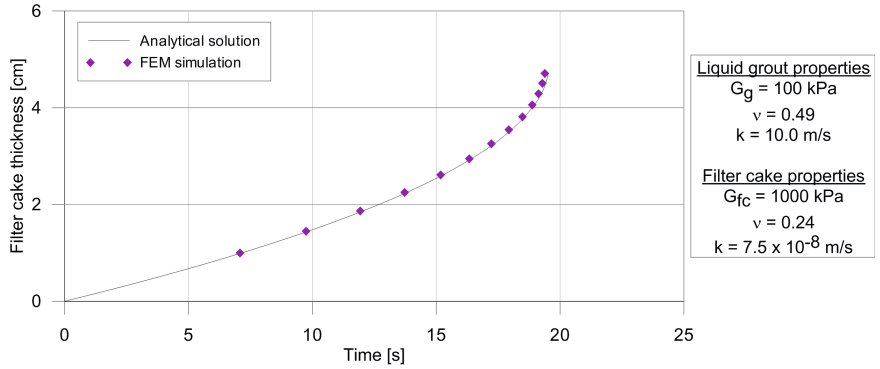

Figure 6.9: Radial filter cake formation at FEM simulation compared to analytical solution.

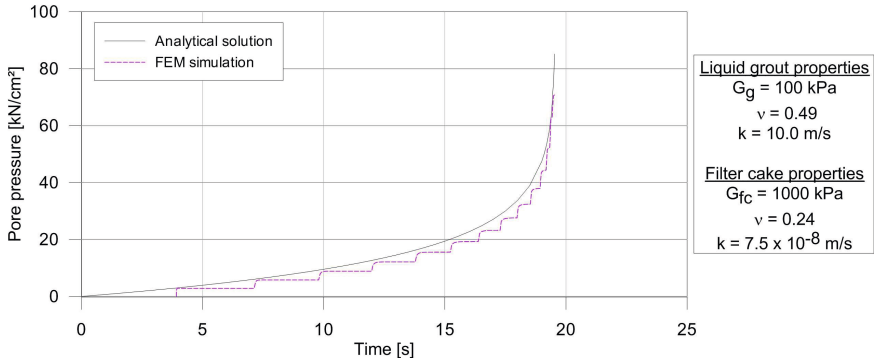

Figure 6.10: Pore pressure development at borehole centre in radial filtration FEM simulation compared to analytical solution.

6.6 Cement grout filtration inside the borehole

After validating the implementation of cement grout filtration, the grouting process during anchor installation was simulated based on the conditions of the Dörverden building site described in Chapter 5. At this site the anchors are vertical and thus axisymmetric symmetry could be employed. The model set-up is presented in Figure 6.11: A 12 m heigh, quasi-axisymmetric section with a 3 m radius and 22.5°angle of soil was modelled. In the model centre, a 9 m long vertical borehole with a radius of 10 cm was modelled, with the soil extending 3 m below the borehole. Instead of modelling the anchor bar directly, a 2.5 cm cavity was left in the borehole centre and this boundary was assumed undeformable and impermeable. Two grouting stages of 3 m grouting length each were simulated. The withdrawal of the casing was taken into account by changing the material properties of the casing elements from ‘steel’ to ‘liquid cement grout’ properties.

6.6.1 Model definition

To achieve a quasi-axisymmetric model, following boundary conditions were applied: tangential deformations were restrained at the side surfaces and radial deformations were restrained at the outer radius. Vertical deformations were omitted at the bottom of the model. Horizontal deformations were also restrained at the elements representing the borehole casing.

Pore pressure boundary conditions were set equal to the groundwater stress distribution at top, bottom and radial sides of the model. The tangential sides were defined impermeable. As initial conditions for the calculation, the expected stress field was assigned to the elements to minimise deformations due to gravity loading in the first step. The self-weight of soil and grout was assigned to the model and pore pressures were set to the expected groundwater pore pressure. Zero effective stress was defined for the liquid grout inside the borehole. The

borehole was modelled ‘wished in place’, meaning that the material in the borehole was already grout at the beginning of the calculation.

For the model two different mesh options were used: In one model (model ‘G_LM’), the element width was increased from 0.5 cm in the borehole towards 50 cm at the outer radius of the model. The general element height was 9.4 cm and only refined towards the borehole bottom to 2.7 cm. The borehole and 10 cm of adjacent soil are modelled using cubic, 8 node elements (C3D8RP) whereas the surrounding soil is modelled using 6 node elements (C3D6P). In the second model (model ‘G_FM’), the mesh was refined: The element height was refined at the borehole bottom and 3 m above, where the casing ends at the first grouting stage. 6 node elements (C3D6P) were used for the entire model. In both models, instead of modelling the anchor rod, a small cavity was left out in the model centre. This cavity was also extended into the soil below the borehole to prevent numerical singularities due to pointy elements. The mesh and boundary conditions are presented in Figures 6.11 and 6.12.

The material properties of the cement grout were defined dependent on the field variable FIELD(1), where a value of zero was assigned to all liquid grout elements and a value of 1 for filter cake elements. One layer of elements was used as interface layer between grout and borehole casing in the regions where the casing was not yet withdrawn. The material properties of these elements were also defined dependent on field variable FIELD(1), so that the material could be changed to simulate the casing withdrawal. To define the initial filtration front, all soil elements were assigned to FIELD(1)=1, even though the material parameters were not dependent on the field variable. Thus, the soil represented the filter material (associated with FIELD(1)=1) and filtration could start in grout elements adjacent to the soil.

Linear-elastic material behaviour was chosen for the soil and casing elements, whereas the Mohr-Coulomb model was used for the grout. For the casing elements a very low permeability approximates an impermeable interface. The low shear stiffness is applied to the interface to simulate frictionless contact between grout and casing and to prevent the grout ‘sticking ’ to the casing and causing unrealistic stresses in the grout. The material of the casing elements is switched to liquid grout properties when the casing is withdrawn in this section. Material properties are presented in Table 6.1.

6.6.2 Calculation steps

STEP 1: Grouting-1

In the first calculation step, instantaneous gravity loading was applied to the entire model and a user defined pore pressure boundary equivalent to the groundwater pressure was applied to the outer radius of the model. The overburden pressure was applied as load to the top surface of the model (except the borehole). Then, grouting of the first 3 m borehole section was simulated: To simulate a pumping rate of 30 l/min a pore-fluid velocity of $\vec{v}$ = -0.021292 m/s was applied to the borehole surface at the top with a surface area

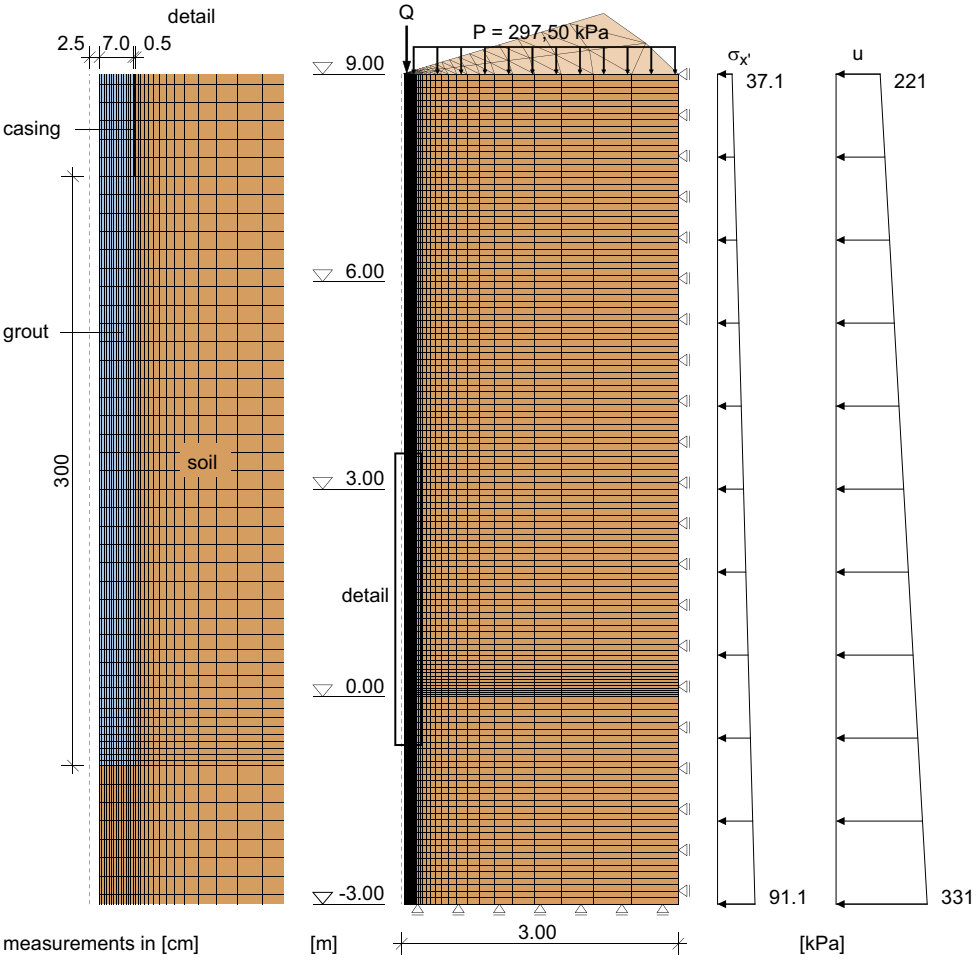

Figure 6.11: 3D-FEM model of the vertical anchor installation ('G_LM').

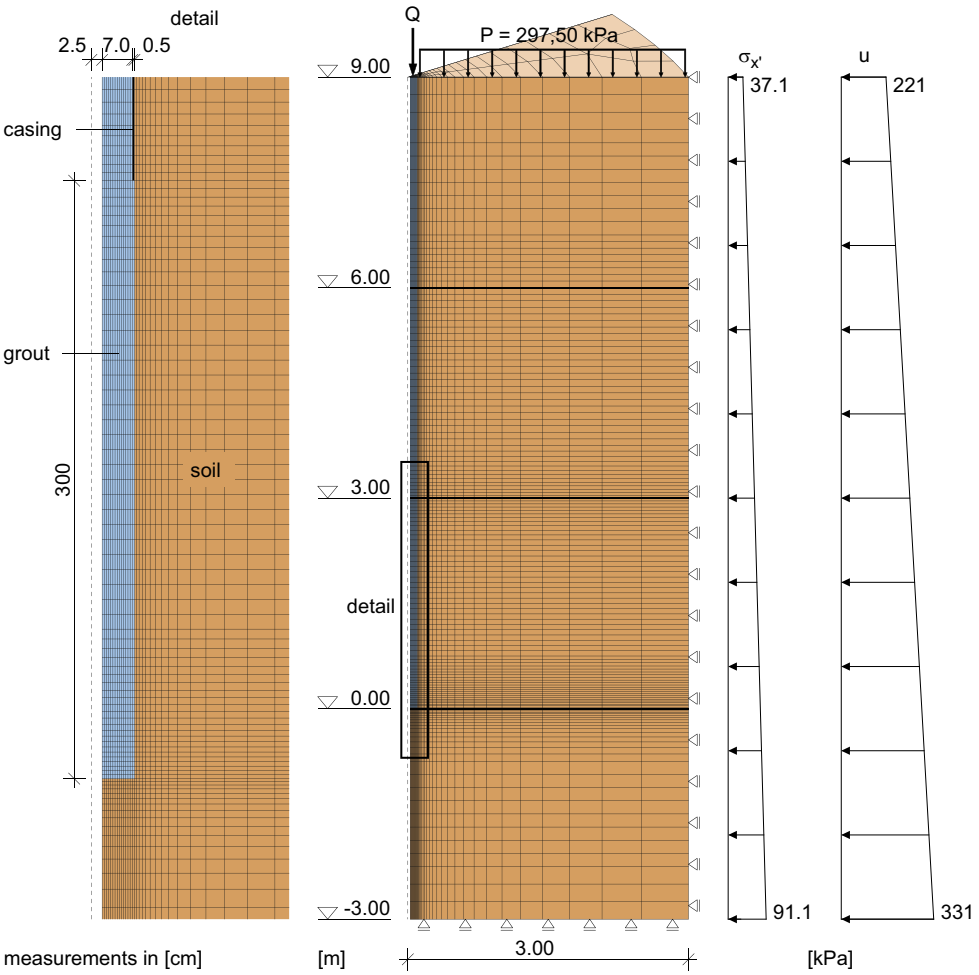

Figure 6.12: 3D-FEM model of the vertical anchor installation (‘G_FM’).

Table 6.1: Material parameters used for the 3D model.

Linear Elastic model				Mohr-Coulomb model			
Parameter		Dense sand	Casing	Parameter		Liquid grout	Solid grout
E	$[MPa]$	42	1×10^{-3}	G	$[MPa]$	1	30
ν	[-]	0.3	0	ν	[-]	0.489	0.3
				m	[-]	0	0
				c'	$[kPa]$	30	30
				φ'	$[^\circ]$	38	38
				ψ	$[^\circ]$	38	38
				σ_{ten}	$[kPa]$	30	30
				CVR	[-]	0.323	
k	$[m/s]$	5×10^{-4}	1×10^{-20}	k	[m/s]	1.0	7.5×10^{-8}

of $A = (0.09^2 - 0.025^2) * \pi = 0.023483\ m^2$. The calculation step was terminated once the grouting pressure of 30 bar was reached in the liquid grout at the top of the borehole.

STEP 2: Unloading-1

In the second calculation step, the release of grouting pressure after grouting the first section was simulated. The pore-fluid velocity at the top of the borehole was set to zero. The duration of this step was set to 60 seconds.

STEP 3: Grouting-2

The second grouting stage was calculated in this step. To simulate the withdrawal of the 3 m casing section, material properties of the elements representing the casing section that is withdrawn were changed to liquid grout properties by changing the field variable to $FIELD(1) = 0$ and the horizontal fixity was released. The constant pore-fluid velocity of -0.021292 m/s was again applied at the borehole top to achieve the constant pumping rate. The step was stopped once the grouting pressure of 30 bar was reached in the liquid grout.

STEP 4: Unloading-2

As in STEP 2 the grouting was stopped by setting the pore-fluid velocity to zero at the borehole top.

6.6.3 Calculation modes

After the first calculations, it was observed that the filter cake progresses far into the borehole casing, which was not expected. It was assumed that in reality the flow inside the casing would flush the filter cake material towards the grouting length to some extend. This Eulerian phenomenon can hardly be reproduced in a Lagrangian FEM calculation. Therefore comparison calculations are carried out, where filtration inside the casing was permitted.

6.6.4 Results of model ‘G_LM’

The filter cake formation and grouting pressure at the borehole centre calculated with the equally meshed model for filtration in the casing (model‘G_LM_A’) and no filtration in the casing (model ‘G_LM_B’) is presented in Figure 6.13.

With both calculation options, the filter cake developed from the borehole walls towards the centre and the thickness was almost even with depth along the grouting length. As shown in Figure 6.13a, the filter cake reaches well into the casing in model ‘G_LM_A’ (where filtration was allowed inside the casing), whereas in model ‘G_LM_B’ the filter cake only reaches up to the point where filtration is permitted. In the first grouting stage, however, the filter cake thickness in the free grouting length and the grouting pressure in the borehole centre were almost identical for both models. The pore pressure in the borehole centre increased disproportionally with time. With increasing filter cake thickness, the hydraulic resistance increases and thus the pressure generated with a constant pumping rate. Due to the decreasing radius of the open cavity, the filtration rate (cm/s) increases towards the borehole centre. The centre pore pressures at 1.5 m, 4.5 m and at top of the model correspond to each other, showing the pressure distribution of a liquid material. In both models, the filter cake does not reach into the borehole centre in the first grouting stage, because the limit pressure of 30 bar is reached previously and pumping is stopped. During the second grouting stage, pore pressures increase much faster in ‘G_LM_A’ than in ‘G_LM_B’, due to the filter cake material already existent in the new grouting length from the first grouting stage. The pore pressure in the first grouting length drops to the groundwater pore pressure, as soon as the filter cake material reaches the borehole centre. In the second grouting length, the pore pressure increases to the grouting pressure of 30 bar but after grouting the pore pressures dissipate gradually toward the groundwater pressure. In ‘G_LM_B’ pore pressures inside the liquid grout increase similarly to the first grouting stage, as no filter cake is existent in the actual grouting length. The pore pressures in the first grouting length drop to groundwater pore pressure as soon as the filter cake reaches the borehole centre. Both calculation options show the full grouting pressure at the top of the model, whereas in the bottom grouting length a lower pressure increase was observed.

The radial deformation at different depths and along the borehole surface are presented for different time increments in Figures 6.14 and 6.15. The deformation increases from zero at the borehole centre towards a peak value at the borehole surface and reduces exponentially from this peak value inside the soil. After unloading, the deformations reduce slightly; mostly at the borehole walls. The filter cake formation in the first grouting stage is very homogeneous with time for both models, resulting in even radial deformations along the grouting length and in the soil. In the second grouting stage however, the results of models ‘G_LM_A’ and ‘G_LM_B’ differ from each other. In the model where filtration is allowed inside the casing, the filter cake already reaches far into the second grouting length at the beginning of the second grouting process. The filter cake developed faster at the bottom than at the top of the grouting length, and reaches the centre before the full grouting pressure is

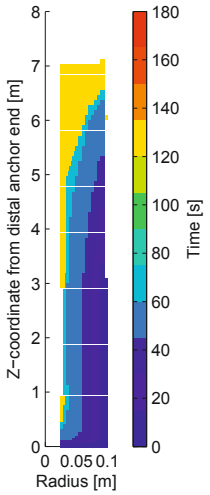

(a) Filter cake 'G_LM_A'.

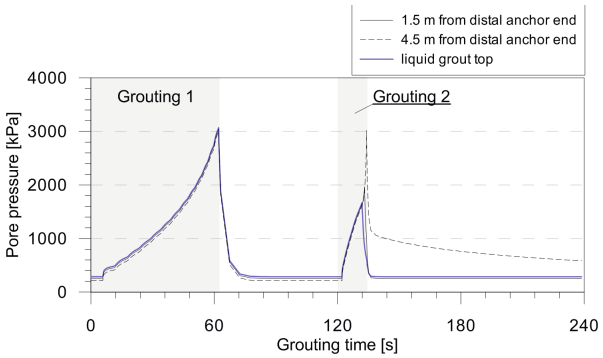

(b) Grouting pressure at borehole centre.

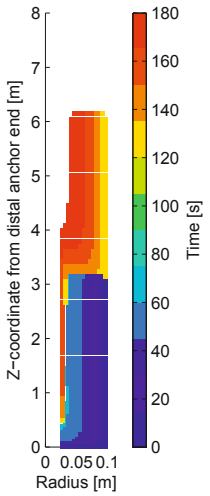

(c) Filter cake 'G_LM_B'.

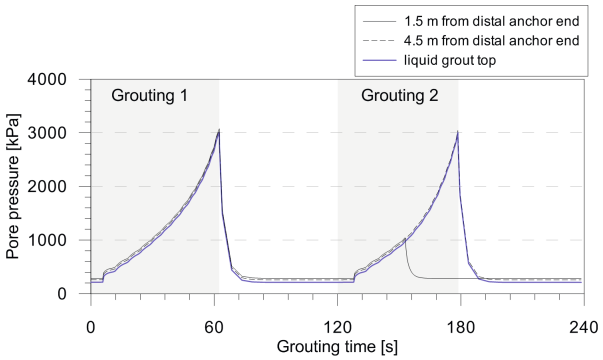

(d) Grouting pressure at borehole centre.

Figure 6.13: Filter cake formation and grouting pressure where filtration within borehole casing is allowed (a, b) or prevented (c, d).

achieved. In contrast, the filter cake in model ‘G_LM_B’ develops similar in both grouting stages and thus, similar deformations are achieved in both grouting sections.

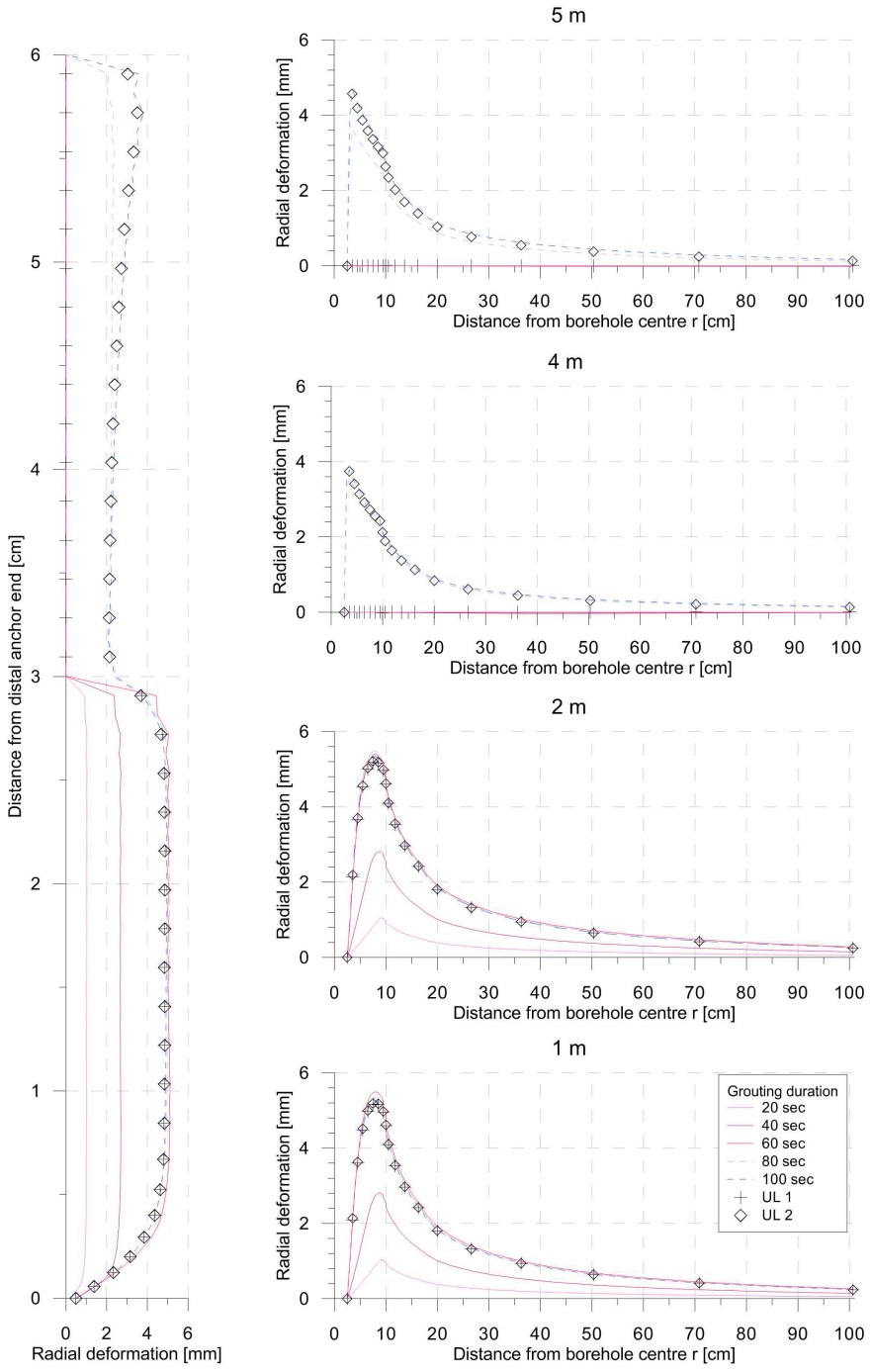

Figure 6.14: Development of radial deformations in model 'G_LM_A' with filtration in the drill casing.

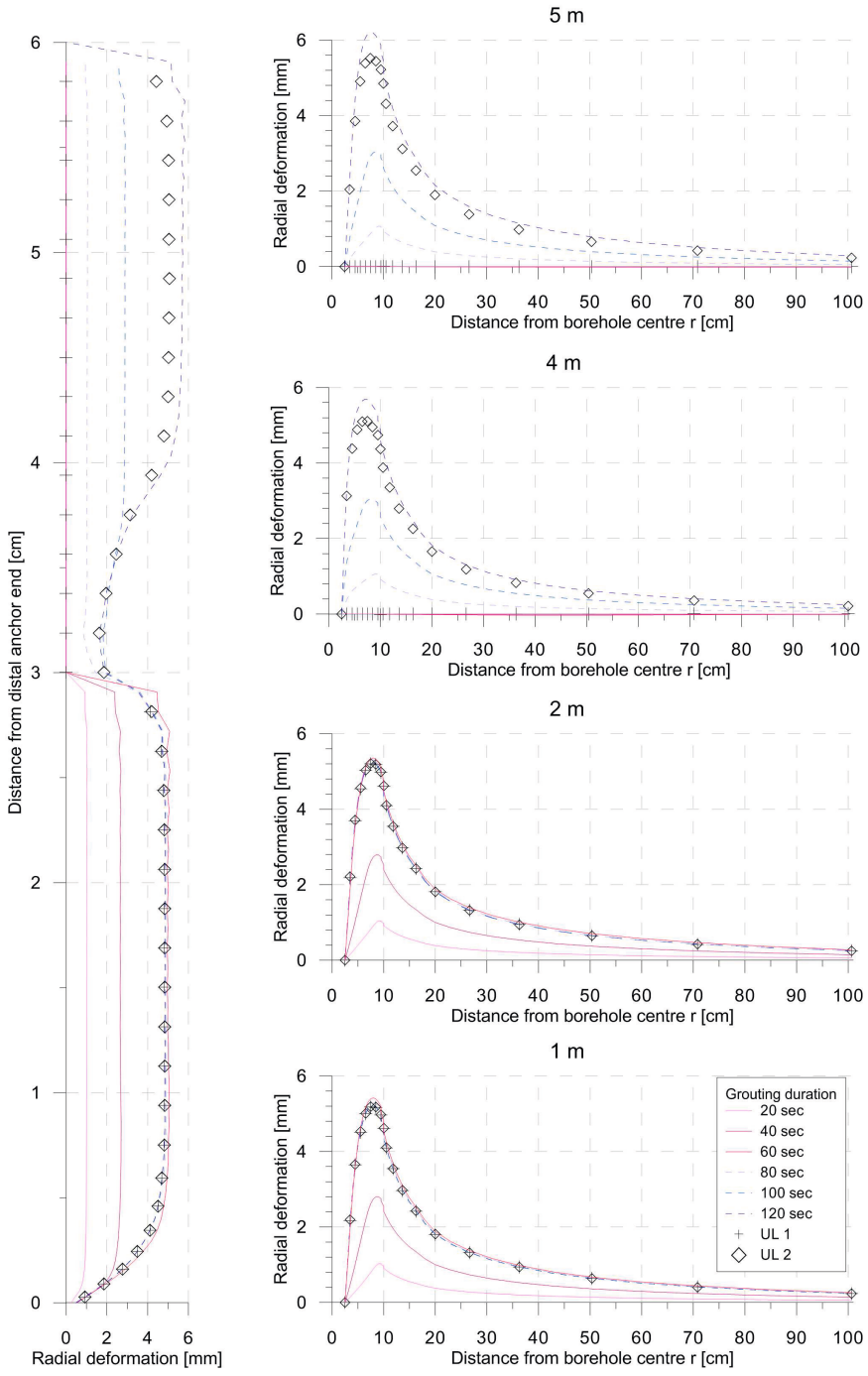

Figure 6.15: Development of radial deformations in model 'G_LM_B' without filtration in the drill casing.

6.6.5 Mesh dependency and filtration direction

The mesh dependency of the model was investigated by mesh refinement. The filter cake formation in the first grouting stage calculated with a refined mesh is presented in Figure 6.16. In model 'G_FM_A' (filtration inside the drill casing) the filter cake formation was similar to the larger mesh, albeit less regular. After 75 seconds grouting time, the filter cake reaches the borehole centre in the middle of the grouting length, but not throughout to the distal anchor end. As this liquid grout is now separated from the liquid grout above, it is not subjected to the grouting pressure any more and does not filtrate completely. This observation was even more distinct in model 'G_FM_B', where filtration inside the casing was permitted. Here, the filter cake developed rapidly at the end of the drill casing and reached the borehole centre after a few seconds. The filter cake plugs the casing just at the opening and the desired grouting pressure is reached before the filter cake builds up in the free grouting length.

This mesh dependency of the numerical simulation was unexpected, especially as a refined mesh should result in more precise calculation results. Possible reasons for the artificial plugging effect with a refined mesh are that numerical singularities are more distinct for smaller elements, whereas they are smeared in larger elements. The local radial filter cake formation at the casing end was caused by a large radial flow component in the element just below the drill casing as showed in Figure 6.17. This horizontal flow component arises from the change of flow direction at the end of the drill casing and is restricted to one single element. It is therefore more distinct in smaller meshes. Inside the casing, flow occurs in vertical direction only, whereas in the free grouting length also a horizontal flow component is apparent. The horizontal flow component leads to filtration of the element just below the casing, even though the main flow direction is still vertical. Thereafter, filtration takes place in the adjacent elements. In reality, no filter cake would build up against the main flow direction, as the particles would be flushed away (similar to the situation inside the borehole casing). For larger elements this filtration against the main flow direction is less significant, as the large peak value just below the drill casing is smeared over a larger area.

6.6.6 Results for filtration in main flow direction only

The effect of filtration against the main flow direction was investigated in comparison calculations carried out with a modified filtration model, where only filtration in main flow direction was considered. To achieve filtration in main flow direction, only discharge of water from the grout is taken into account, if the main flow direction is directed towards the filtration front. Figure 6.18 shows the filter cake formation with time in models 'G_LM_B_filtdir' and 'G_FM_B_filtdir', where only filtration in a main flow direction was allowed. The filter cake forms more smoothly within the borehole geometry, but the filtration time is much longer than for the previous models. This is because in this model the balance between pumping rate at the top of the borehole and filter cake volume increase is not maintained,

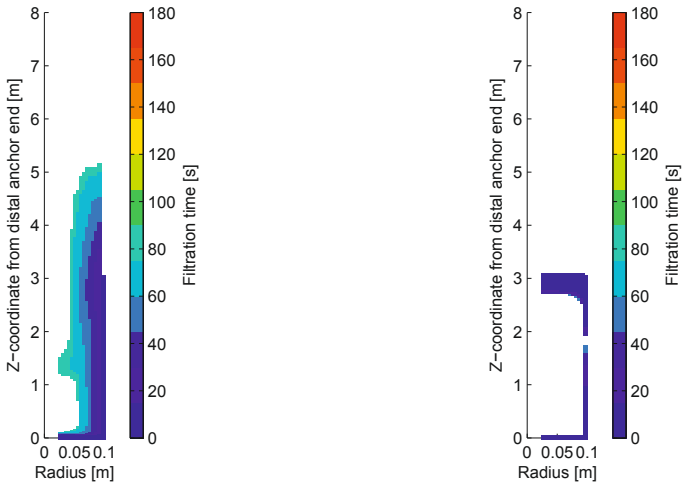

(a) Filter cake ‘G_FM_A’. (b) Filter cake ‘G_FM_B’.

Figure 6.16: Filter cake formation during the first grouting stage for refined mesh.

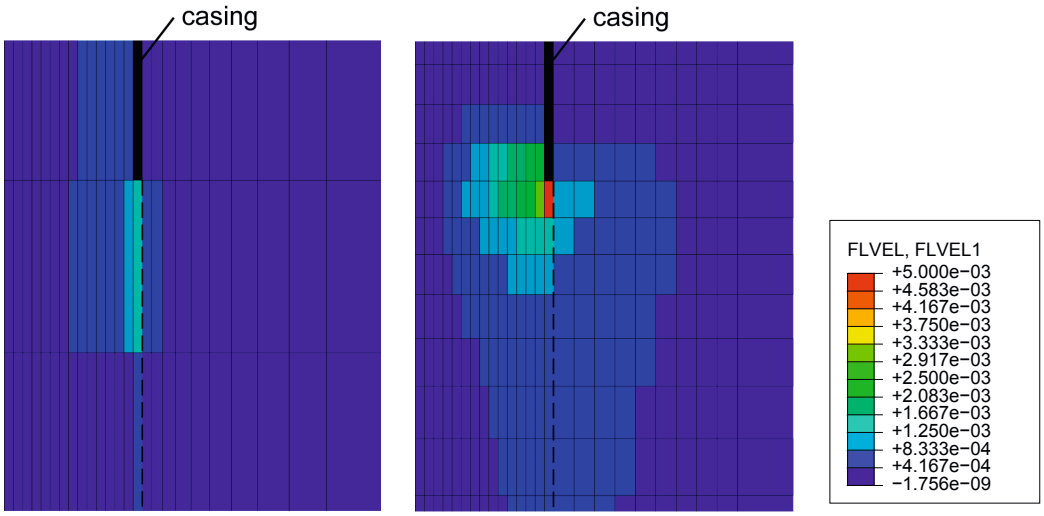

(a) Large mesh. (b) Small mesh.

Figure 6.17: Radial flow velocity in m/s at beginning of grouting length.

as the discharge of water from the borehole is disregarded if it is not directed into the main flow direction. In reality the suspension would drain due to filtration against the main flow direction, but would then be flushed downwards by the current. Due to the gradual increase of filter cake thickness with depth, the radial deformations on the borehole cavity are less uniform than for the regular model (Appendix C, Figure C.7).

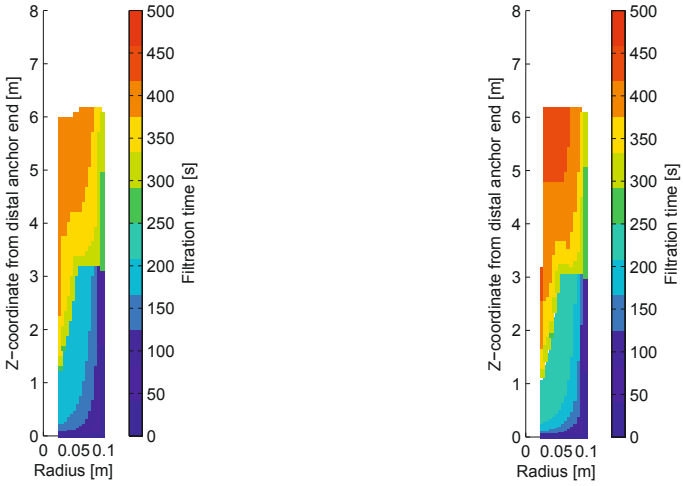

(a) Filter cake ‘G_LM_B_filtdir’.

(b) Filter cake ‘G_FM_B_filtdir’.

Figure 6.18: Filter cake formation for filtration in main flow direction only.

6.6.7 Summary

In the models ‘G_LM_A’ and ‘G_LM_B’, the filter cake formed evenly at the borehole walls of the first grouting length resulting in homogeneous deformations along the grouting length after grouting. In the second grouting stage, the radial deformations after grouting were much smaller in model ‘G_LM_A’ than in model ‘G_LM_B’, where deformations in both grouting lengths were almost identical. Filtration inside the borehole casing is only likely to occur at the bottom because the liquid grout flows inside it and would flush any existing filter cake down. Considering this effect, model ‘G_LM_B’ represents the grouting process better than model ‘G_LM_A’. Calculations with the modified filtration model, which takes into account filtration in the main flow direction only, showed a more gradient filter cake formation with increasing filter cake thickness along the borehole towards the bottom. The filtration time was much longer in this model because the balance of inflow of liquid grout and filter cake formation is not maintained. Therefore, the initial filtration model, taking into account filtration in all directions, gives a better estimation of the filtration time. The shape of the filter cake is likely to lie between the initial model and the modified model

with filtration in main flow direction only. Corresponding to the filter cake shape, the radial deformations along the borehole casing are more equally distributed in the regular model, whereas it increases with depth in the modified model.

6.7 Parametric study - Radial flow

The influences of different soil and grout properties were investigated in parametric studies, using the model shown in Figure 6.19. This model is a 20 cm thick horizontal section of the 3D-filtration model presented in Section 6.6. As in the original model, a cavity of 2.5 cm was left out in the borehole centre to represent the anchor steel bar and to apply a radial pore-fluid velocity to the model.

6.7.1 Model definition

The boundary conditions of the wedge were similar to the original model, with tangential constraints at the sides and radial constrains at the centre and outer diameter of the model. Vertical deformations were constrained at the top and bottom boundaries to achieve plane-strain conditions. To achieve plane flow conditions, the top and bottom boundaries were defined impermeable and also the tangential sides were defined impermeable. In this simplified model, gravity loading was disregarded and the stresses assumed uniform with depth. The in-situ pore pressure was applied as uniform boundary condition on the outer model radius. The assumed in-situ, before-drilling, effective stresses and pore pressures at a depth of 1 m above the anchor end were assigned as uniform initial stress field to the elements. Zero effective stress was assigned to the grout elements. For the entire model, 8-node cubic elements with reduced integration (C3D8RP) were used. The mesh and applied loads are presented in Figure 6.19. Similar to the previous models, the material properties of the cement grout were defined field variable dependent to distinguish between liquid and solid properties. The filtration model with Mohr-Coulomb failure criterion was used for the grout, whereas the Hardening Soil model with small-strain stiffness (HSsmall) was chosen for the soil.

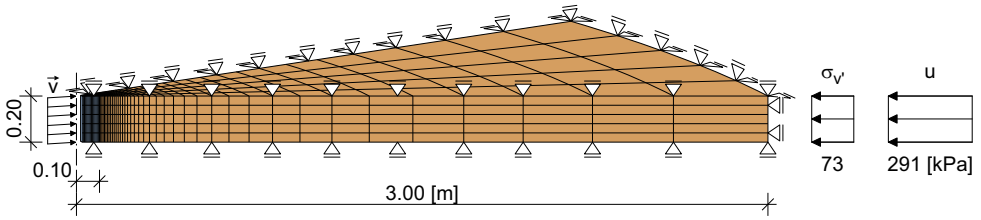

Figure 6.19: Plane strain filtration model.

The parametric studies were based on a reference parameter set given in Table 6.2. For the sand two reference parameter sets were used: One representing a loose packing (‘loose

sand') and one representing a dense packing ('dense sand'). The material parameters were determined using empirical formula for quartz sands to correlate relative density (RD) to soil parameters as proposed by Brinkgreve et al. (2010).

All parametric studies were carried out with both parameter sets for the sand, results for the 'loose sand' parameter set are, however, partly presented in the appendix.

Table 6.2: Material parameters used for the parametric study.

		HSsmall model				Mohr-Coulomb model	
Parameter		Loose sand	Dense sand	Parameter		Liquid grout	Solid grout
E_{50}^{ref}	$[MPa]$	20	45	G^{ref}	$[MPa]$	1	11
E_{oed}^{ref}	$[MPa]$	20	45				
E_{UR}^{ref}	$[MPa]$	60	135				
m	[-]	0.6	0.5	m	[-]	0.75	0.75
p^{ref}	$[kPa]$	100	100	p^{ref}	$[kPa]$	100	100
ν_{UR}	[-]	0.2	0.2	ν	[-]	0.489	0.24
c'	$[kPa]$	0.01	0.01	c'	$[kPa]$	0	30
φ'	$[^\circ]$	32.2	37.4	φ'	$[^\circ]$	38	38
ψ	$[^\circ]$	2.2	7.4	ψ	$[^\circ]$	8	8
R_f	$[-]$	0.96	0.91				
σ_{ten}	$[kPa]$	0.01	0.01				
G_0	$[MPa]$	80	110	CVR	[-]	0.323	
$\gamma_{0.7}$	[-]	1.7×10^{-4}	1.3×10^{-4}				
k	[m/s]	5.0×10^{-4}	5.0×10^{-4}	k	[m/s]	1.0	7.5×10^{-8}

6.7.2 Calculation steps

The model section covers a horizontal slice of the model and thus, only one grouting stage was modelled.

STEP 1: Grouting

In the first calculation step, grouting was simulated by applying a constant pore-fluid velocity $\overrightarrow{v}_{grout}$ in radial direction to the cavity in the borehole centre, corresponding to the desired pumping rate of liquid grout at top of the borehole. Similar to the previous full 3D borehole model a pumping rate of 30 l/min with a limiting grouting pressure of 30 bar was applied, unless different parameters are stated. The calculation step was terminated once the limit grouting pressure was exceeded or the filtration front reached the borehole centre (all grout elements changed from liquid to filter cake state).

STEP 2: Unloading

In the second calculation step unloading of the soil after grouting was simulated. The pore-fluid velocity at the borehole centre was set to zero, defining the surface impermeable at the same time.

6.7.3 Radial stresses and deformations using HSsmall model for the soil

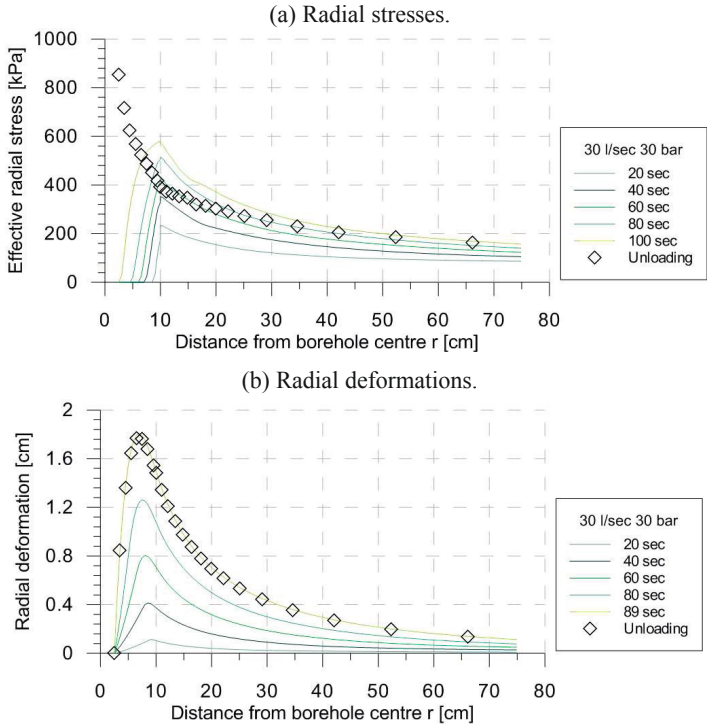

Figure 6.20: Results for grouting in ‘loose sand’ with 30 l/min and a limiting grouting pressure of 30 bar.

The radial stress distribution after grouting and unloading was calculated with the reference parameter set for the grout and the two material sets for the soil (‘loose sand’ and ‘dense sand’), as given in Table 6.2. The simulation results for different grouting durations are presented in Figures 6.20 and 6.21. For both material sets, full filtration was achieved before the limiting grouting pressure of 30 bar was reached. Taking into account plastic soil behaviour, the grouting pressures and radial stresses during and after grouting are much lower than for linear-elastic soil. When the borehole is expanded during grouting, radial stresses increase but the tangential stresses reduce until failure. A plastic zone forms around the borehole and radial stresses do not increase further. Also the radial stresses reduce significantly after unloading compared to the stresses during grouting, in contrast to the calculations with linear-elastic soil, where radial stresses were almost fully retained after unloading. In the ‘dense sand’ larger radial stresses are retained after grouting than in the ‘loose sand’. Due to the larger stiffness the borehole deformation was smaller than for the ‘loose sand’ and therefore larger grouting pressures were achieved.

(a) Radial stresses.

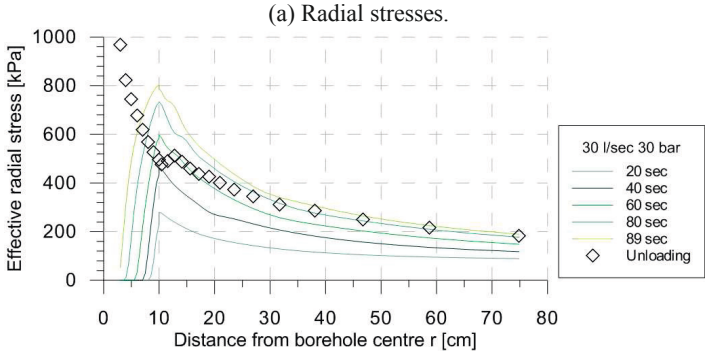

(b) Radial deformations.

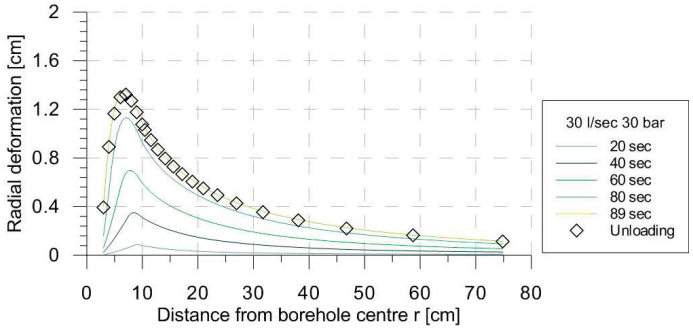

Figure 6.21: Results for grouting in ‘dense sand’ with 30 l/min and a limiting grouting pressure of 30 bar.

6.7.4 Variation of grouting parameters

The influence of the pumping rate and the limiting grouting pressure was investigated in a parametric study: For limiting grouting pressures of 10, 20 and 30 bar the pumping rate was varied from 10 l/min to 130 l/min (33.33 to 43.33 l/min per m grouting length respectively), using the reference material parameter sets given in Table 6.2. A constant pore fluid velocity corresponding to the pumping rate was applied at the borehole centre until the limiting grouting pressure was reached in the liquid grout or the filtration was completed and all grout elements switched to filter cake material.

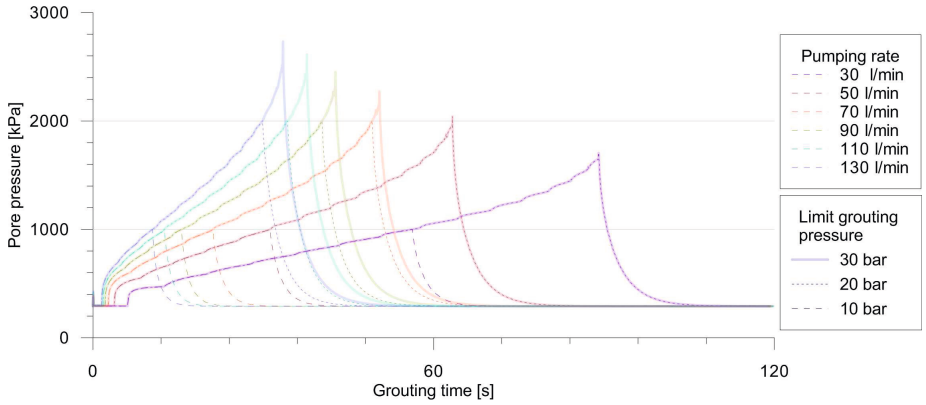

Figure 6.22: Grouting pressure development for different pumping rates in ‘dense sand’.

The pore pressure build-up at the borehole centre is presented for different pumping rates in Figures 6.22 and C.8 for the dense and loose sand respectively. The pumping rate clearly influences the achieved grouting pressures in the liquid grout. The higher the pumping rate, the higher the achieved pressures. For the simulation in the dense sand maximum grouting pressures up to 27 bar were reached at a pumping rate of 130 l/min. Pressures exceeding 20 bar were reached for pumping rates larger than 60 l/min and 10 bar grouting pressure was reached for all pumping rates. In cases where the specified limit grout pressure was not reached during grouting, the calculation was stopped when all grout elements were filtered out. In reality the filter cake would progress inside the casing and the grouting pressure would therefore increase at top of the casing anyway.

The resulting radial stresses at the borehole walls after grouting and unloading are presented in Figures 6.23 and C.9. The filled symbols represent simulations where the limit grouting pressure was reached and open symbols indicate cases where the grouting process was stopped because filtration was completed.

For the cases where full filtration occurred before the limit grouting pressure was reached, the radial stresses at the borehole walls after grouting increase with increasing pumping rate because higher grouting pressures were achieved. In cases were the limit grout pressure was reached, stresses after grouting increase slightly with increasing pumping rates but remain at

a constant level at higher pumping rates. After unloading, residual radial stresses increased with increasing pumping rate if full filtration had been achieved before the limiting pressure was reached, whereas the pumping rate is insignificant when the limit grouting pressure was reached.

(a) Radial stresses at maximum grouting pressure.

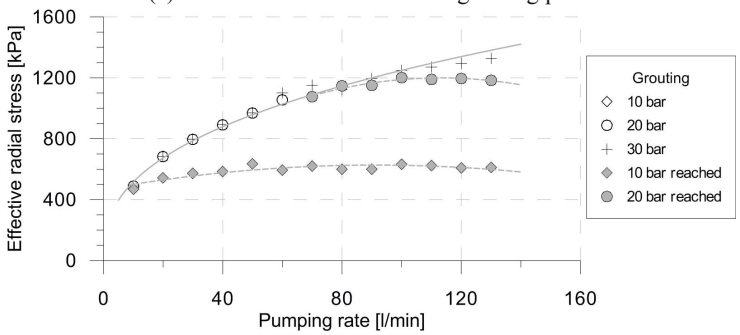

(b) Radial stresses after unloading.

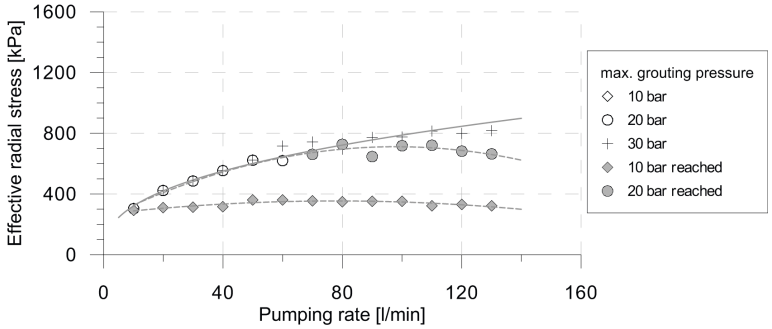

Figure 6.23: Radial stresses at borehole walls after grouting in ‘dense sand’ with varying grouting pressures and pumping rates.

6.7.5 Variation of filter cake stiffness

The influence of the filter cake stiffness G_{fc} on the simulation results was investigated by varying G_{fc} from 3 to 11 MPa, where the stress exponent m = 0.6 was taken for G_{fc} = 3 MPa and 5 MPa and m = 0.75 for G_{fc} = 7 MPa, 9 MPa and 11 MPa to meet the ranges of the virgin and reloading stress-strain curve from oedometer tests respectively. The remaining parameters for grout and soil were taken from the reference parameter set.

During all calculations full filtration of the cement grout occurred before the limit grouting pressure of 30 bar was reached. Figures 6.24 and C.10 show that the filter cakes’ stiffness does not influence the radial stresses during grouting. After unloading, however, slightly

higher pressures are retained for a stiffer filter cake, as it better retains the soil's back-deformation. The variation of residual radial stresses is around 150 kPa for the loose and 200 kPa for the dense sand. This effect of larger radial stresses is only apparent in a thin zone around the grout body.

(a) Radial stresses at maximum grouting pressure.

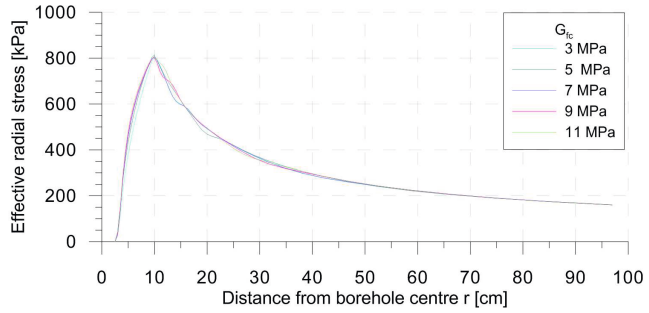

(b) Radial stresses after unloading.

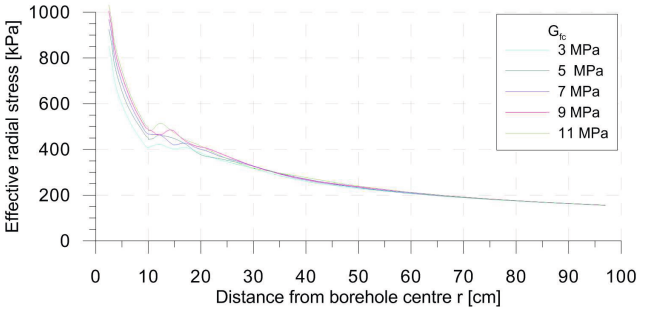

(c) Radial stresses at borehole walls at maximum grouting pressure and after unloading.

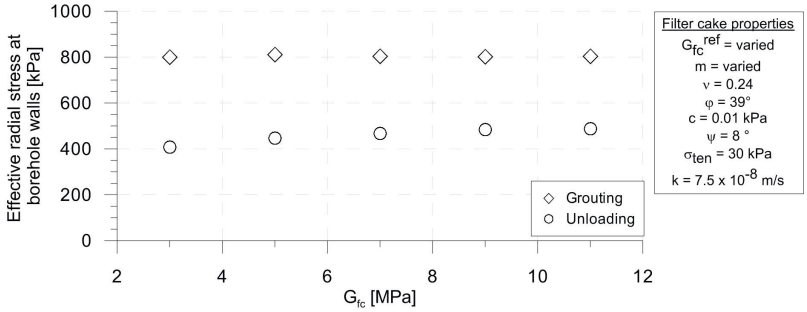

Figure 6.24: Parameter variation of filter cake stiffness G_{fc} in 'dense sand'.

6.7.6 Variation of filter cake permeability

The filter cake permeability was varied from 2.5×10^{-8} m/s to 1.25×10^{-7} m/s. The remaining parameters for grout and soil were again taken from the reference parameter set.

During all calculations the filtration of the liquid grout was completed before the limit grouting pressure of 30 bar was reached. The results presented in Figures 6.25 and C.11 show that for a less permeable filter cake higher radial stresses evolved during grouting, due to the higher hydraulic resistance of the filter cake. This trend remains after unloading. The variations of residual radial stresses range from 200 kPa for the 'loose sand' to 300 kPa for the 'dense sand' for filter cake permeabilities in the range observed during laboratory tests (3.5×10^{-8} m/s to 1.25×10^{-7} m/s).

(a) Radial stresses at maximum grouting pressure.

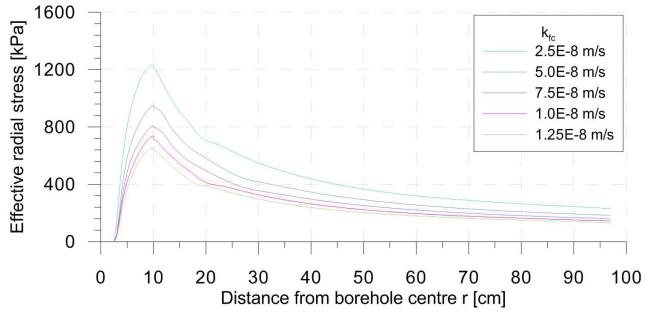

(b) Radial stresses after unloading.

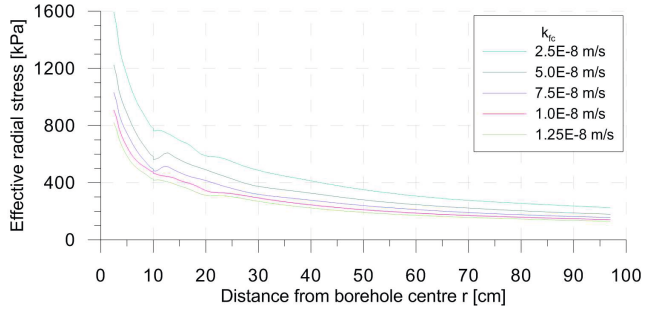

(c) Radial stresses at borehole walls at maximum grouting pressure and after unloading.

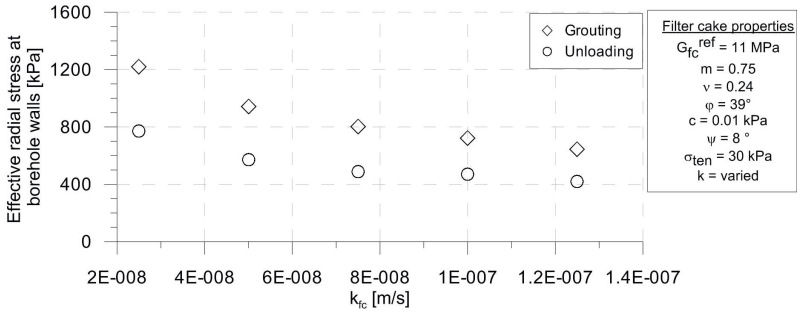

Figure 6.25: Parameter variation of filter cake permeability k_{fc} in 'dense sand'.

6.7.7 Variation of soil permeability

The soil permeability was varied between $k_{soil} = 1 \times 10^{-3}$ m/s and 1×10^{-5} m/s representing coarse to fine sands and 1×10^{-6} m/s representing silt.

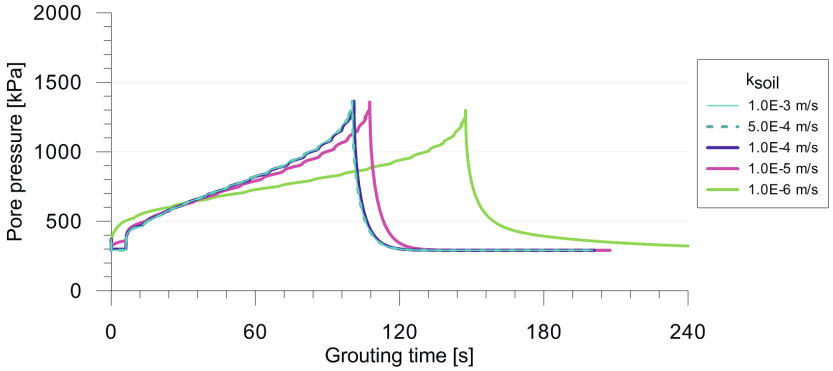

Figure 6.26: Grouting pressure development in ‘loose sand’.

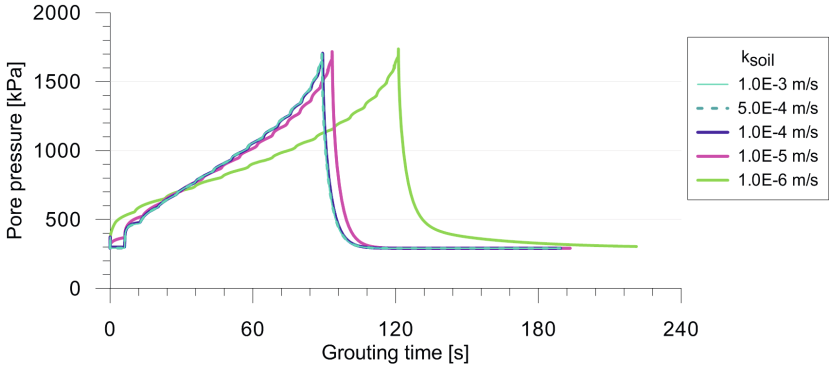

Figure 6.27: Grouting pressure development in ‘dense sand’.

The grouting pressure build-up is presented in Figures 6.26 and 6.27. The filtration time was identical for permeabilities between 1×10^{-3} and 1×10^{-4} m/s, for $k_{soil} = 1 \times 10^{-5}$ m/s the filtration time is slightly longer and for a permeability of 1×10^{-6} m/s, the filtration time increased significantly. Yet at all tests the same grouting pressure was reached.

The radial stress distribution after grouting and unloading is presented in Figures 6.28 and C.12. As for the grouting pressure build-up the radial stresses are identical for permeabilities in the range of sands. For permeabilities representing silts, the radial stresses at the borehole walls were slightly lower than for sands due to higher pore pressures in the soil.

(a) Radial stresses at maximum grouting pressure.

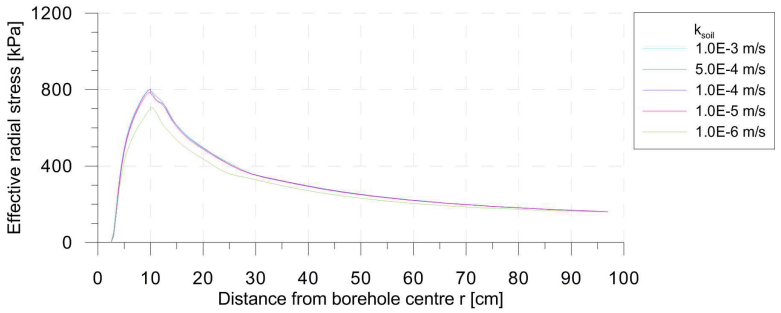

(b) Radial stresses after unloading.

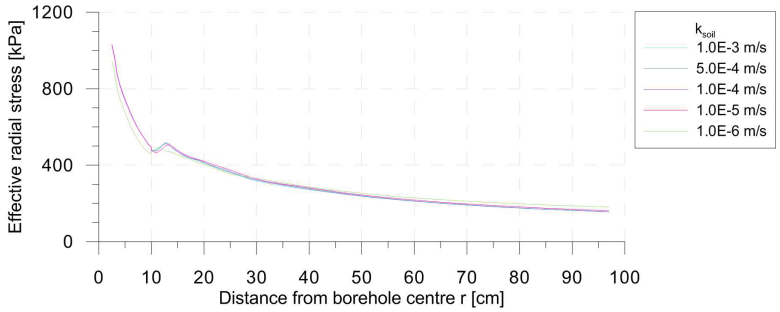

(c) Radial stresses at borehole walls at maximum grouting pressure and after unloading.

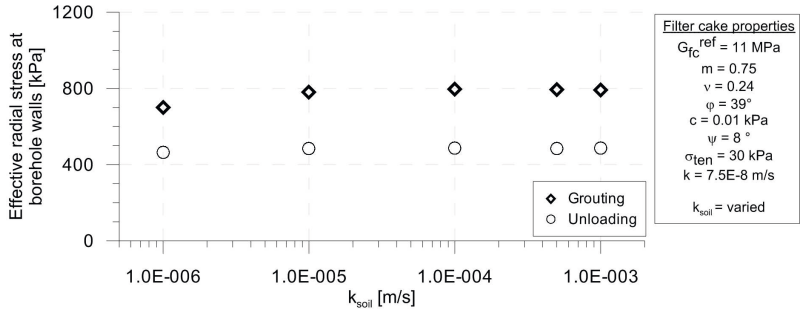

Figure 6.28: Parameter variation of soil permeability k_{soil} in ‘dense sand’.

6.8 Chapter summary

The two-phase filtration model was implemented into a finite element model to simulate cement grout filtration inside the borehole. Validations for one-dimensional and radial flow showed the applicability of the model. The flow of the liquid phase was approximated by assigning high permeability and low stiffness to the 'liquid grout' elements. This approximation simulates the flow of the suspension, with the particle concentration remaining constant. In cases where filtration against the main flow direction occurs, the transport of suspension with higher particle concentration can therefore not be simulated and the filter cake builds up at the location of drainage. A variation of the model was introduced, where only filtration in main flow direction is considered. This model gives a more irregular filter cake shape than the initial model, it does, however, not fully comply with the two-phase filtration model because the balance of discharge and filter cake build-up is violated. This leads to unrealistic filtration time. The real filter cake shape is assumed to lie between both versions of the filtration model.

The filter cake formation calculated with both models was found relatively homogeneous along the grouting length, what allowed for the use of a plane strain vertical section of the model to determine stresses in the soil and carry out parametric studies.

The properties of the surrounding soil influence the pressures achieved during grouting as well as the radial stresses retained thereafter. For the 'loose sand' material set with lower stiffness and friction angle, lower grouting pressures and radial stresses were achieved than for the 'dense sand'.

Variations of the grouting parameters showed that the value of radial effective stresses on the borehole walls after grouting directly relates to the grouting pressure that could be achieved. The maximum grouting pressure that is reached during grouting depends on the soil stiffness, permeability and pumping rate. With higher pumping rates, higher grouting pressures are obtained before all grout in the borehole filtrates. For very high pumping rates, however, the grouting pressure is reached with only a thin filter cake which then in turn does not resist the back-deformation of the soil and less stresses are retained.

Parameter variations of the filter cake permeability showed considerable variations of the achieved grouting pressure and residual radial stresses for permeabilities in the range of the laboratory tests. The filter cake permeability directly defines the grouting pressure which can be achieved for a certain pumping rate. The radial stress was then a percentage of the grouting pressure.

The soil permeability also influences the filtration process. For permeabilities in the range of coarse to fine sand the results were almost identical, but for much lower permeabilities a significant different filtration behaviour and stress distribution was determined. This confirms the general experience that applying grouting pressure in semi-permeable or impermeable soils does not have the same positive effect than in permeable soils.

It was also found that the value of the applied grouting pressure directly influences the

radial effective stresses on the borehole walls remained after unloading and thus the pull-out capacity of the grout body. The parametric study showed that for the range of parameters likely to occur during real anchor installation, a liquid grouting pressure of 30 bar in the borehole centre is rarely obtainable. The achievement of grouting pressures around 10 bar to 15 bar seems more likely. Any larger grouting pressures would be the result of filtration inside the drill casing. This complies with the results of various anchor tests reported by Ostermayer (1975), who stated that for grouting pressures above 10 bar no increase in anchor capacity was achieved. During their studies the higher grouting pressures might only have occurred within the casing and therefore not increased the effective stresses on the borehole walls.

Chapter 7

Concluding remarks

7.1 Summary

The effects of pressure grouting during installation of grouted ground anchors in non-cohesive soils were investigated. It shed light on the process of cement grout filtration and the material properties of cement grout filter cake were determined. Additionally the grouting process was observed in-situ and based on the findings, finally, modelled numerically.

Reviewing previous studies revealed that different concepts of the processes taking place during anchor installation exist. This is probably because the observations were made on studies with varying installation conditions, which might have influenced the processes taking place. For anchor installation in sand, the majority of sources state that during grouting excess water is filtered from the grout suspension in the borehole and no injection into the soil takes place. It is assumed that a filter cake builds up which transfers the grouting pressure to the soil. This concept complies with theoretical considerations on groutability and excavations of grout anchors in sand, which showed a clear distinction between anchor body and soil. In literature it was, however, not clarified whether only a thin filter cake builds up actioning like a membrane on the soil or if the entire grout filters inside the borehole. The amount of grouting pressure being transferred to the soil and remaining after grouting was also unknown.

Excavations of anchors revealed that a straight shaft grout body is created in sand. Anchors where hydro-fracturing of the soil was reported are probably created with bentonite added to the grout. Referring to studies on hydro-fracturing in sands, it, however, seems unlikely that the soil fractures during conventional anchor installation in sand. No reports exist where fracturing during installation of grouted ground anchors was confirmed by excavations.

Even though there is consensus in literature that applying pressure to the cement grout increases the anchor capacity, the significance of the magnitude of the applied pressure remained unclear.

To analytically describe the cement grout filtration process, two approaches were mainly used in literature: the two-phase filtration model and classical consolidation theory. Those require the void ratio and permeability of the filter cake or the coefficient of consolidation and a mean permeability of the grout respectively.

In the presented study a series of filtration tests with varying water contents and grouting pressures were carried out to investigate the filtration process of cement grouts and to determine sufficient calculation parameters. It was found that the grout filtrates quickly and a stiff filter cake builds up with a clear phase change from liquid grout to filter cake. The filter cake then consolidates further due to the applied load. The filtration process was found to be a combination of filtration and consolidation: In a first phase water is expelled from the liquid grout until the cement particles contact each other and a filter cake builds up, which then consolidates. Immediately after filtration, the mechanical properties of the filter cake material were investigated in triaxial, oedometer and permeability tests.

From the laboratory filtration tests it was found that

- cement grout does not infiltrate sand
- with higher grouting pressures the filtration time reduces
- with higher grouting pressures the void ratio of the filter cake reduces
- with lower initial water content the void ratio of the filter cake reduces

The scatter of results within the tests were however larger than the influence of grouting pressure and water content and no correlations could be drawn between those factors and the filter cake properties. But using mean values for all tests, both approaches, the two-phase filtration model and consolidation theory were found appropriate to back-calculate the filtration tests and estimate the filter cake thickness with time. A filter cake water content of w/c_{fc} = 0.3 and a permeability of $k_{fc} = 7.5 \times 10^{-8}$ m/s were determined from the filtration tests and fitted well for back-calculations with the two-phase filtration model.

The two-phase filtration model directly yields the filter cake thickness, whereas when using consolidation theory the degree of consolidation at which the grout is considered filter cake needs to be defined. While one set of parameters (k_{fc} and w/c_{fc}) is sufficient to back-calculate all tests of the series with the two-phase filtration model, for the consolidation model the coefficient of consolidation c_v needed to be adjusted to the applied grouting pressure in order to receive appropriate results and is therefore not generally applicable, especially for varying grouting pressures.

Additional in-situ measurements of the grouting pressures inside the borehole proved that filtration takes place during grouting and that the entire grout in the grouting length filtrates. Soundings confirmed that grouting increases the radial stresses in the soil adjacent to the grout body.

Even though the soil conditions were similar at the different test sites, the measured grouting pressures and filtration times varied significantly. This is ascribed to the different installation techniques (drilling method and grouting pressure) applied. However, full filtration of the cement grout was achieved at all sites. Measurements of the grouting pressure inside the borehole showed that

- initially the grout acts as liquid and suspension pressure is distributed hydrostatically

- the grout in the grouting length filtrates and becomes a friction material causing an anisotropic stress distribution
- whereas the grout inside the casing is still liquid
- full filtration of the grout in the grouting length was achieved regardless installation technique
- the grout filters even without applied grouting pressure
- increased radial stresses remain after grouting
- filtration leads to low water contents of the grout which could cause swelling of the grout body during setting and therefore lead to an increase of radial stresses

DMT and CPT soundings in the soil showed that radial stresses next to the grouting length increased significantly during and after grouting. However, too little data was available to determine correlations between grouting pressure and radial stresses after grouting.

Based on previous findings, the process of cement grout filtration was simulated by applying the finite element method. Filtration during grouting was accounted for by switching the material properties of the grout from 'liquid grout' to 'filter cake', using a filter criterion adapted from the two-phase filtration model. In a coupled flow-deformation analysis, the phase change of the grout due to filtration as well as consolidation of the created filter cake was taken into account. The filter cake formation was simulated inside the borehole by applying a constant pumping rate rather than a constant pressure. The calculations showed that a relatively homogeneous filter cake builds up along the borehole walls in the free grouting length and that the filter cake reaches the borehole centre after a short grouting period. In the range of sands, the permeability of the soil does not influence the filtration process significantly. With a constant pumping rate the grouting pressure is obtained due to the hydraulic resistance of the filter cake and therefore depends on its permeability and the pumping rate. But also the soil properties affect the grouting pressure. For weaker soils larger borehole deformations occur, releasing the established grout pressure. The radial stresses on the anchor body/soil interface directly relate to the reached grouting pressure, but the residual stresses after grouting depend on the thickness of the filter cake, which retains the soil from moving back inwards after grouting. The achieved grouting pressures were very sensitive to the filter cake permeability and showed considerable scatter for permeabilities in the range determined in laboratory tests.

Even though the anchor geometry and reached grouting pressures varied between the test in Venhaus and Dörverden, the radial stress increase measured in DMT and DMTA soundings in Venhaus were in the range of the simulated values: Simulated and measured radial stresses at a distance of 40 cm from the anchor axis increased in the range of 100 and 300 kPa for grouting pressures between 20 and 30 bar.

7.2 Conclusions and recommendations for practice

Cement grouting during anchor installation was found to be a complex process influenced by various interacting factors. The effect of cement grouting on the residual stresses on the grout body were identified depending on the

- pumping rate
- achieved grouting pressure
- soil properties
- grout properties
- applied drilling method
- used flushing liquid

Even though in particular the pumping rate significantly influences the grouting process, it was disregarded in previous studies. And if the anchor installation was considered at all, only the applied grouting pressure was taken into account.

Considering grouting in permeable soils, it was found that the grouting pressure is a result of the pumping rate and filter cake permeability. The pressure in the liquid grout increases once the filter cake builds up, due to its increasing hydraulic resistance. The soil itself does not provide sufficient hydraulic resistance to generate grouting pressures of several bars without the filter cake and pumping rates possible with conventional grout pumps. The grouting pressure increases gradually during in-situ anchor installation, as the filter cake builds up. The higher the pumping rate, the higher are the achieved grouting pressures. If a limit grouting pressure is defined at which the grouting process is stopped, the grouting pressure might be reached at a thin filter cake only, which in turn results in lower residual stresses after grouting.

Figure 7.1 presents schematic results of the FEM simulations of grouting in dense sands. The maximum grouting pressure that is achieved in the borehole centre before full filtration of the grout directly correlates to the pumping rate (Figure 7.1a). The remaining radial stresses on the grout body also increase with pumping rate, as long as full filtration is reached. If grouting is stopped at a specific limiting pressure level before full filtration is achieved, the residual stresses reduce with increasing pumping rates, because a thinner filter cake is achieved compared to lower pumping rates (Figure 7.1b). In addition to the presented FEM model comparison calculations with varying soil pressures were carried out. The shaded areas in Figure 7.1 indicate the range of results of simulations with soil pressures varying from $\sigma'_H = 50\ kPa$ to $\sigma'_H = 100\ kPa$. The comparison calculations showed that the initial soil pressure has only little influence on the results, especially if the limiting grouting pressure was reached. But for full filtration, higher grouting pressures were achieved in calculations with higher initial soil pressures. This effect was also observed at the remaining radial stresses on the grout body. Larger radial stresses were achieved with higher initial soil pressures, possibly due to the larger soil stiffness.

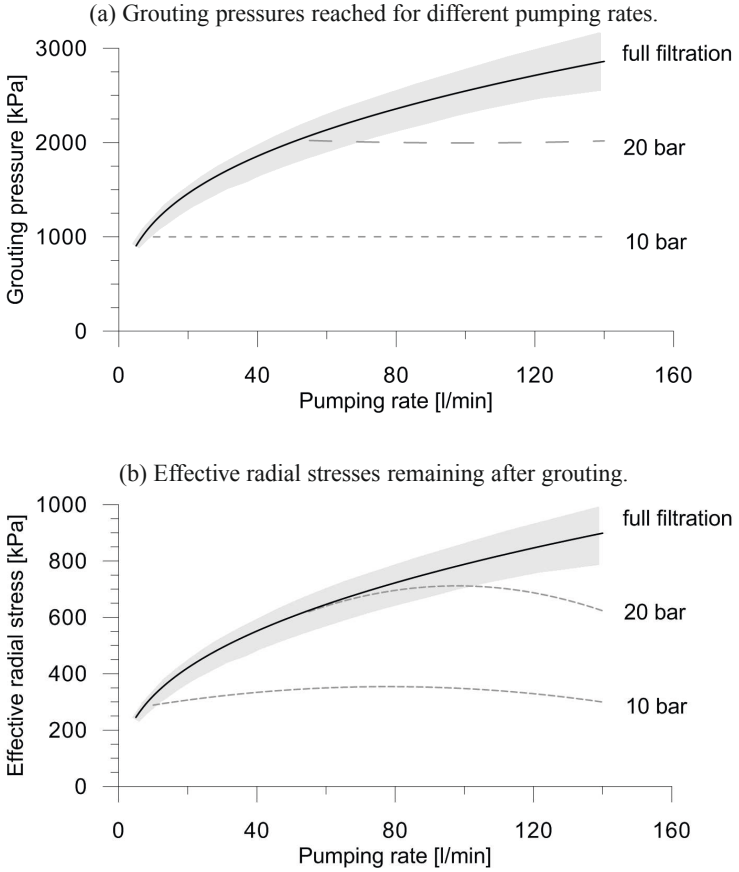

Figure 7.1: Schematic presentation of grouting pressures and radial effective stresses on the grout body surface after unloading. FEM simulation with borehole diameter 20 cm, steel bar diameter 5 cm and 3m grouting length.

To increase the radial effective stresses as much as possible, in practice full filtration should be anticipated with a preferably high grouting pressure, aiming optimal balance between pumping rate and limit grouting pressure. If necessary the grouting length can be reduced in order to obtain larger pumping rates per m grouting length.

To detect the time of full filtration in the grouting length, one should monitor the grouting pressure development. When grouting is continued beyond the point of full filtration in the grouting length, the filter cake progresses into the drill casing. At this point the grouting pressure increases exponentially and the casing should be withdrawn further. A too long grouting duration bears the risk of grout filtration in the cavity between casing and soil, which can get the casing stuck. This applies especially for boreholes drilled with outward flushing, since the cavity between casing and soil is larger than for inward flushing.

It is recommended to previously determine the maximum grouting pressure which can be reached inside the borehole without filtration inside the casing. This would provide maximum effect of grouting and minimize the risk of casing being stuck during the grouting process.

The presented study shows that the filtration of cement grout due to water expulsion is critical during anchor installation, which explains the difference between grouting in non-cohesive (permeable) soils and cohesive (impermeable) soils. In permeable soils the filtration of cement grout plays the major role, whereas in impermeable soils the grouting pressure is only transferred as excess pore pressure without significant filtration. Therefore the radial stresses reduce as soon as grouting is stopped because the soil can move back into the borehole without being restrained by a stiff filter cake. This explains why post grouting is successful in cohesive soils: First of all, it is only possible to fracture the initial grout body, because the water content remained relatively high resulting in a lower strength, and then the expansion of the grout body increases the radial stresses that could not be achieved during grouting.

Observations during in-situ anchor installation showed that for drilling with external flushing only low grouting pressures could be achieved because the grout was pressed upwards between casing and soil. If a filter cake builds up at this position, it might cause the casing to be stuck in the borehole. Drilling with external flushing enlarges the grout body and creates a more irregular anchor surface, which might be favourable to introduce anchor loads, but it also disturbs the surrounding soil. To minimise these effects, drilling with internal flushing should be preferred.

The use of packers might be useful to separate the grouting length from the remaining borehole and prevent grout being pressed upwards between drill casing and borehole and could help to reach the desired grouting pressure. However, it seems unnecessary with respect to maintain the grouting pressure for a period of time because in non-cohesive soils the grouting pressure will reduce immediately after pumping is stopped due to water draining from the grout. In impermeable soils it might however be helpful because no filtration takes place and the liquid grout pressure is maintained by the packers until the grout cures.

If bentonite is added to the drilling or grouting liquid, it decreases the permeability of the filter cake. In view of the presented study, adding bentonite to the flushing liquid is not advisable because it could hinder the filtration of the grout during grouting and support that the grout is flushed upwards between casing and soil.

7.3 Recommendation for further work

The presented field tests aimed to investigate anchor installation, as it is carried out in practice, and therefore, no specifications were made regarding the installation technique. In the light of the presented study it would be interesting to carry out field tests under more controlled conditions, where the pumping rate, amount of grout and grouting pressures are recorded precisely. This would allow to back-calculate the tests and to validate the presented FEM model.

The sensors used to measure total stresses in the borehole during grouting were calibrated in water. The test results indicate that as soon as the grout filtrates some arching around the sensors could have reduced the measured total stresses. For further in-situ measurements it would be recommended to calibrate the sensors in cement grout and cement grout filtrate in order to evaluate these effects. Also the durability of the sensors and casings could be improved in order to achieve reliable long term measurements.

Time dependent changes of radial stresses on the grout body and thus, changes of anchor capacity some time after anchor installation were not investigated within this study. Field observation and literature suggests that the radial stresses increase during curing of the grout due to a swelling process. It would be very interesting to investigate this volume increase of cement grouts with low water contents due to swelling. Also time dependent relaxation of the effective stresses created during grouting would be of interest.

The numerical simulations showed that the filter cake permeability influences the grouting pressure that can be achieved. Adding small amounts of bentonite to the grout decreases the permeability of the filter cake and might support the effect of pressure grouting. However, reducing the permeability too much by adding too much bentonite could hinder the grout filtration, so that only a thin filter cake builds up by the time the desired grouting pressure is achieved. In that case, the grouting pressure would not be retained and the quality of the grout body would be reduced. Further work is required to evaluate the benefits and risks of using bentonite during anchor installation and to find an optimal amount of bentonite to support the benefits of grouting.

Further, the influence of drilling methods and grout types could be investigated in more detail.

The presented PhD study represents a foundation for further research on the installation effects of grouted ground anchors. Knowing the processes of cement grouting during anchor installation and the effects on the stress state in the soil is prerequisite to determine the anchor pull-out capacity numerically. For a realistic simulation of the load bearing mechanisms

following items should be investigated further and included into the FEM model:

- The effects of grouting on the soil properties due to stress change and compaction, for example by applying a material model with state dependent soil parameters (void-ratio dependent φ and ψ).
- The interlocking of the grout and soil surface.
- The volume increase due to swelling.
- Progressive failure/debonding of the anchor body.

References

ABAQUS 6.11 (2011a). Abaqus user subroutines reference manual. In *Online Documentation*. Dassault Systèmes.

ABAQUS 6.11 (2011b). *Online Documentation*. Dassault Systèmes.

Abuel-Naga, H. M. and Pender, M. J. (2012). Modified terzaghi consolidation curves with effective stress-dependent coefficient of consolidation. *Géotechnique Letters*, 2(2):43–48.

Ahverdov, I. N. (1981). Foundations of concrete physics. *Stroiizdat, Moscow, Russia (in Russian, see Kleyner and Krizek (1995))*.

Akbulut, S. and Saglamer, A. (2002). Estimating the groutability of granular soils: a new approach. *Tunnelling and Underground Space Technology Tunnelling and Underground Space Technology*, 17(4):371–380.

Altenhöfer, C. (2013). *Geotechnischer Bericht zum Neubau der Schleusenanlage Venhaus. BAW-Nr. A39520210119-2 - April 2013*. Bundesanstalt für Wasserbau. Internal report, unpublished.

Barley, A. D. and Windsor, C. R. (2000). Recent Advantages in Ground Anchor and Ground Reinforcement Technology with Reference to the Development of the Art. In *GEO 2000 International Conference on Geotechnical and Geotechnical Engineering, Melbourne, 19th - 24th November 2000*.

BBRI (2008). *Proceedings of the International Symposium 'Ground Anchors - Limelette test field results'.*, volume 1. Belgian Building Research Institute.

Benz, T. (2007). Small-strain stiffness of soils and its numerical consequences. In *Mitteilung des Instituts für Geotechnik*, volume 55. Universität Stuttgart, Stuttgart.

Bergholz, K. (2011). *Bewertung dynamischer Probebelastungen von Bohrpfählen - Geotechnischer Untersuchungsbericht. BAW-Nr. A39520270002 - August 2011*. Bundesanstalt für Wasserbau. Internal report, unpublished.

Bezuijen, A. (2010). *Compensation Grouting in Sand - Experiments, Field Experiences and Mechanisms*. PhD thesis, Delft University of Technology.

Bezuijen, A. and Talmon, A. M. (2003). Grout the foundation of a bored tunnel. In *Proc. int. conf. on Foundations 'Innovations, Observations, Design & Practice' (ICOF 2003 Dundee)*, London. Thomas Telford.

Bolton, M. D. and McKinley, J. D. (1997). Geotechnical properties of fresh cement grout - pressure filtration and consolidation tests. *GEOTECHNIQUE*, 47(2):347–352.

Bornemann, R. (2005). *Untersuchungen zur Modellierung des Frisch- und Festbetonverhaltens erdfeuchter Betone*. Kassel Univ. Press, Kassel.

Bürger, R., F., C., and H., K. K. (2001). Phenomenological model of filtration processes: 1. cake formation and expression. *Chemical Engineering Science*, 56:4537–4553.

Brinkgreve, R. B. J., Engin, E., and Engin, H. K. (2010). Validation of empirical formulas to derive model parameters for sands. In Benz, T. and Nordal, S., editors, *Numerical Methods in Geotechnical Engineering NUMGE 2010*, London. Taylor Francis Group.

Brinkgreve, R. B. J., Engin, E., and Swolfs, W. M. (2012). *PLAXIS 2D 2012*. Plaxis bv, Delft, Netherlands.

Carman, P. C. (1956). *Flow of gases through porous media.* Butterworths Scientific Publications, London.

Casagrande, A. and Fadum, R. E. (1940). *Notes on soil testing for engineering purposes*. Harvard University, Graduate School of Engineering, Cambridge, Mass.

Cornelius, V. and Mehlhorn, G. (1982). *Tragfähigkeitsuntersuchungen im Verankerungsbereich von Verpressankern und Pfählen mit kleinem Durchmesser für den Anwendungsbereich Lockergestein : Abschlussbericht*. Technische Hochschule Darmstadt, Inst. für Massivbau, Darmstadt.

De Paoli, B., Bosco, B., Granata, R., and Bruce, D. A. (1992a). Fundamental observations on cement based grouts (1): Traditional materials. In Borden, R. H., Holtz, R. O., and Juran, I., editors, *ASCE Specialty Conference on Grouting, Soil Improvement and Geosynthetics*, volume 1, pages 474–485.

De Paoli, B., Bosco, B., Granata, R., and Bruce, D. A. (1992b). Fundamental observations on cement based grouts (2): Microfine cements In Borden, R. H., Holtz, R. O., and Juran, I., editors, *ASCE Specialty Conference on Grouting, Soil Improvement and Geosynthetics*, volume 1.

Hazen, A. (1893). *Some physical properties of sands and gravels, with special reference to their use in filtration.*, pages 541–556. Number Public Document No 34. Massachusetts State Board of Health.

Hong, C.-Y., Yin, J.-H., Pei, H.-F., and Zhou, W.-H. (2013). Experimental study on the pull-out resistance of pressure-grouted soil nails in the field. *Canadian Geotechnical Journal*, 50(7):693–704.

Jelinek, R. and Ostermayer, H. (1976). *Verpreßanker in Böden*. Mitteilungen aus dem Lehrstuhl und Prüfamt für Grundbau und Bodenmechanik der TU München. Lehranstalt und Prüfamt für Grundbau und Bodenmechanik, TH München.

Jessberger, H. L. (1963). Theorie und Praxis eines neuzeitlichen Verankerungsverfahrens. *Die Bautechnik*, 7:226–232.

Kabir, M. A. and Gamwo, I. K. (2011). Filter cake formation on the vertical well at high temperature and high pressure: Computational fluid dynamics modeling and simulations. *Journal of Petroleum and Gas Engineering*, 7.2:146–164.

Kleyner, I. and Krizek, R. J. (1995). Mathematical Model for Bore-Injected Cement Grout Installations. *Journal of geotechnical engineering.*, 121(11):782–788.

Lee, D. J. and Wang, C. H. (2000). Theories of cake filtration and consolidation and implications to sludge dewatering. *Water Research*, 34(1):1–20.

Lee, S.-W., Kim, T.-S., Sim, B.-K., Kim, J.-S., and Lee, I.-M. (2012). Effect of pressurized grouting on pullout resistance and group efficiency of compression ground anchor. *Can. Geotech. J. Canadian Geotechnical Journal*, 49(8):939–953.

Littlejohn, G. S. (1970). Soil anchors. In *Proceedings of the Conference on Ground Engineering, London*, pages 33–44. ICE.

Littlejohn, G. S. (1980). Design estimation of the ultimate load-holding capacity of ground anchors. *Ground Engineering*, 13(8):25–39.

Marchetti, S. (1975). A New in Situ Test for the Measurement of Horizontal Soil Deformability. In *Proceedings of the conference on In Situ Measurement of Soil Properties*, volume 2 of *Specialty Converence of the Geotechnical Engineering Divison ASCE*, pages 255–259, Raleigh, North Carolina. North Carolina State University, ASCE.

Marchetti, S., Monaco, P., Totani, G., and Calabrese, M. (2001). The Flat Dilatometer Test (DMT) in Soil Investigations - A Report by the ISSMGE Committee TC16. In of the ISSMGE Technical Committee 16 on Ground Property Characterisation from In-situ Testing, R., editor, *IN SITU 2001, Intnl. Conf. On In situ Measurement of Soil Properties, Bali, Indonesia*.

Mayer, G. (1983). *Untersuchungen zum Tragverhalten von Verpressankern in Sand*. PhD thesis, Technische Universität Berlin.

McKinley, J. D. (1993). *Grouted ground anchors and the soil mechanics aspects of cement grouting.* PhD thesis, Cambridge Univ. (United Kingdom).

McKinley, J. D. and Bolton, M. D. (1999). Technical papers - A geotechnical description of fresh cement grout - Filtration and consolidation behaviour. *Magazine of concrete research.*, 51(5):295–307.

Mecsi, J. (2013). *Geotechnical Engineering examples and solutions using the cavity expanding therory : pressuremeters, piles, grouted soil anchors.* Hungarian Geotechnical Society, Budapest.

Ostermayer, H. and Barley, T. (2002). *Geotechnical Engineering Handbook*, volume 2, chapter 2.5 Ground Anchors, pages 169–215. John Wiley & Sons.

Ostermayer, H. (1975). Construction Carrying Behavior and Creep Characteristics of Ground Anchors. In *Diaphragm walls & anchorages : proceedings of the conference organized by the Institution of Civil Engineers and held in London, 18-20 September 1974*.

Ostermayer, H. (1993). 40 Jahre Spezialtiefbau 1953 - 1993. Technische und rechtliche Entwicklungen. Festschr. f. Karlheinz Bauer zum 65. Geburtstag. pages S.65–96. Werner.

Ostermayer, H. (2001). Verpressanker. In *Grundbau Taschenbuch*, volume 2, pages 167–210. Ernst & Sohn, 6. edition.

Ostermayer, H. and Werner, H.-U. (1972). Neue Erkenntnisse und Entwicklungstendenzen in der Verankerungstechnik. In Prof. Dr. Ing. R. Jelinek, editor, *Mitteilungen aus dem Institut für Grundbau und Bodenmechanik der TEchnischen Universität München*. Deutsche gesellschaft für Erd- und Grundbau e.V., Essen.

Paproth, E. and Paproth, H. (1966). Zementstein als Mittel zum Aufbau von Zug- und Druckpfählen sowie von Pfahlwänden. *Die Bautechnik*, 11:385–391.

Picandet, V., Rangeard, D., Perrot, A., and Lecompte, T. (2011). Permeability measurement of fresh cement paste. *Cement and Concrete Research*, 41(3):330–338.

Reschke, T. (2001). *Der Einfluss der Granulometrie der Feinstoffe auf die Gefügeentwicklung und die Festigkeit von Beton*. Verlag Bau + Technik, Düsseldorf.

Scheele, F. (1982). *Tragfähigkeit von Verpreßankern in nichtbindigem Boden : Neue Erkenntnisse durch Dehnungsmessungen im Verankerungsbereich.* PhD thesis, TU München.

Schmertmann, J. H. (1983). Revised Procedure for Calculating K_0 and OCR from DMT's with $I_D > 1.2$ and which Incorporates the Penetration Measurement to Permit Calculating the Plane Strain Friciton Angle. In *DMT Digest No. 1*. GPE Inc., Gainesville, FL.

Schmertmann, J. H. (1988). Guidelines for Using the CPT, CPTU and Marchetti DMT for Geotechnical Design. Report FHWA-PA-87-023+24 Vol. 3-4., U.S. Dept. of Transportation, Federal Highway Administration, Office of Research and Special Studies.

Schwab, R. (2008). *Neue Schleuse Dörverden - Baugrund- und Gründungsgutachten. BAW-Nr. A39520210028 - Februar 2008*. Bundesanstalt für Wasserbau. Internal report, unpublished.

Semprich, S. and Stadler, G. (2002). *Geotechnical Engineering Handbook*, volume 2, chapter 2.2 Grouting in Geotechnical Engineering, pages 57–90. John Wiley & Sons.

Shields, J. R. (1978). Load Transfer in Pressure Injected Anchors. *Journal of the Geotechnical Engineering Division*, 104(9):1183–1196.

Taylor, D. W. (1948). *Fundamentals of soil mechanics.* J. Wiley, New York.

Terzaghi, K., Peck, R. B., and Mesri, G. (1996). *Soil mechanics in engineering practice*, volume 3. Wiley and Sons, Inc, New York.

Tomboy, O. and Huybrechts, N. (2008). Excavation of the Anchors Measurements and Observations. In Belgian Building Research Institute, editor, *PROCEEDINGS INTERNATIONAL SYMPOSIUM GROUND ANCHORS* , volume 1.

Warner, J. (2004). *Practical Handbook of Grouting - Soil, Rock, and Structures*. John Wiley & Sons, Norwich, NY.

Werner, H.-U. (1972). *Die Tragkraft langzylindrischer Erdanker zur Verankerung von Stützwänden unter besonderer Berücksichtigung der lagerungsdichte kohäsionsloser Böden.* PhD thesis, Rijksuniversiteit Ghent.

Werner, H.-U. (1975). Das Tragverhalten von gruppenweise angeordneten Erdankern. *Die Bautechnik*, 11:387–390.

Wernick, E. (1978). *Tragfähigkeit zylindrischer Anker in Sand unter besonderer Berücksichtigung des Dilatanzverhaltens*. PhD thesis, Karlsruhe.

Wichter, L. and Meiniger, W. (2000). *Verankerungen und Vernagelungen im Grundbau*. Ernst & Sohn, Berlin.

Xanthakos, P. P. (1991). *Ground Anchors and Anchored Structures*. Wiley, New York.

Zebovitz, S., Krizek, R. J., and Atmatzidi, D. K. (1989). Injection of fine sands with very fine cement grout. *Journal of Geotechnical Engineering*, 115(12):1717–1733.

Zinati, F. F., Farajzadeh, R., Currie, P. K., and Zitha, P. L. J. (2009). Modeling of external filter cake build-up in radial geometry. *Petroleum Science and Technology Petroleum Science and Technology*, 27(7):746–763.

Appendix A

Laboratory test results

Table A.1: Test parameters and results from test series No 1. e_{fc} and w/c_{fc} calculated from h_{ini}, w/c_{ini}, and δ_{fin}.

Test	w/c_{ini} [-]	h_{ini} [mm]	p_{ini} [kPa]	δ_{max} [mm]	e_{ini} [-]	e_{fc} [-]	w/c_{fc} [-]
1_1_045	0.45	80	92	13.9	1.42	1.00	0.32
1_2_045	0.45	80	92	14.1	1.42	0.99	0.31
1_3_045	0.45	80	197	14.8	1.42	0.97	0.31
2_1_045	0.45	80	201	14.5	1.42	0.98	0.31
2_2_045	0.45	80	190	13.4	1.42	1.01	0.32
2_3_045	0.45	80	101	13.3	1.42	1.02	0.32
4_1_045	0.45	80	494	15.5	1.42	0.95	0.30
4_2_045	0.45	80	494	16.1	1.42	0.93	0.30
4_3_045	0.45	80	491	15.3	1.42	0.95	0.30
5_1_045	0.45	80	994	16.2	1.42	0.93	0.29
5_2_045	0.45	80	1003	16.1	1.42	0.93	0.30
5_3_045	0.45	80	996	15.0	1.42	0.96	0.31
6_2_045	0.45	80	466	14.5	1.42	0.98	0.31
7_1_060	0.60	80	482	25.7	1.89	0.96	0.31
7_2_060	0.60	80	500	27.4	1.89	0.90	0.29
8_1_060	0.60	80	996	25.4	1.89	0.97	0.31
8_2_060	0.60	80	1004	26.2	1.89	0.94	0.30
9_1_050	0.50	80	503	23.9	1.58	0.81	0.26
9_2_050	0.50	80	497	21.7	1.58	0.88	0.28
10_1_050	0.50	80	1015	23.8	1.58	0.81	0.26
10_2_050	0.50	80	1024	23.7	1.58	0.81	0.26
10_3_050	0.50	80	494	22.1	1.58	0.86	0.27
11_1_040	0.40	80	196	10.5	1.26	0.96	0.31
11_2_040	0.40	80	197	10.8	1.26	0.96	0.30
12_1_050	0.50	80	1422	25.9	1.58	0.74	0.24
12_2_050	0.50	80	1453	21.7	1.58	0.88	0.28
12_3_050	0.50	80	1434	19.1	1.58	0.96	0.30
13_1_045	0.45	80	1476	17.2	1.42	0.90	0.29
13_2_045	0.45	80	1501	18.4	1.42	0.86	0.27
14_1_040	0.40	80	508	15.0	1.26	0.84	0.27
14_2_040	0.40	80	491	12.2	1.26	0.92	0.29
14_3_040	0.40	80	485	13.4	1.26	0.88	0.28
15_1_040	0.40	80	1019	13.8	1.26	0.87	0.28
15_2_040	0.40	80	982	14.2	1.26	0.86	0.27
16_1_060	0.60	80	1437	27.4	1.89	0.90	0.29
16_2_060	0.60	80	1437	24.5	1.89	1.00	0.32
16_3_060	0.60	80	1455	24.2	1.89	1.01	0.32
17_1_050	0.50	80	190	16.5	1.58	1.05	0.33
17_2_050	0.50	80	197	16.5	1.58	1.04	0.33
17_3_050	0.50	80	203	16.5	1.58	1.05	0.33
18_1_040	0.40	80	1439	16.7	1.26	0.79	0.25
18_2_040	0.40	80	1480	16.2	1.26	0.80	0.25
18_3_040	0.40	80	1472	15.4	1.26	0.83	0.26
19_1_060	0.60	80	194	23.1	1.89	1.05	0.33
19_2_060	0.60	80	186	24.2	1.89	1.02	0.32
19_3_060	0.60	80	195	22.5	1.89	1.08	0.34

Table A.2: Test parameters and results from test series No 1, with additional sand layer. e_{fc} and w/c_{fc} calculated from h_{ini}, w/c_{ini}, and δ_{fin}.

Test	w/c_{ini} [-]	h_{ini} [mm]	p_{ini} [kPa]	δ_{max} [mm]	e_{ini} [-]	e_{fc} [-]	w/c_{fc} [-]
3_1_045_S	0.45	80	191	11.6	1.42	1.07	0.34
3_2_045_S	0.45	80	470	11.6	1.42	1.07	0.34
3_3_045_S	0.45	80	483	16.9	1.42	0.91	0.29

Table A.3: Test parameters and results from test series No 2. e_{fc} and w/c_{fc} calculated from h_{ini}, w/c_{ini}, and δ_{fin}.

Test	w/c_{ini} [-]	h_{ini} [mm]	p_{ini} [kPa]	δ_{max} [mm]	e_{ini} [-]	e_{fc} [-]	w/c_{fc} [-]
2-2-1_040	0.40	127	506	16	1.26	0.98	0.31
2-2-2_040	0.40	140	489	16	1.26	1.00	0.32
2-3-1_040	0.40	140	518	20	1.26	0.94	0.30
2-3-2_040	0.40	140	509	20	1.26	0.94	0.30
2-4-1_040	0.40	138	512	21	1.26	0.92	0.29
2-4-2_040	0.40	140	503	20	1.26	0.94	0.30
2-5-1_040	0.40	141	489	20	1.26	0.94	0.30
2-5-2_040	0.40	138	508	21	1.26	0.91	0.29
2-6-1_040	0.40	140	514	15	1.26	1.01	0.32
2-6-2_040	0.40	140	512	15	1.26	1.02	0.32
2-7-1_040	0.40	140	975	21	1.26	0.92	0.29
2-7-2_040	0.40	140	1073	21	1.26	0.93	0.29

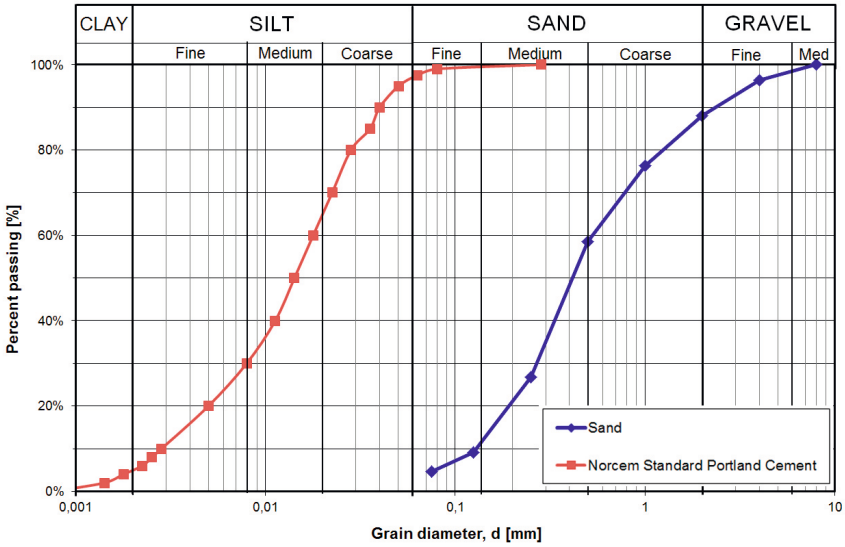

Figure A.1: Particle size distribution of Norcem standard Portland cement and sand used as filter material in filtration tests.

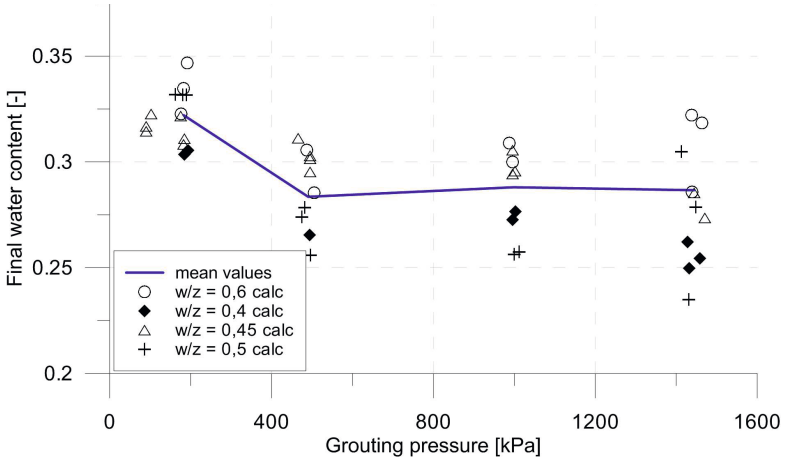

Figure A.2: Water contents w/c_{fc} for different grouting pressures calculated from h_{ini}, w/c_{ini}, and δ_{fin}.

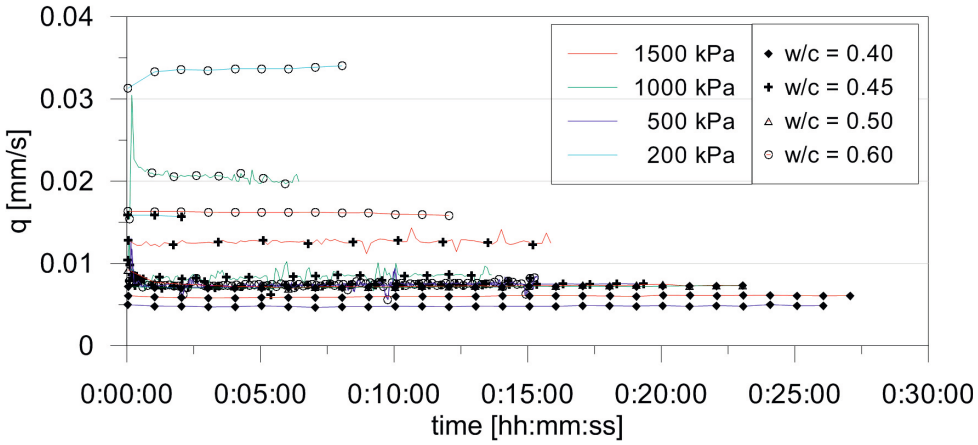

Figure A.3: Discharge rate measured during permeability tests.

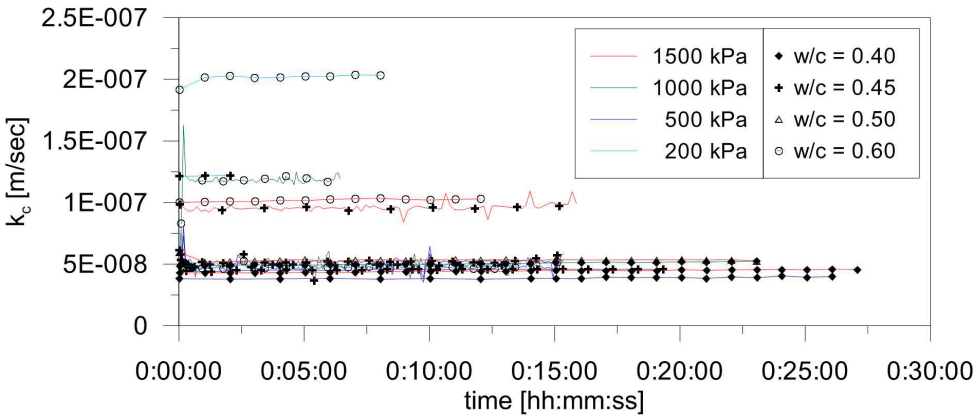

Figure A.4: Permeability during permeability tests.

Appendix B

Field test results

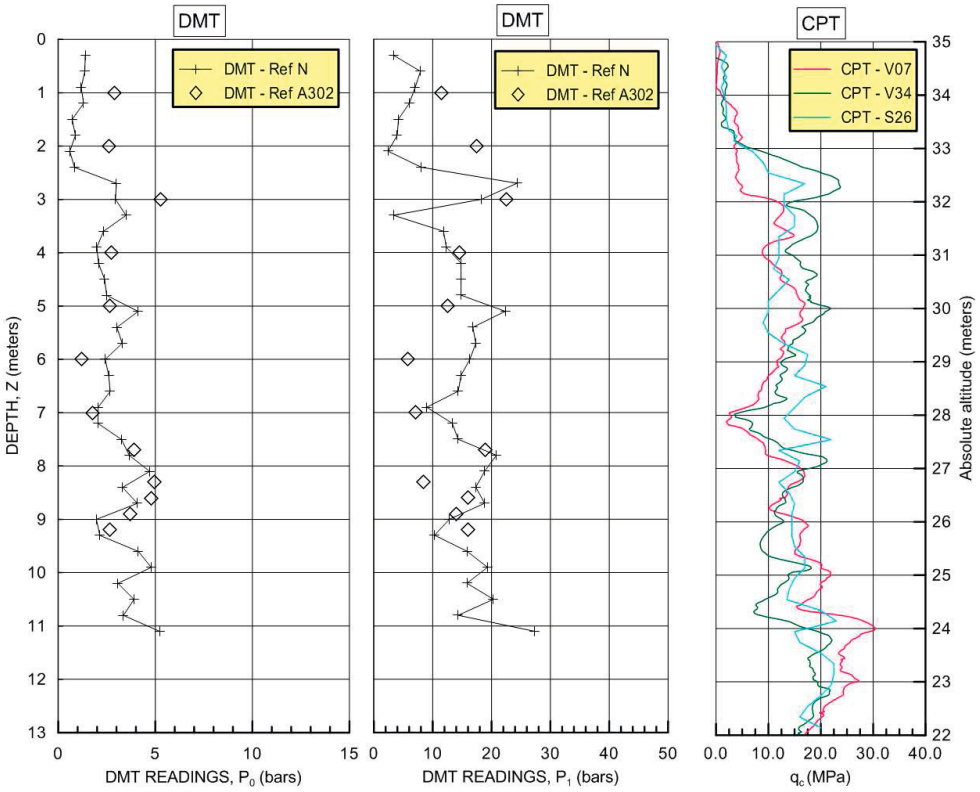

Figure B.1: Comparison of DMT and CPT measurements before anchor installation in Venhaus.

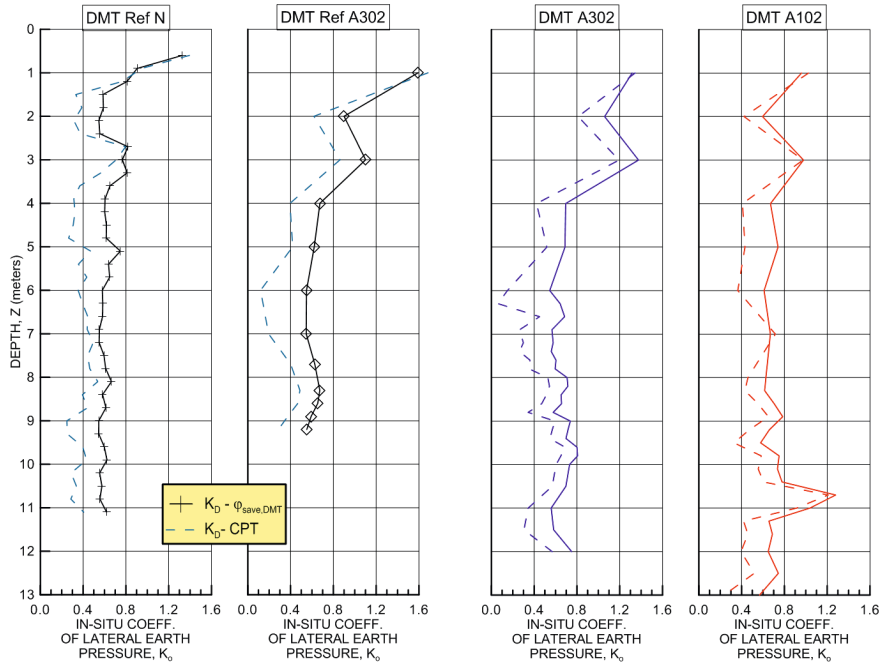

Figure B.2: Comparison of K_0 values determined from DMT tests in Venhaus. Correlation $K_0 - K_D - \phi_{save,DMT}$ (solid line) and correlation $K_0 - K_D - q_c$ (dashed line).

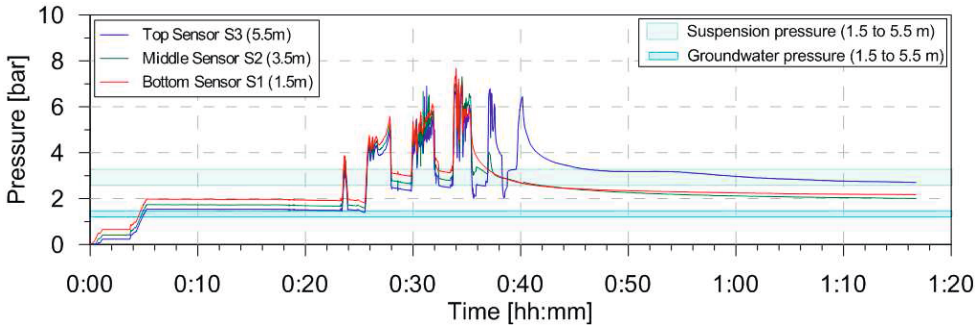

Figure B.3: Grouting pressure measured during installation of Anchor 7 in Horstwalde.

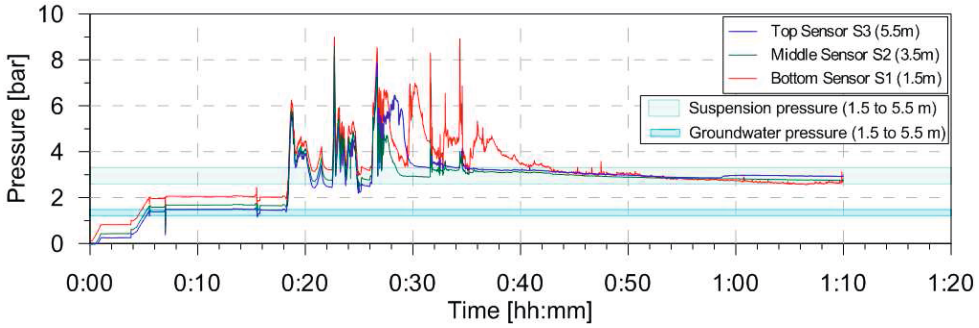

Figure B.4: Grouting pressure measured during installation of Anchor 10 in Horstwalde.

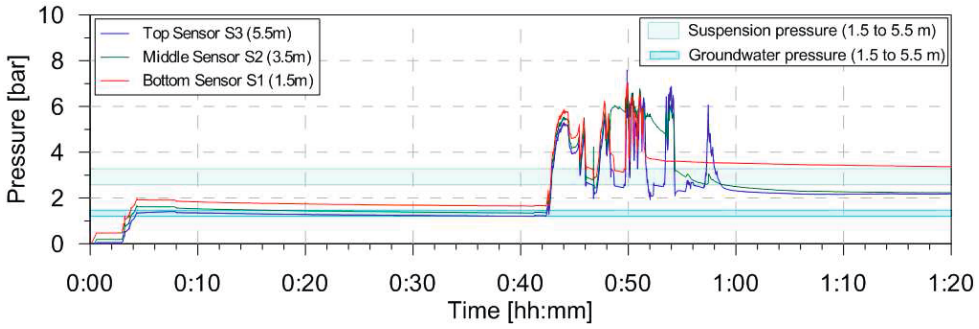

Figure B.5: Grouting pressure measured during installation of Anchor 19 in Horstwalde.

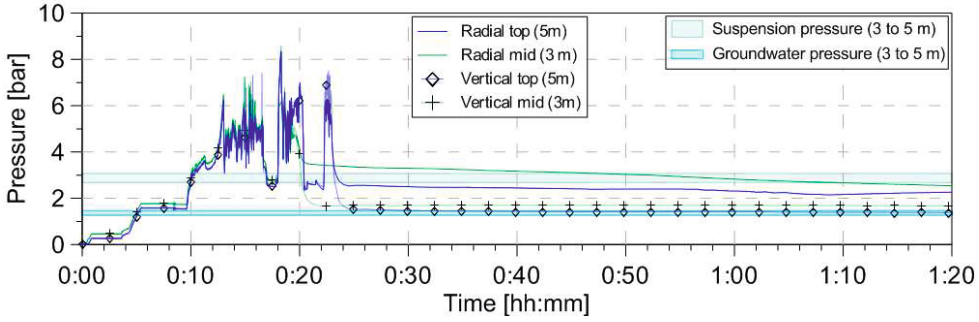

Figure B.6: Grouting pressure measured during installation of Anchor 8 in Horstwalde.

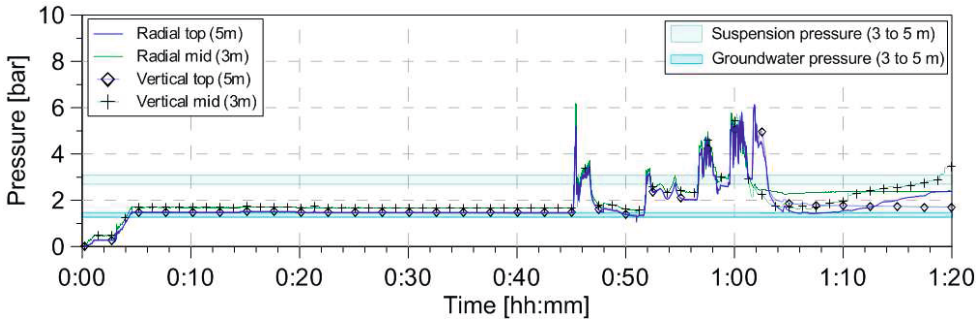

Figure B.7: Grouting pressure measured during installation of Anchor 13 in Horstwalde.

Appendix C

Numerical simulations

C.1 Constitutive laws

In the following section a short description of the constitutive laws that were used in the FEM simulations is given.

C.1.1 The Linear Elastic model

The Linear Elastic model was used for the cement grout and soil in validation calculations. The required model parameters are presented in Table C.1. The used Linear Elastic model assumes an elastic stress-strain relationship after Hooke. The stiffness matrix is defined by two independent constants, for example the Young's modulus E and Poisson's ratio ν.

Table C.1: Material parameters for the Linear Elastic model.

Parameter		Description
E	$[kPa]$	Young's modulus
ν	[-]	Poisson's ratio

C.1.2 The Mohr-Coulomb model

The Mohr-Coulomb model was used to model the cement grout inside the borehole. It is a elastic-perfect plastic constitutive model, featuring a stress dependent stiffness formulation. Table C.2 shows the material parameters required for the model:

Table C.2: Material parameters for the Mohr-Coulomb model.

Parameter		description
E_{50}^{ref}	$[kPa]$	Secant modulus for primary triaxial loading
m	[-]	Exponent of the Ohde/Janbu law
p^{ref}	$[kPa]$	Reference stress for stiffness parameters
ν	[-]	Poisson's ratio
c'	$[kPa]$	Cohesion
φ'	$[^\circ]$	Friction angle
ψ	$[^\circ]$	Dilatancy angle
σ_{ten}	$[kPa]$	Tensile strength

Strength parameters

The Mohr-Coulomb model employs the Mohr-Coulomb yield surface which is defined by the friction angle φ' and cohesion c' (Figure C.1). The parameter σ_{ten} defines the maximum tensile strength of the material. The dilatancy angle ψ describes the volumetric behaviour of the soil under deviatoric loading. In simple shear ψ corresponds to the angle of the deviation of the grain movement to the direction of shearing. In a triaxial test the dilatancy angle can be determined as shown in Figure C.3.

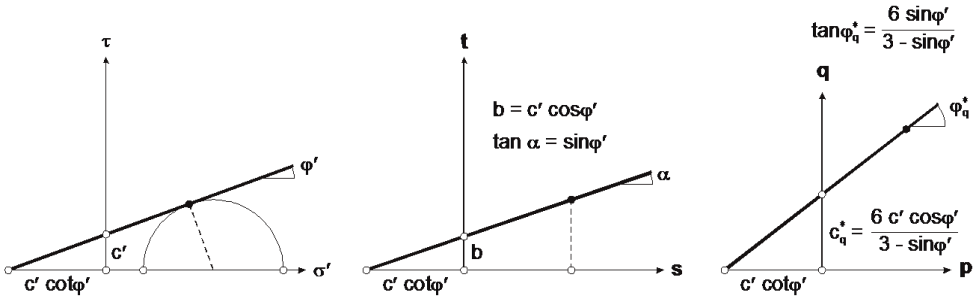

Figure C.1: Visualisation of the Mohr-Coulomb failure criterion.

Stiffness parameters

The elastic stiffness matrix of the used Mohr-Coulomb model is based on the parameters ν and E^{ref}. The stiffness is defined dependent on the isotropic mean pressure $\sigma_m = \frac{1}{3}(\sigma_1 + \sigma_3 + \sigma_3)$ using the exponential law after Ohde/Janbu as

$$E = E^{ref} \left(\frac{\sigma_m}{p^{ref}} \right)^m , \tag{C.1}$$

where p^{ref} is the reference mean isotropic stress (usually 100 kPa) and m the stress exponent. In the Mohr-Coulomb model, elastic stresses are assumed until the material fails and the stress path reaches the yield surface. In this model it is not accounted for material hardening or softening.

C.1.3 The Hardening Soil model with small-strain stiffness

The Hardening Soil model with small-strain stiffness (HSsmall) was used to model the soil in the parametric study. It is a double hardening model, adding two yield surfaces to the Mohr-Coulomb failure criterion. Therefore, irreversible plastic shear strains due to primary deviatoric loading as well as irreversible volumetric strains due to primary isotropic loading are taken into account. Further, a stress dependent stress-strain relationship and a distinction between primary loading and reloading/unloading is covered. Following material parameters are required for the model:

Table C.3: Material parameters for the HSsmall model.

Parameter		Description
E_{50}^{ref}	$[kPa]$	Secant modulus for primary triaxial loading
E_{oed}^{ref}	$[kPa]$	Tangent modulus for oedometric loading
E_{UR}^{ref}	$[kPa]$	Secant modulus fo run- and reloading
m	[-]	Exponent of the Ohde/Janbu law
p^{ref}	$[kPa]$	Reference stress for stiffness parameters
ν_{UR}	[-]	Poisson's ratio unloading-reloading
c'	$[kPa]$	Cohesion (Mohr-Coulomb)
φ'	$[^\circ]$	Friction angle (Mohr-Coulomb)
ψ	$[^\circ]$	Dilatancy angle
R_f	$[-]$	Failure ratio
σ_{ten}	$[kPa]$	Tensile strength
G_0	$[kPa]$	Shear modulus for small strains
$\gamma_{0.7}$	[-]	Shear strain for $G = 0.7G_0$

Strength parameters and dilatancy angle

In the HSsmall model the Mohr-Coulomb failure criterion is employed which is defined by the friction angle φ and the cohesion c as explained in Section C.1.2. During virgin loading (no plastic strains) the yield surface expands until the maximum value is reached, but does not shrink during unloading. The parameter σ_{ten} defines the maximum tensile strength of the material. The dilatancy angle ψ describes the volumetric behaviour of the soil under deviatoric loading (see C.1.2).

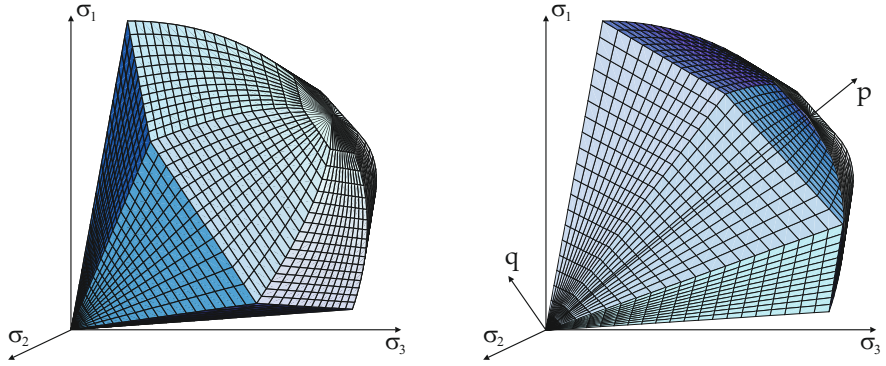

Figure C.2: Yield surface of the HSsmall model in principal stress space.

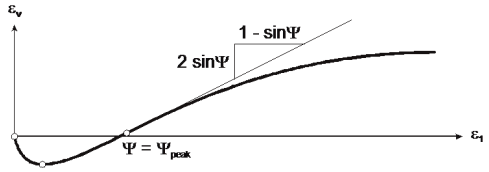

Figure C.3: Determination of ψ in a drained, triaxial test.

Stiffness parameters

The elastic stiffness matrix of the Hardening Soil model is quantified using the parameters ν_{ur} and E_{ur}^{ref}. If no plastic straining occurs (stresses inside the yield surfaces) these elastic parameters in combination with the parameter m and the small-strain formulation described below identify the stress strain behaviour of the model. The elastic Poisson's ratio ν_{ur} and the elastic stiffness E_{ur}^{ref} can be determined in a triaxial test. The secant stiffness E_{ur}^{ref} is determined in an un-/reloading loop. The stress dependent stiffnesses are defined with the exponential law after Ohde/Janbu as

$$E_{UR} = E_{ur}^{ref}\left(\frac{\sigma_3 + c\ cot\varphi'}{p^{ref} + c\ cot\varphi}\right)^m,\ E_{50} = E_{50}^{ref}\left(\frac{\sigma_3 + c\ cot\varphi'}{p^{ref} + c\ cot\varphi}\right)^m\ and$$
$$E_{oed} = E_{oed}^{ref}\left(\frac{\sigma_1 + c\ cot\varphi'}{p^{ref} + c\ cot\varphi}\right)^m \tag{C.2}$$

where p^{ref} is the reference stress (usually 100 kPa) and m the stress exponent.

As shown in Figure C.4 E_{50} represents the secant modulus in primary triaxial loading reaching 50 percent of the ultimate deviatoric stress q_f. The ultimate deviatoric stress q_f is defined by the shear strength. The ratio of q_f and q_a is given by the failure ratio R_f. When assuming $R_f = 1.0$ an asymptotic approach of the stress strain curve to the ultimate deviatoric stress ($q_f = q_a$) is given. Smaller values of R_f yield non-asymptotic stress strain curves, similar to the one shown in Figure C.4. E_{50}^{ref} corresponds to 100 kPa cell pressure (for p^{ref} = 100 kPa). E_{oed}^{ref} represents the tangent modulus in an oedometer test for $p^{ref} = \sigma_1$ = 100 kPa.

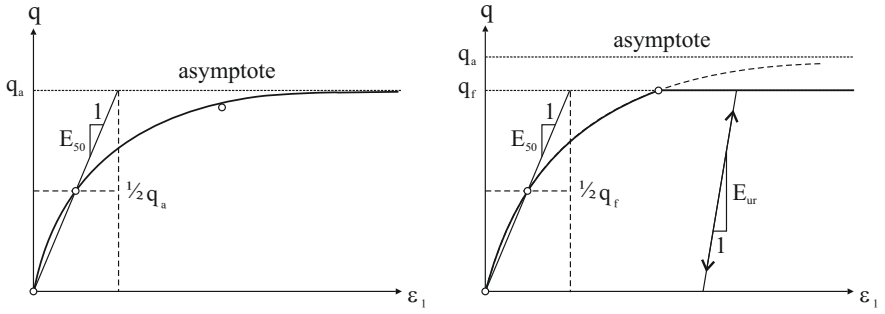

Figure C.4: Definition of E_{ur} and E_{50} in a drained triaxial test.

Small-strain stiffness

The Hardening Soil model with small-strain stiffness takes into account that for small-strains a manifold larger soil stiffness is observed than for larger strains. In addition to the secant stiffness E_{UR} for un- and reloading for large strains, the shear modulus G_0 is defined for very small strains. The Poisson's ratio ν_{UR} is, however, used for all strain ranges. The small-strain shear modulus can be determined from special laboratory tests, but using empirical values usually gives appropriate results. Figure C.5 shows a stiffness reduction curve. The parameter $\gamma_{0.7}$ defines the shear strain at which the actual shear modulus equals $G = 0.7\, G_0$.

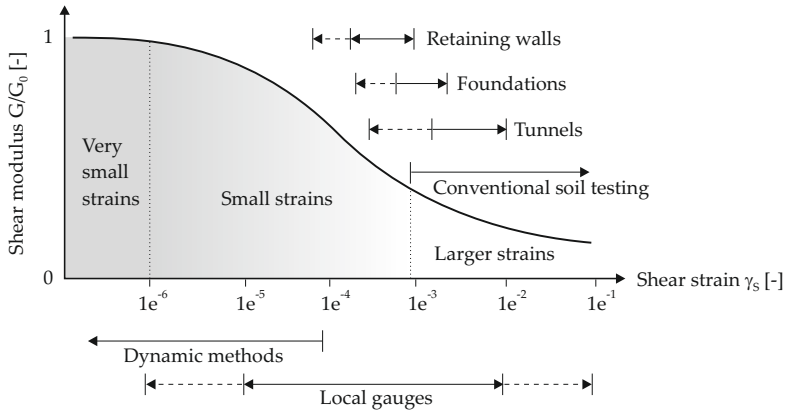

Figure C.5: Definition of small strains.

C.2 Implementation of the two-phase filtration model into FEM

C.2.1 Element connectivity

The algorithm **'ele_con'** reads the list of elements and corresponding nodes from the input file and compares each node of one element to each node of the whole model. The number of common nodes of two elements defines the element connectivity. Cubic elements with 8 nodes and 6 faces have a common face with 4 common nodes, a common edge with 2 common nodes or only a common corner with 1 common node.

Box C.1: Algorithm 'ele_con' for element connectivity

read input file List of elements and their nodes
loop $Element1 = 1..N$
  loop $Element2 = 1..N$
    number of common nodes = 0
    loop $NodeEl1 = 1..8$
      loop $NodeEl2 = 1..8$
        if $NodeEl1 = NodeEl2 \; and \; Element1 \neq Element2$ **then**
          number of common nodes = number of common nodes + 1
        end if
      end loop
    end loop
    write Common bock 'neighbour'
  end loop
end loop

The element connectivity is stored in a three-dimensional common block named 'neighbour'. For each element number, the element number of the neighbouring elements are stored. Then, for each combination the number of common nodes, the contact surface area A and the normal vector of this surface $\overrightarrow{n}_0$ are stored. In a three-dimensional model one element has between 7 and 26 neighbours.

Box C.2: Connectivity of Element 1 stored in common block 'neighbour'

Element No 1

Neighbouring Element No	Number of common nodes	Contact surface properties A	nx	ny	nz
2	4	1.000	0.000	-1.000	0.000
6	4	1.000	0.000	0.000	-1.000
7	2	0.000	0.000	0.000	0.000
26	4	1.000	-1.000	0.000	0.000
27	2	0.000	0.000	0.000	0.000
31	2	0.000	0.000	0.000	0.000
32	1	0.000	0.000	0.000	0.000

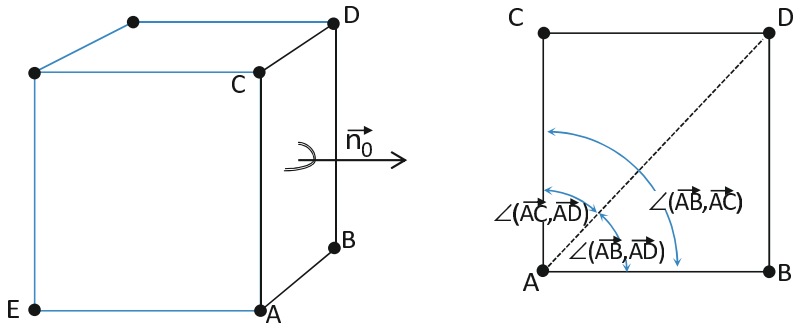

Figure C.6: Definition of normal vector and element face area (A,B,C,D).

Flow of one element to a neighbouring element occurs through a common face. The discharge through this face is calculated from the pore-fluid velocity vector $\overrightarrow{v}$, which is provided for each material point as a result of the previous calculation step. To calculate the discharge though an element face, the area and orientation of the face is now determined. The normal vector $\overrightarrow{n}_0$ of the element face is determined with the cross product of the vectors between three nodes on the surface $(\overrightarrow{AB}, \overrightarrow{AC})$ with

$$\overrightarrow{n_0} = \frac{\overrightarrow{AB} \times \overrightarrow{AC}}{|\overrightarrow{AB} \times \overrightarrow{AC}|} \,. \tag{C.3}$$

This normal vector is perpendicular to the element face, but, depending on the order of the nodes ABC, it could point inwards or outwards of the element. To determine the direction of the normal vector, a reference vector is constructed perpendicular to the subjected element face, starting from a Node P on the opposite face of the element:

$$\overrightarrow{PS} = \frac{\overrightarrow{PA} * \overrightarrow{n_0}}{|\overrightarrow{n_0}|^2} * \overrightarrow{n_0}. \tag{C.4}$$

If the normal vector points in the same direction than this vector, it points outwards of the element. Otherwise it needs to be reversed.

The area of the quadrilateral element surface is determined by dividing it into two triangles, as shown in Figure C.6. The triangle areas are then calculated using the vector product:

$$A_{\triangle ABD} = 0.5|\overrightarrow{AB} \times \overrightarrow{AD}| A_{\triangle ACD} = 0.5|\overrightarrow{AC} \times \overrightarrow{AD}| \,. \tag{C.5}$$

To avoid overlapping triangles, the positions of nodes A,B,C,D around the element face needs to be known. The node order is assessed by an algorithm which identifies the node diagonal to node A by comparing the angles between vectors $\overrightarrow{AB}, \overrightarrow{AC}$ and $\overrightarrow{AD}$ and then defines which nodes form the triangles for calculation (Box C.3).

Box C.3: Calculate area of quadrilateral element surface A,B,C,D

1. Calculate cosine angles between vectors AB,AC,AD

$$cos\angle(\overrightarrow{AB}, \overrightarrow{AD}) = \frac{\overrightarrow{AB} * \overrightarrow{AD}}{|\overrightarrow{AB}||\overrightarrow{AD}|}$$

$$cos\angle(\overrightarrow{AD}, \overrightarrow{AC}) = \frac{\overrightarrow{AD} * \overrightarrow{AC}}{|\overrightarrow{AD}||\overrightarrow{AC}|}$$

$$cos\angle(\overrightarrow{AB}, \overrightarrow{AC}) = \frac{\overrightarrow{AB} * \overrightarrow{AC}}{|\overrightarrow{AC}||\overrightarrow{AD}|}$$

2. Calculate triangular area

if $cos\angle(\overrightarrow{AB}, \overrightarrow{AD}) < (cos\angle(\overrightarrow{AD}, \overrightarrow{AC}))\ and\ cos\angle(\overrightarrow{AB}, \overrightarrow{AC})$ **then**
$A_{ABC} = 0.5|\overrightarrow{AB} \times \overrightarrow{AC}| + 0.5|\overrightarrow{AC} \times \overrightarrow{AD}|$

else if $(cos\angle(\overrightarrow{AB}, \overrightarrow{AD})\ and\ cos\angle(\overrightarrow{AD}, \overrightarrow{AC})) < cos\angle(\overrightarrow{AB}, \overrightarrow{AC}))$ **then**
$A_{ABC} = 0.5|\overrightarrow{AB} \times \overrightarrow{AD}| + 0.5|\overrightarrow{AC} \times \overrightarrow{AD}|$

else
$A_{ABC} = 0.5|\overrightarrow{AB} \times \overrightarrow{AC}| + 0.5|\overrightarrow{AB} \times \overrightarrow{AD}|$
end if

C.2.2 Calculating the filtration front

Two versions of the filtration model were used to calculate cement grout filtration. In the standard model, the discharge into all neighbouring filter cake elements was taken into account. For the modified model, only filtration in the main flow direction of the liquid grout was allowed. To achieve this, only discharge of water from the grout is taken into account, if the main flow direction is directed towards the filtration front. Both options are presented in Boxes C.4 and C.5, respectively. For the considered surface between two elements the velocity vector perpendicular to the surface $\overrightarrow{v_{n0}}$ is determined and the discharge is calculated taking into account the surface area and integrating over time. This procedure is repeated for all neighbouring elements. Once the filter criterion is met, the material properties are changed.

For the modified version with filtration in main flow direction only, the relative flow direction is evaluated from the angle between the flow velocity vector $\overrightarrow{v}$ and the normal vector $\overrightarrow{n_0}$. For an angle below $45°$ the discharge is considered valid and taken into account to calculate the filtration. The adjusted code to access cement grout filtration is presented in Box C.5.

Box C.4: Algorithm to calculate filtration front - standard model

Require: : List of neighbour elements(Element No., Surf. area A, Normal vector $\overrightarrow{n_0}$), Element volume V_{El}, pore fluid velocity vector $\overrightarrow{v}$
  if Element is grout ($FIELD1 = 0$) **then**
    loopNeighbobour=1..N
      if Neighbour is filter cake ($FIELD1 = 1$) **then**
        $\overrightarrow{v_{n0}} = (\overrightarrow{V} * \overrightarrow{n_0}) * \overrightarrow{n_0}$
        $Q_{act} = Q_{act} + \overrightarrow{V_{n0}} * A * \delta t$
      end if
    end loop
    $Q = Q + Q_{act}$
    $Q_{max} = filtcrit * V_{El}$
    if $Q > Q_{max}$ **then**
      Element changes to filter cake material
      $FIELD1 = 1$
    end if
  end if

Box C.5: Algorithm to calculate filtration front in main flow direction - modified model

Require: List of neighbour elements (Element No., Surf. area A, Normal vector $\overrightarrow{n_0}$), Element volume V_{El}, pore fluid velocity vector $\overrightarrow{V}$
if Element is grout ($FIELD1 = 0$) **then**
loopNeighbobour=1..N
if Neighbour is filter cake ($FIELD1 = 1$) **then**
$\angle(\overrightarrow{V}, \overrightarrow{n_0}) = \frac{\overrightarrow{V} * \overrightarrow{n_0}}{|\overrightarrow{V}| * |\overrightarrow{n_0}|}$
if $\angle(\overrightarrow{V}, \overrightarrow{n_0}) \leq 45°$ **then**
$\overrightarrow{V_{n0}} = (\overrightarrow{V} * \overrightarrow{n_0}) * \overrightarrow{n_0}$
$Q_{act} = Q_{act} + \overrightarrow{V_{n0}} * A * \delta t$
end if
end if
end loop
$Q = Q + Q_{act}$
$Q_{max} = filtcrit * V_{El}$
if $Q > Q_{max}$ **then**
Element changes to filter cake material
$FIELD1 = 1$
end if
end if

C.3 ABAQUS Model

C.3.1 General information

ABAQUS is a comprehensive program package for finite-element analysis for a wide variety of engineering problems. For geotechnical engineering, for example, it covers total and effective stress analyses for stress-strain calculations or fully coupled pore fluid flow analyses to calculate consolidation problems or steady or transient groundwater flow. Also heat transfer, mass diffusion and many other applications can be applied. The material models available for soils are linear-elastic behaviour, or elastic-plastic behaviour with classical 'Mohr-Coulomb', 'Drucker-Prager', or critical state 'Cam-Clay' failure criterion. Other constitutive models can be implemented as user defined materials. For all calculations presented in this work, the analysis product ABAQUS/Standard version 6.11 was used, a FEM tool which solves a system of equations implicitly at each calculation increment. For convenience it is only referred to as 'ABAQUS', as other tools such as ABAQUS/Explicit and ABAQUS/DCF analysis, are not considered within this work. Some brief information about the program limited to aspects concerning the work presented here is given in the following sections. A comprehensive documentation of the capabilities and implementation of the code is given in ABAQUS 6.11 (2011b).

Conventions

The units used in an ABAQUS simulation can be freely chosen by the user, as long as they are self consistent. No units are built in into the code. Therefore, the calculation parameters have to be defined with special care in order to achieve self-consistent results for derived units. Within this work following SI units were chosen:

- length [m]
- force [kN]
- mass [kg]
- time [s]

The ABAQUS analysis is divided in calculation steps, for each new step, boundary conditions and loads might be changed. One calculation step is solved in step increments, which sizes depend on the nonlinearity of the analysis or the maximum prescribed value.

The stress convention within ABAQUS is defined according to common structural mechanics: pressure is negative and tension is positive. Pore pressures are positive.

ABAQUS element types

ABAQUS provides an extensive variety of element types, which are described in ABAQUS 6.11 (2011b) in detail. For the grout,3D-continuum brick elements with 8 nodes and reduced integration were chosen (C3D8RP). These elements have one material point (integration point) in the centre. For the soil also C3D8RP and in some models C3D8P elements were used. The C3D8P elements are fully integrated and provide 8 material points. For all stress-displacement element types, the degrees of freedom are assigned to the same number:

- 1: x-displacement
- 2: y-displacement
- 3: z-displacement
- ...
- 8: Pore pressure, hydrostatic fluid pressure
- ...

Usually, the displacements in x-, y-, and z-direction coincide with the global coordinate system, except if a lokal transformation is defined at a node, then the local 1-, 2-, and 3-directions are used.

ABAQUS field and state variables

ABAQUS distinguishes between state and field variables. They are used to store data for output purposes or to store and change values and re-use them during the calculation. In the user defined subroutines both variable types can be used in an equivalent way, only that not all subroutines can read or update both variable types. For example, the user defined material subroutine (UMAT) can only access state variables, but not user defined field variables. Therefore, in the presented code the variable defining the material properties of the grout is assigned to the field variable FIELD(1) and the state variable STATEV(2) accordingly.

ABAQUS input file

An ABAQUS simulation consists of three parts: preprocessing, simulation and postprocessing. In the preprocessing stage the model parameters such as geometry, mesh, material properties, initial and boundary conditions, loads and calculation variables are defined in an input file. This input file can be generated with a preprocessor program, or simply by creating a text file in an text editor. The input file ($*.inp$) is used to create the model from which the calculation is carried out.

If user subroutines are used to increase the program's functionality they have to be referred to in the input file. This applies for user defined material models, boundary conditions, solution dependent material properties or many more.

C.3.2 ABAQUS Subroutines

A variety of user subroutines are available in the ABAQUS package. They enable the user to customise the code and implement non-standard features. The user subroutines are written in the program language FORTRAN and compiled automatically before the calculation of the ABAQUS job is started. A comprehensive description of the available subroutines is given in the ABAQUS user manual (ABAQUS 6.11 (2011a)). The subroutines utilised within this work are now covered briefly:

User defined material model (UMAT)

The subroutine UMAT is applied to implement user defined material behaviour. The user defined material models Hardening Soil with small-strain stiffness (HSsmall) and a classical Mohr-Coulomb approach (MC) are implemented to simulate the soil and grout behaviour respectively. The material properties are assigned dependent on state variables, so that it is possible to change the material properties during calculation by changing the state variables.

User defined boundary conditions (DISP)

The subroutine DISP is used to change the magnitude of a prescribed boundary condition at all nodes listed in a user-subroutine-defined boundary condition. This option is used to define changing pore pressure boundary conditions with depth.

User defined amplitude (UAMP)

User defined amplitudes are used, where a boundary condition of zero effective stress is needed. This is the case for the validation of seepage forces, where a constant flow is applied to a boundary, and free deformation is allowed. In ABAQUS only deformation or total stress boundary conditions (loads) can be applied. In order to achieve a ‘zero-effective-stress boundary’, a load with the magnitude of the pore pressure is applied, to cancel each other out with respect to effective stresses. In the input file this load is defined with a magnitude of one and assigned to the user defined amplitude, which is a multiplier of the load magnitude. This amplitude is supposed to have the same value as the pore pressure at the considered surface. Therefore, the pore pressure is written in a sensor output, which is defined in the input file. This sensor output is then enquired by the subroutine UAMP and used to define the amplitude value. This method only gives approximately zero effective stresses, depending on the pore pressure change in one increment, because the sensor value is written in the previous step. The larger the pore pressure change within one increment, the larger is the effective stress at the boundary.

C.3.3 Calculating field variables and updating state variables (USDFLD)

In this subroutine material point data can be accessed for all elements of which the material properties are dependent on user defined field variables. It can be used to calculate solution-dependent material properties and to update state variables. This subroutine can also be used to include any code features which are to be conducted at specific time points, steps, elements or material points, because the subroutine it is called at each calculation increment and for each material point.

This subroutine is used to change the material properties of the grout when it filters. The filter criterion is checked for each material point, and if it is met, the state variable which defines the material properties is updated. Also the field variables are changed, which define the permeability.

C.4 Implementation of filtration in ABAQUS

To simulate the filtration process in ABAQUS, following adjustments were made to the program:

- Idenfification of neighbouring elements
- Identification of filtration front
- Assessing filter criterion
- Changing mechanical properties when cement filters
- Changing permeability when cement filters

The principles behind the code implemented to accomplish these tasks is explained in section 6.2. In this section it is explained how the code can be implemented into the ABAQUS context. First of all, the element connectivity is determined in the subroutine ‘get_ele_con’, which is called from the subroutine USDFLD at the material point and first time increment. The element connectivity is written in a common block and available for all other subroutines. With this information now the neighbours of each element are known. In the subroutine USDFLD it is now checked whether the current element is located at the filtration front and if the filter criterion is met. State and field variables are then changed accordingly.

C.4.1 Change of material properties due to filtration

Once the grout filtrates, its state changes from a viscous fluid to a solid filter cake with significant strength and stiffness. The permeability decreases due to the denser packing of particles. Assuming the two-phase filtration theory, this change of material properties occurs instantaneously when filtration takes place. To model this change of material behaviour in ABAQUS, the material properties are assigned dependent on state and field variables, which in turn change if the material state changes due to filtration.

In ABAQUS defining a solution dependent permeability is straight forward: the permeability can be directly defined as a function of the desired field variable (here: FIELD(1)) in the input file.

The material properties for the user defined soil model cannot be defined field-variable dependent in the input file. In the user subroutine UAMT only state variables are available and therefore the material properties need to be defined dependent on state variables. The material model was then adapted to calculate the actual value of the material properties, dependent on the current value of the state variable. Within the material model the state variable is accessed before calculation and the state-variable dependent material properties determined.

C.4.2 Prescribed pore-fluid velocity and zero effective stress boundaries

In some validation models a zero effective stress, constant velocity boundary condition is required. ABAQUS however, only provides deformation or total stress (load) boundary conditions. If neither the deformation is restrained nor a pressure applied to a boundary, zero total stress is assumed, meaning that if pore pressures develop at this boundary, also effective stresses occur to maintain zero total stresses. Therefore, to achieve zero effective stress at that boundary, a (total) pressure load equal to the pore pressure is applied. The pore pressure, however, is unknown, as it is a result of the calculation and varying with time, in case of constant pore-fluid velocity boundary. The filter cake thickness changes during calculation and consequently the pore pressure changes due to the increasing hydraulic resistance. To solve that problem, the pore pressure is written in a history output and assigned to a śensor; which makes the value available for ABAQUS user subroutines. The applied pressure load is defined amplitude dependent, with an unity value. Using a user defined amplitude UAMP, where the amplitude value is set equal to the actual pore pressure (sensor) value, the value of the load is updated to the sensor value. This is however an explicit solution as the sensor value is taken from the previous calculation step and therefore the applied load will vary from the actual pore pressure. For that reason it is important to limit the step size to reduce the pore pressure change in one increment and achieve appropriate results.

C.4.3 Assigning initial field variable values

The properties of the user defined material model for the grout, which is specified in the subroutine UMAT, are defined dependent on field- and state variables which are assigned to the material points (material points). However the initial values of the field variables can only be assigned to element nodes in the input file. They are then interpolated from the element nodes to the material points prior the first calculation step. This interpolation results in unintended field variable values at material points lying between areas of different values (materials). In order to obtain the desired field variables at all material points, the material points with incorrect field variable values are identified in the first time increment in the subroutine USDFLD and assigned to the desired values. After correcting the field variables, the state variable defining the material property $(STATEV(2))$ are assigned accordingly.

C.4.4 State variables

Various state variables are used to extend the ABAQUS functionality, define solution dependent material properties and provide additional output parameters. Following state variables are used in the calculation:

- STATEV(1): – Variable already occupied in UMAT –
- STATEV(2): Material index $(= FIELD(1))$
- STATEV(3): Relative discharge (Q_{act}/Q_{max})
- STATEV(4): Total discharge (Q)
- STATEV(5): Identifier for plastic material state

C.5 Fortran source code

C.5.1 Advancing filtraiton front: USDFLD subroutine

```
1 !-----------------------------------------------------------------------
2 !234567890123456789012345678901234567890123456789012345678901234567890
3 !-----------------------------------------------------------------------
4 ! Implementation of two-phase filtration model in ABAQUS
5 !-----------------------------------------------------------------------
6 ! by Xenia Stodieck 2014
7 !-----------------------------------------------------------------------
8 ! Within the ABAQUS subroutine USDFLD the advancing filtration front
9 ! is identified and a filter criterion is accessed
10 ! Only for Element Type C3D8RP
11 ! Calculation is terminated for a defined pore pressure or if filter
12 ! or filter cake reaches a certain element
13 !-----------------------------------------------------------------------
14 !     xN0:          Normal vector on element face
15 !     xVEL:         Porefluid velocity vector
16 !     xVN0:         Normalized velocity vector
17 !     xIntVol:      Integration point volume (Element volume for C3D8RP)
18 !     xMatInd:      Material index  0=liquid or 1=filter cake
19 !     xNEIGHBOUR:   Common block storing connectivity
20 !     xPor:         Pore pressure
21 !     xQ_act:       Discharge of element in actual increment
22 !     xQ:           Cumulative discharge of element
23 !     xQ_max:       Discharge defining filter criterion
24 !-----------------------------------------------------------------------
25 !     filtel():     Material index actual element
26 !     filtelold():  Material index of actual element in previous increment
27 !     filtcheck:    Number of specified elements that are filter cake
28 !     increment:    Previous increment number
29 !     elcheck:      Index if element is on filtration front
30 !-----------------------------------------------------------------------
31 !     STATEV(2):  Material index (0=liquid or 1=filter cake)
32 !     STATEV(3):  Relative discharge xQ/(xQ_max)
33 !     STATEV(4):  Total discharge xQ
34 !-----------------------------------------------------------------------
35
36       SUBROUTINE USDFLD(FIELD,STATEV,PNEWDT,DIRECT,T,CELENT,
37      1 TIME,DTIME,CMNAME,ORNAME,NFIELD,NSTATV,NOEL,NPT,LAYER,
38      2 KSPT,KSTEP,KINC,NDI,NSHR,COORD,JMAC,JMATYP,MATLAYO,
39      3 LACCFLA)
40
41       INCLUDE 'ABA_PARAM.INC'
42
43       CHARACTER*80 CMNAME,ORNAME
44       CHARACTER*3  FLGRAY(15)
```

```
45        DIMENSION FIELD(NFIELD),STATEV(NSTATV),DIRECT(3,3),
46       1 T(3,3),TIME(2)
47        DIMENSION ARRAY(15),JARRAY(15),JMAC(*),JMATYP(*),
48       1 COORD(*)
49        real xVEL(3),xN0(3),xVN0(3)
50        real xNEIGHBOUR(45000,26,6)
51        real xMatInd
52        real filtel(45000),filtelold(45000)
53        integer m,loop,ADNO,ADEL,elcheck,increment
54        common /kNEIGHBR/ xNEIGHBOUR
55        common /kFilt/ filtel
56        common /kFiltOld/ filtelold
57        common /kIncrement /increment
58
59 !------------------------------------------------------------------
60 !      Terminating analysis when grouting pressure limit is reached or
61 !      all elements are filtrated
62 !      -> definition of elements numbers for exit criterion required
63 !------------------------------------------------------------------
64
65        IF (TIME(1) .NE. 0 .AND. NOEL .EQ. 963)    THEN
66          CALL GETVRM('POR',ARRAY,JARRAY,FLGRAY,JRCD,JMAC,JMATYP,MATLAYO,
67       2          LACCFLA)
68          xPOR=ARRAY(1)
69          IF (xPOR .GT. 3000.) THEN
70             CALL XIT ! Exit when grouting pressure is exceeded!
71          END IF
72        ELSE IF (TIME(1) .NE. 0 .AND. NOEL .EQ. 1) THEN
73         filtcheck=0
74         DO ele=951,955 ! Insert centre element numbers
75            filtcheck=filtcheck+filtelold(ele)
76         END DO
77         IF (filtcheck .EQ. 5.) THEN
78            CALL XIT ! Exit when filter cake reaches centre!
79         END IF
80        END IF
81
82 !------------------------------------------------------------------
83 !      Adjust material index for interpolation elements in first step
84 !      -> values need to be checked for each new model!
85 !------------------------------------------------------------------
86
87        IF (TIME(1) .EQ. 0) THEN
88           filtel(NOEL)=FIELD(1)
89           IF (FIELD(1) .EQ. 1.5 .OR. FIELD(1) .EQ. 1.75) THEN
90              filtel(NOEL)=0.
91           END IF
92           filtelold=filtel ! filtelold is updated one increment
93 !                          delayed in case increment fails to converge
```

```
94            increment=KINC    ! Stores the previous increment number
95          END IF
96
97 !-------------------------------------------------------------------------
98 !         Get element connectivity in first increment
99 !-------------------------------------------------------------------------
100         IF (NOEL .EQ. 1) THEN
101           IF (TIME(2) .EQ. 0) THEN
102             CALL get_elem_con
103           ELSE
104           IF (KINC .EQ. increment) THEN !Increment is repeated
105 !           use previous material index if increment is repeated
106             filtel=filtelold
107           ELSE !New increment
108             filtelold=filtel   !update filtelold
109             increment=KINC     !update increment
110           END IF
111           END IF
112         END IF
113
114 !-------------------------------------------------------------------------
115 !       Get current velocity
116 !-------------------------------------------------------------------------
117         CALL GETVRM('FLVEL',ARRAY,JARRAY,FLGRAY,JRCD,JMAC,JMATYP,
118        1 MATLAYO,LACCFLA)
119         xV = ( ARRAY(3))
120         xVEL(1)=ARRAY(2)
121         xVEL(2)=ARRAY(3)
122         xVEL(3)=ARRAY(4)
123
124 !-------------------------------------------------------------------------
125 !       Get material point volume
126 !-------------------------------------------------------------------------
127         CALL GETVRM('IVOL',ARRAY,JARRAY,FLGRAY,JRCD,JMAC,JMATYP,
128        1 MATLAYO,LACCFLA)
129         xIntVol = ARRAY(1)
130
131 !-------------------------------------------------------------------------
132 !         Access filtration criterion
133 !-------------------------------------------------------------------------
134         xMatInd=filtel(NOEL)   !Material index  0=liquid or 1=filter cake
135         elcheck=0
136
137         IF (xMatInd .EQ. 0) THEN   !Material is grout
138           xQ_act =0
139           !Find adjacent elements who are filter cake
140           DO loop=1,26    !Go through all neighbouring elements
141             ADEL=xNEIGHBOUR(NOEL,loop,1) ! Number of neighbour element
142             ADNO=xNEIGHBOUR(NOEL,loop,2) ! Number of common nodes
```

```
143             IF (ADNO .EQ. 4 .AND. filtel(ADEL) .GE. 1) THEN
144                 elcheck=1 !Element is filter element
145                 xN0(1)=xNEIGHBOUR(NOEL,loop,4)
146                 xN0(2)=xNEIGHBOUR(NOEL,loop,5)
147                 xN0(3)=xNEIGHBOUR(NOEL,loop,6)
148                 xskal=dot_product(xVEL,xN0)
149                  IF (xskal .GT. 0) THEN !Flow outwards
150                     DO i=1,3
151 !                       Transpose velocity vector
152                        xVN0(i)=dot_product(xVEL,xN0)*xN0(i)
153                     END DO
154                     xVneu=(dot_product(xVN0,xVN0))**0.5
155                  ELSE
156                     xVneu=0
157                  END IF
158                  xQ_act = xQ_act+ xVneu*xNEIGHBOUR(NOEL,loop,3)*DTIME
159             END IF
160          END DO
161          IF(elcheck .EQ. 1) THEN !Element is on filtration front
162             xQ_max = 0.323*xIntVol
163             xQ=STATEV(4)+xQ_act
164             IF (xQ .GE. xQ_max) THEN
165                 filtel(NOEL) = 1.
166                STATEV(3) = 1.
167              Else IF (xQ .GT. 0.) THEN
168                 STATEV(3) = xQ/(xQ_max)
169              END IF
170              STATEV(4) = xQ
171           END IF
172        End IF
173
174 ! Write actual material definition in FIELD variable
175        FIELD(1) = filtel(NOEL)
176
177 ! Store as a solution dependent state variable
178        STATEV(2) = filtel(NOEL)
179
180 ! IF error, write comment to .DAT file:
181        IF(JRCD.NE.0)THEN
182        WRITE(6,*) 'REQUEST␣ERROR␣IN␣USDFLD␣FOR␣ELEMENT␣NUMBER␣',
183       1       NOEL,'INTEGRATION␣POINT␣NUMBER␣',NPT
184        END IF
185        RETURN
186        END
187 !-----------------------------------------------------------------------
```

C.5.2 Element connectivity: get_elem_con subroutine

```
1 !------------------------------------------------------------------------------
2 !234567890123456789012345678901234567890123456789012345678901234567890
3 !------------------------------------------------------------------------------
4 ! Identify Neighbouring Elements/ Common nodes
5 ! Determination of node connectivity based on ele_con.for available at
6 !   http://www.eng-tips.com/viewthread.cfm?qid=269244
7 !------------------------------------------------------------------------------
8 !    ncnt:       Number of nodes in the model
9 !    nelcnt:     Number of elements in the model
10 !   num_neighbours: Number of neighbours
11 !   xNEIGHBOUR: Common block storing connectivity
12 !   nodes:        Matrix with node number and coordinates
13 !   ele:          Matrix with element number (1,...) and nodes (...,2-9)
14 !   ab,ac,ad:     Vectors between a, b and c
15 !   A:            Element surface area
16 !   W1, W2, W3:   Cosine of angle between vectors
17 !------------------------------------------------------------------------------
18
19       subroutine get_elem_con
20        include 'ABA_PARAM.INC'
21 !
22 !       Declaration of variables
23 !
24       character*256 jobname,outdir,filename,input
25       real xNEIGHBOUR(45000,26,6)
26       integer ele(45000,9)
27       real nodes(46000,4)
28       real ab(3),ac(3),ad(3),A,W1,W2,W3,xn(3),xn0(3),pa(3),PS(3)
29       integer com_nodes
30       real com_nodes_nr(5,3)
31       integer ele_loop1,ele_loop2,count,ncheck,comncheck
32       common /kNEIGHBR/ xNEIGHBOUR
33       common /kELEMENTS/ ele
34
35 !------------------------------------------------------------------------------
36 !       Open INP file for reading.
37 !------------------------------------------------------------------------------
38
39       CALL getjobname(jobname,lenjobname)
40       CALL getoutdir(outdir,lenoutdir)
41       filename=outdir(1:lenoutdir)//'\'//
42      1        jobname(1:lenjobname)//'.inp'
43       OPEN(unit=101,file=filename(1:lenoutdir+
44      1        lenjobname+5),status='old')
45
46       ncnt=0
```

```
47        nelcnt=0
48        count=0
49
50 !-------------------------------------------------------------------------
51 !       Skip down to *Node in input File
52 !-------------------------------------------------------------------------
53        DO WHILE (index(input,'*Node')==0)
54           read(101,'(a)')input
55        END DO
56
57 !-------------------------------------------------------------------------
58 !       Read in node coordinates
59 !-------------------------------------------------------------------------
60        DO WHILE (.TRUE.)
61           read(101,*)input
62           IF (index(input,'*')==0) THEN
63             backspace(101)
64             ncnt=ncnt+1
65             read(101,*)nodes(ncnt,1),nodes(ncnt,2),
66       1          nodes(ncnt,3),nodes(ncnt,4)
67           ELSE
68             EXIT
69           END IF
70        END DO
71
72 !-------------------------------------------------------------------------
73 !       Skip down to *Element in input File
74 !-------------------------------------------------------------------------
75        DO WHILE (index(input,'*Element')==0)
76           read(101,'(a)')input
77        END DO
78
79 !-------------------------------------------------------------------------
80 !        Read in element nodal connectivity
81 !-------------------------------------------------------------------------
82         DO WHILE (.TRUE.)
83           read(101,*)input
84           IF (index(input,'*')==0) THEN
85              backspace(101)
86              nelcnt=nelcnt+1
87              read(101,*)ele(nelcnt,1),ele(nelcnt,2),
88       1             ele(nelcnt,3),ele(nelcnt,4),ele(nelcnt,5),
89       2             ele(nelcnt,6),ele(nelcnt,7),ele(nelcnt,8),
90       3             ele(nelcnt,9)
91           ELSE
92              EXIT
93           END IF
94         END DO
95
```

```
!------------------------------------------------------------------------
!       Get element connectivity
!------------------------------------------------------------------------
!      Loop over all elements (El1)
       DO ele_loop1=1,nelcnt
          num_neighbours=1
!
!    Compare to all elements (El2)
          DO ele_loop2=1,nelcnt
             elecheck=0
             com_nodes=0
             com_nodes_nr=0
!
!    Compare all nodes of El1 to all nodes of El2
             DO nlp1=2,9
                ncheck=0

!     Ask if node is common
                IF (ele(ele_loop2,nlp2)==ele(ele_loop1,nlp1)) THEN

!     Ask if compared elements are unequal
                   IF (ele_loop1/=ele_loop2) THEN
                      com_nodes=com_nodes+1

!     Write coordinates of common nodes
                      com_nodes_nr(com_nodes,1)=nodes(ele(ele_loop2,nlp2),2)
                      com_nodes_nr(com_nodes,2)=nodes(ele(ele_loop2,nlp2),3)
                      com_nodes_nr(com_nodes,3)=nodes(ele(ele_loop2,nlp2),4)
                      elecheck=1    !Elements are neighbours
                      ncheck=1      !nlp1 is a common node!
                      xNEIGHBOUR(ele(ele_loop1,1),num_neighbours,1)
     1                     =ele(ele_loop2,1)
                      xNEIGHBOUR(ele(ele_loop1,1),num_neighbours,2)
     1                     =com_nodes
                   END IF
                END IF
             END DO !nlp2

             IF (elecheck .EQ. 1 .AND. ncheck .EQ. 0) THEN !One node which is
     not common
                com_nodes_nr(5,1)=nodes(ele(ele_loop1,nlp1),2)
                com_nodes_nr(5,2)=nodes(ele(ele_loop1,nlp1),3)
                com_nodes_nr(5,3)=nodes(ele(ele_loop1,nlp1),4)
                comncheck=1
             ELSE IF (elecheck .EQ. 1 .AND. npl1 .EQ. 9 .AND.
     1            comncheck .EQ. 0) THEN !In case common nodes are npl1=6 to
     9
                com_nodes_nr(5,1)=nodes(ele(ele_loop1,2),2)
                com_nodes_nr(5,2)=nodes(ele(ele_loop1,2),3)
```

```
143               com_nodes_nr(5,3)=nodes(ele(ele_loop1,2),4)
144               write(6,*)'***ERROR: Check uncommon node between'
145               write(6,*)'Element',ele_loop1,'and element',ele_loop2
146             END IF
147           END DO !nlp1
148           IF (elecheck .EQ. 1) THEN
149               num_neighbours=num_neighbours+1
150
151 !-------------------------------------------------------------------------
152 !              Calculation of area between neighbours
153 !-------------------------------------------------------------------------
154               IF (com_nodes .EQ. 4) THEN
155                  DO count=1,3
156                     ab(count)=com_nodes_nr(2,count)-com_nodes_nr(1,count)
157                     ac(count)=com_nodes_nr(3,count)-com_nodes_nr(1,count)
158                     ad(count)=com_nodes_nr(4,count)-com_nodes_nr(1,count)
159                     pa(count)=com_nodes_nr(1,count)-com_nodes_nr(5,count)
160                  END DO
161
162 !                Cosine of angle between vectors
163                W1=dot_product(ab,ad)/((dot_product(ab,ab))
164       1            **0.5*(dot_product(ad,ad))**0.5)
165                W2=dot_product(ad,ac)/(dot_product(ad,ad)
166       1            **0.5*dot_product(ac,ac)**0.5)
167                W3=dot_product(ab,ac)/(dot_product(ab,ab)
168       1            **0.5*dot_product(ac,ac)**0.5)
169
170 !              Calculate Area
171                IF (W1 .LT. W2 .and. W1 .LT. W3) THEN
172                  A=0.5*(dot_product(ab,ab)*dot_product(ac,ac)
173       1              -(dot_product(ab,ac))**2)**0.5+0.5*(dot_product(ad,ad)
174       2               *dot_product(ac,ac)-(dot_product(ad,ac))**2)**0.5
175                Else If (W3 .LT. W2 .and. W3 .LT. W1) THEN
176                  A=0.5*(dot_product(ab,ab)*dot_product(ad,ad)
177       1              -(dot_product(ab,ad))**2)**0.5+0.5*(dot_product(ad,ad)
178       2               *dot_product(ac,ac)-(dot_product(ad,ac))**2)**0.5
179                Else If (W2 .LT. W1 .and. W2 .LT. W3) THEN
180                  A=0.5*(dot_product(ab,ab)*dot_product(ad,ad)
181       1              -(dot_product(ab,ad))**2)**0.5+0.5*(dot_product(ab,ab)
182       2               *dot_product(ac,ac)-(dot_product(ab,ac))**2)**0.5
183                End If
184                  xNEIGHBOUR(ele(ele_loop1,1),num_neighbours-1,3)=A
185
186 !-------------------------------------------------------------------------
187 !            Calculation of normal Vector
188 !-------------------------------------------------------------------------
189                   xn(1)=ab(2)*ac(3)-ab(3)*ac(2)
190                   xn(2)=ab(3)*ac(1)-ab(1)*ac(3)
191                   xn(3)=ab(1)*ac(2)-ab(2)*ac(1)
```

```
192                 xn0=xn/(dot_product(xn,xn)**0.5)
193
194 !               Perpendicular vector from uncommon point to plane
195                 PS=dot_product(pa,xn0)*xn0
196
197 !               Check if vector points outward of element
198                 IF (dot_product(PS,xn0) .LT. 0) THEN
199                     xn0=-1*xn0
200                 End If
201
202                     DO count=1,3
203                         xNEIGHBOUR(ele(ele_loop1,1),num_neighbours-1
204       1                             ,count+3)=xn0(count)
205                     END DO
206
207                     ab=0
208                     ac=0
209                     ad=0
210                     A=0
211                     W1=0
212                     W2=0
213                     W3=0
214
215                 END IF
216               END IF
217             END DO !ele_loop2
218           END DO   !ele_loop1
219           close(101)
220
221 !-------------------------------------------------------------------------
222         return
223         END subroutine get_elem_con
224 !-------------------------------------------------------------------------
```

C.6 Results of FEM simulations

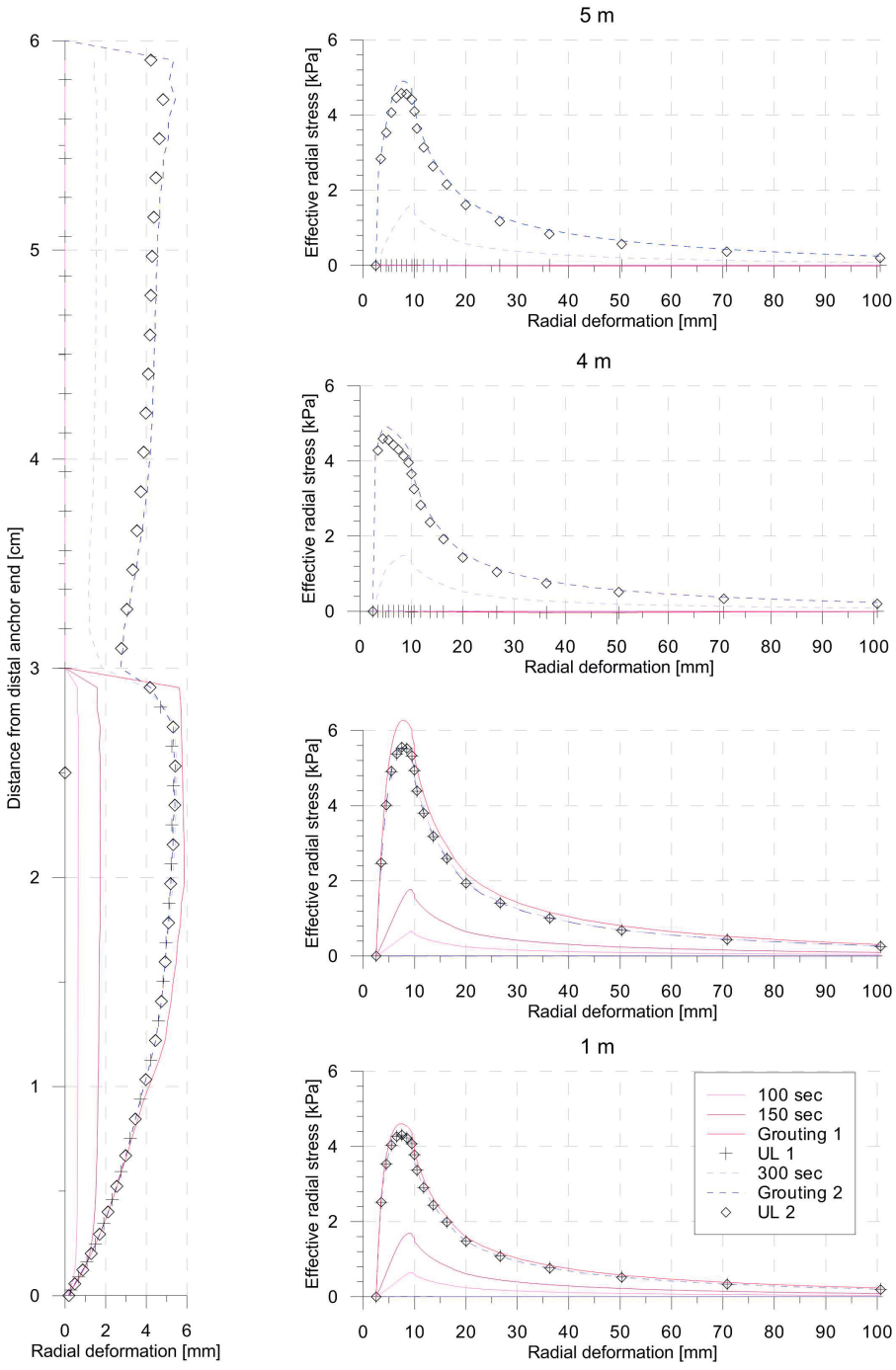

Figure C.7: Development of radial deformations in model ‘G_LM_B_filtdir’.

C.7 Parameter study results for the material set ‘loose sand’

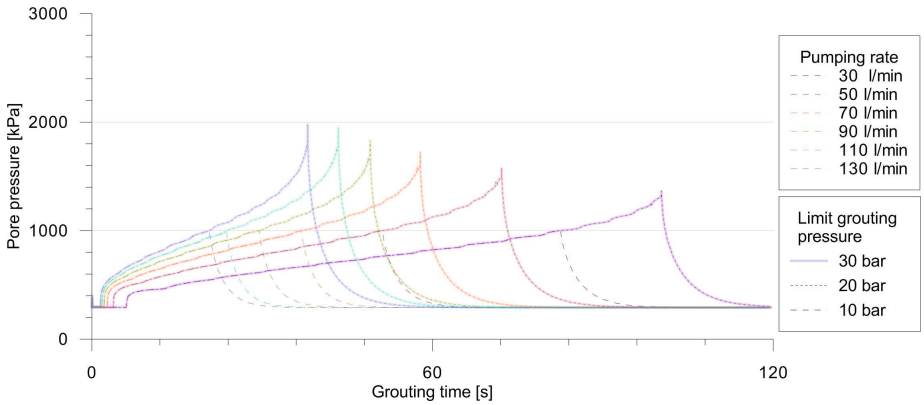

Figure C.8: Grouting pressure development for different pumping rates in ‘loose sand’.

Table C.4: Results of parametric study with varying pumping rates in 'loose sand' and 10 bar limiting grouting pressure.

Model	Pumping rate	Max. grouting pressure P	Filter cake thickness	σ'_G (STEP1)	σ'_{UL} (STEP2)	σ'_{UL}/σ'_G	σ'_{UL}/P
	[l/min]	[kPa]	[cm]	[kPa]	[kPa]		
	l/min	kPa	cm	kPa	kPa		
W_HS_PAR1	10	974.05	7.5	392.0	264.3	63%	29%
W_HS_PAR2	20	1000.48	6.0	474.7	314.2	57%	31%
W_HS_PAR3	30	1000.02	5.0	525.4	338.7	55%	31%
W_HS_PAR4	40	1000.14	4.5	556.5	361.0	54%	32%
W_HS_PAR5	50	1000.16	4.0	537.8	329.4	57%	36%
W_HS_PAR6	60	1000.54	4.0	582.0	366.7	61%	36%
W_HS_PAR7	70	1000.18	3.5	589.6	351.7	57%	35%
W_HS_PAR8	80	1001.67	3.5	617.9	383.0	58%	35%
W_HS_PAR9	90	1000.46	3.0	547.1	328.6	59%	35%
W_HS_PAR10	100	1000.22	3.0	549.0	349.9	56%	35%
W_HS_PAR11	110	1002.67	3.0	617.6	411.6	52%	32%
W_HS_PAR12	120	1000.01	3.0	597.6	378.2	55%	33%
W_HS_PAR13	130	1002.44		601.0	361.2	52%	32%

Table C.5: Results of parametric study with varying pumping rates in 'loose sand' and 20 bar limiting grouting pressure.

Model	Pumping rate	Max. grouting pressure P	Filter cake thickness	σ'_G (STEP1)	σ'_{UL} (STEP2)	σ'_{UL}/σ'_G	σ'_{UL}/P
	[l/min]	[kPa]	[cm]	[kPa]	[kPa]		
W_HS_PAR1	10	974.05	7.5	392.0	264.3	62%	27%
W_HS_PAR2	20	1211.34	7.5	521.0	350.7	62%	29%
W_HS_PAR3	30	1363.60	7.5	576.1	399.2	61%	29%
W_HS_PAR4	40	1481.31	7.5	638.8	459.9	62%	29%
W_HS_PAR5	50	1576.24	7.5	700.9	501.3	64%	31%
W_HS_PAR6	60	1662.87	7.5	667.4	465.8	59%	31%
W_HS_PAR7	70	1723.02	7.5	743.8	562.8	62%	33%
W_HS_PAR8	80	1765.42	7.5	750.1	558.8	63%	36%
W_HS_PAR9	90	1829.56	7.5	815.9	605.5	56%	32%
W_HS_PAR10	100	1900.59	7.5	768.7	512.2	60%	36%
W_HS_PAR11	110	1991.99	7.5	769.7	572.8	61%	36%
W_HS_PAR12	120	1948.73	7.5	891.7	646.8	57%	34%
W_HS_PAR13	130	1979.39	7.5	770.8	541.0	56%	33%

Table C.6: Results of parametric study with varying pumping rates in 'loose sand' and 30 bar limiting grouting pressure.

Model	Pumping rate	Max. grouting pressure P	Filter cake thickness	σ'_G (STEP1)	σ'_{UL} (STEP2)	σ'_{UL}/σ'_G	σ'_{UL}/P
	[l/min]	[kPa]	[cm]	[kPa]	[kPa]		
W_HS_PAR1	10	974.05	7.5	392.0	264.3	62%	27%
W_HS_PAR2	20	1211.34	7.5	521.0	350.7	62%	29%
W_HS_PAR3	30	1363.60	7.5	576.1	399.2	61%	29%
W_HS_PAR4	40	1481.31	7.5	638.8	459.9	62%	29%
W_HS_PAR5	50	1576.24	7.5	700.9	501.3	64%	31%
W_HS_PAR6	60	1662.87	7.5	667.4	465.8	65%	33%
W_HS_PAR7	70	1723.02	7.5	743.8	562.8	64%	33%
W_HS_PAR8	80	1765.42	7.5	750.1	558.8	62%	29%
W_HS_PAR9	90	1829.56	7.5	815.9	605.5	65%	32%
W_HS_PAR10	100	1900.59	7.5	768.7	512.2	62%	30%
W_HS_PAR11	110	1991.99	7.5	769.7	572.8	64%	31%
W_HS_PAR12	120	1948.73	7.5	891.7	646.8	62%	31%
W_HS_PAR13	130	1979.39	7.5	770.8	541.0	62%	30%

Table C.7: Results of parametric study with varying pumping rates in 'dense sand' and 10 bar limiting grouting pressure.

Model	Pumping rate	Max. grouting pressure P	Filter cake thickness	σ'_G (STEP1)	σ'_{UL} (STEP2)	σ'_{UL}/σ'_G	σ'_{UL}/P
	[l/min]	[kPa]	[cm]	[kPa]	[kPa]		
W_HS_PAR1	10	1000.2	6.50	467.9	292.8	63%	29%
W_HS_PAR2	20	1000.2	4.50	542.4	309.0	57%	31%
W_HS_PAR3	30	1000.3	3.50	571.3	311.9	55%	31%
W_HS_PAR4	40	1000.2	3.00	584.1	315.3	54%	32%
W_HS_PAR5	50	1002.6	3.00	635.2	361.4	57%	36%
W_HS_PAR6	60	1000.8	2.50	593.6	361.4	61%	36%
W_HS_PAR7	70	1001.6	2.50	620.8	353.6	57%	35%
W_HS_PAR8	80	1001.3	2.00	600.4	349.8	58%	35%
W_HS_PAR9	90	1000.0	2.00	598.6	351.9	59%	35%
W_HS_PAR10	100	1001.5	2.00	631.7	352.7	56%	35%
W_HS_PAR11	110	1000.7	2.00	623.6	323.6	52%	32%
W_HS_PAR12	120	1002.4	2.00	608.2	331.7	55%	33%
W_HS_PAR13	130	1000.7	1.50	612.6	320.9	52%	32%

Table C.8: Results of parametric study with varying pumping rates in 'dense sand' and 20 bar limiting grouting pressure.

Model	Pumping rate	Max. grouting pressure P	Filter cake thickness	σ'_G (STEP1)	σ'_{UL} (STEP2)	σ'_{UL}/σ'_G	σ'_{UL}/P
	[l/min]	[kPa]	[cm]	[kPa]	[kPa]		
W_HS_PAR1	10	1114.8	7.50	490.4	303.4	62%	27%
W_HS_PAR2	20	1463.7	7.50	681.8	424.2	62%	29%
W_HS_PAR3	30	1706.0	7.50	795.8	486.3	61%	29%
W_HS_PAR4	40	1885.3	7.50	890.5	555.8	62%	29%
W_HS_PAR5	50	2041.2	7.50	967.9	623.9	64%	31%
W_HS_PAR6	60	2001.3	7.00	1,056.7	621.4	59%	31%
W_HS_PAR7	70	2002.7	6.50	1,075.5	662.4	62%	33%
W_HS_PAR8	80	2001.2	6.50	1,147.2	726.7	63%	36%
W_HS_PAR9	90	2000.8	6.50	1,150.1	647.7	56%	32%
W_HS_PAR10	100	2001.6	6.00	1,201.0	719.8	60%	36%
W_HS_PAR11	110	2000.1	5.50	1,190.4	721.8	61%	36%
W_HS_PAR12	120	2001.7	5.00	1,196.3	682.7	57%	34%
W_HS_PAR13	130	2004.7	5.00	1,183.7	665.9	56%	33%

Table C.9: Results of parametric study with varying pumping rates in 'dense sand' and 30 bar limiting grouting pressure.

Model	Pumping rate	Max. grouting pressure P	Filter cake thickness	σ'_G (STEP1)	σ'_{UL} (STEP2)	σ'_{UL}/σ'_G	σ'_{UL}/P
	[l/min]	[kPa]	[cm]	[kPa]	[kPa]		
W_HS_PAR1	10	1114.8	7.50	490.4	303.4	62%	27%
W_HS_PAR2	20	1463.7	7.50	681.8	424.2	62%	29%
W_HS_PAR3	30	1706.0	7.50	795.8	486.3	61%	29%
W_HS_PAR4	40	1885.3	7.50	890.5	555.8	62%	29%
W_HS_PAR5	50	2041.2	7.50	967.9	623.9	64%	31%
W_HS_PAR6	60	2160.1	7.50	1,099.8	716.8	65%	33%
W_HS_PAR7	70	2272.8	7.50	1,150.1	741.8	64%	33%
W_HS_PAR8	80	2375.2	7.50	1,122.7	694.7	62%	29%
W_HS_PAR9	90	2451.8	7.50	1,195.7	773.6	65%	32%
W_HS_PAR10	100	2542.3	7.50	1,249.9	774.2	62%	30%
W_HS_PAR11	110	2663.0	7.50	1,269.8	813.1	64%	31%
W_HS_PAR12	120	2613.3	7.50	1,292.7	798.2	62%	31%
W_HS_PAR13	130	2733.9	7.50	1,327.7	818.3	62%	30%

(a) Radial stresses at maximum grouting pressure.

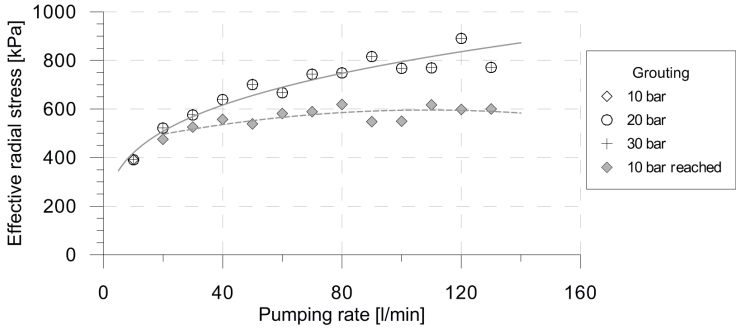

(b) Radial stresses after unloading.

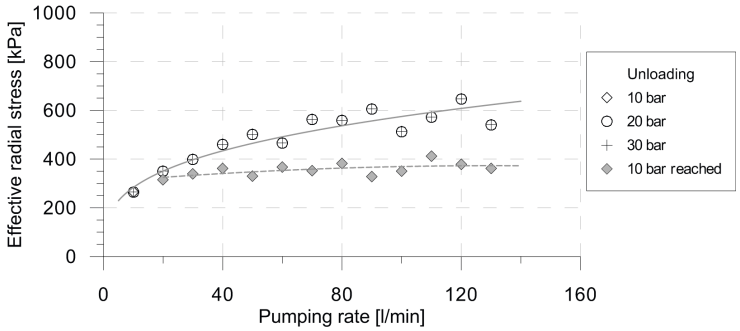

Figure C.9: Radial stresses at borehole walls after grouting in ‘loose sand’ with varying grouting pressures and pumping rates.

(a) Radial stresses at maximum grouting pressure.

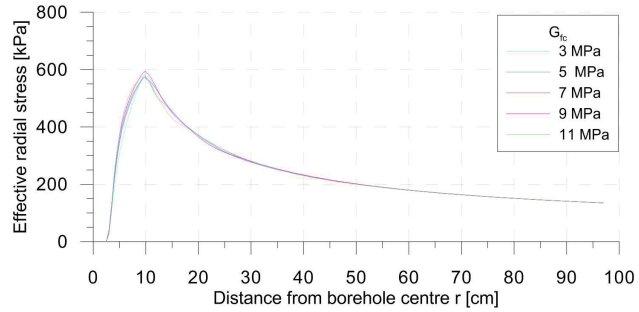

(b) Radial stresses after unloading.

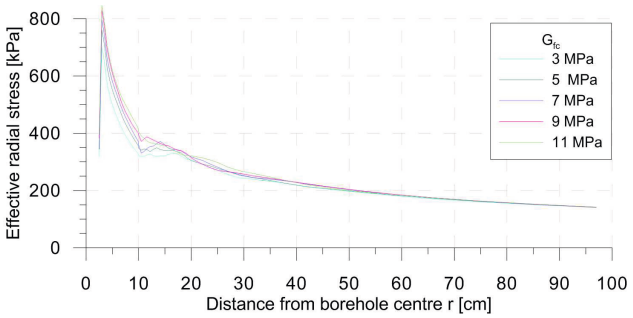

(c) Radial stresses at borehole walls at maximum grouting pressure and after unloading.

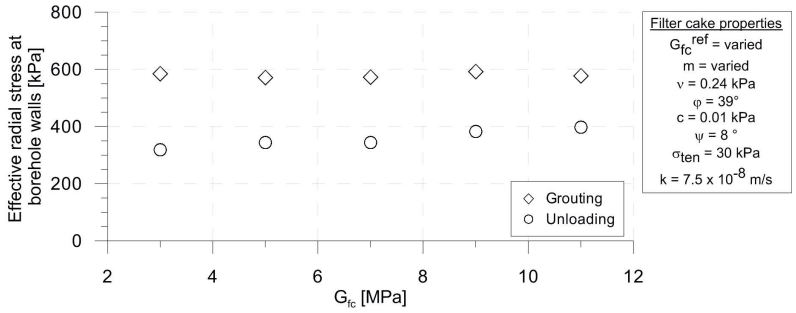

Figure C.10: Parameter variation of filter cake stiffness G_{fc} in ‘loose sand’.

(a) Radial stresses at maximum grouting pressure.

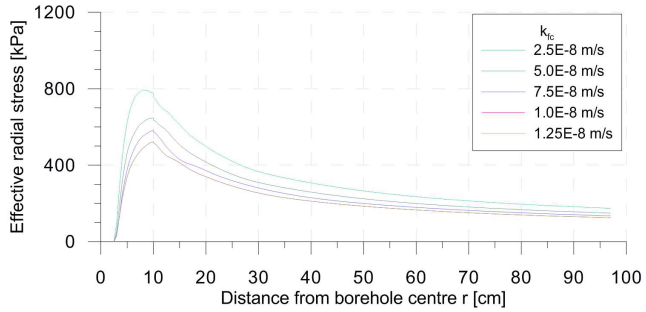

(b) Radial stresses after unloading.

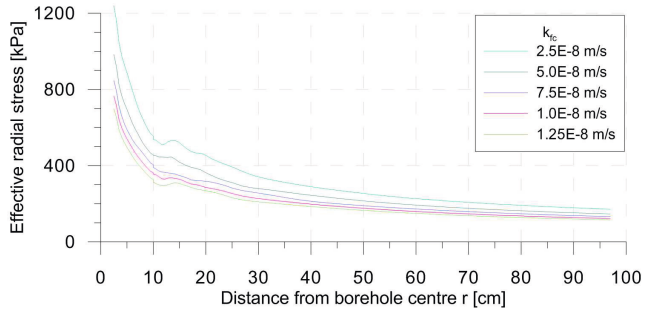

(c) Radial stresses at borehole walls at maximum grouting pressure and after unloading.

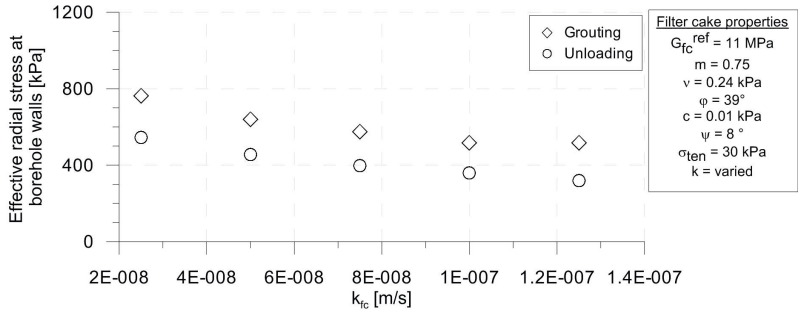

Figure C.11: Parameter variation of filter cake permeability k_{fc} in 'loose sand'.

(a) Radial stresses at maximum grouting pressure.

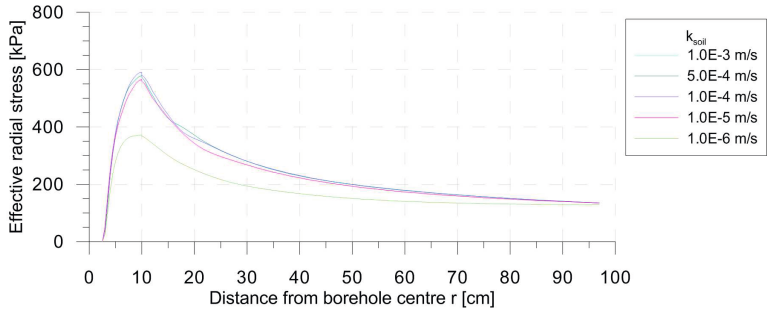

(b) Radial stresses after unloading.

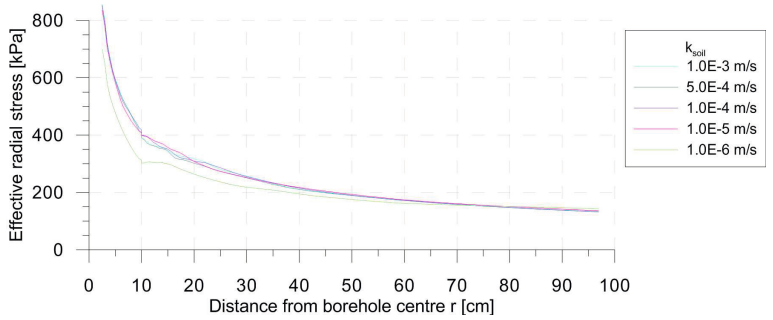

(c) Radial stresses at borehole at maximum grouting pressure and unloading.

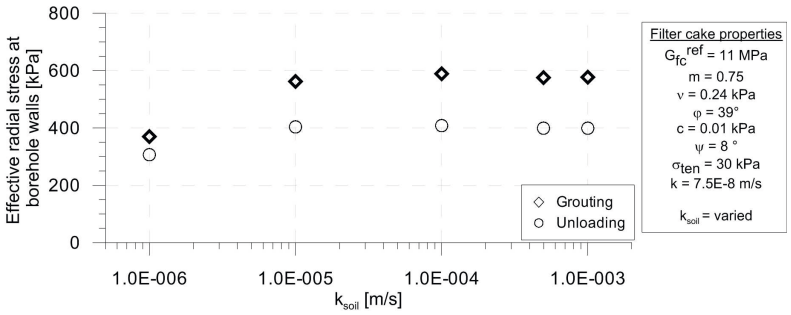

Figure C.12: Parameter variation of soil permeability k_{soil} in 'loose sand'.